National Library of Canada
Bibliothèque nationale du Canada

Canadian Theses Service
Service des thèses canadiennes

Ottawa, Canada
K1A 0N4

NOTICE

The quality of this microform is heavily dependent upon the quality of the original thesis submitted for microfilming. Every effort has been made to ensure the highest quality of reproduction possible.

If pages are missing, contact the university which granted the degree.

Some pages may have indistinct print especially if the original pages were typed with a poor typewriter ribbon or if the university sent us an inferior photocopy.

Reproduction in full or in part of this microform is governed by the Canadian Copyright Act, R.S.C. 1970, c. C-30, and subsequent amendments.

AVIS

La qualité de cette microforme dépend grandement de la qualité de la thèse soumise au microfilmage. Nous avons tout fait pour assurer une qualité supérieure de reproduction.

S'il manque des pages, veuillez communiquer avec l'université qui a conféré le grade.

La qualité d'impression de certaines pages peut laisser à désirer, surtout si les pages originales ont été dactylographiées à l'aide d'un ruban usé ou si l'université nous a fait parvenir une photocopie de qualité inférieure.

La reproduction, même partielle, de cette microforme est soumise à la Loi canadienne sur le droit d'auteur, SRC 1970, c. C-30, et ses amendements subséquents.

NL-339 (r. 88/04) c

Canada

THE UNIVERSITY OF ALBERTA

HIGH-PRESSURE SCALED MODEL DESIGN TECHNIQUES FOR THERMAL RECOVERY PROCESSES

by

Kevin Kimber

(C)

A THESIS

SUBMITTED TO THE FACULTY OF GRADUATE STUDIES AND RESEARCH

IN PARTIAL FULFILLMENT OF THE REQUIREMENTS FOR THE DEGREE

OF DOCTOR OF PHILOSOPHY

IN

PETROLEUM ENGINEERING

DEPARTMENT OF MINING, METALLURGICAL AND PETROLEUM ENGINEERING

EDMONTON, ALBERTA

SPRING 1989

National Library of Canada
Bibliothèque nationale du Canada

Canadian Theses Service
Service des thèses canadiennes

Ottawa, Canada
K1A 0N4

The author has granted an irrevocable non-exclusive licence allowing the National Library of Canada to reproduce, loan, distribute or sell copies of his/her thesis by any means and in any form or format, making this thesis available to interested persons.

L'auteur a accordé une licence irrévocable et non exclusive permettant à la Bibliothèque nationale du Canada de reproduire, prêter, distribuer ou vendre des copies de sa thèse de quelque manière et sous quelque forme que ce soit pour mettre des exemplaires de cette thèse à la disposition des personnes intéressées.

The author retains ownership of the copyright in his/her thesis. Neither the thesis nor substantial extracts from it may be printed or otherwise reproduced without his/her permission.

L'auteur conserve la propriété du droit d'auteur qui protège sa thèse. Ni la thèse ni des extraits substantiels de celle-ci ne doivent être imprimés ou autrement reproduits sans son autorisation.

ISBN 0-315-52863-X

Canada

THE UNIVERSITY OF ALBERTA

RELEASE FORM

NAME OF AUTHOR	Kevin Kimber
TITLE OF THESIS	High-Pressure Scaled Model Design Techniques for Thermal Recovery Processes
DEGREE	Doctor of Philosophy
YEAR	1989

Permission is hereby granted to the University of Alberta Library to reproduce single copies of this thesis and to lend or sell such copies for private, scholarly or scientific research purposes only.

The author reserves other publication rights, and neither the thesis nor extensive extracts from it may be printed or otherwise reproduced without the author's written permission.

Kevin Kimber

2011 141 Avenue
Edmonton, Alberta T5Y 1P4

DATE: March 29, 1989

THE UNIVERSITY OF ALBERTA

FACULTY OF GRADUATE STUDIES AND RESEARCH

The undersigned certify that they have read, and recommend to the Faculty of Graduate Studies and Research for acceptance, a thesis entitled:

HIGH-PRESSURE SCALED MODEL DESIGN TECHNIQUES

FOR THERMAL RECOVERY PROCESSES

submitted by Kevin Kimber in partial fulfillment of the requirements for the degree of Doctor of Philosophy in Petroleum Engineering.

Dr. S.M. Farouq Ali (Supervisor)

Dr. J.M. Whiting

Dr. D.D. Flock

Dr. R.G. Bentsen

Dr. K. Nandakumar

Dr. J.P. Batycky (External Examiner)

Date: March 17, 1989

To my wife and parents,

who provide the inspiration for everything I do

ABSTRACT

New scaling techniques for design of steam injection experiments are developed and tested in this research project. The requirements for scaling steam-additive processes are derived and five approaches to satisfying a relaxed set of these requirements identified.

One limitation of scaling techniques is their inability to simultaneously satisfy all of the criteria governing the scaling of a process. A novel approach, in which some of the requirements of geometric similarity are relaxed in order to scale other aspects of the process, is examined in this study. Each approach offers different advantages. The most appropriate approach must be selected in order to scale a particular field situation.

When using current techniques, different porous media and different pressure conditions than found in the field are required. As a result, properties which depend on pressure (e.g. PVT properties) or porous media (e.g. relative permeabilities) may not be scaled accurately. Three of the new scaling approaches allow the use of field porous media and pressure conditions.

A high-pressure scaled model facility was designed and constructed in order to compare the capabilities of the scaling approaches. Experimental results from a large model are compared with those from smaller models which were designed using each scaling approach. Initial experiments led to design criteria improvements in approaches which relaxed

some aspects of geometric similarity. Other experiments examined the capabilities of each approach when used to predict such parameters as energy and temperature distribution, oil production rate, water-oil ratio, steam zone size and steam breakthrough.

The scaling approaches which use field porous media and pressure conditions yielded results for the steam processes studied which were in agreement with those from an accepted approach from the literature which was tested as well. The new approaches provide scaling options which may be better for steam processes using additives (PVT properties must be scaled), processes using pressure cycles (fluid compressibilities must be scaled), and processes requiring the use of the same porous media as found in the field.

ACKNOWLEDGEMENTS

I wish to express my sincere appreciation to my academic supervisor, Dr. S.M. Farouq Ali, and to my project manager, Dr. T.W. Stone, for their valuable guidance, encouragement, and thoughtful suggestions throughout the preparation of this thesis.

I feel indebted to the Alberta Research Council and the Alberta Oil Sands Technology and Research Authority for funding this study and for providing a superb environment in which to carry out this work.

I would further like to thank all the staff at the Alberta Research Council who participated directly or indirectly in the completion of this thesis. In particular, I would like to thank Doug Lillico for his valuable discussions and helpful suggestions.

TABLE OF CONTENTS

	Page
ABSTRACT	v
ACKNOWLEDGEMENTS	vii
LIST OF TABLES	xi
LIST OF FIGURES	xii
LIST OF PLATES	xvii
NOMENCLATURE	xviii
1. INTRODUCTION	1
2. OBJECTIVES	3
3. LITERATURE REVIEW	4
3.1 Background for scaling Steam Processes	4
3.1.1 Scaling Theories	5
3.1.2 Scaled Experimental Studies	5
4. PRESENTATION AND DISCUSSION OF THEORETICAL DEVELOPMENT	10
4.1 Additional Mechanisms to be Considered for Steam-plus-additive Processes	10
4.1.1 Dispersion	10
4.1.2 Stability of Steam Fronts	11
4.1.3 Non-equilibrium Mass Transfer	13
4.2 Derivation of Scaling Groups	14
4.2.1 Inspection Analysis	14
4.2.2 Dimensional Analysis	19
4.3 Approaches to Satisfying the Scaling Criteria	22
4.3.1 Approach #1 - Same Fluids, Different Porous Media, Different Pressure, Drop Geometric Similarity	27
4.3.2 Approach #2 - Same Fluids, Same Porous Medium, Same Pressure Drop, Geometric Similarity	29
4.3.3 Approach #3 - Same Fluids, Same Porous Medium, Same Pressure Drop, Geometric Similarity Relaxed	31
4.3.4 Approach #4 - Same Fluids, Same Porous Medium, Same Pressure Drop, Geometric Scaling Relaxed	32
4.3.5 Approach #5 - Same Fluids, Different Porous Media, Different Pressure Drop, Geometric Scaling Relaxed	33
4.4 Comparison of the Five Scaling Approaches	35

Page

5. EXPERIMENTAL INVESTIGATION 41

5.1 Experimental Strategy 41

5.2 Design of the Scaled Experiments 42
5.2.1 Field Data and Operating Conditions 42
5.2.2 Experimental Design 43
5.2.3 Experimental Apparatus 51
5.2.4 Experimental Procedure 58

6. ANALYSIS PROCEDURE 64

6.1 Porosity 64

6.2 Permeability 65

6.3 Production Rate 65

6.4 Saturation 66

6.5 Steam Zone Volume 66

6.6 Pressure Data 67

6.7 Temperature Measurement and Energy Balance 67
6.7.1 Energy Losses to the Insulation 70
6.7.2 Energy Losses to the Surrounding Formations 70
6.7.3 Energy Losses to the Steel Model 71

6.8 Produced Steam Quality and Steam Breakthrough 73

6.9 Scale-Up of Experimental Results 74
6.9.1 Temperature 74
6.9.2 Time 75
6.9.3 Energy 76
5.9.4 Production Rate 76
6.9.5 Cumulative Production 77
6.9.6 Pressure 77

7. PRESENTATION AND DISCUSSION OF EXPERIMENTAL RESULTS 79

7.1 Approaches #3 and #4 82

7.2 Approaches #1, #2, and #3 90
7.2.1 Temperature Distribution 97
7.2.2 Energy Distribution 112
7.2.3 Production 122
7.2.4 Steam Zone Volume 137
7.2.5 Production Quality and Steam Breakthrough 137
7.2.6 Pressure Data 147
7.2.7 Quantitative Comparisons 150

Page

7.3 Heat Losses to the Insulation....158

7.4 Repeatability....158

8. CONCLUSIONS....164

9. RECOMMENDATIONS FOR FURTHER STUDIES....168

REFERENCES....169

APPENDIX A - INITIAL AND BOUNDARY CONDITIONS....172

APPENDIX B - DEVELOPMENT OF THE RELAXED SCALING CRITERIA....175

APPENDIX C - DIFFERENTIAL EQUATIONS IN DIMENSIONLESS FORM....179

APPENDIX D - SCALING ANISOTROPIC POROUS MEDIA....184

APPENDIX E - OIL PROPERTIES....185

APPENDIX F - AVERAGE BLOCK TEMPERATURE....188

APPENDIX G - NEW CRITERIA FOR APPROACHES #3 AND #4....190

LIST OF TABLES

Table		Page
1.	Summary of Previous Scaled Steam Experiments	7
2.	Constitutive Relationships and Constraints	17
3.	Mass Balance For Oil in Terms of the Dimensionless Variables and Their Reference Quantities	18
4.	Similarity Groups from Inspectional Analysis	20
5.	Dimensionless Properties and Conditions to be Satisfied	21
6.	Variables for Dimensional Analysis	23
7.	Similarity Groups from Dimensional Analysis	25
8.	Influence of Various Similarity Groups on Each Approach	36
9.	Field Information	44
10.	Model Information	46
11.	Comparison of 5-Spot Pressure Distribution	68
12.	Characteristics of Each Experimental Run	80
13.	Dimensionless Time Matches for Each Approach and the Associated Errors	106

LIST OF FIGURES

Figure		Page
1.	A brief description of the five high-pressure scaling techniques examined in this study	28
2.	Examples of the inability of Approach #1 to satisfy the scaling requirements for fluid properties	48
3.	Schematic of experimental apparatus	52
4.	Details of the injection well used in the models	56
5.	Thermocouple locations	60
6.	Schematic of assembled model	63
7.	Triangular cells used to analyze energy distribution	69
8.	A comparison of the measured and ideal (scaled) heat losses to the surrounding formations for Run 8	72
9.	Comparison of the energy losses to the surrounding formations of the large model to those predicted using Approaches #3 and #4 (Runs 44, 34, 24)	84
10.	Comparison of the energy contained in the reservoir of the large model to those predicted using Approaches #3 and #4 (Runs 44, 34, 24)	85
11.	Comparison of the energy contained in the produced fluids of the large model to those predicted using Approaches #3 and #4 (Runs 44, 34, 24)	86
12.	Comparison of the production rate of water and condensed steam in the large model to those predicted using Approaches #3 and #4 (Runs 44, 34, 24)	87
13.	Comparison of the fraction of the reservoir occupied by steam in the large model to those predicted using Approaches #3 and #4 (Runs 44, 34, 24)	88
14.	Comparison of the estimated quality of the produced steam from the large model to those predicted using Approaches #3 and #4 (Runs 44, 34, 24)	89

Figure — Page

15. Improvement in prediction of energy losses to the surrounding formations using Approach #3 (Run 46) 91

16. Improvement in prediction of energy contained within the reservoir using Approach #3 (Run 46) 92

17. Improvement in prediction of energy contained in the produced fluids using Approach #3 (Run 46) 93

18. Improvement in predicted production rate using Approach #3 (Run 46) 94

19. Improvement in prediction of steam zone volume using Approach #3 (Run 46) 95

20. Improved estimate of the quality of the produced steam using Approach #3 (Run 46) 96

21. Sectioned views for vertical (View A-A) and horizontal (View B-B) temperature profiles 99

22. Step-by-step advancement of temperature within the large model (Run 45) during a steam-oil-water experiment 100

23. Comparison of the vertical temperature profile for the large model (Run 45) at t_D=0.165 to that predicted using Approach #2 (Run 39) 102

24. Comparison of the vertical temperature profile for the large model (Run 45) at t_D=0.142 to that predicted using Approach #1 (Run 43) 103

25. Comparison of the vertical temperature profile for the large model (Run 45) at t_D=0.136 to that predicted using Approach #3 (Run 47) 104

26. Comparison of the horizontal temperature profile for the large model (Run 8) to those predicted using Approach #1 (Run 28) and #2 (Run 13) at t_D=0.400 108

27. Comparison of the horizontal temperature profile for the large model (Run 11) to those predicted using Approach #1 (Run 27) and #2 (Run 16) at t_D=0.400 109

28. Comparison of the horizontal temperature profile for the large model (Run 44) to those predicted using Approach #1 (Run 42), #2 (Run 38) and #3 (Run 46) at t_D=0.400 110

Figure — Page

29. Comparison of the horizontal temperature profile for the large model (Run 10) to those predicted using Approach #1 (Run 30) and #2 (Run 15) at t_D=0.400 111

30. Comparison of the horizontal temperature profiles for the steam-oil-water experiments 113

31. Energy distribution during a large model experiment (Run 8) at an injection rate of 6.9 m^3/day 114

32. Comparison of energy lost to the surrounding formations of the large model (Run 44) to that predicted by each scaling approach (Runs 42, 38, 46) 116

33. Comparison of energy lost to the surrounding formations of the large model (Run 45) to that predicted by each scaling approach (Runs 43, 39, 47) 117

34. Comparison of the energy contained within the reservoir of the large model (Run 44) to that predicted by each scaling approach (Runs 42, 38, 46) 118

35. Comparison of the energy contained within the reservoir of the large model (Run 45) to that predicted by each scaling approach (Runs 43, 39, 47) 119

36. Comparison of the energy contained in the production fluids of the large model (Run 44) to that predicted by each scaling approach (Runs 42, 38, 46) 120

37. Comparison of the energy contained in the production fluids of the large model (Run 45) to that predicted by each scaling approach (Runs 43, 39, 47) 121

38. The energy distribution in the large model (Run 8) and that predicted using Approach #2 (small model, Run 13) 123

39. The energy distribution in the large model (Run 11) and that predicted using Approach #2 (small model, Run 16) 124

40. The energy distribution in the large model (Run 9) and that predicted using Approach #2 (small model, Run 14) 125

41. The energy distribution in the large model (Run 10) and that predicted using Approach #2 (small model, Run 15) 126

42. Comparison of the production rate of the large model (Run 44) to that predicted using Approach #1 (Run 42) 128

Figure — Page

43. Comparison of the production rate of the large model (Run 44) to that predicted using Approach #2 (Run 38).....129

44. Comparison of the production rate of the large model (Run 44) to that predicted using Approach #3 (Run 46).....130

45. Comparison of the cumulative production from the large model (Run 44) to those predicted using Approaches #1 (Run 42), #2 (Run 38) and #3 (Run 46).....132

46. Comparison of the oil production rate of the large model (Run 45) to that predicted using Approach #1 (Run 43).....133

47. Comparison of the oil production rate of the large model (Run 45) to that predicted using Approach #2 (Run 39).....134

48. Comparison of the oil production rate of the large model (Run 45) to that predicted using Approach #3 (Run 47).....135

49. Comparison of the oil/water ratio for the large model (Run 45) to those predicted using Approaches #1 (Run 43), #2 (Run 39) and #3 (Run 47).....136

50. Comparison of the fraction of the pore volume occupied by steam in the large model (Run 44) to those estimated using Approaches #1 (Run 42), #2 (Run 38) and #3 (Run 46).....138

51. Comparison of the fraction of the pore volume occupied by steam in the large model (Run 45) to those estimated using Approaches #1 (Run 43), #2 (Run 39) and #3 (Run 47).....139

52. Estimated quality of the produced steam for large model experiments at various injection rates (Runs 8,11,44,15).....141

53. Comparison of the quality of the produced steam for the large model to the predictions of each scaling approach for a series of steam-water experiments with scaled injection rates of 55.3 m^3/day.....142

54. Comparison of the quality of the produced steam for the large model (Run 45) to the prediction made using Approach #1 (Run 43).....143

55. Comparison of the quality of the produced steam for the large model (Run 45) to the prediction made using Approach #2 (Run 39).....144

Figure — Page

56. Comparison of the quality of the produced steam for the large model (Run 45) to the prediction made using Approach #3 (Run 47) 145

57. Comparison of the horizontal temperature profiles for a steam-water experiment (Run 49) and a steam-oil-water experiment (Run 45) 146

58. Comparison of the injection pressure for the large model (Run 45) to those predicted using Approaches #1 (Run 43), #2 (Run 39) and #3 (Run 47). The dimensionless injection pressure is defined as $p_D=p_i/p_R$. 148

59. Comparison of the pressure drop across the large model (Run 45) to those predicted using Approaches #1 (Run 43), #2 (Run 39) and #3 (Run 47). The dimensionless pressure drop is defined as $\Delta p_D=\Delta p/p_R$. 149

60. Injection pressure comparisons which minimize the effect of model permeability 151

61. Pressure drop comparisons which minimize the effect of model permeability 152

62. Average errors in predicting energy distribution for each scaling approach for a series of steam-water experiments (Runs 44, 42, 38, 46) 153

63. Average errors in predicting energy distribution for each scaling approach for a series of steam-oil-water experiments (Runs 45, 43, 39, 47) 155

64. Average relative errors in predicting produced steam quality, steam zone volume, and production rate for a series of steam-water experiments (Runs 44, 42, 38, 46) 156

65. Average relative errors in predicting produced steam quality, steam zone volume, oil/water ratio and production rate for a series of steam-oil-water experiments (Runs 45, 43, 39, 47) 157

66. Repeatability of large model experiments (Runs 41 and 45) 160

67. Repeatability of Approach #1 experiments (Runs 14 and 38) 161

68. Repeatability of Approach #2 experiments (Runs 29 and 42) 162

69. Repeatability of Approach #3 experiments (Runs 19 and 34) 163

LIST OF PLATES

Plate		Page
1.	Pressure vessel which housed the scaled model	54
2.	A large and a small model illustrating the location of the thermocouple ports	54
3.	A large and small model illustrating the 1/8th of a 5-spot geometry used	57
4.	Three of the small models illustrating the different thicknesses required by the various scaling approaches	57
5.	A scaled model with the overburden and thermocouples in place	61
6.	A fully assembled scaled model, ready to be placed in the pressure vessel	61

NOMENCLATURE

a	scaling factor
A_{iw}	area open for flow in an injection or production well
C_{ij}	concentration of component j in phase i
C_p	heat capacity
D^*	molecular diffusion coefficient
D^*_{eff}	effective diffusion coefficient for a porous medium
D_T	transverse hydrodynamic dispersion coefficient
D_L	longitudinal hydrodynamic dispersion coefficient
$\bar{D}_i$	convective dispersion tensor of the i phase
$\bar{D}^*_{ij}$	molecular diffusion tensor of the j component within the i phase
$\bar{D}_{ij}$	hydrodynamic dispersion tensor of the j component within the i phase
d_p	mean particle diameter in the porous medium
E	energy
F	formation electrical resistivity factor
f	a general function
g	acceleration due to gravity
H	height or thickness of the reservoir or model
h_i	enthalpy of the i phase
I_s	instability number
K_{jik}	equilibrium K-value for component j partitioning between phases i and k
k_{hj}	thermal conductivity of j
$\bar{k}_i$	effective permeability tensor of the i phase
k	absolute permeability

L	length of the reservoir or model
M	hypothetical property
M_{eq}	equivalent mobility ratio
P_c	capillary pressure
p_i	pressure of the i phase
S_i	saturation of the i phase
T	temperature
t	time
U_i	internal energy of the i phase
v	superficial velocity
w	slot width
W	width of the reservoir or model
W_{ij}	injection rate of component j within phase i
x_i	Cartesian coordinates
z	elevation of reservoir above a datum
α	thermal diffusivity
ϕ	porosity of reservoir
ρ_i	density of the i phase
μ_i	viscosity of the i phase
σ_{ik}	interfacial tension between the i and k phases
χ	inhomogeneity factor

<u>subscripts</u>

a	air
c	cap rock or base rock
d	downstream

D	dimensionless quantity
g	gas phase
gs	additive component of gaseous phase
gw	water component of gaseous phase
i	initial
iw	located at the injection well
irr	irreducible
m	model
n	normal to the boundary
o	oleic phase
oo	oil component of oleic phase
os	additive component of oleic phase
p	prototype
pw	located at the production well
R	reference quantity
r	reservoir rock
s	additive component
sat	saturation
ss	stainless steel
st	steam
u	upstream
w	aqueous phase
ww	water component of aqueous phase
x	x_1-direction
y	x_2-direction
z	x_3-direction

1. INTRODUCTION

Steam injection, and in particular steamflooding, accounts for over 80 percent of all enhanced oil production. Thus, prediction of steamflood performance is of great importance to the petroleum industry. For a number of years, emphasis has been placed on improving the efficiency of steamflooding processes. Many laboratory studies have been conducted in an effort to achieve this goal. Some of the experiments were designed to study the various mechanisms of a given process and to extend the results for making field predictions by use of numerical simulators. Other experiments, referred to as "scaled experiments," were designed to allow the relative influence of the various mechanisms observed in an experiment to be similar to that expected in the field and to permit interpretation of the results to predict field performance.

Physical models are a valuable adjunct to numerical simulators. In the case of steam injection, numerical simulators are still inadequate in a number of respects, such as grid size and orientation, process description, and rock-fluid interactions. The limitations of physical models include their inability to satisfy all of the scaling criteria. This research attempts to make contributions in this area.

Some of the requirements for designing scaled experiments of steamflooding processes are contradictory. Consequently, one or more of these requirements must be relaxed. Choosing which requirements to relax depends on the particular process being modelled. Scaling of the phenomena considered to be least important to a particular process might

be relaxed without significantly affecting the major features of the process. Different choices for relaxation will lead to different scaling techniques. Suitable scaling techniques for steam injection experiments are developed and verified, and conditions are identified under which particular scaling approaches are found to be most suitable to particular recovery processes (e.g. steam additives, thin reservoirs, gas caps, bottom water, etc.).

2. OBJECTIVES

The broad objectives of this work are to develop and verify suitable scaling techniques for steam injection experiments, and to identify the conditions under which a particular technique is most suitable for a given recovery process. The first objective is to develop scaling techniques which permit the use of field pressure conditions or field porous media in the scaled models. Such theories may allow scaled model investigations to include steam additives which are influenced by pressure and temperature, compressibility effects of reservoir fluids, condensation and solubility effects, distillation, and rock-fluid interactions.

The next objective is to verify these techniques experimentally. Complete verification requires large financial and human resources and, of necessity, includes field pilots. The initial steps in this verification process are taken in the experimental portion of this work. The objectives of the experimental part of this study were as follows:

1) To design, construct, and operate a high-pressure scaled model apparatus;
2) To verify that the novel concepts developed for the new scaling approaches are valid;
3) To evaluate the importance of scaling pressure conditions and the significance of what is relinquished to do so; and
4) To assess the relative usefulness of each scaling approach in predicting a number of parameters important to steam injection processes.

3: LITERATURE REVIEW

Scaling theories for studying isothermal systems were first presented by Leverett et al.[1] They studied radial flow near an oil well and linear flow through layered sands. Rapoport and Leas[2] studied linear floods in greater detail and presented scaling laws governing stabilized flow for corefloods. A detailed study of the major scaling parameters governing waterfloods was presented by Croes and Schwarz.[3] Scaling laws were extended by Geertsma et al.[4] to cover hot water injection. These parameters were later used by Baker[5,6] in his experimental studies of heat flow during thermal processes.

3.1 BACKGROUND FOR SCALING STEAM PROCESSES

The scaling of steam processes is even more complex than scaling hot water processes. The scaling techniques must now include the effects of three phase flow with a condensing gas where pressure conditions are more critical and gravity segregation more severe. The techniques are used to predict the effect of various parameters on the production response of a reservoir undergoing steam injection. The parameters include injection rate, production pressure, slug size, completion intervals, well pattern geometry, steam additives, the existence of bottom water, reservoir heterogeneities, and steam quality. Scaled models are also used to calibrate numerical models and provide insight into the effects of mechanisms that may not be properly incorporated in numerical simulators.

3.1.1 Scaling Theories

A number of approaches to scaling steam processes have been used by previous investigators. Farouq Ali and Redford[7] presented a review of the approaches used. The various approaches differ in degree of scaling complexity and may be divided into two broad categories: high-pressure models (operating at field pressures) and low-pressure models (operating under vacuum). The scaling criteria used most widely for low-pressure models are those presented by Stegemeier et al.[8] The criteria used most widely for high-pressure models are those presented by Pujol and Boberg.[9] High-pressure models use the same fluids as found in the prototype (field). Certain high temperature/pressure phenomena such as rock-fluid interactions, fluid properties, emulsification, steam distillation, gas solubility, and compressibility effects may be scaled in a better manner with high-pressure models than with low-pressure ones. Low-pressure models are easier to build and operate, and may yield more accurate temperature and velocity distributions due to improved scaling of the pressure-temperature relationship for saturated steam. Such models usually require a fluid with properties different from those of the fluid in the prototype to satisfy all the criteria considered to be important. In practice, it is difficult to find fluids that can satisfy these criteria, and as with high-pressure models, compromises must be made.

3.1.2 Scaled Experimental Studies

Several investigators have studied steam processes using scaled models

in the past. Various fields, exhibiting a wide variety of characteristics, were examined. The studies vary in geometry represented, material used to represent the porous media, permeability of the porous media, type of oil used to represent the field oil, and pressure at which the model was operated. Table 1 lists these studies and indicates some of the major differences. The remainder of this section is devoted to discussing these experiments in more detail.

Pujol and Boberg[9] demonstrated the difficulty of simultaneously scaling viscous, gravity and capillary forces in a steamflood. They investigated the use of surfactants to bring the capillary forces into scale, but concluded that this introduced too many undesirable changes to the process to be a suitable solution. However, through numerical studies they demonstrated that capillary forces can be neglected for viscous oils. Bursell and Pittman[10] used a high-pressure scaled model representing one-eighth of a five-spot pattern to study the effects of reservoir thickness, oil viscosity, and steam injection temperature on sweep efficiency, residual oil, and oil recovery. They used field oils ranging in viscosity from 650 to 26 600 mPa•s and found that scaled model results correlated very well with data from pilot operations. Huygen[11] and Huygen and Lowry,[12] using an approach in which only the heat flow is considered in scaling, developed a high-pressure model which used field crudes and crushed sandstone. He studied the effects of oil viscosity, initial oil saturation, and distillation residue on oil recovery. Huygen and Lowry[12] used Pujol and Boberg's scaling laws to construct a high-pressure model of a Wabasca tar sand. They investigated the influence of steam rate and initial oil saturation of a

Table 1. Summary of previous scaled steam experiments.

Author	Geometry	Medium	Permeability (μm^2)	Type of Oil	Viscosity (20°C) (mPa•s)	Pressure (kPa)
Niko[15]	1/6 of a well	sand	700-1900*	various	600-8000*	<100*
Pujol[9]	1/8 of 5-spot	sand	400	?	100 000	3550
Pursley[13]	1/8 of 5-spot	frac sand	200-1200	Cold Lake	100 000	3550
Bursell[10]	1/8 of 5-spot	sand	215	various	450-26 600	275-1830
Huygen[11]	1/2 of 5-spot	crushed Berea	18	various	3.6-70 000	430-5920
Ehrlich[14]	1/4 of 5-spot	sand	10-30	Wabasca	100 000	1690
Stegemeier[8]	line drive	glass beads	2600-5200	Dutrex blend	271	80
Doscher[20]	1/8 of 5-spot	glass beads	2000	Dutrex 419	600	30
Singhal[19]	1/12 of 7-spot	glass beads	170	Rapeseed/Shellflex	70	210
Huygen[12]	1/4 of 5-spot	sand	32	Wabasca	100 000	2240
Proctor[17]	1/4 of 5-spot	glass beads	4217	Faxam 10	250	20
Sufi[16]	1/12 of 7-spot	glass beads	1668	Sun Chem. synthetic	15 000*	40
Kimber	1/8 of 5-spot	sand	2-4	Esso base oil	30	2450
Nasr[23]	1/8 of 5-spot	sand	240	Cold Lake	100 000	2170

* N/A, but estimated from other parameters

reservoir with a communicating bottom-water zone on oil recovery. Pursley[13] applied Pujol and Boberg's high-pressure scaling criteria to a study of the Cold Lake, Alberta oil sands. He studied the influence of pattern size, bottom water, a gas cap, reservoir heterogeneities, and steam quality on reservoir response. Ehrlich[14] also used Pujol and Boberg's scaling rules in his model of the Wabasca, Alberta, heavy oil field. He examined the effects of horizontal flow barriers and caustic as an additive to steam drives. The scaling groups made no allowance for the presence of caustic.

Niko and Troost[15] used low-pressure scaled models to study single-well cyclic steam stimulation processes. Their models represented one-sixth of a single well pattern, and a hydraulic analog was used to represent the fluid compressibilities. From the experiments they concluded that the production performance of a steam stimulated well was relatively insensitive to the injection rate and soak time over a wide range of values. Stimulated oil production was proportional to the drawdown, and the increase in productivity index was higher when the viscosity of the oil was higher.

Stegemeier et al.[8] developed a set of scaling criteria for vacuum models which has served as the basis for a number of steamflood studies. They studied a number of reservoirs, including the Peace River reservoir, using this approach. Prats[16] applied these scaling rules to a model of Peace River tar sand. He found the vacuum pressures suitable for simulating the vaporization phenomena associated with pressure blowdown in the pressure cycling process. Proctor[17] investigated various aspects

of steamflooding the thin Aberfeldy oil reservoir of the Lloydminster, Alberta area using the criteria developed by Stegemeier et al. Sufi[18] used low-pressure scaled models to study enhancement of injectivity for a tar sand reservoir. He found that injectivity could be improved by using a hot waterflood for a period of time prior to the commencement of a steamflood. Singhal,[19] using similar criteria but scaling mobility rather than permeability, modelled a seven-spot pattern of Lloydminster type heavy oil. Doscher[20] and co-workers developed scaling criteria for vacuum models similar to those of Stegemeier et al.; however, they were based on the integral form of the thermal energy balance over the steam zone as developed by Yortsos.[21] Doscher's model used the Kern River, California reservoir as its prototype. Butler and Chung[22] developed two-dimensional scaled reservoir models to test the steam-assisted gravity drainage theory. They found approximate agreement with numerical predictions for recovery from the AOSTRA Underground Test Facility.

In order to study steam processes in which additives might be used to improve the process, high-pressure models in which the same fluids, under similar conditions of pressure and temperature, are required. Some phenomena, such as the irreducible saturations or the relative permeabilities, may be scaled better if the same porous medium as is found in the prototype could be used in the model. None of the high or low-pressure scaling approaches discussed allow similar conditions of pressure or the same porous medium to be used in the model. Approaches which would permit their use and furthermore provide the scaling requirements for steam additives are desirable.

4. PRESENTATION AND DISCUSSION OF THEORETICAL DEVELOPMENT

To date, there has been no rigorous presentation of the scaling requirements for a steam-plus-additive process. Pursley[13] generated a partially scaled model of the process in which he simply added solvent to his steamflood model. Kennedy and Crawford[24] presented a non-rigorous set of criteria which treated the process as a steam recovery process plus a miscible drive process. They concluded that scaling of the combined steam and solvent processes could not be achieved as the scaling requirements for the flow rate in the steam recovery process contradicted the scaling requirements for the flow rate in the miscible drive process. Scaling of the process is possible, and using a rigorous approach, the scaling requirements are developed in this chapter.

4.1 ADDITIONAL MECHANISMS TO BE CONSIDERED FOR STEAM-PLUS-ADDITIVE PROCESSES

4.1.1 Dispersion

A number of mechanisms may be important in the steam-plus-additive process. One of the least understood is dispersion. Pozzi and Blackwell[25] studied the scaling of isothermal miscible displacements. They determined that under specified conditions, the requirements of geometric similarity and gravitational scaling can be relaxed to allow scaling of miscible displacements whether transverse mixing is by molecular diffusion or by convective dispersion. In a scaled study of immiscible carbon dioxide displacement of heavy oil in a very thin reservoir,

Rojas[28] found very little dependence of CO_2 or brine breakthrough recoveries on scaled displacements having superficial velocities above 1 m/d. He also found that breakthrough recoveries depended very little on the transverse dispersion group, $(D_T L/W^2 v)$, provided it was less than 0.0004 or on the longitudinal dispersion group, $(D_T L/D_L W)$, provided it was less than 0.3 (see Nomenclature for a definition of the terms).

In the past, several models for expressing the dispersion tensor in terms of macroscopic variables representing the microscopic configuration of the phase under consideration and the velocity field have been suggested. Bear and Bachmat[27] showed that for isotropic media where an orthonormal coordinate system parallel to the flow is selected, the dispersion tensor becomes

$$\bar{D} = \begin{pmatrix} D_L & 0 & 0 \\ 0 & D_T & 0 \\ 0 & 0 & D_T \end{pmatrix} .$$

An isotropic media will be assumed in this study, and therefore, this model is appropriate for use in this work.

4.1.2 Stability of Steam Fronts

The phenomenon of the stability of one fluid displacing another has been investigated by Chuoke et al.[28], Saffman and Taylor,[29] Miller,[30] Bentsen,[31] and many others. Criteria for determining the stability of a system are available. Bentsen[31] suggested that displacements may be divided, by means of an instability number, into three types: 1) a stable region in which the displacement is stable and the recovery is independent of the instability number, 2) a pseudostable region in which

the recovery is again independent of the instability number but displacement efficiencies are much lower, and 3) a transition region in which recovery efficiency is dependent on the instability number. In order to scale this phenomenon, both the prototype and the model should be in the stable region, the pseudostable region, or have the same value for the instability number.

This phenomenon may not be as important for steam injection processes as for waterflooding processes. Steam is not as conducive to the formation and growth of viscous fingers. In simple terms, small steam fingers, if formed, tend to lose heat at a relatively rapid rate, resulting in condensation and disappearance of the steam and thus, the finger. Miller[38] has presented a stability analysis of steam displacing water. He concluded that heat transfer from the hot fluid, as well as condensation of the injected fluid, would tend to have a stabilizing influence on the displacement. A more general analysis of this problem which allowed for the description of a dynamic interface, was provided by de la Cruz et al.[32] They showed that the increased stability is due to a trade-off between the stabilizing effect of phase change, which increases with steam velocity, and the destabilizing effect of mobility which will increase as well.

A common reservoir engineering parameter used as a measure of the stability of a displacement front in the absence of capillary and gravity forces is the ratio of the pressure gradient, $\partial p/\partial n$, normal to and on the downstream side of the displacement front to that on the

upstream side. Based on this concept, Prats[33] defines an equivalent mobility ratio for steam drives as:

$$M_{eq} = \left(\frac{v_w \mu_w}{k_{rw}}\right)_d \left(\frac{k_{rst}}{v_{st}\mu_{st}}\right)_u .$$

Combarnous and Sourieau[34] evaluated the quantity, $(v_{st}\mu_{st})/(v_w\mu_w)$, for piston-like displacement of water by steam and found that displacement by saturated steam is stable for temperatures up to 190°C and that superheated steam leads to even more stable displacements. Inclusion of the saturation distributions upstream and downstream of the displacement front would expand the temperature range over which the equivalent mobility ratio is favourable. However, in the case of steam displacing a very viscous oil, conditions under which steam channelling might occur are encountered.

4.1.3 Non-equilibrium Mass Transfer

Laboratory experiments are conducted on a shorter time scale than field projects. Consequently, it is possible for non-equilibrium phenomena to be significant in the experiments but to be insignificant in the field. Non-equilibrium effects, such as diffusive mass transfer of components within a phase, are often described using a relationship such as Fick's equation. When mass transfer occurs between one phase and another, the description of the process may be more complex. This description may include such complex phenomena as interfacial turbulence, spontaneous emulsification, and interfacial accumulation. Hirasaki[35] describes these phenomena, and states conditions under which they may be significant. The more complex situations are normally described using mass transfer coefficients, which account for both the diffusive mass

transfer within each phase and the interfacial mass transfer. Scaling groups derived using equations which describe diffusive mass transfer will identify the conditions necessary to scale diffusion controlled mass transfer. For situations when interfacial mass transfer dominates the non-equilibrium effects a more suitable description may be required in order to obtain the scaling requirements necessary to scale this mechanism.

4.2 DERIVATION OF SCALING GROUPS

A set of scaling groups for the steam-plus-additive process can be derived using either dimensional and/or inspectional analyses. Dimensional analysis requires knowledge of the complete set of relevant variables influencing the process. Inspectional analysis requires the variables in a set of equations which fully describe the process. Dimensional analysis often yields a more complete set of similarity groups, but the physical meaning of the similarity groups themselves is generally more apparent from inspectional analysis. Usually some scaling requirements must be relaxed. For this reason, inspectional analysis is often preferred. Dimensional analysis is usually used in conjunction with inspectional analysis to ensure that important groups are not omitted. Geertsma et al.[4] described these techniques in detail.

4.2.1 Inspectional Analysis

In order to derive the scaling groups by inspectional analysis, the governing partial differential equations, initial and boundary conditions, constitutive relationships, and constraints were formulated.

These were then rewritten in terms of the dimensionless variables and their reference quantities and the various similarity groups were identified.

The porous medium was assumed to be homogeneous and isotropic in the formulation of the governing partial differential equations. This was necessary as the macroscopic flow equations may not apply to heterogeneous systems and scaling at the macroscopic level may not apply at the megascopic level. The process was treated as three-phase flow (oleic, aqueous, gaseous). Mass transfer was assumed to result from diffusion, convection, and dispersion. There is mass transfer of the additive within the oleic phase and within the gaseous phase. Oil was assumed to exist in the oleic phase only, while water was assumed to be present in the gaseous or aqueous phases. Darcy's, Fourier's, and Fick's equations were assumed to be valid. The system was assumed to be in local thermodynamic equilibrium. Rock compressibility and thermal expansion were assumed to be negligible effects. The kinetic, potential and viscous dissipation energies were assumed to be negligible compared to thermal energy, which may be transported by convection or conduction. This led to the following governing equations.

Mass Balance of Oil

$$\frac{\partial}{\partial t}(\phi S_o C_{oo} \rho_o) = \nabla \cdot \left(C_{oo} \frac{\rho_o \bar{k}_o}{\mu_o} \cdot (\nabla p_o + \rho_o g \nabla Z) + \phi S_o (\bar{D}_o + \bar{D}^*_{oo}) \cdot \nabla (C_{oo} \rho_o)\right) \quad \ldots\ldots\ldots (1)$$

Mass Balance of an Additive

$$\frac{\partial}{\partial t}(\phi S_o C_{oo} \rho_o + \phi S_g C_{go} \rho_g) = \nabla \cdot \left(C_{oo} \frac{\rho_o \bar{k}_o}{\mu_o} \cdot (\nabla p_o + \rho_o g \nabla Z) + C_{go} \frac{\rho_g \bar{k}_g}{\mu_g} \cdot (\nabla p_g + \rho_g g \nabla Z)\right)$$
$$+ \nabla \cdot \left(\phi S_o (\bar{D}_o + \bar{D}^*_{oo}) \cdot \nabla (C_{oo} \rho_o) + \phi S_g (\bar{D}_g + \bar{D}^*_{go}) \cdot \nabla (C_{go} \rho_g)\right) \quad \ldots\ldots (2)$$

Mass Balance of Water

$$\frac{\partial}{\partial t}(\phi S_g C_{gw}\rho_g + \phi S_w \rho_w) = \nabla\cdot\left(C_{gw}\frac{\rho_g \bar{k}_g}{\mu_g}\cdot(\nabla p_g + \rho_g g\nabla Z) + \frac{\rho_w \bar{k}_w}{\mu_w}\cdot(\nabla p_w + \rho_w g\nabla Z)\right)$$
$$+ \nabla\cdot(\phi S_g(\bar{D}_g + \bar{D}^*_{gw})\cdot\nabla(C_{gw}\rho_g)) \quad \ldots\ldots(3)$$

Energy Balance

$$\phi\frac{\partial}{\partial t}(\rho_g S_g U_g + \rho_w S_w U_w + \rho_o S_o U_o) + (1-\phi)\rho_r\frac{\partial U_r}{\partial t} = \nabla\cdot(k_{hr}\nabla T)$$
$$+ \nabla\cdot\left(\frac{\rho_g h_g \bar{k}_g}{\mu_g}\cdot(\nabla p_g + \rho_g g\nabla Z) + \frac{\rho_w h_w \bar{k}_w}{\mu_w}\cdot(\nabla p_w + \rho_w g\nabla Z) + \frac{\rho_o h_o \bar{k}_o}{\mu_o}\cdot(\nabla p_o + \rho_o g\nabla Z)\right) \ldots\ldots(4)$$

These four equations represent the conservation of mass and energy. They contain 110 variables and thus require additional constitutive equations and constraints together with the appropriate initial and boundary conditions to complete a well-posed problem. Table 2 lists the constitutive relationships and constraints and Appendix A shows a possible set of boundary conditions.

Each variable or property can be written in dimensionless form by dividing it by some characteristic reference quantity. For example, for the general property M, $M_D = M/M_R$, where M_D is the dimensionless form of the property M, and M_R is some constant characteristic reference quantity. By substituting $M_R M_D$ for M in the partial differential equations, the set of equations take the form shown in Table 3 for the mass balance of oil. Appendix C lists the dimensionless mass balances for the other components as well as for the energy balance. Note that a Cartesian coordinate system of x_1, x_2, x_3 has been used, where x_2 represents the vertical coordinate. The reference quantities in the square

Table 2. Constitutive relationships and constraints.

1) $S_g + S_o + S_w = 1$

2) $C_{oo} + C_{os} = 1$

3) $C_{gs} + C_{gw} = 1$

4) $\rho_o = \rho_o(p_o, T, C_{os})$

5) $\rho_g = \rho_g(p_g, T, C_{gs})$

6) $\rho_w = \rho_w(p_w, T)$

7) $\mu_o = \mu_o(p_o, T, C_{os})$

8) $\mu_g = \mu_g(p_g, T, C_{gs})$

9) $\mu_w = \mu_w(p_w, T)$

10) $C_{gw} = K_{wgw}(p, T, C_{gw})$

11) $C_{gs}/C_{os} = K_{sgo}(p, T, C_{gs}, C_{os})$

12) $p_g = P_{cgo}(S_g, S_o, S_w) + p_o$

13) $p_w = p_o - P_{cow}(S_g, S_o, S_w)$

14) ϕ = constant

15) g = constant

16) ρ_r = constant

17-25) $\bar{k}_o = \bar{k}_o(S_g, S_o, S_w, k)$

26-34) $\bar{k}_g = \bar{k}_g(S_g, S_o, S_w, k)$

35-43) $\bar{k}_w = \bar{k}_w(S_g, S_o, S_w, k)$

44-61) $\bar{D}_o + \bar{D}^*_{oo} = \bar{D}_{oo}(D_{Loo}, D_{Too})$

62-70) $\bar{D}_o + \bar{D}^*_{os} = \bar{D}_{os}(D_{Los}, D_{Tos})$

71-88) $\bar{D}_g + \bar{D}^*_{gs} = \bar{D}_{gs}(D_{Lgs}, D_{Tgs})$

89-97) $\bar{D}_g + \bar{D}^*_{gw} = \bar{D}_{gw}(D_{Lgw}, D_{Tgw})$

98) $h_g = h_g(p, T, C_{gw})$

99) $h_w = h_w(p, T)$

100) $h_o = h_o(p, T, C_{os})$

101) $U_r = U_r(T)$

102) $U_g = h_g - P_g/\rho_g$

103) $U_w = h_w - P_w/\rho_w$

104) $U_o = h_o - P_o/\rho_o$

105) $k_{hr} = k_{hr}(T)$

106) $z = z(x_1, x_2, x_3)$

Table 3. Mass balance for oil in terms of the dimensionless variables and their reference quantities.

$$\left[\frac{\phi_R S_{oR} C_{ooR} \rho_{oR}}{t_R}\right] \frac{\partial}{\partial t_D} \left(\phi_D S_{oD} C_{ooD} \rho_{oD}\right) = \left[\frac{C_{ooR} \rho_{oR} k_{oR} p_{oR}}{x_{1R}^2 \mu_{oR}}\right] \frac{\partial}{\partial x_{1D}} \left(\frac{C_{ooD} \rho_{oD} k_{oD}}{\mu_{oD}} \frac{\partial p_{oD}}{\partial x_{1D}}\right)$$

$$+ \left[\frac{C_{ooR} \rho_{oR}^2 k_{oR} g_R z_R}{\mu_{oR} x_{1R}^2}\right] \frac{\partial}{\partial x_{1D}} \left(\frac{C_{ooD} \rho_{oD}^2 k_{oD} g_D}{\mu_{oD}} \frac{\partial z_D}{\partial x_{1D}}\right) + \left[\frac{C_{ooR} \rho_{oR} k_{oR} p_{oR}}{x_{2R}^2 \mu_{oR}}\right] \frac{\partial}{\partial x_{2D}}$$

$$\left(\frac{C_{ooD} \rho_{oD} k_{oD}}{\mu_{oD}} \frac{\partial p_{oD}}{\partial x_{2D}}\right) + \left[\frac{C_{ooR} \rho_{oR}^2 k_{oR} g_R z_R}{\mu_{oR} x_{2R}^2}\right] \frac{\partial}{\partial x_{2D}} \left(\frac{C_{ooD} \rho_{oD}^2 k_{oD} g_D}{\mu_{oD}} \frac{\partial z_D}{\partial x_{2D}}\right)$$

$$+ \left[\frac{C_{ooR} \rho_{oR} k_{oR} p_{oR}}{x_{3R}^2 \mu_{oR}}\right] \frac{\partial}{\partial x_{3D}} \left(\frac{C_{ooD} \rho_{oD} k_{oD}}{\mu_{oD}} \frac{\partial p_{oD}}{\partial x_{3D}}\right) + \left[\frac{C_{ooR} \rho_{oR}^2 k_{oR} g_R z_R}{\mu_{oR} x_{3R}^2}\right] \frac{\partial}{\partial x_{3D}}$$

$$\left(\frac{C_{ooD} \rho_{oD}^2 k_{oD} g_D}{\mu_{oD}} \frac{\partial z_D}{\partial x_{3D}}\right) + \left[\frac{\phi_R S_{oR}^D L_{ooR} C_{ooR} \rho_{oR}}{x_{1R}^2}\right] \frac{\partial}{\partial x_{1D}} \left(\phi_D S_{oD}^D L_{ooD} \frac{\partial}{\partial x_{1D}} \left(C_{ooD} \rho_{oD}\right)\right)$$

$$+ \left[\frac{\phi_R S_{oR}^D T_{ooR} C_{ooR} \rho_{oR}}{x_{2R}^2}\right] \frac{\partial}{\partial x_{2D}} \left(\phi_D S_{oD}^D T_{ooD} \frac{\partial}{\partial x_{2D}} \left(C_{ooD} \rho_{oD}\right)\right)$$

$$+ \left[\frac{\phi_R S_{oR}^D T_{ooR} C_{ooR} \rho_{oR}}{x_{3R}^2}\right] \frac{\partial}{\partial x_{3D}} \left(\phi_D S_{oD}^D T_{ooD} \frac{\partial}{\partial x_{3D}} \left(C_{ooD} \rho_{oD}\right)\right)$$

brackets represent the coefficient for that term in the equation. All coefficients have the same dimensions. Similarity groups are determined by dividing the entire equation by one of these coefficients. This yields the dimensionless forms of the equations and their similarity groups or dimensionless coefficients. The dimensionless forms of the other governing equations are obtained in a similar manner. Stegemeier et al.[8] provide a good account of this procedure. The set thus produced may be replaced by any other set obtained from the products of the groups and any other group raised to any power. This allows for some simplification and leads to the similarity groups listed in Table 4.

In practice, certain simplifying assumptions must be made in order to reduce the similarity groups to a set of scaling criteria. It is more straightforward and less confusing to omit the mechanisms assumed to be insignificant from the equations in the form shown in Table 3 and rederive the similarity groups, than it is to simplify the similarity groups listed in Table 4 based on these assumptions. This is the purpose of representing the equations in the long notation shown in Table 3. In addition to the partial differential equations, constraints, initial conditions, and boundary conditions, the constitutive relationships in dimensionless form must be the same for the model and the prototype. Table 5 lists those required.

4.2.2 Dimensional Analysis

The similarity groups may also be derived using dimensional analysis. After the relevant variables for the process are selected, the similar-

Table 4. Similarity groups from inspectional analysis.

$$\frac{H}{L}, \frac{W}{L}, \frac{\rho_{oR} g_R Z_R}{p_{oR}}, \frac{k_{oR} \rho_{oR} h_{oR} p_{oR}}{\mu_{oR} k_{hrR} T_R}, \frac{\rho_{rR} U_{rR}}{\rho_{wR} h_{wR}}, \frac{h_{oR}}{h_{wR}}, \frac{h_{gR}}{h_{wR}}, \frac{\mu_{oR} k_{gR}}{\mu_{gR} k_{oR}}, \frac{\mu_{oR} k_{wR}}{\mu_{wR} k_{oR}}$$

$$\frac{w_{wwR} \mu_{wR}}{\rho_{wR} k_{wR} p_{wR} L}, \frac{w_{owR}}{w_{wwR}}, \frac{w_{gwR}}{w_{wwR}}, \frac{w_{gsR}}{w_{wwR}}, \phi_R, \frac{\alpha_{cR}}{\alpha_{rR}}, \frac{S_{wiR}}{S_{wR}}, \frac{S_{giR}}{S_{wR}}, \frac{T_{iR}}{T_R}, \frac{p_{oiR}}{p_{oR}}$$

$$\frac{p_{pwR}}{p_{oR}}, \frac{p_{gR}}{p_{wR}}, \frac{p_{oR}}{p_{wR}}, \frac{p_{cgoR}}{p_{wR}}, \frac{p_{cowR}}{p_{wR}}, \frac{A_{iwR}}{L^2}, \frac{S_{oR}}{S_{wR}}, \frac{S_{gR}}{S_{wR}}, \frac{\rho_{oR}}{\rho_{wR}}, \frac{\rho_{gR}}{\rho_{wR}}, \frac{Z_R}{L}$$

$$\frac{\mu_{oR} D_{LosR}}{k_{oR} p_{oR}}, \frac{D_{LooR}}{D_{LosR}}, \frac{D_{LgsR}}{D_{LosR}}, \frac{D_{LgwR}}{D_{LosR}}, \frac{D_{TooR}}{D_{LosR}}, \frac{D_{TgsR}}{D_{LosR}}, \frac{D_{TgwR}}{D_{LosR}}, \frac{D_{TosR}}{D_{LosR}}$$

Table 5. Dimensionless properties and conditions to be satisfied.

$T_{satD}(P_{satD})$

ρ_{iD} (p_D, T_D, C) i = o, w, g

$k_{iD}(S_{oD}, S_{wD}, S_{gD})$ i = o, w, g

$\mu_{iD}(T_D)$ i = o, w, g

P_{coiD} $(S_{iD}, \rho_i, \sigma_i, k)$ i = g, w

$z_D(x_{1D}, x_{2D}, x_{3D})$

$D_{LiD}(D_i^*, F, \phi, v, \sigma, d_p)$ i = os, gs, oo, gw

$D_{TiD}(D_i^*, F, \phi, v, \sigma, d_p)$ i = os, gs, oo, gw

$h_{iD}(p_D, T_D, c)$ i = o, w, g

$K_{iD}(p_D, T_D, C)$ i = wgw, sgo

ity groups can be determined using the Buckingham π-theorem. Loomis and Crowell[36] provide a good account of this procedure. The symbols, dimensions, and a description of the variables selected are listed in Table 6. The similarity groups derived by this method are shown in Table 7.

Using this approach, a few new groups which did not appear while using inspectional analysis have been introduced. The reason for this is that some of these variables were not considered in the formulation of the governing equations. New groups include the Reynolds number, $(\rho v k^{1/2}/\mu)$, which relates viscous to inertial forces, and the ratio, k/L^2, which relates pore diameter to the overall dimensions. Inertial effects may not be important for cases of practical interest. Therefore, their scaling requirements are usually relaxed. The group, $\sigma/P_c k^{1/2}$, which scales capillary forces, did not appear explicitly by inspectional analysis, but the requirement that the dimensionless capillary pressures be the same functions of their dimensionless variables in the models as they are in the field implies that this group or a similar one be satisfied.

4.3 APPROACHES TO SATISFYING THE SCALING CRITERIA

The similarity groups derived in the previous sections represent the complete set of scaling criteria which must be satisfied in order to scale the process as defined by the governing equations, constitutive relationships, constraints, and conditions. This set of criteria is very difficult to satisfy, and consequently, some of the scaling

Table 6. Variables for dimensional analysis.

Symbol	Dimensions	Description
l	L	well spacing
h	L	thickness of system
w	L	width of system
ρ_w	M/L^3	density of aqueous phase
ρ_g	M/L^3	density of gas phase
ρ_o	M/L^3	density of oleic phase
ρ_r	M/L^3	density of reservoir rock
g	L/t^2	acceleration due to gravity
p_w	M/Lt^2	pressure of aqueous phase
p_g	M/Lt^2	pressure of gas phase
p_o	M/Lt^2	pressure of oleic phase
h_w	L^2/t^2	enthalpy of aqueous phase
h_g	L^2/t^2	enthalpy of gas phase
h_o	L^2/t^2	enthalpy of oleic phase
U_r	L^2/t^2	internal energy of reservoir rock
k_w	L^2	effective permeability to the aqueous phase
k_o	L^2	effective permeability to the oleic phase
k_g	L^2	effective permeability to the gas phase
μ_w	M/Lt	viscosity of aqueous phase
μ_o	M/Lt	viscosity of oleic phase
μ_g	M/Lt	viscosity of gas phase
k_{hr}	ML/Tt^3	thermal conductivity of the reservoir
T	T	temperature
ϕ		porosity
D_{Loa}	L^2/t	longitudinal dispersion of additive into the oleic phase
D_{Toa}	L^2/t	transverse dispersion of additive into the oleic phase
D_{Lga}	L^2/t	longitudinal dispersion of additive into the gas phase
D_{Tga}	L^2/t	transverse dispersion of additive into the gas phase
D_{Loo}	L^2/t	longitudinal dispersion of oil into the oleic phase
D_{Too}	L^2/t	transverse dispersion of oil into the oleic phase
D_{Lgw}	L^2/t	longitudinal dispersion of water into the gas phase
D_{Tgw}	L^2/t	transverse dispersion of water into the gas phase

Table 6. (continued)

Symbol	Dimensions	Description
P_{cgo}	M/Lt^2	gas-oil capillary pressure
P_{cow}	M/Lt^2	oil-water capillary pressure
W_{ww}	M/t	injection rate of water
W_{gw}	M/t	injection rate of water in the gas phase
W_{gs}	M/t	injection rate of additive in the gas phase
W_{os}	M/t	injection rate of additive in the oleic phase
σ_{go}	M/t^2	interfacial tension between the gas and oleic phases
σ_{ow}	M/t^2	interfacial tension between the oleic and aqueous phases
v	L/t	superficial velocity

Table 7. Similarity groups from dimensional analysis.

Scaling Group	Description
(H/L)	geometric factor
(W/L)	geometric factor
$(\rho_w g H/p_w)$	ratio of gravitational to viscous forces
(p_g/p_w)	ratio of gas and aqueous phase pressures
(p_o/p_w)	ratio of oleic and aqueous phase pressures
$(\rho_w h_w k_w p_w/\mu_w k_{hr} T)$	ratio of convective to conductive heat transfer
$(\rho_r U_r/\rho_w h_w)$	ratio of energy stored in reservoir to that stored in aqueous phase
(ρ_g/ρ_w)	ratio of gas and aqueous phase densities
(ρ_o/ρ_w)	ratio of oleic and aqueous phase densities
(ρ_r/ρ_w)	ratio of reservoir and aqueous phase densities
(h_g/h_w)	ratio of gas and aqueous phase enthalpies
(h_o/h_w)	ratio of oleic and aqueous phase enthalpies
ϕ	porosity factor
(μ_g/μ_w)	ratio of gas and aqueous phase viscosities
(μ_o/μ_w)	ratio of oleic and aqueous phase viscosities
$(k_g\mu_w/\mu_g k_w)$	ratio of gas and aqueous phase viscous forces
$(k_o\mu_w/\mu_o k_w)$	ratio of oleic and aqueous phase viscous forces
$(\phi D_{Low}\mu/k_o p_o)$	ratio of dispersive forces to viscous forces
(D_{Tos}/D_{Los})	ratio of transverse and longitudinal dispersion of additive in oil
(D_{Lgs}/D_{Los})	ratio of longitudinal dispersion of additive in the gas and oleic phases
(D_{Tgs}/D_{Los})	ratio of transverse dispersion of additive in gas phase to longitudinal dispersion of additive in oleic phase
(D_{Loo}/D_{Los})	ratio of longitudinal dispersion of oil in oleic phase to longitudinal dispersion of additive in oleic phase
(D_{Lgs}/D_{Los})	ratio of longitudinal dispersion of water in gas phase to longitudinal dispersion of additive in oleic phase
(D_{Too}/D_{Los})	ratio of transverse dispersion of oil in oleic phase to longitudinal dispersion of additive in oleic phase
(D_{Tgw}/D_{Los})	ratio of transverse dispersion of water in gas phase to longitudinal dispersion of additive in oleic phase
(P_{cgo}/p_w)	ratio of gas-oil capillary pressure to aqueous phase pressure

Table 7. (continued)

Scaling Group	Description
(P_{cow}/p_w)	ratio of water-oil capillary pressure to aqueous phase pressure
$(W_{ww}h_w/k_{hr}TL)$	ratio of injected energy to conductive heat transfer
$(W_{ww}\mu_w/\rho_w k_w L p_w)$	ratio of injection rate to viscous forces
(W_{gw}/W_{ww})	ratio of steam and water injection rates
(W_{gs}/W_{ww})	ratio of gaseous additive and water injection rates
(W_{os}/W_{ww})	ratio of liquid additive and water injection rates
$(\rho_w v\phi L^2/W_{ww})$	relates injection rate and superficial velocity
$(\rho_w v k^{1/2}/\mu_w)$	Reynolds Number for water
(k/L^2)	ratio of permeability to system dimensions
$(\sigma_{ow}/P_{cow}\ k^{1/2})$	ratio of capillary to viscous forces
$(\sigma_{go}/\sigma_{ow})$	ratio of gas-oil interfacial tension to oil-water interfacial tension

requirements must be relaxed. A number of subsets of this complete set can be identified, depending on which scaling requirements are relaxed. Limiting the subsets to those that use the same fluids in the model as are found in the prototype, five approaches for high-pressure models were developed. These are illustrated in Figure 1. Approach #1 was first developed by Pujol and Boberg[9] and has been used by a number of investigators in the past.

4.3.1 Approach #1 - Same Fluids, Different Porous Media, Different Pressure Drop, Geometric Similarity

In order to satisfy the groups that scale geometry, viscous forces and gravitational forces, the pressure drop in the model must be different from that in the prototype. This requires a different porous medium. Approach #1, which was proposed by Pujol and Boberg,[9] allows these scaling requirements to be met but violates some of the requirements of the constitutive relationships, constraints, and boundary conditions. For example, the pressure-temperature relationship for saturated steam cannot be scaled using this method. This leads to an improper match of the boundary conditions for temperature and poor scaling of heat losses from the steam zone. Steam density and other properties which depend on pressure cannot be scaled properly either. The effects of dispersion and capillary forces are not scaled. As a result of the different porous media, the irreducible saturations and the relative permeability may not be scaled adequately.

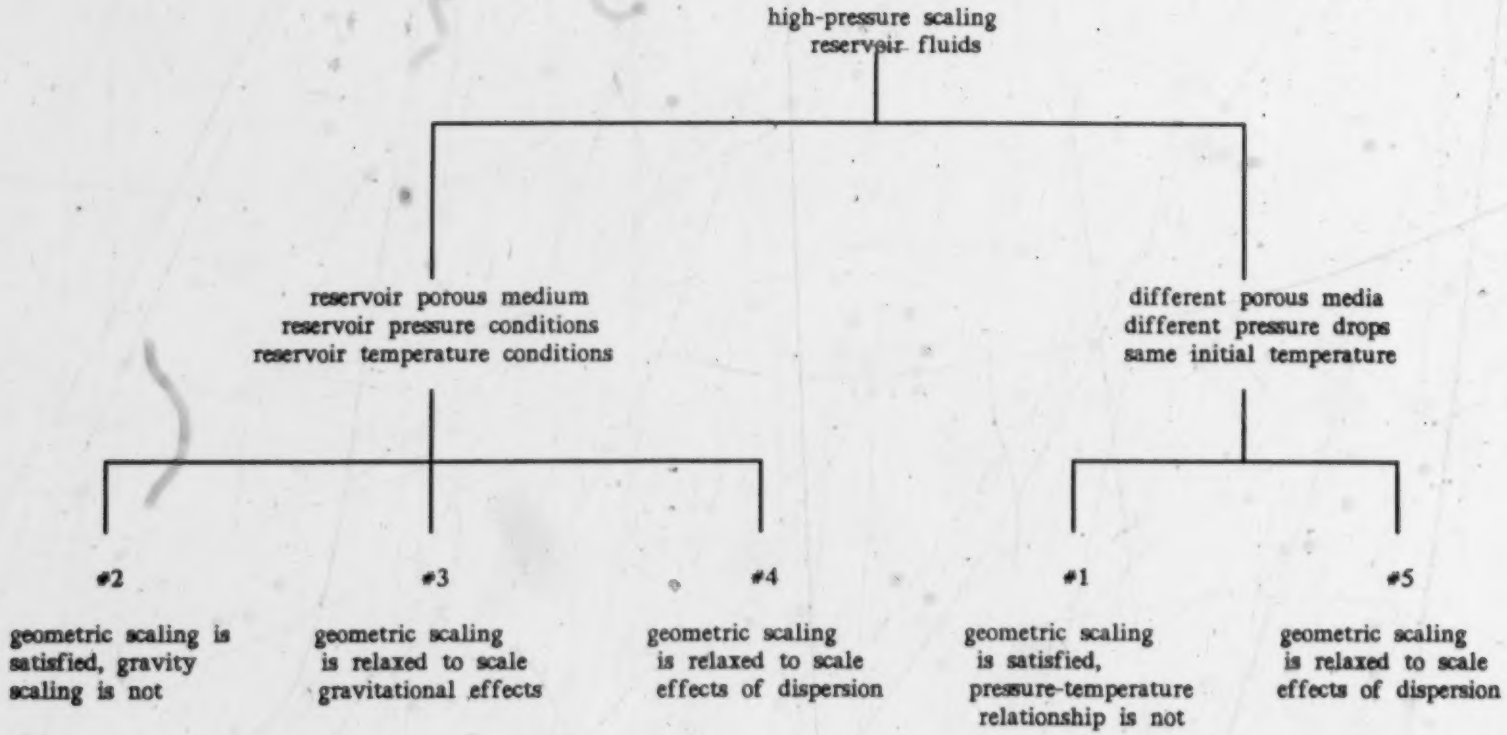

Figure 1. A brief description of the five high-pressure scaling techniques examined in this study.

The relaxed requirements for this approach are listed below. Their detailed development is similar to that given in Appendix B.

Scaling Groups: Approach #1

$$\frac{H}{L}, \frac{W}{L}, \frac{k_{oR}\rho_{oR}h_{oR}p_{oR}}{\mu_{oR}k_{hrR}T_R}, \frac{\rho_{rR}U_{rR}}{\rho_{wR}h_{wR}}, \frac{h_{oR}}{h_{wR}}, \frac{h_{gR}}{h_{wR}}, \frac{\mu_{oR}k_{gR}}{\mu_{gR}k_{oR}}, \frac{\mu_{oR}k_{wR}}{\mu_{wR}k_{oR}}, \frac{w_{osR}}{w_{wsR}}, \frac{w_{gwR}}{w_{wsR}}, \frac{w_{gsR}}{w_{wsR}}, \phi_R, \frac{\alpha_{cR}}{\alpha_{rR}}$$

$$\frac{S_{wiR}}{S_{wR}}, \frac{S_{giR}}{S_{wR}}, \frac{T_{iR}}{T_R}, \frac{\rho_{oR}}{\rho_{wR}}, \frac{\rho_{gR}}{\rho_{wR}}, \frac{\rho_{oR}g_RL}{p_{oR}}, \frac{w_{wsR}\mu_{wR}}{\rho_{wR}k_{wR}p_{wR}L}, \frac{A_{iwR}}{L^2}, \frac{S_{oR}\mu_{oR}D^*_{ooR}}{k_{oR}p_{oR}F_R}, \frac{D^*_{ooR}}{D^*_{oosR}}, \frac{D^*_{gsR}}{D^*_{oosR}}, \frac{D^*_{gwR}}{D^*_{oosR}}$$

In addition to these requirements, all of the dimensionless properties must be the same functions of their dimensionless variables for the prototype and the model. The implications of these scaling criteria for a model reduced in length by a scaling factor of "a" and employing the same fluids as the prototype are: 1) α_c, ϕ, S_{wi}, S_{gi}, F, T_i, ΔT_{max} must remain the same; 2) H, W, Δp_{max}, W_{ww}, W_{os}, W_{gw}, W_{gs} must be reduced by "a"; 3) k must be increased by "a"; and thus 4) t will be reduced by "a^2." This approach is suitable for steam-only processes, particularly if gravitational effects are very important. Additives may not be scaled properly using this approach as their PVT relationships will not be scaled.

4.3.2 Approach #2 - Same Fluids, Same Porous Medium, Same Pressure Drop, Geometric Similarity

To overcome some of the difficulties identified in Approach #1, the initial pressure and temperature as well as the maximum pressure and temperature change must be the same in the model as in the prototype. This would allow the properties which depend on pressure to be more

accurately scaled. In addition, using the same porous medium would allow better scaling of the irreducible saturations and the relative permeabilities. These changes would permit the effects of diffusion, the viscous forces, and heat transfer to be properly scaled while maintaining geometric similarity. Gravitational forces would not be scaled properly using this approach. In processes dominated by gravitational effects this will be a serious limitation. The effects of dispersion at high flow rates may not be scaled properly either.

The relaxed requirements for this approach are listed below. The method of development of this set of criteria is given in Appendix B.

Scaling Groups: Approach #2

$$\frac{H}{L}, \frac{W}{L}, \frac{k_{oR}\rho_{oR}h_{oR}p_{oR}}{\mu_{oR}k_{hrR}T_R}, \frac{\rho_{rR}U_{rR}}{\rho_{wR}h_{wR}}, \frac{h_{oR}}{h_{wR}}, \frac{h_{gR}}{h_{wR}}, \frac{\mu_{oR}k_{gR}}{\mu_{gR}k_{oR}}, \frac{\mu_{oR}k_{wR}}{\mu_{wR}k_{oR}}, \frac{\rho_{oR}}{\rho_{wR}}, \frac{\rho_{gR}}{\rho_{wR}}, \frac{w_{osR}}{w_{wwR}}, \frac{w_{gwR}}{w_{wwR}}, \frac{w_{gsR}}{w_{wwR}}, \phi_R$$

$$\frac{\alpha_{cR}}{\alpha_{rR}}, \frac{S_{wiR}}{S_{wR}}, \frac{S_{giR}}{S_{wR}}, \frac{T_{iR}}{T_R}, \frac{p_{iR}}{p_{oR}}, \frac{p_{pwR}}{p_{oR}}, \frac{w_{wwR}\mu_{wR}}{\rho_{wR}k_{wR}p_{wR}L}, \frac{A_{iwR}}{L^2}, \frac{S_{oR}\mu_{oR}D^*_{ooR}}{k_{oR}p_{oR}F_R}, \frac{D^*_{ooR}}{D^*_{osR}}, \frac{D^*_{gsR}}{D^*_{osR}}, \frac{D^*_{gwR}}{D^*_{osR}}$$

In addition to these requirements, all of the dimensionless properties must be the same functions of their dimensionless variables for the prototype and the model. The implications of these scaling criteria for a model reduced in length by a scaling factor of "a" and employing the same fluids as the prototype are: 1) α_c, Δp_{max}, p_i, p_{pw}, ΔT_{max}, T_i, k, ϕ, S_{wi}, S_{gi}, F must remain the same; 2) H, W, W_{ww}, W_{os}, W_{gw}, W_{gs} must be reduced by "a"; and thus 3) t will be reduced by "a^2." This approach is suitable for steam and steam-plus-additive processes. It is restricted to processes in which gravitational effects may not be important, such as high injection rates in thin formations. The PVT relationships for steam and additives as well as diffusion within each phase will be scaled.

4.3.3 Approach #3 - Same Fluids, Same Porous Medium, Same Pressure Drop, Geometric Scaling Relaxed

In order to combine the advantages of using the same fluids, the same porous medium, and similar pressure and temperature conditions with proper scaling of the gravitational effects, some of the requirements of geometric similarity must be relaxed. If geometric similarity is relaxed and if the vertical pressure gradient due to viscous and capillary forces is small, the viscous and gravitational forces may be scaled for horizontal reservoirs. Heat conduction in the vertical direction, capillary forces, and the effects of dispersion may not be scaled adequately.

The relaxed requirements for this approach are listed below. The method of development of this set of scaling criteria is similar to that given in Appendix B for Approach #2. The most significant difference is the choice of the reference quantity for the vertical coordinate, x_2. It now becomes

$$x_{2R} = \rho_{oR}\, g_R\, L^2/p_{oR} \qquad (5)$$

Scaling Groups: Approach #3

$$\frac{W}{L},\ \frac{k_{oR}\rho_{oR}h_{oR}p_{oR}}{\mu_{oR}k_{hrR}T_R},\ \frac{\rho_{rR}U_{rR}}{\rho_{wR}h_{wR}},\ \frac{h_{oR}}{h_{wR}},\ \frac{h_{gR}}{h_{wR}},\ \frac{\mu_{oR}k_{gR}}{\mu_{gR}k_{oR}},\ \frac{\mu_{oR}k_{wR}}{\mu_{wR}k_{oR}},\ \frac{\rho_{oR}}{\rho_{wR}},\ \frac{\rho_{gR}}{\rho_{wR}},\ \frac{\alpha_{rR}}{\alpha_{rR}}$$

$$\frac{w_{osR}}{w_{wwR}},\ \frac{w_{gwR}}{w_{wwR}},\ \frac{w_{gsR}}{w_{wwR}},\ \phi_R,\ \frac{S_{wiR}}{S_{wR}},\ \frac{S_{giR}}{S_{wR}},\ \frac{T_{iR}}{T_R},\ \frac{p_{iR}}{p_{oR}},\ \frac{p_{pwR}}{p_{oR}},\ \frac{k_{hcR}T_RL}{w_{wwR}h_{wR}}$$

$$\frac{\rho_{oR}g_RL^2}{H\,p_{oR}},\ \frac{w_{wwR}\mu_{wR}}{\rho_{wR}^2k_{wR}g_RL^2},\ \frac{A_{iwR}p_{oR}}{L^3\rho_{oR}g_R},\ \frac{S_{oR}\mu_{oR}D^*_{ocoR}}{k_{oR}p_{oR}F_R},\ \frac{D^*_{ocR}}{D^*_{ocR}},\ \frac{D^*_{gcR}}{D^*_{ocR}},\ \frac{D^*_{gwR}}{D^*_{ocR}}$$

In addition to these requirements, all of the dimensionless properties must be the same functions of their dimensionless variables for the

prototype and the model. The implications of these scaling criteria for a model reduced in length by a scaling factor of "a" and employing the same fluids as the prototype are: 1) α_c, Δp_{max}, p_i, p_{pw}, ΔT_{max}, T_i, k, ϕ, S_{wi}, S_{gi}, F must remain the same; 2) k_{hc}, W must be reduced by "a"; 3) H, W_{ww}, W_{ow}, W_{gw}, W_{go} must be reduced by "a^2"; 4) the reservoir must be horizontal; and thus 5) t will be reduced by "a^2." This approach is suitable for steam and steam-plus-additive processes which require gravitational scaling, and is restricted to very thick formations because of the relatively large reduction in reservoir thickness.

4.3.4 Approach §4 - Same Fluids, Same Porous Medium, Same Pressure Drop, Geometric Scaling Relaxed

The effects of dispersion at high flow rates are not scaled by any of the previous approaches. These effects are very difficult to scale completely. The aim of Approach §4 is to scale processes dominated by transverse dispersion. The viscous and dispersive effects are balanced at the expense of improperly scaling gravitational or capillary effects. The advantages of satisfying the requirements of the relative permeabilities, irreducible saturations, and most of the dimensionless properties and boundary conditions are maintained. Considering the effects that must be relaxed to achieve more rigorous scaling of dispersion, the suitability of this approach for steam recovery processes is uncertain.

The relaxed requirements for this approach are listed below. The method of development of this set of scaling criteria is similar to that given in Appendix B for Approach §2. The most significant difference is the

choice of the reference quantity for the vertical coordinate, x_2. It now becomes

$$x_{2R} = (\phi_R S_{oR} \gamma_R d_{pR} L)^{1/2}. \qquad (6)$$

Scaling Groups: Approach #4

$$\frac{W}{L}, \frac{k_{oR}\rho_{oR}h_{oR}P_{oR}}{\mu_{oR}k_{hR}T_R}, \frac{\rho_{rR}U_{rR}}{\rho_{oR}h_{oR}}, \frac{h_{oR}}{h_{wR}}, \frac{h_{gR}}{h_{oR}}, \frac{\mu_{oR}k_{gR}}{\mu_{gR}k_{oR}}, \frac{\mu_{oR}k_{wR}}{\mu_{wR}k_{oR}}, \frac{\rho_{oR}}{\rho_{wR}}, \frac{\rho_{gR}}{\rho_{wR}}, \frac{a_{oR}}{a_{rR}}$$

$$\frac{w_{owR}}{w_{wwR}}, \frac{w_{gwR}}{w_{wwR}}, \frac{w_{goR}}{w_{woR}}, \frac{S_{wiR}}{S_{oR}}, \frac{S_{giR}}{S_{oR}}, \frac{T_{iR}}{T_R}, \frac{P_{iR}}{P_{oR}}, \frac{P_{pwR}}{P_{oR}}, \frac{k_{hoR}T_R L}{w_{woR}h_{wR}}, \phi_R, \frac{d_p}{k^{1/2}}$$

$$\frac{D_{TooR}}{D_{TooR}}, \frac{D_{TgwR}}{D_{TooR}}, \frac{D_{TgoR}}{D_{TooR}}, \frac{\phi_R S_{oR}\gamma_R d_{pR} L}{H^2}, \frac{w_{woR}\mu_{wR}}{\rho_{oR}k_{woR}P_{woR}H}, \frac{LH}{A_{iwR}}, \frac{S_{oR}\mu_{oR}D_{TooR}L^2}{k_{oR}P_{oR}H^2}$$

In addition to these requirements, all of the dimensionless properties must be the same functions of their dimensionless variables for the prototype and the model. The implications for a model reduced in length by a scaling factor of "a" and employing the same fluids as the prototype are: 1) a_c, ϕ, Δp_{max}, P_i, P_{pw}, ΔT_{max}, T_i, k, S_{wi}, S_{gi}, F must remain the same; 2) W must be reduced by "a"; 3) H, W_{ww}, W_{ow}, W_{gw}, W_{go} must be reduced by "$a^{1/2}$"; 4) k_{hc} must be increased by "$a^{1/2}$"; and thus 5) t will be reduced by "a^2." This approach is suitable for processes which require scaling of dispersion but allow the gravitational effects to be relaxed. Injection of liquid additives in a hot waterflood might be one application. This process is restricted to very thin formations because of the relatively small reduction in reservoir thickness.

4.3.5 Approach #5 - Same Fluids, Different Porous Medium, Different Pressure Drop, Geometric Scaling Relaxed

Relaxation of the scaling of gravitational effects is the major shortcoming of Approach #4. Proper scaling of the viscous and gravitational

forces while still scaling transverse dispersion is the objective of using Approach #5. This requires a different maximum pressure change and a different porous medium resulting in many of the same weaknesses inherent in Approach #1. Another drawback to this approach is that time is scaled down by the four-fifths power of the scaling factor rather than its square, making the experiments rather lengthy. Neither the effects of the capillary forces nor heat conduction within the reservoir can be scaled using this approach. The pressure-temperature relationship for saturated steam and the boundary conditions for temperature may be poorly scaled as well.

The relaxed requirements for this approach are listed below. The method of development of this set of criteria is similar to that given in Appendix B. The choice of the reference quantity for the vertical coordinate, x_2, is the same as that selected for Approach #3 in Equation (5).

Scaling Groups: Approach #5

$$\frac{W}{L}, \frac{\rho_{oR} g_R L^2}{H p_{oR}}, \frac{\rho_{rR} U_{rR}}{\rho_{wR} h_{wR}}, \frac{h_{oR}}{h_{wR}}, \frac{h_{gR}}{h_{wR}}, \frac{\mu_{oR} k_{gR}}{\mu_{gR} k_{oR}}, \frac{\mu_{oR} k_{wR}}{\mu_{wR} k_{oR}}, \frac{\rho_{oR}}{\rho_{wR}}, \frac{\rho_{gR}}{\rho_{wR}}, \frac{\alpha_{cR}}{\alpha_{rR}}$$

$$\frac{w_{wwR}\mu_{wR}}{\rho_{wR} k_{wR} p_{wR} H}, \frac{w_{osR}}{w_{wwR}}, \frac{w_{gwR}}{w_{wwR}}, \frac{w_{gsR}}{w_{wwR}}, \frac{S_{wiR}}{S_{wR}}, \frac{S_{giR}}{S_{wR}}, \frac{T_{iR}}{T_R}, \frac{p_{iR}}{p_{oR}}, \frac{p_{pwR}}{p_{oR}}, \frac{k_{hcR} T_R L}{w_{wwR} h_{wR}}, \phi_R$$

$$\frac{D_{TooR}}{D_{TosR}}, \frac{D_{TgsR}}{D_{TosR}}, \frac{D_{TgwR}}{D_{TosR}}, \frac{D_{TooR}}{D^*_{TooR}}, \frac{S_{oR}\mu_{oR} D_{TooR} L^2}{k_{oR} p_{oR} H^2}, \frac{S_{oR}\gamma_R d_{pR} L}{H^2}, \frac{LH}{A_{iwR}}, \frac{d_p}{k^{1/2}}$$

In addition to these requirements, all of the dimensionless properties must be the same functions of their dimensionless variables for the prototype and the model. The implications for a model reduced in length by a scaling factor of "a" and employing the same fluids as the

prototype are: 1) ϕ, S_{wi}, S_{gi}, F, T_i, ΔT_{max} must remain the same; 2) L, W must be reduced by "a"; 3) k must be increased by "$a^{2/5}$"; 4) Δp_{max}, W_{ww}, W_{os}, W_{gw}, W_{ge} must be reduced by "$a^{8/5}$"; 5) H must be reduced by "$a^{2/5}$"; and thus 6) t will be reduced by "$a^{4/5}$." Although the effects of both gravity and dispersion are scaled using this approach, it may not have a useful application for steam processes as the pressure conditions and the conduction of energy within the reservoir are not scaled.

4.4 COMPARISON OF THE FIVE SCALING APPROACHES

Table 8 lists a number of important similarity groups and an estimate of how the simplifications of the various approaches might change the influence of each in a model scaled down by a factor of "a." These groups may be determined by the appropriate ratio of coefficients from the equations in the form shown in Table 3.

Approach #2 is the most suitable for systems in which gravitational forces do not play an important role. This approach is expected to be most applicable to processes dominated by viscous forces. The effects of gravitational forces will be reduced in a model employing this approach. Conditions under which relaxation of these effects causes significant errors have not been established, but for steam processes this may be quite restrictive. Rojas,[26] in an isothermal study of the immiscible displacement of heavy oil by CO_2, found oil recovery to be independent of the model/prototype ratio of gravitational forces to viscous forces for values of $(kv)_m/(kv)_p < 5$.

Table 8. Influence Of Various Similarity Groups On Each Approach.

Group/Approach	#1	#2	#3	#4	#5
a) mass transport					
$visc_x/visc_y$	√	√	$\downarrow a^2$	$\uparrow a$	$\uparrow a^{6/5}$
$visc_x/grav_y$	√	$\uparrow a$	√	$\uparrow a^{3/2}$	√
$visc_x/cap_x$	$\downarrow a^{1/2}$	√	√	√	$\downarrow a^{7/5}$
$visc_x/cap_y$	$\downarrow a^{1/2}$	√	$\downarrow a^2$	$\uparrow a$	$\downarrow a^{1/5}$
$visc_y/grav_y$	√	$\uparrow a$	$\uparrow a^2$	$\uparrow a^{1/2}$	$\downarrow a^{6/5}$
$grav_y/cap_y$	$\downarrow a^{1/2}$	$\downarrow a$	$\downarrow a^2$	$\downarrow a^{1/2}$	$\downarrow a^{1/5}$
$visc_y/cap_y$	$\downarrow a^{1/2}$	√	√	√	$\downarrow a^{7/5}$
$disp_y/visc_x$	$\uparrow a^{3/2}$	$\uparrow a$	$\uparrow a^3$	√	√
$disp_y/grav_y$	$\uparrow a^{3/2}$	$\uparrow a^2$	$\uparrow a^3$	$\uparrow a^{3/2}$	√
b) energy transport					
$cond_x/cond_y$	√	√	$\downarrow a^2$	$\uparrow a$	$\uparrow a^{6/5}$
$cond_x/visc_x$	√	√	√	√	$\uparrow a^{6/5}$
$cond_x/grav_y$	√	$\uparrow a$	√	$\uparrow a^{3/2}$	$\uparrow a^{6/5}$
$visc_{wx}/visc_{gx}$	?	√	√	√	?
$visc_{wx}/grav_{gy}$	?	$\uparrow a$	√	$\uparrow a^{3/2}$	?
c) others					
$T_{sat}(p_{sat})$	x	√	√	√	x
k_r	?	√	√	√	?
Sw_{irr}	?	√	√	√	?
$\rho(p)$	x	√	√	√	x
h(p)	x	√	√	√	x
I_s	$\downarrow a^2$	$\downarrow a$	$\downarrow a$ to $\downarrow a^3$	$\downarrow a$ to √	$\downarrow a^{13/5}$ to $\downarrow a^{7/5}$
B.C.0 prod. well	x	√	√	√	x

KEY:
- √ indicates that the group is satisfied
- x indicates that the group is not satisfied
- ↓ indicates that the influence of the group is reduced
- ↑ indicates that the influence of the group is increased
- ? indicates that the influence of the group is uncertain
- a is the scaling factor by which the major dimension in the prototype has been reduced in the model

A region between an upper and lower limit may exist in which Approach #2 is suitable. The lower limit may represent the point at which gravitational effects must be scaled more rigorously and the upper limit where dispersion must be scaled more rigorously. The ratio of viscous and gravitational forces is scaled most accurately using Approach #1. Approach #1, used by a number of previous investigators, can not be used to accurately scale: the pressure-temperature relationship for saturated steam, the steam temperature at the wells, the energy carried in the steam phase, the steam density, and the latent heat of vaporization. In addition, use of a different porous medium may alter irreducible saturations and relative permeabilities.

Field fluids and porous medium are used in Approach #3, thereby increasing the likelihood that the relative permeabilities and the irreducible saturations are scaled correctly. This approach also allows the steam density, the latent heat of vaporization, the pressure-temperature relationship for saturated steam, the injection temperature, and the energy carried in the steam to be scaled correctly. The ratio of capillary and gravitational forces is not satisfied using this approach. Since the influence of the capillary forces will be enhanced in a model employing this approach, the ability to scale gravitational effects may be limited. Energy will be conducted at an increased rate in the vertical direction within the reservoir because the thickness is reduced, thereby increasing the temperature gradient. This should not be a serious problem in the steam zone where temperatures are all near saturation temperature and heat transfer due to conduction will be minimal, or in the cold liquid zone where the effect of conductive heat

transfer will be small as well. However, if the hot liquid region is very large, an appreciable vertical temperature gradient may exist and heat losses by conduction to the surrounding formations may be greater than allowed for. Baker[5,6] found that heat losses in a steamflood experiment were a function of time only and did not vary with injection rate. In addition to the effects of capillary forces and vertical temperature gradients, the effects of transverse dispersion will be enhanced in a model using Approach #3.

The only methods which properly scale diffusion are Approaches #1 and #2. Diffusion, however, may not be an important mechanism for cases of practical interest, and relaxing this scaling requirement would be reasonable. Convective dispersion, on the other hand, may be more important and is not easily scaled. Peters[37] found that it was more important to match the ratio of viscous to capillary forces in the transverse direction than in the longitudinal direction in order to match recovery at breakthrough for two-dimensional immiscible core displacements. From Table 8 it can be seen that only Approach #2 satisfies this criterion. Pozzi and Blackwell[25] describe conditions for isothermal miscible processes under which the scaling of viscous and dispersive forces can be achieved by relaxing geometric and gravitational scaling requirements. The limits determined by Pozzi and Blackwell between which this was successful were $20 \leq (v\mu L/kg\Delta\rho H) \leq 0.4\ (L/H)^2$. The scaling of transverse dispersion is attempted in Approaches #4 and #5 by relaxing the requirement of geometric similarity. In order to scale transverse dispersion using Approach #4, scaling of the gravitational and capillary forces and the vertical conduction of energy within the reservoir must

be relaxed. This approach does, however, satisfy the requirements of relative permeability, irreducible saturations, heat content in the steam and water phases, steam density, the saturation pressure-saturation temperature relationship, and the injection temperature. The gravitational forces are in balance with the viscous and dispersive forces when using Approach #5. However, this approach suffers many of the same drawbacks as Approach #1 as a large reduction in pressure drop is required as well. In order to scale conduction, time must be scaled down by the square of the scaling factor. The criteria of this approach require time to be scaled down by the four-fifths power of the scaling factor. Therefore, conduction is scaled poorly using Approach #5.

Permeability across the bedding plane of a sand can often be appreciably different from that parallel to the bedding plane. Appendix D shows that gravitational effects due to a vertical and horizontal permeability contrast in the field can be scaled using uniform sands and Approaches #1 and #3. This technique is only applicable to horizontal reservoirs in which the vertical pressure gradient is insignificant. For Approach #1, gravitational effects are scaled using the group, $(\rho g k_y L/k_x \Delta p)$, instead of, $(\rho g L/\Delta p)$, and for Approach #3, $(\rho g k_y L^2/k_x H \Delta p)$, instead of, $(\rho g L^2/H\Delta p)$. When the vertical permeability of the reservoir is less than its horizontal permeability, the significance of relaxing the scaling of gravitational effects when using Approach #2 is reduced and the applicability of Approach #3 is expanded.

Other phenomena that have not been considered in the scaling criteria, but which may be important in certain circumstances, are distillation,

emulsification, gas solubility, rock-fluid interactions, and temperature dependence of rock properties. Approaches #2, #3, and #4, which allow the use of the same fluids and the same porous medium, and result in the same pressure drop and temperature change should be superior methods for simulating many of these phenomena even though they have not been scaled rigorously.

In each of the five approaches, emphasis is placed on scaling different aspects of a recovery process. The choice of any one approach depends on the importance of the phenomena which are not scaled by that approach. For example, if gravitational effects are believed to be of major significance to the process, it is unlikely that Approaches #2 and #4 would be satisfactory methods to use. The degree to which a phenomenon is not scaled is also an important consideration. If a particular phenomenon is considered to be insignificant in the prototype and its scaling requirements relaxed, it is important that this phenomenon remains insignificant in the scaled experiment. For example, Approach #3 may be selected for scaling a process because the effects of transverse dispersion are considered to be minor in the prototype and the other aspects are properly handled using this approach. The effect of transverse dispersion in the model will be magnified by the cube of the scaling factor using Approach #3. If the effect is still considered to be insignificant, this approach would be suitable. Table 8 can be used as a guide for selecting a high-pressure scaling approach which would be most suited for a particular process.

5. EXPERIMENTAL INVESTIGATION

5.1 EXPERIMENTAL STRATEGY

A series of experiments was designed to develop and test four of the high-pressure scaling approaches (#1, #2, #3, and #4). Approach #5 was not studied experimentally, as even in theory it appeared to be very limited for application to thermal processes. The experimental strategy was to scale down a field reservoir in order to design a series of experiments in a large model. Approach #2 and a scaling factor of 100 were used. The results were expressed in dimensionless form. The large model was then scaled down using each scaling approach so as to design a series of experiments using smaller models. These dimensionless results were then compared with those of the large model in order to determine the relative value of each scaling approach when used to predict the results of the large model. It should be noted that the large model was only twice the size of the smaller models, as necessitated by expefimental considerations.

The first experimental phase consisted of 35 experiments involving the injection of steam into cold, water-saturated sand. The use of a two-phase steam-water system simplified evaluation of the different approaches. The objective of this experimental phase was to ensure that the four scaling approaches could be used to scale the mechanisms of heat transfer and steam zone development. All four approaches were studied over a wide range of injection rates, with some experiments being duplicated.

The second experimental phase consisted of 10 experiments in which steam was injected into oil-saturated sand. The oil selected was a 30 mPa•s oil. This phase was used to screen the relative value of Approaches #1, #2, and #3 when used to scale oil production rates and sweep efficiencies. These experiments were also used to examine the importance of using field pressure conditions versus the accurate scaling of gravitational effects.

5.2 DESIGN OF THE SCALED EXPERIMENTS

To design a scaled experiment for a steam injection process, a number of steps must be followed. These include:

1) identification of field data and operating conditions,
2) selection of the most appropriate scaling approach, and
3) design of the scaled model.

In this study, these steps were used to design a large model using Approach #2 and then followed again using all the scaling approaches to design the smaller models based on the large model. It was not necessary to scale down a field reservoir to design the large model, but doing so ensured a representative balance of the various mechanisms and parameters involved in the recovery process.

5.2.1 Field Data and Operating Conditions

The first step is to characterize the reservoir being studied and identify the operating conditions which will be used. Some parameters,

such as permeability, may best be represented as a distribution. A decision must be made regarding whether to represent it as a distribution or as an average value. A compromise between practical difficulties and the influence of the distribution on the process must be made. Table 9 lists the idealized field information which will be used to design the large scaled model in this study.

5.2.2 Experimental Design

The scaling groups listed in Section 4.3 for each approach are applied in order to design each model. The characteristic reference quantities listed in the sections are replaced by representative constants. The first parameter to be determined is the scaling factor or the ratio of length in the prototype to that in the model. It is usually determined by the maximum physical size available for the experiment. In this study, the maximum size available is 60 cm. Therefore, the scaling factor, a, is determined as follows:

a = (prototype well spacing/model well spacing)
= (60 m/0.6 m) = 100 (large model)
= (0.6 m/0.3 m) = 2 (small model).

The remaining design of the experiments will incorporate these scaling factors.

Geometry. The well-spacing has already been selected. In Approaches #1 and #2, use is made of the geometric scaling group, (H/L), to determine

Table 9. Field Information.

Well spacing	60 m
Well diameter	0.2 m
Porosity	0.36
Permeability	2 μm^2
Formation type	unconsolidated sand
Reservoir temperature	27°C
Reservoir thickness	10 m
Geometry	5-spot
Production pressure	400 or 1700 kPa
Injection rate	7-110 m^3/day
Steam quality	1.0
Thermal conductivity of cap rock	0.6 W/(m K)
Heat capacity of cap rock	1.9 J/(cm^3 K)

the model thickness. Thus, for the large model,

$$(H_p)/(H_m) = (L_p)/(L_m) = a$$

$$H_m = 10 \text{ m}/100 = 0.1 \text{ m} .$$

The desired geometry is a five-spot pattern. To minimize the scaling factor by which the prototype must be reduced in order to fit in the pressure vessel, the smallest element of symmetry, one-eighth of a five-spot pattern, is represented. This leads to a triangular model which has a 60 cm diagonal, two 42.4 cm sides, and a thickness of 10 cm. Dimensions for the other models are listed in Table 10. The undesired heat losses through the walls of the model can be reduced if one-quarter of a five-spot pattern is selected because a lower temperature boundary will result, but this will lead to a larger scaling factor.

In Approach #3 and #4, different scaling groups are used to determine the model thickness. For Approach #3, $(H\Delta p/\rho g L^2)$, a group for scaling gravitational effects is used. For Approach #4, $(H/(\phi S_w \chi d_p L)^{1/2})$, a group for scaling the effects of transverse dispersion is used. Approach #3 will be practical for only thick reservoirs and low scaling factors because the model thickness may become impractically small. Approach #4 is most suitable for thin formations as the model may become too thick to be practical.

Fluid properties. Every dimensionless fluid property must be the same function of dimensionless pressure and temperature for the model as it is for the field. By using field fluids in the model, fluid properties such as density, viscosity, and heat capacity, are scaled. Note that this is strictly true only for scaling approaches that scale the

Table 10. Model Information.

	Large Model	#1	#2	#3	#4
Well spacing	60 cm	30 cm	30 cm	30 cm	30 cm
Well slot width	0.079 cm	0.039 cm	0.039 cm	0.039 cm	0.039 cm
Porosity	0.36	0.36	0.36	0.36	0.36
Permeability	2 μm^2	4 μm^2	2 μm^2	2 μm^2	2 μm^2
Formation type	uc sand	uc sand	uc sand	uc sand	uc sand
Reservoir fluids - water exps.	100% water	100% water	100% water	100% water	100% water
- oil exps.	85% oil	85% oil	85% oil	85% oil	85% oil
Reservoir temperature	27°C	27°C	27°C	27°C	27°C
Reservoir thickness	10 cm	5 cm	5 cm	2.5 cm	7.1 cm
Geometry	1/8 of 5-spot	1/8 of 5-spot	1/8 of 5-spot	1/8 of 5-spot	1/8 of 5-spot
Production pressure - water exps	1700 kPa	1700 kPa	1700 kPa	1700 kPa	1700 kPa
- oil exps.	400 kPa	400 kPa	400 kPa	400 kPa	400 kPa
Injection rate	0.1-1.6 cm^3/s	.05-0.8 cm^3/s	.025-0.4 cm^3/s	0.05-0.8 cm^3/s	.071-1.13 cm^3/s
Steam quality	1.0	1.0	1.0	1.0	1.0
Thermal conductivity of cap rock	0.6 W/(m K)	0.6 W/(m K)	0.6 W/(m K)	0.3 W/(m K)	0.85 W/(m K)
Heat capacity of cap rock	1.9 J/(cm^3 K)	1.9 J/(cm^3 K)	1.9 J/(cm^3 K)	1.0 J/(cm^3 K)	2.7 J/(cm^3 K)

uc - unconsolidated

pressure and temperature conditions accurately. This condition is not satisfied in Approach #1. Even though the same fluids are used in Approach #1, properties which depend on pressure, such as the saturation temperature and density of steam, are not scaled properly. Two examples of this are shown in Figure 2. Selection of the same fluids allows the scaling groups, (h_{st}/h_s) and (ρ_{st}/ρ_s), to be satisfied. It also leads to a reduction of the group scaling the fluid mobilities, $(\mu_s k_{st}/\mu_{st} k_s)$, to a group scaling effective fluid permeabilities, (k_{st}/k_s).

Thermal Properties of the Surrounding Formations. Design of the material over-lying and underlying the reservoir formation is very important as heat losses to these formations play a major role in thermal processes. In Approaches #1 and #2, use is made of the scaling group, (α_c/α_r), a ratio of the thermal diffusivity of the reservoir and the cap rock, to design the thermal properties of the surrounding formations. Therefore,

$$(\alpha_c)_m = (\alpha_c/\alpha_r)_p \cdot (\alpha_r)_m \ .$$

Since these scaling approaches allow field porous media to be used in the model, and it has been determined that the same fluids will be used, then,

$$(\alpha_c)_m = (\alpha_c)_p$$
$$(\alpha_c)_m = 3.2 \times 10^{-7} \ m^2/s \ .$$

When using Approaches #3 and #4, the conductivity and heat capacity must be scaled independently using the two scaling groups, $(k_{hc}t/(\rho C_p)_c L^2)$ and

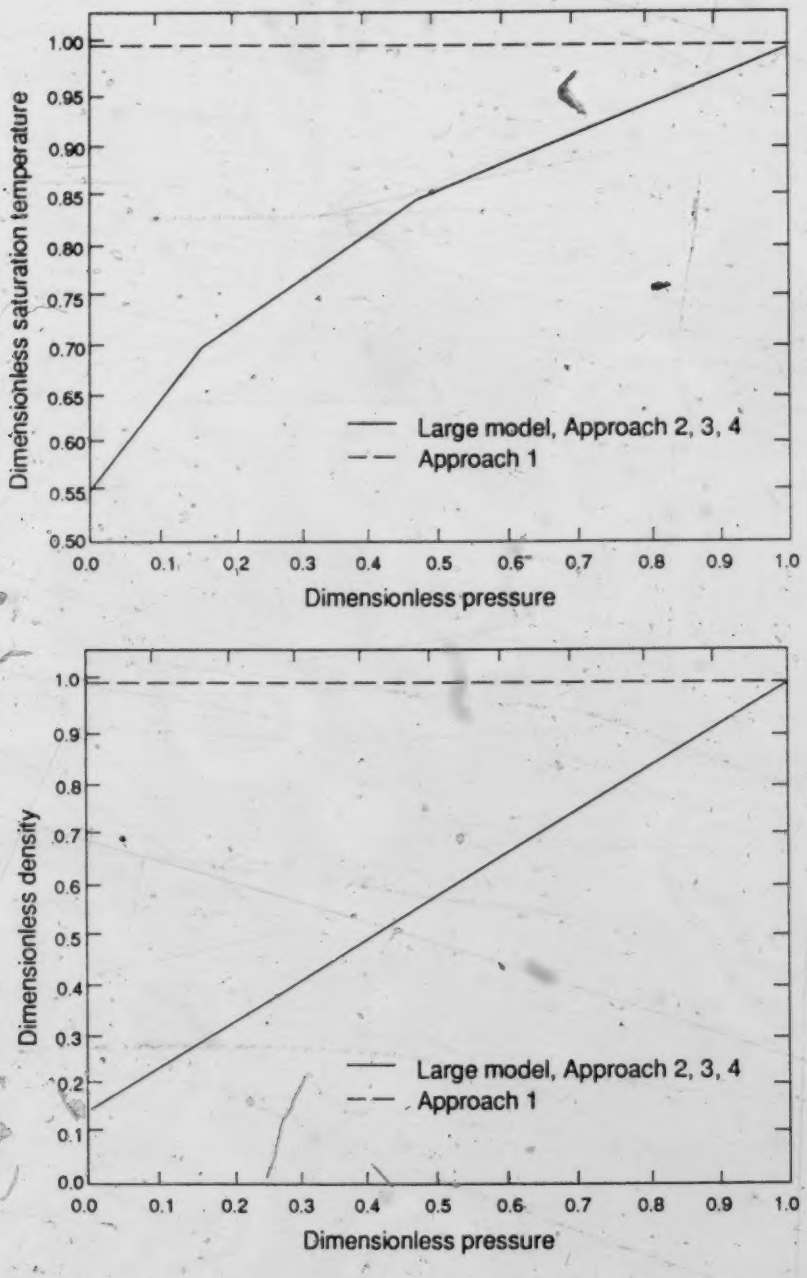

Figure 2. Examples of the inability of Approach #1 to satisfy the scaling requirements for fluid properties.

$(k_{hc}\Delta TL/W_{st}h_w)$. This is necessary because, using these approaches, scaling of the vertical temperature gradient in the reservoir is relaxed. Some practical difficulties may be encountered when searching for a material with the thermal properties that satisfy these requirements. The thicknesses of the overburden and underburden are selected to ensure that the boundary effects on these formations are not significant over the duration of the experiment, i.e. the temperature on the exterior surfaces is near the initial temperature.

Pressure Conditions. Using Approaches #2 and #3, the pressure drop and the production pressure must be the same as those encountered in the field in order to scale the fluid properties properly. This requires that

$$(p_{pw})_m = (p_{pw})_p = 1700 \text{ kPa (water runs)}$$

or

$$= 400 \text{ kPa (oil runs)} .$$

In Approach #1, the pressure drop is scaled using the gravitational group, $(\Delta p/\rho_w gH)$, leading to a substantially smaller pressure drop. Consequently, the best compromise for pressure conditions using Approach #1 is to make the injection pressure equal to the field injection pressure and the production pressure equal to the injection pressure minus the required pressure drop.

Permeability. The group, $(k\rho_w h_w \Delta p/\mu_w k_{hr}\Delta T)$, is used to scale permeability for all of the approaches. In Approaches #2 and #3, the same

fluids, the same pressure drop, the same temperature change, and the same thermal conductivity are used, therefore, the same absolute permeability is required. This allows the field porous media to be used in the model. Approach #1 requires a much smaller pressure drop, and therefore, a much larger permeability would be required to satisfy this scaling group.

Injection Rate. In Approaches #1, #2 and #3, the injection rate is scaled using the group, $(W_{st}\mu_w/\rho_w k\Delta pH)$. Thus, for the large model,

$$
\begin{aligned}
(W_{st}/\rho_w)_m &= (W_{st}\mu_w/\rho_w k\Delta pH)_p \cdot (k\Delta pH/\mu_w)_m \\
&= (W_{st}/\rho_w H)_p \cdot (H)_m \\
&= (55.3\ m^3/d\ /\ 10\ m) \cdot (0.1\ m) \\
&= 0.553\ m^3/d
\end{aligned}
$$

Only one-eighth of this flow rate is required because only one-eighth of the five-spot pattern is represented by the model; thus, $(W_{st}/\rho_w) = 0.0691\ m^3/d$. For Approaches #3 and #4, this group would lead to lower and higher injection rates, respectively, i.e. 0.000691 m^3/day and 0.691 m^3/day.

Well Design. If the well diameter was scaled down in size by a factor of 100, it would be too small to be practical. To overcome this, a technique was developed by Stegemeier et al.[8] to represent the well as a slot. The slot width is determined using the scaling group, (A_{iw}/LH).

Therefore,

$$(A_{iw})_m = (A_{iw}/LH)_p \cdot (LH)_m$$

$$= (\pi d_{well} H/LH)_p \cdot (LH)_m$$

$$= (\pi\ 0.2\ m \cdot 10\ m \cdot 0.6\ m \cdot 0.1\ m)/(60\ m \cdot 10\ m)$$

$$= 0.000628\ m^2$$

$$w = (A_{iw}/H)_m$$

$$= (0.000628\ m^2/0.1\ m) = 0.0063\ m$$

Since only one-eighth of the well is being represented, the slot width, w, is 7.85×10^{-4}m.

Steam Quality. The steam quality is scaled using the scaling group, (W_{st}/W_w). This means that the mass fraction of injected steam and water must be the same in the field and the model. Therefore, the quality of injected steam must be 1.0 for the model. A summary of model characteristics for the large model and each small model is given in Table 10.

5.2.3 Experimental Apparatus

The experimental apparatus consisted of an injection facility, a production facility, and a pressure vessel (Figure 3). The injection facility supplied steam to the model at the desired rate, temperature, pressure, and quality. The production facility collected the produced fluids at the desired production pressure and determined the production rates. A pressure vessel housed the model and allowed a confining pressure to be applied to the reservoir.

The injection facility consisted of a pump and three heat exchangers. A Jefri positive displacement pump suitable for injecting water at rates

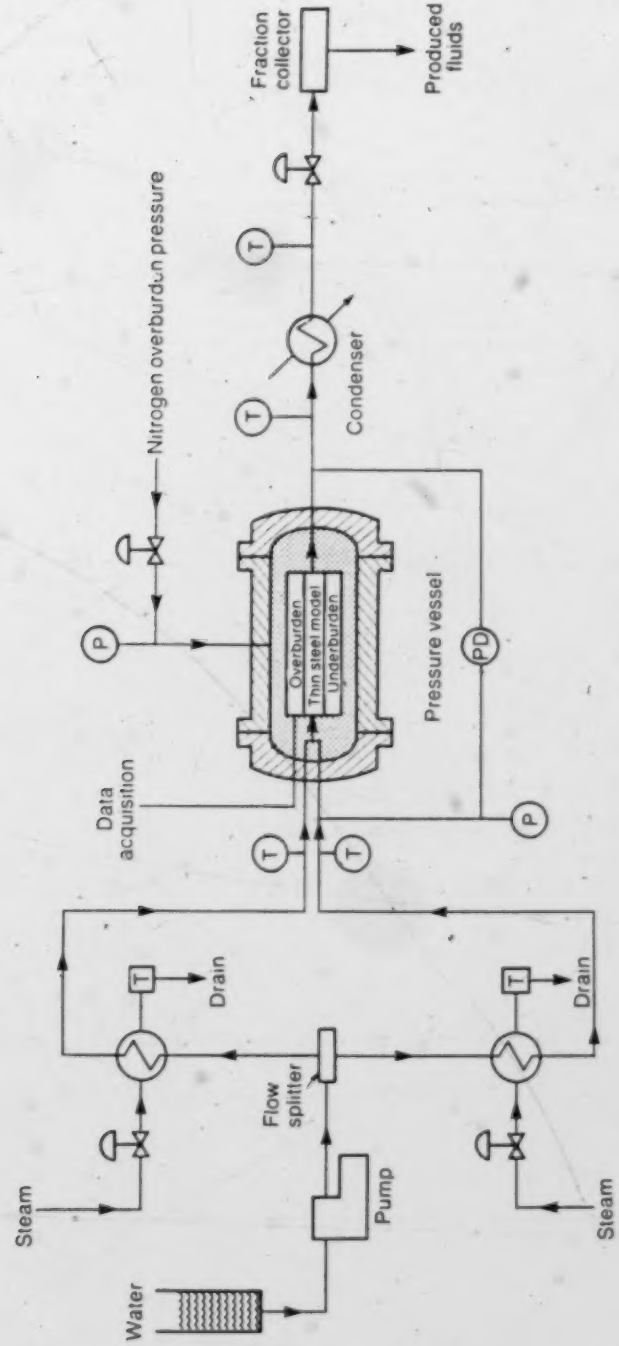

Figure 3. Schematic of experimental apparatus.

of 0.005-1.999 cm^3/s and at pressures up to 6.9 MPa was used. The water then passed into a double-tube heat exchanger where utility steam, controlled at pressures between 0 and 4.1 MPa, was used to superheat the water by about 50°C. The superheated steam then passed into a second heat exchanger, also heated by utility steam, in which the pressure was set to within 100 kPa above the saturation pressure of the desired injection temperature. This heat exchanger was also a double-tube exchanger and extended through the pressure vessel to maintain the superheat of the injected steam. The slightly superheated steam (typically 10°C) was then maintained through the final 10 cm of injection tubing using an electrical heat tape and a temperature controller which monitored the injection temperature.

The production system consisted of a condenser, a back-pressure regulator, and a fraction collector. The produced fluids passed out of the pressure vessel and into the condenser, which cooled them to about 28°C. They then passed through a Nicola back-pressure regulator which maintained the desired production pressure to within 1 kPa. Finally, the fluids were collected using a fraction collector that deposited them into 30 ml test tubes at time intervals of 6-600 seconds.

The pressure vessel (Plate 1) that housed the assembled scaled model allowed up to 9.0 MPa of overburden pressure to be applied to the flexible walls of the reservoir model. Nitrogen gas was used to apply an overburden pressure of 4.5 MPa. The pressure vessel end caps permitted an injection line, a bypass line, a production line, a heat tape power cable, and 120 thermocouple extension wires to pass into the vessel.

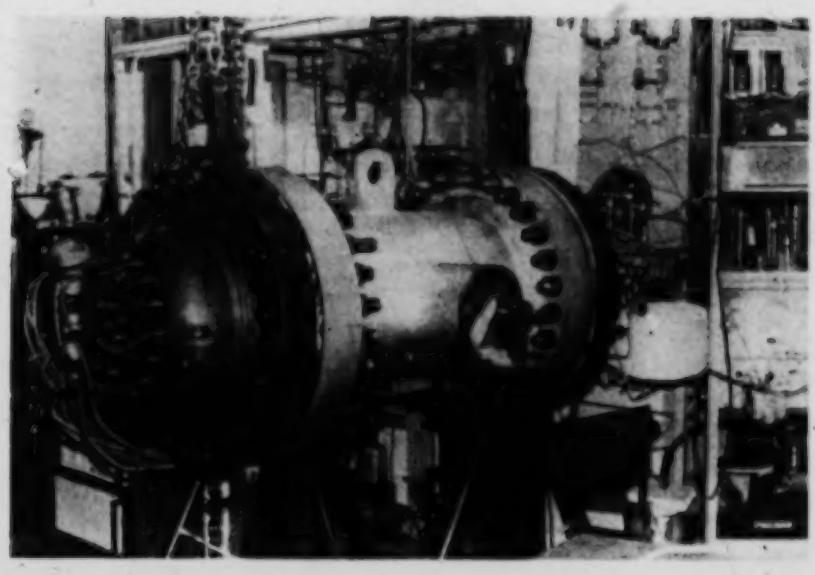

Plate 1. Pressure vessel which housed the scaled model.

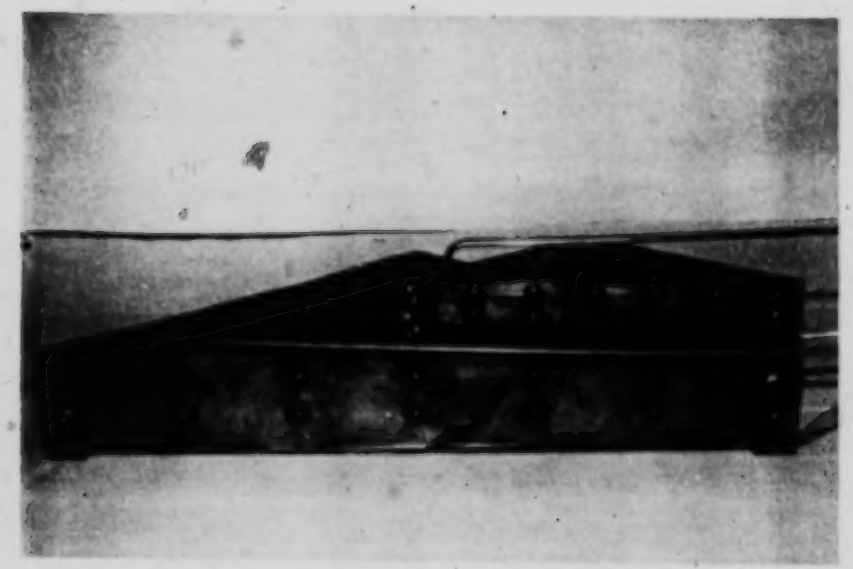

Plate 2. A large and a small model illustrating the location of the thermocouple ports.

Temperatures, injection pressure, pressure drop, and heat flux voltages were recorded using a PDP 11/44 computer and a Fluke Datalogger.

The models were constructed of 24-gauge 316 stainless steel. Wells were fabricated from 316 stainless steel, with a slot of an appropriate width representing the well inside the model. Two screens, one of 325 mesh, then one of 50 mesh, were tack welded over the slots to prevent sand from entering the wells. Each well had ports which permitted tubing for conducting fluids and a thermocouple for monitoring temperature to be attached. A well is illustrated in Figure 4. The model wall between the two wells contained 10 ports for thermocouple probes (Approach #3's small model had only 5 ports) that monitored temperature at 28 locations throughout the model (Plate 2). A port at the right angle corner allowed the model to be filled with sand. Plate 3 shows one of the large and one of the small models that were used. Note that they represent one-eighth of a five-spot pattern. Plate 4 shows the small models; the left one was used for Approach #3, the middle one for Approach #1 and #2, and the right one for Approach #4.

A mixture of bitumen and solid particles was used to simulate the overburden and underburden. Bitumen was used because of its highly viscous, semisolid characteristics which permitted molding to shape and ensured good thermal contact on the deformed surface of the model. Solid particles were mixed in and the resulting thermal properties were determined by Tempest Geophysical Consultants Limited. A mixture of bitumen and glass beads yielded the desired thermal conductivity of 0.6 W/m^2K, and a mixture of bitumen and wood particles resulted in the desired thermal conductivity of 0.3 W/m^2K.

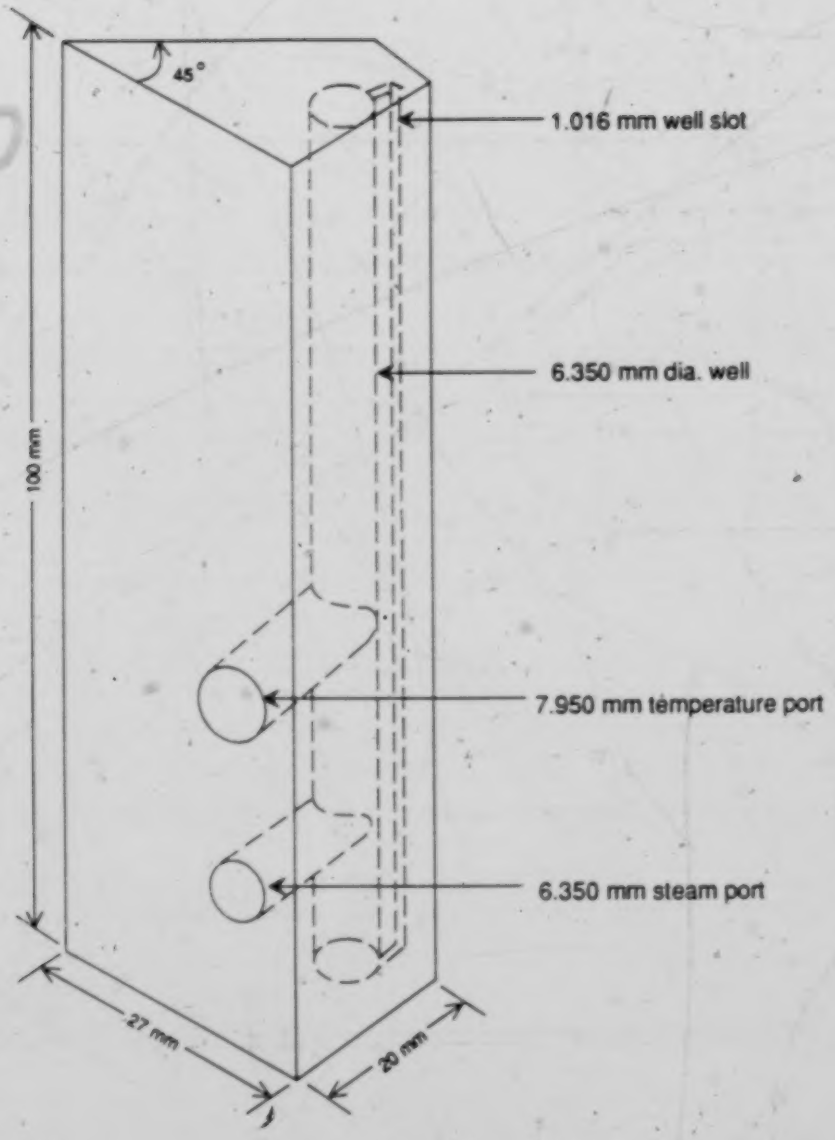

Figure 4. Details of the injection well used in the models. The height of the well is tailored to the particular model. The production well is similar.

Plate 3. A large and a small model illustrating the 1/8th of a 5-spot geometry used.

Plate 4. Three of the small models illustrating the different thicknesses required by the various scaling approaches.

5.2.4 Experimental Procedure

Preparation for an experiment normally took six weeks. The actual experiment could be completed in a matter of hours. The entire procedure consisted of the following steps:

1) preparation of the model;
2) preparation of the surrounding formations;
3) saturation;
4) performance of an experiment.

Each step will be discussed in detail.

Preparation of the Model. The triangular model was fabricated from 24-gauge stainless steel. All the joints were welded. Thermocouple ports, a sand fill port, and the injection and production wells were also welded in place. Leaks in the model were a major problem, as the nitrogen gas used to confine the reservoir will leak through the smallest of holes. A helium leak detector was used to find all leaks in the welds at this point.

The model was then packed with clean Ottawa sand. The sand was poured through the fill port at about 15 g/min and vibrated to achieve a very dense packing of the sand grains. The level of vibration was sufficient for visual detection of sand grain motion at the surface, if carefully observed. This technique led to reproducible porosity and permeability measurements (ϕ=0.370±0.017, k=2.5±0.5). Small core tests showed that a

a -200 +325 mesh cut of F-140 sand yielded about a 2 μm^2 porous medium and that a -150 +200 cut would yield about a 4 μm^2 one. Glass beads were not used to represent the porous media, because initial tests with high-pressure steam revealed that the beads became a consolidated, almost impermeable, mass.

The model was then placed in a pressure vessel and deformed by applying 5.0 MPa of confining nitrogen pressure. Porosity of the model was determined by measuring its weight in air and in water. Thermocouple probes were inserted into the model to monitor the temperature inside, and 56 thermocouples were also welded to the exterior of the model to monitor its surface temperature (see Figure 5 for thermocouple locations).

Preparation of Surrounding Formations. Packing of the bitumen and glass bead mixture, selected to simulate the overburden and the underburden, was done at this point. The unconsolidated nature of this material allowed good thermal contact at the surface of the model. A triangular frame constructed of one-quarter inch plywood, for holding the underburden, was packed as densely as possible with the mixture. The model was then placed on top, and the frame for holding the overburden was set in place. Overburden was packed into this frame. Thermocouple probes were inserted into the overburden and underburden to monitor the temperature in these regions (see Figure 5 for thermocouple locations). Plate 5 shows the model with the overburden and thermocouples in place. Mineral wool insulation was packed around the model, overburden, and underburden to represent as closely as possible the zero heat flux boundaries.

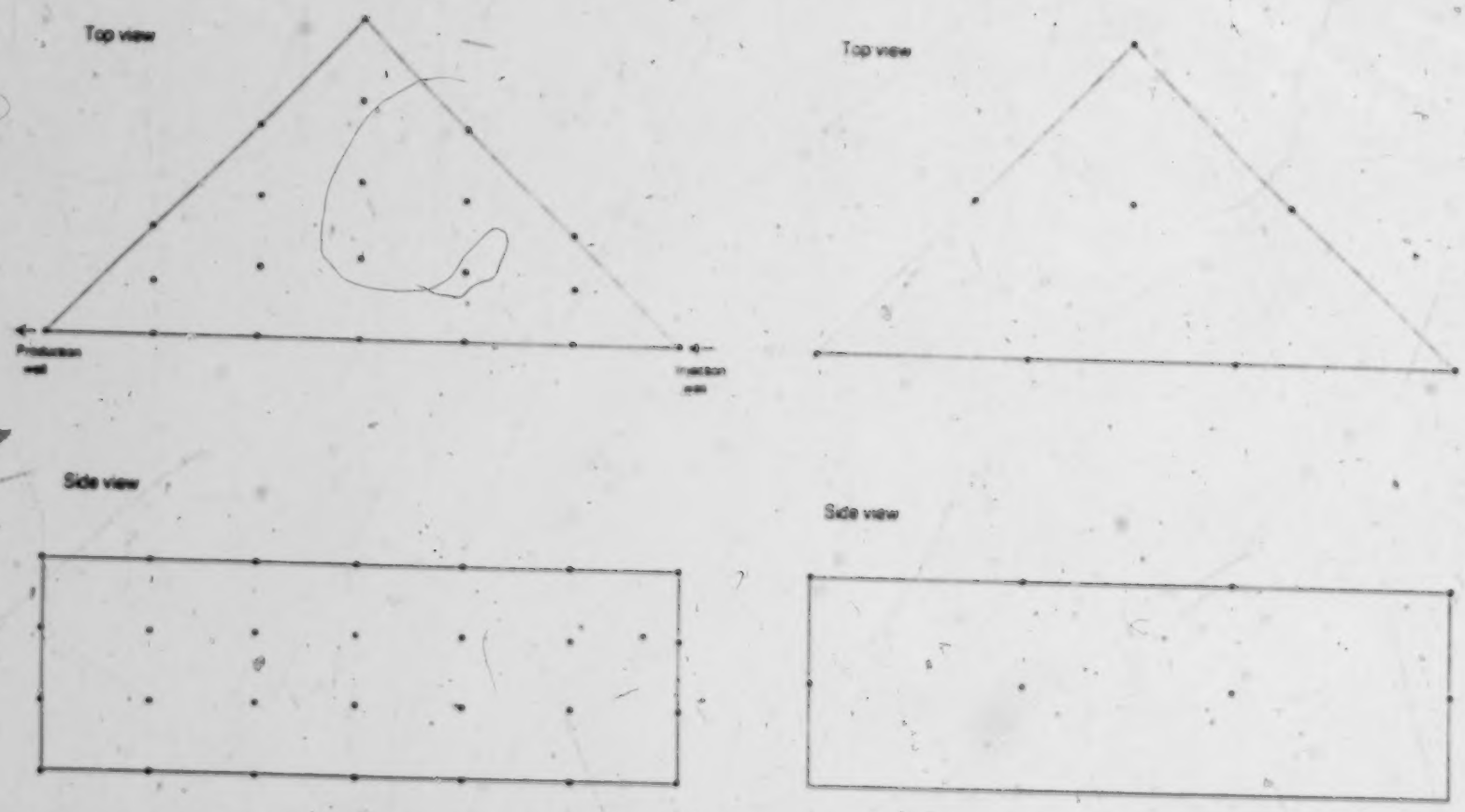

Figure 5. Location of thermocouples in the model (left) and overburden (right). The underburden locations are similar to those in the overburden.

Plate 5. A scaled model with the overburden and thermocouples in place.

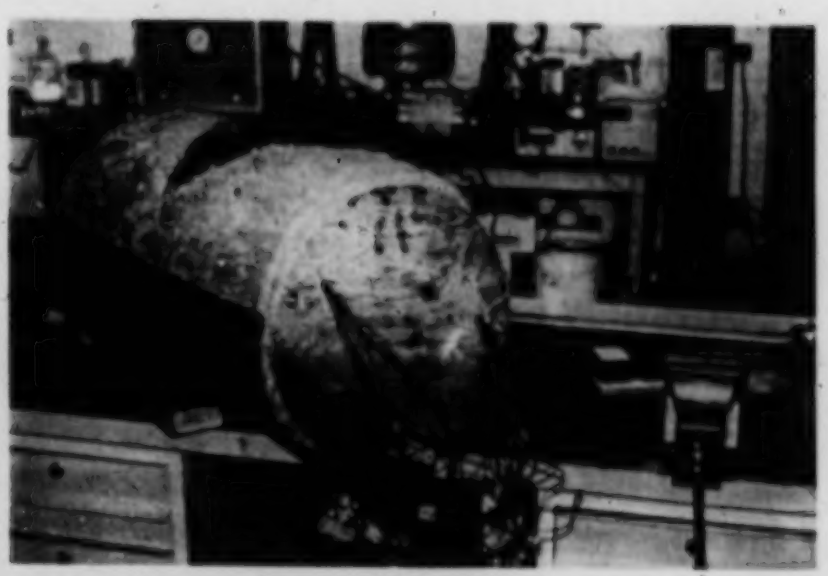

Plate 6. A fully assembled scaled model, ready to be placed in the pressure vessel.

Saturation. The assembled model (Plate 6, Figure 6) was placed in the pressure vessel and a confining pressure of 4.5 MPa was applied. After evacuating the air from the model, it was flooded with water. For the experiments involving oil saturation, 1.5 pore volumes of oil were injected into the fill port and produced from each well. The model was positioned upright to take advantage of gravitational segregation. It was then returned to its normal position and another pore volume of oil was injected into the injection well and produced from the production well. The oil used was Esso Uniflo base oil. It contains no additives, but many of the light and heavy ends are removed (see Appendix E for a list of properties).

Performance of an Experiment. The heat exchangers were preheated to the desired conditions by bypassing the injected water around the model. Steam was then injected at the desired rate and temperature (slightly superheated to ensure a steam quality of 100% for these experiments). Temperatures, injection pressure, and pressure drop were monitored using the data acquisition system. Produced fluids were collected after being passed through a back-pressure regulator set to the desired production pressure. A fraction collector allowed production rate and cumulative production to be estimated throughout the experiment. The oil and water were separated and the respective amounts were used to calculate the water-oil ratios.

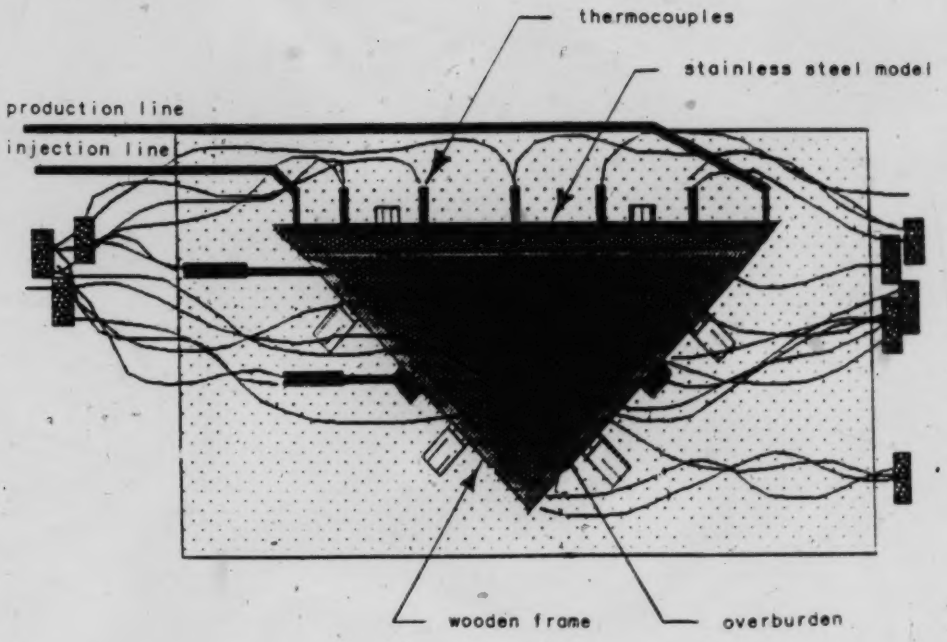

Figure 6. Schematic of assembled model.

6. ANALYSIS PROCEDURE

Many parameters were measured directly or inferred from other measurements. Their method of determination is discussed in the following sections. The parameters measured directly include injection pressure, pressure drop, temperature, injection rate, and production. These data, together with the basic properties of the materials utilized were used in the analyses of the experiments. The techniques by which these parameters were scaled up for comparisons of the results are then outlined.

6.1 POROSITY

The porosity of each model was calculated using a material balance. The weight of the empty model, the model filled with sand, and the filled model immersed in water were used to calculate the porosity. The volume of air in the model was calculated using Equation 7.

$$V_a = \left\{ W_3 - W_2 \left[\frac{(\rho_{ss} - \rho_w)}{(\rho_{ss} - \rho_a)} - \frac{(\rho_{sand} - \rho_w)}{(\rho_{sand} - \rho_a)} \right] - W_1 \frac{(\rho_{sand} - \rho_w)}{(\rho_{sand} - \rho_a)} \right\} / (\rho_a - \rho_w) \qquad (7)$$

where V_a = volume of air in the model

W_3 = weight of packed model immersed in water

W_2 = weight of empty model

W_1 = weight of packed core.

The pore volume is therefore equal to this calculated volume of air minus the volume of the lines entering and leaving the model. The porosity was calculated using Equation 8.

$$\phi = V_{pore}/(V_{pore}+(W_1-W_2)/\rho_{sand}) . \qquad (8)$$

6.2 PERMEABILITY

The permeability of the model was calculated using Muskat's[38] single-phase solution for the pressure drop in a five-spot pattern. Water was injected at three injection rates, while the temperature of the water and the pressure drop across the model were being monitored. Equation 9 was then used to calculate absolute permeability.

$$k = \frac{810600\ \mu\ Q\ [\ln(d/r_w)-0.6190]}{\pi\ H\ \Delta p} \qquad (9)$$

where k = absolute permeability (md)

μ = water viscosity (cp)

Q = water injection rate (cm^3/s)

H = thickness of model (cm)

Δp = pressure drop (kPa)

d/r_w = ratio of interwell spacing to well radius.

The ratio, d/r_w, was estimated to be 750. Note that the accuracy of this estimate is not critical, as doubling or halving it would increase or decrease the permeability by only 12%.

6.3 PRODUCTION RATE

Production rate was estimated after condensing and collecting the produced fluids in a fraction collector. The volume of water and/or oil

was measured and divided by the time interval of collection to give the average rate over that interval. During the oil experiments, the total rate was estimated as described, but the oil-water ratio was estimated by calculating the quantity of oil and water leaving the production well during a particular time interval. This was necessary because approximately 150 cm^3 of tubing existed between the production well and the fraction collector, and although the production rate was known immediately, the fluid production was delayed.

6.4 SATURATION

The weight of oil remaining in the model was determined at the Alberta Research Council analytical lab using the Dean Stark extraction procedure. This remaining oil was added to the produced oil for determination of the total amount of oil that initially saturated the model. Based on the calculated pore volume for the model, the initial saturations of oil and water were determined.

6.5 STEAM ZONE VOLUME

An experiment would begin with the constant injection of cold, deionized water into a series of heat exchangers (Figure 3), thereby injecting steam into the model at the desired temperature, pressure, and quality. The steam entered the model and fluids were subsequently produced at the production well. These produced fluids were cooled, depressurized, collected, and measured. The volume of the reservoir occupied by steam was inferred from the measured injection and production rates using a

volumetric balance. It was assumed that the steam occupied the hottest regions of the reservoir. The volume of the fluids within the reservoir was then corrected for temperature and pressure. This volume was used to compare steam zone development in the various experiments and to assist in calculation of the energy distributions.

6.6 PRESSURE DATA

Pressure data were used to determine fluid properties and compare pressure drop history over time. Pressure drop data were also recorded during a waterflood to determine whether or not the one-eighth five-spot element of symmetry exhibited a pressure distribution typical of a five-spot pattern. Four pressure taps were used to monitor the pressure drop over various regions of the model during waterflooding. These measured values were compared to theoretical values for a five-spot pattern flowing a single phase. The measured and theoretical values were similar, confirming that the one-eighth five-spot element of symmetry suitably represented a five-spot pattern (Table 11).

6.7 TEMPERATURE MEASUREMENT AND ENERGY BALANCE

The 120 temperatures measured were processed using computer programs that provided temperature profiles and energy distributions for various parts of the model. For purposes of analyzing the energy distribution, the model was divided into 112 triangular cells (Figure 7). Average temperature, fluid and rock properties, and energy content for each cell over each time interval were calculated. The details of estimating an

Table 11. Comparison of 5-spot Pressure Distribution.

	Measured (% of total pressure drop)	Theoretical
Δp_1	52%	46%
Δp_2	10%	8%

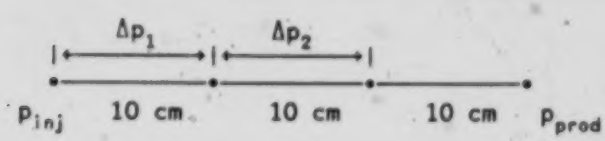

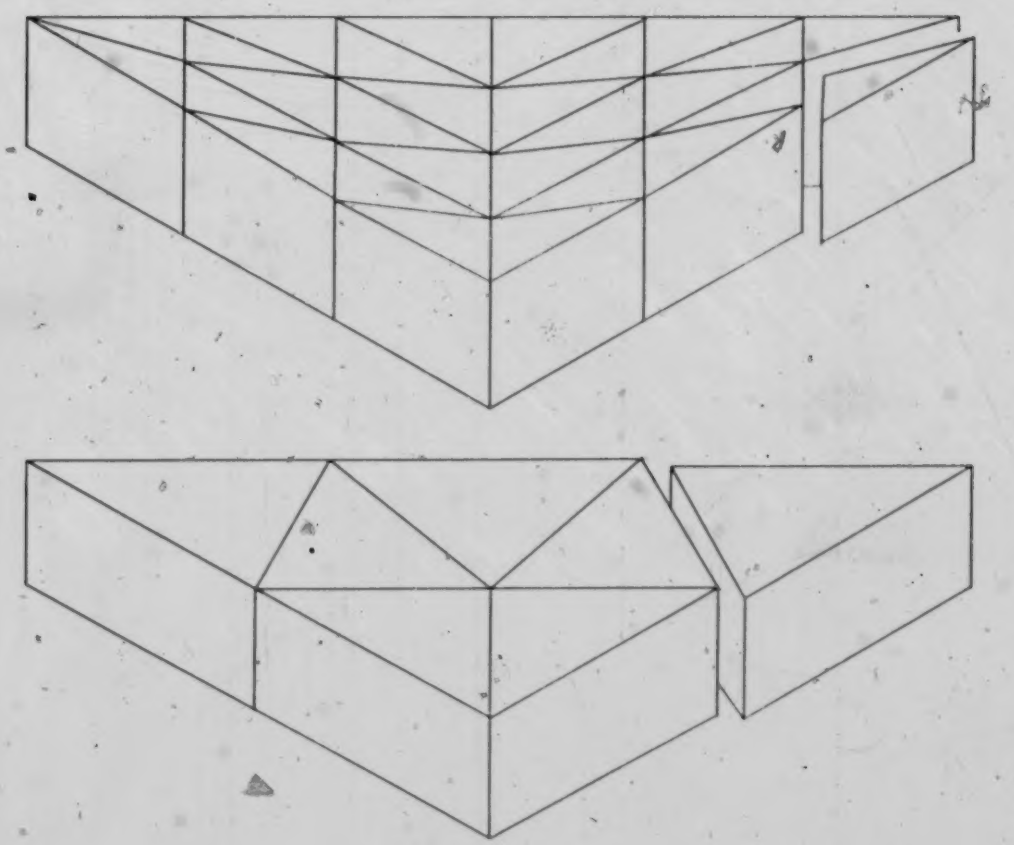

Figure 7. Illustration of the triangular cells used to analyze energy distribution in the model (top) and the over/underburden (bottom).

average block temperature are outlined in Appendix F. The cells in the various regions were then combined to yield energy distribution in the overburden, underburden, reservoir, and produced fluids. Energy losses from the model to the insulation, from the surface of the overburden and underburden to the pressure vessel, and to the thin steel model were estimated.

6.7.1 Energy Losses to the Insulation

Energy lost to the insulation was estimated using Equation 4, a one-dimensional transient solution assuming infinite insulation thickness.[39]

$$q = \frac{k_h A}{\sqrt{\pi \alpha}} \left\{ \frac{(T_1 - T_0)}{\sqrt{t}} + \sum_{i=2}^{n} \frac{(T_i - T_{i-1})}{\sqrt{t - t_i^*}} \right\} . \qquad (10)$$

Temperature, T, is assumed to be equal to the average skin temperature of the entire model at each time step. The thermal conductivity of the rock wool insulation is assumed to be 0.0415 W/mK and its heat capacity, 0.837 kJ/kgK.

6.7.2 Surrounding Formation Energy Losses

As an experiment progressed, the material representing the overburden and underburden became warm. The lateral boundaries were insulated so as to approximate the no-heat flow condition, but energy was lost in an undesirable manner from the upper and lower boundary. If the pressure vessel had been larger, and thicker overburden and underburden could have been used, part of this lost energy would have been desirable (i.e.

scaled losses to the surrounding formations). Equation 4 was used to estimate the scaled portion of these heat losses, with the remainder attributed to unscaled losses. The unscaled portion limited the duration of each experiment as it must not significantly affect the results of the experiment. In Figure 8, the actual (measured) losses and the ideal (desired) losses for the longest experiment are shown. A significant difference is not evident until 600 minutes into this experiment.

6.7.3 Energy Losses To The Steel Model

The maximum amount of energy which could be stored in the steel of the large model was about 240 kJ, and in the small model, about 105 kJ. Approximately 21 000 kJ were injected into the large model, and about 2750 kJ into the small model. Although the drain on the injected energy was more significant for the small models, it was still less than 4% of the total injected energy.

The insulation on the lateral boundaries of the model was not perfect and consequently some energy was lost through these surfaces. The surface area of the lateral boundaries of the small models was one-quarter that of the large models, but the injected energy was only one-eighth, making energy losses more significant for the small models. As is shown in Section 7.3, however, these losses are small.

The effect of energy being conducted along the skin of the model was studied numerically using a transient, two-dimensional radial simulation. Energy conducted along the steel sheet had an insignificant

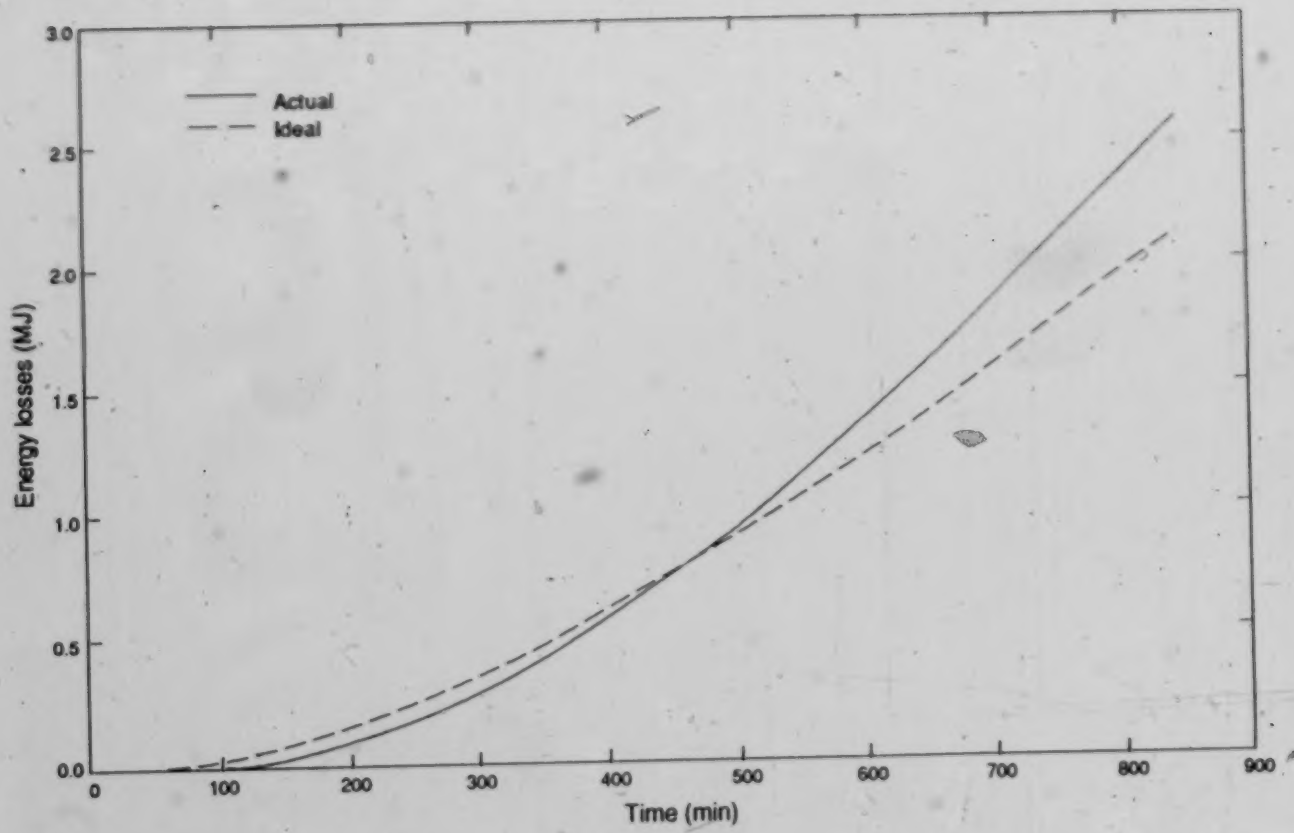

Figure 8. A comparison of the measured and ideal (scaled) heat losses to the surrounding formations for Run 8. Due to the finite thicknesses of the surrounding formations, the actual losses exceed those which are desired in the latter part of the experiment.

effect on the temperature distribution because the sheet was very thin (0.6 mm) and the heat sink created by the surrounding formations was large.

6.8 PRODUCED STEAM QUALITY AND STEAM BREAKTHROUGH

By combining production data, temperature and pressure data, and the energy balance, the quality of steam at the production well was calculated. Until the fluids in the production well reached saturation conditions, the quality of the produced steam was known to be zero. During this time, the unscaled heat losses were estimated from the energy balance. Once the production well was at saturation conditions, the undesired heat losses were assumed to remain the same fraction of the injected energy, and the steam quality at the production well was calculated from the energy balance. This assumes that heat losses had reached steady-state conditions. This may not have been true, particularly for experiments which were shorter and which exhibited early steam breakthrough. For these experiments, it is more likely that the heat losses were increasing because they were still in the transient regime. The accuracy of the estimated heat losses and the frequency of their estimation makes attempts to model them very difficult. The assumption of steady-state based on data obtained just previous to saturation conditions reaching the production well gives the most reasonable estimate. The point in time at which live steam first breaks through at the production well can then be estimated, providing another check in the scaling of steam zone development.

6.9 SCALE-UP OF EXPERIMENTAL RESULTS

The objective of using a scaled experiment is to predict the field response to a particular process. To accomplish this, the experimental results must be scaled up. In order to make comparisons between the results of the large and small models, the results must be expressed on the same scale. This can be achieved either by expressing both sets of results in dimensionless form or by scaling the small model results up so as to predict the large model. Both result in an identical comparison. Scaling up of time, energy, production, temperature, and pressure are outlined below.

6.9.1 Temperature

Temperature is scaled up using the scaling group,

$$T_D = (T - T_i)/(T_{max} - T_i),$$

which normalizes if between its maximum and initial values. Therefore,

$$T_p = (T_{max} - T_i)_p \cdot ((T - T_i)/(T_{max} - T_i))_m + (T_i)_p .$$

The subscripts "p" and "m" refer, in general terms, to a field prototype and a model. By replacing T_p with T_{large} and T_m with T_{small}, temperature in the large model can be predicted from the small model. If the same initial and maximum temperatures are used in the model and the field or in the large model and the small model, the direct readings of temperature can be used for predictions (i.e. $T_p = T_m$).

6.9.2 Time

Time is scaled using the group,

$$t_D = (tW_{st}/\phi\rho_o HL^2),$$

which relates time to the injection rate and the pore volume. Therefore,

$$t_p = (tW_{st}/\phi\rho_o HL^2)_m \cdot (\phi\rho_o HL^2/\tfrac{1}{8}W_{st})_p$$

or

$$t_{large} = (tW_{st}/\phi\rho_o HL^2)_{small} \cdot (\phi\rho_o HL^2/W_{st})_{large}$$

where the subscripts "large" and "small" refer to the large and small models, respectively. The "one-eighth" which appears in the relationship for time between the prototype and the model results from representing the field by a one-eighth element of symmetry. The quantity, ϕHL^2, was determined from the measurements of pore volume and porosity. This minimizes the influence of small variations in model dimensions. For the purpose of comparing the results of the large and small models, $t_D=0$ was considered to be the instant in time at which production started. The delay in start time was approximately one minute from the time that steam was diverted from the bypass to the injection well. The delay was a result of changes in the injection pressure and the collapsing of steam in the injection and bypass lines. This delay was not the same for the small models as the large ones, consequently the most consistent technique for matching the start time of the experiments

was to match the times at which the injection wells reached steam saturation temperature.

6.9.3 Energy

Energy in the reservoir, lost to the surrounding formations, injected, or produced is scaled up using the scaling group,

$$E_D = (E/\phi\rho_w h_{st} HL^2),$$

which relates the calculated energy to the energy contained in one pore volume of steam. Scaling of energy is calculated as:

$$(\tfrac{1}{8} E)_p = (E/\phi\rho_w h_{st} HL^2)_m \cdot (\phi\rho_w h_{st} HL^2)_p$$

or

$$E_{large} = (E/\phi\rho_w h_{st} HL^2)_{small} \cdot (\phi\rho_w h_{st} HL^2)_{large}$$

The representative enthalpy used in comparing the large and small models was the enthalpy of steam at the injection temperature of 230°C. Again, the one-eighth term results from using an element of symmetry.

6.9.4 Production Rate

Production rate is scaled using the group,

$$(W_{pw})_D = (W_{pw}/W_{iw}),$$

which relates the production rate and the injection rate. Scale up of production rate is calculated as:

$$(W_{pw})_p = (W_{pw}/W_{iw})_m \cdot (W_{iw})_p \ .$$

By replacing W_p with W_{large} and W_m with W_{small}, production rate in the large model can be predicted from the small model.

6.9.5 Cumulative Production

Cumulative production is scaled using the group,

$$(Q_{pw})_D = (Q_{pw}/\phi HL^2) \ .$$

This leads to:

$$(\tfrac{1}{8} Q_{pw})_p = (Q_{pw}/\phi HL^2)_m \cdot (\phi HL^2)_p$$

or

$$(Q_{pw})_{large} = (Q_{pw}/\phi HL^2)_{small} \cdot (\phi HL^2)_{large}$$

6.9.6 Pressure

Injection pressure and pressure drop are scaled using the groups,

$$(p_{iw})_D = p_{iw}/p_R$$

$$\Delta p_D = \Delta p/p_R \ .$$

In theory, any representative pressure can be used to non-dimensionalize pressure. An important consideration when selecting a representative pressure is to ensure that the fluid properties which depend on pressure are properly scaled. This is discussed in Section 5.2.2. Often, previous investigators have scaled pressure using $\Delta p/(p_{max}-p_{pw})$, thereby forcing the dimensionless pressure between 0.0 and 1.0. This assumes that the injection pressure does not affect the process or that it is specified by another scaling requirement. It is also important to select a representative pressure which does not depend on the accuracy of satisfying the design requirements of the model. For example, if the maximum injection pressure is selected, its value will not only depend on the design of the experiment but on the modeller's ability to represent permeability, wells, and other practical aspects of the experiments. The representative pressure selected for use in this study is the saturation pressure of steam at the injection temperature of 230°C.

7. PRESENTATION AND DISCUSSION OF EXPERIMENTAL RESULTS

As discussed in Section 5.1, the experimental program was performed in two stages. Phase I consisted of 30 experiments, and was used to study four scaling approaches in which steam was injected into cold, completely water-saturated sand. Four injection rates, spanning a typical range for field steamflood operations were examined. In the second phase, three scaling approaches using one injection rate were studied. The reservoir was 85% saturated with oil.

Each model was prepared as outlined in Section 5.2.4. The operating conditions and model characteristics specific to each experiment are listed in Table 12. The scaled injection rates varied from 6.9 m^3/day to 110 m^3/day in field terms. Production pressure during the water-only experiments was approximately 1700 kPa and during the oil experiments, 400 kPa. The desired absolute permeabilities for the large model, Approach #1, Approach #2, and Approach #3 were 2.0 μm^2, 4.0 μm^2, 2.0 μm^2, and 2.0 μm^2, respectively. Desired porosity for all the models was 36%. The desired initial formation temperature was 27°C and the desired initial oil saturation was 85% for the oil experiments. The measured values of these parameters for each experiment are listed in Table 12.

The results of these experiments are reported and discussed in the following sections. The capabilities of each approach were analyzed by comparing the results of large model experiments to those predicted using the results from smaller scaled models and each of the scaling approaches. These comparisons were made for a number of different

Table 12. Characteristics of each experimental run.

Run #	Scaling Approach	Model Size (cm)	Injection Rate (cm^3/s)	Production Pressure (kPa)	Absolute Permeability (darcy)	Porosity	Pore Volume (cc)	Initial Water Saturation	Initial Temperature (°C)	Overburden Type	Over/Underburden Energy @ t_D=2 (% of injected)	Steam Breakthrough (t_D)	Final Oil Saturation
7		60x10	0.400	1700	2.2	0.360	3338.8	1.0	24.0	G & B	33	0.82	
11		60x10	0.400	1700	2.2	0.360	3338.8	1.0	27.0	G & B	32	0.67	
8		60x10	0.100	1965	2.2	0.360	3338.8	1.0	27.4	G & B	60	----	
9		60x10	0.800	1700	2.2	0.360	3338.8	1.0	26.2	G & B	18	0.55	
40		60x10	0.800	1700	2.0	0.362	3230.9	1.0	26.2	G & B	19	0.60	
44		60x10	0.800	1700	1.9	0.360	3147.3	1.0	26.2	G & B	19	0.61	
10		60x10	1.600	1600	2.2	0.360	3338.8	1.0	25.2	G & B	14	0.43	
12	#2	30x5	0.200	1700	3.0	0.377	418.7	1.0	27.3	G & B	36	1.02	
16	#2	30x5	0.200	1700	3.0	0.377	418.7	1.0	26.3	G & B	37	1.06	
13	#2	30x5	0.050	1965	3.0	0.377	418.7	1.0	28.8	G & B	70	----	
14	#2	30x5	0.400	1700	3.0	0.377	418.7	1.0	24.6	G & B	23	0.79	
37	#2	30x5	0.400	1700	2.2	0.366	399.8	1.0	26.2	G & B	22	0.68	
38	#2	30x5	0.400	1700	2.2	0.366	399.8	1.0	33.1	G & B	22	0.62	
15	#2	30x5	0.800	1600	3.0	0.377	418.7	1.0	28.4	G & B	17	0.91	
17	#3	30x2.5	0.100	1700	3.4	0.410	204.9	1.0	28.1	G & B			
21	#3	30x2.5	0.100	1700	3.4	0.410	204.9	1.0	25.7	G & B			
32	#3	30x2.5	0.100	1700	2.8	0.363	196.6	1.0	31.2	G & B			
36	#3	30x2.5	0.100	1700	2.8	0.363	196.6	1.0	29.9	G & B			
18	#3	30x2.5	0.025	1965	3.4	0.410	204.9	1.0	29.0	G & B	69	----	
33	#3	30x2.5	0.025	1965	2.8	0.363	196.6	1.0	29.3	G & B	101	----	
19	#3	30x2.5	0.200	1700	3.4	0.410	204.9	1.0	25.8	G & B	39	1.08	
34	#3	30x2.5	0.200	1700	2.8	0.363	196.6	1.0	29.4	G & B	43	1.15	
20	#3	30x2.5	0.400	1600	3.4	0.410	204.9	1.0	27.6	G & B			
35	#3	30x2.5	0.400	1600	2.8	0.363	196.6	1.0	24.3	G & B			
46	#3*	30x2.5	0.200	1700	2.8	0.363	196.6	1.0	27.2	G & W	30	0.83	
22	#4	30x7.1	0.283	1700	2.6	0.363	575.9	1.0	26.0	G & B			

Table 12. (continued)

Run #	Scaling Approach	Model Size (cm)	Injection Rate (cm^3/s)	Production Pressure (kPa)	Absolute Permeability (darcy)	Porosity	Pore Volume (cc)	Initial Water Saturation	Initial Temperature (°C)	Overburden Type	Over/Underburden Energy @ t_D=2 (% of injected)	Steam Breakthrough (t_D)	Final Oil Saturation
23	#4	30x7.1	0.071	1965	2.6	0.363	575.9	1.0	28.4	G & B			
24	#4	30x7.1	0.566	1700	2.6	0.363	575.9	1.0	25.2	G & B	17	0.79	
25	#4	30x7.1	1.131	1600	2.6	0.363	575.9	1.0	26.3	G & B			
27	#1	30x5	0.200	1700	4.4	0.357	386.2	1.0	28.1	G & B	38	1.24	
31	#1	30x5	0.200	1700	4.4	0.357	386.2	1.0	28.4	G & B	38	1.33	
28	#1	30x5	0.050	1965	4.4	0.357	386.2	1.0	29.9	G & B	73	----	
29	#1	30x5	0.400	1700	4.4	0.357	386.2	1.0	24.5	G & B	24	0.87	
42	#1	30x5	0.400	1700	5.2	0.393	422.4	1.0	27.7	G & B	22	0.64	
30	#1	30x5	0.800	1600	4.4	0.357	386.2	1.0	26.5	G & B	17	1.07	
41		60x10	0.600	400	2.0	0.362	3230.9	0.146	23.9	G & B	21	0.54	0.17
45		60x10	0.600	400	1.9	0.360	3147.3	0.147	25.6	G & B	18	0.50	0.16
39	#2	30x5	0.300	400	2.2	0.366	399.8	0.126	31.2	G & B	20	0.53	0.12
43	#1	30x5	0.300	400	5.2	0.393	422.4	0.177	25.8	G & B	20	0.59	0.10
47	#3*	30x2.5	0.150	400	2.8	0.363	196.6	0.195	28.2	W & B	27	0.64	0.16

* improved version
G & B - glass and bitumen
W & B - wood particles and bitumen

parameters: temperature distribution, energy distribution, production rate, steam zone size, produced steam quality, steam breakthrough, pressure profiles, and oil-water ratios. The results were expressed in dimensionless form and plotted against dimensionless time. The curves for the large model and each scaling approach were then compared by plotting them on the same figure. More quantitative comparisons were also made by determining the average error in the prediction of each parameter for each approach. These are also presented in the following sections. Some experiments were repeated to demonstrate their repeatability. However, only a few replicate runs were performed because of the expense and length of these experiments. Some replicate runs simply consisted of resaturating the models, while others consisted of rebuilding, repacking, and resaturating the models. These experiments are discussed in one of the following sections.

7.1 APPROACHES #3 AND #4

One of the objectives of the Phase I water-only experiments was to screen the capabilities of each of four scaling approaches for a process that involved many of the complex features of an oil recovery process but which permitted simpler analysis of the results and identification of the causes of scaling differences. Each approach was used to predict steam zone size, production rate, produced steam quality, and energy distribution. The quality of the predictions was then compared. In general, results obtained using Approaches #1 and #2 were satisfactory; these will be discussed in detail in the following sections. Results obtained using Approaches #3 and #4 were much less satisfactory.

The requirements of geometric similarity are relaxed in Approaches #3 and #4. This is done in order to scale gravitational effects in Approach #3 and transverse dispersion in Approach #4. Predictions made using these approaches are compared to the large model results in Figures 9-14. Comparison is made of the various parameters expressed in dimensionless form. The definition of the dimensionless quantity for each parameter was given in Section 6.9. The predictions made in each of these figures using Approach #4 are reasonable, but those made using Approach #3 are poor. The estimated size of the steam zone (shown in Figure 13) is much smaller, and the predicted production rate (shown in Figure 12) as the steam zone develops is much lower. As can be seen in Figure 14, steam is predicted to arrive at the production well much later (large model $t_D \simeq 0.6$, Approach #3 $t_D \simeq 1.2$) and is of a lower quality. Energy losses to the surrounding formations are much higher, and energy contained within the produced fluids is much lower for Approach #3 (see Figures 9 and 11). Too much energy is being transported into the overburden and the underburden using Approach #3, resulting in these inferior predictions.

A review of the theory governing these scaling approaches revealed that when geometric similarity is altered, as is the case in these two approaches, a more detailed scaling development for the boundary conditions of the reservoir is required. The development is given in Appendix G. Rather than design the surrounding formations using the scaling group, (α_c/α_r), which is a ratio of the thermal diffusivities of the reservoir and the cap rock, the conductivity and heat capacity must be scaled independently using the two scaling groups, $(k_{hc}t/(\rho C_p)_c L^2)$ and $(k_{hc}\Delta TL/W_{st}h_w)$.

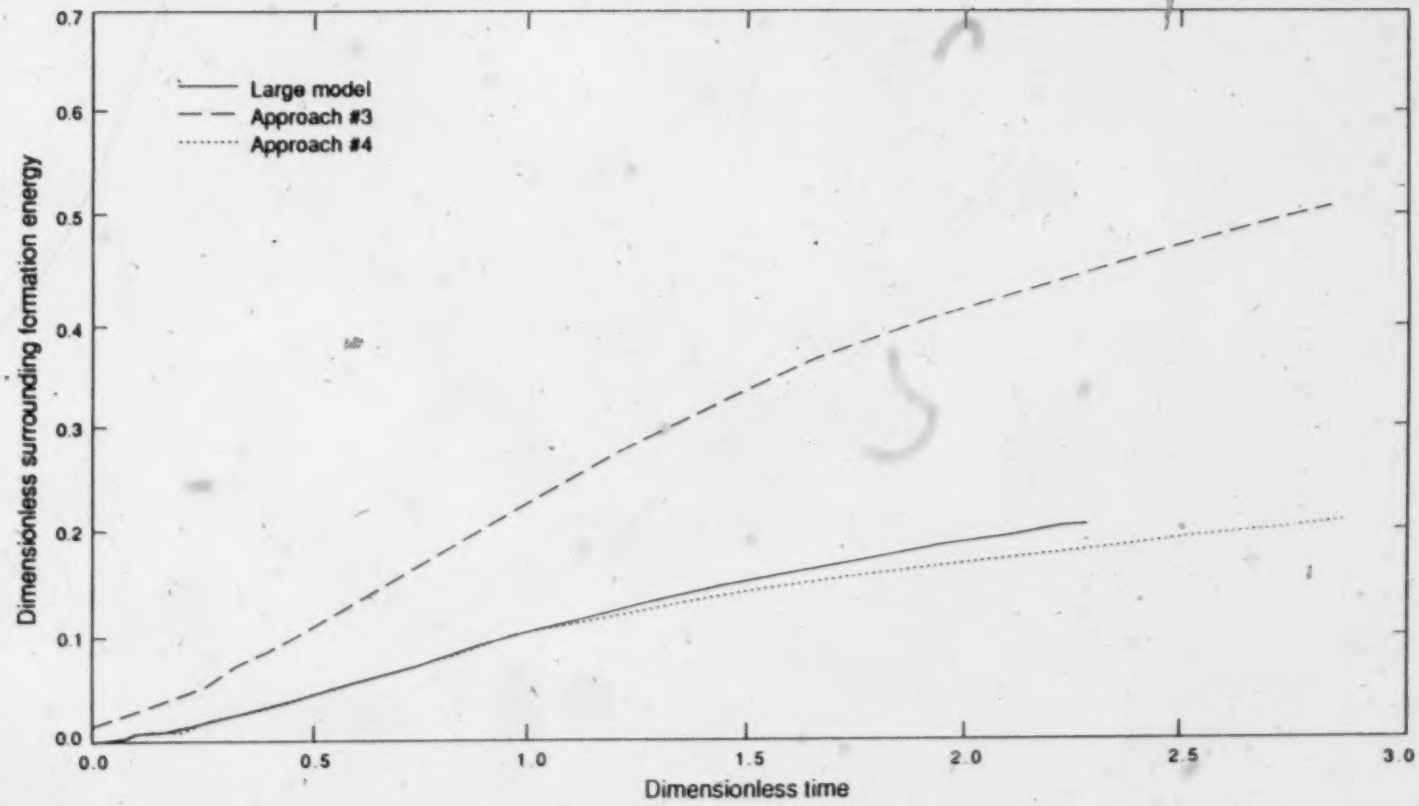

Figure 9. Comparison of the energy losses to the surrounding formations of the large model to those predicted using Approaches #3 and #4 (Runs 44, 34, 24).

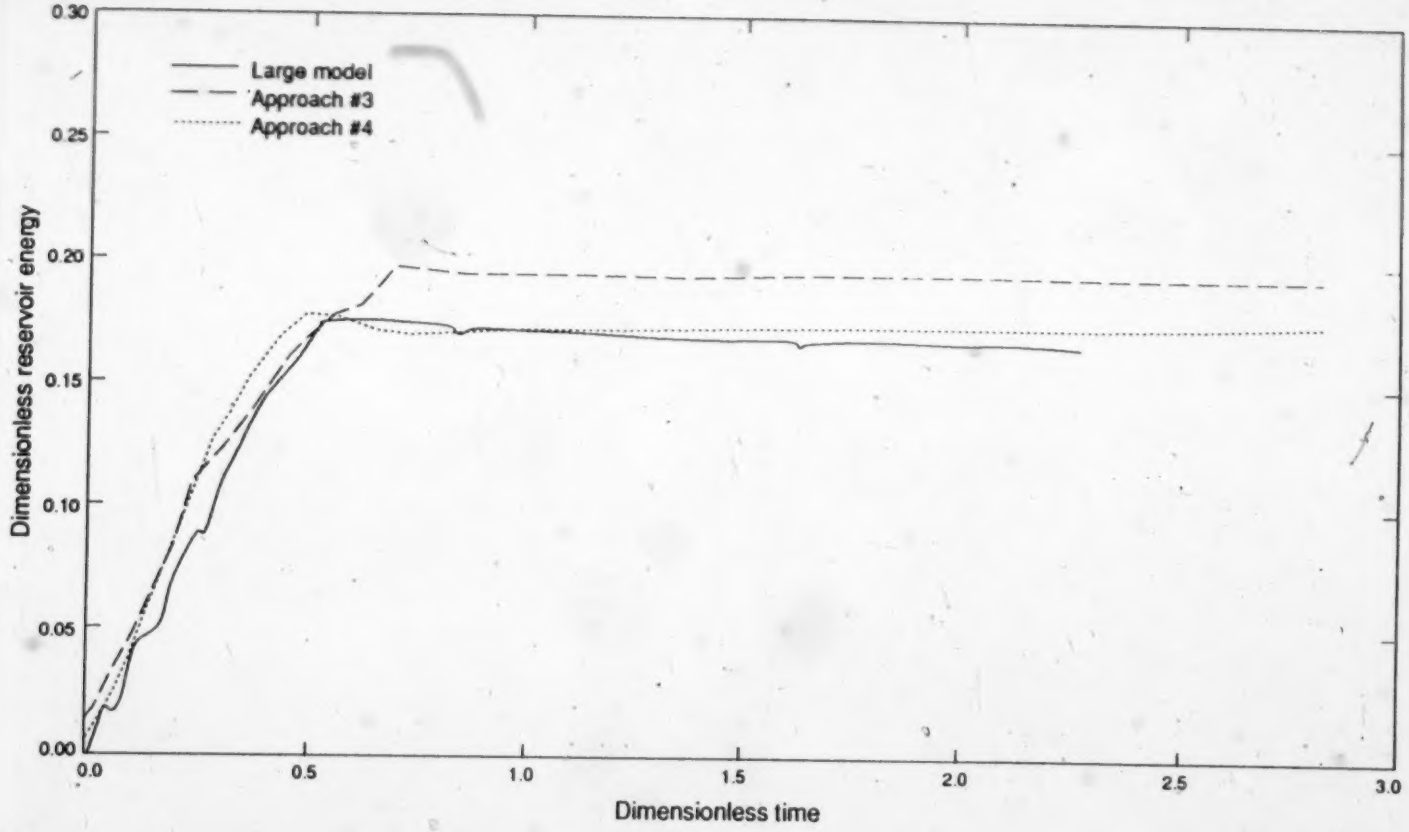

Figure 10. Comparison of the energy contained in the reservoir of the large model to those predicted using Approaches #3 and #4 (Runs 44, 34, 24).

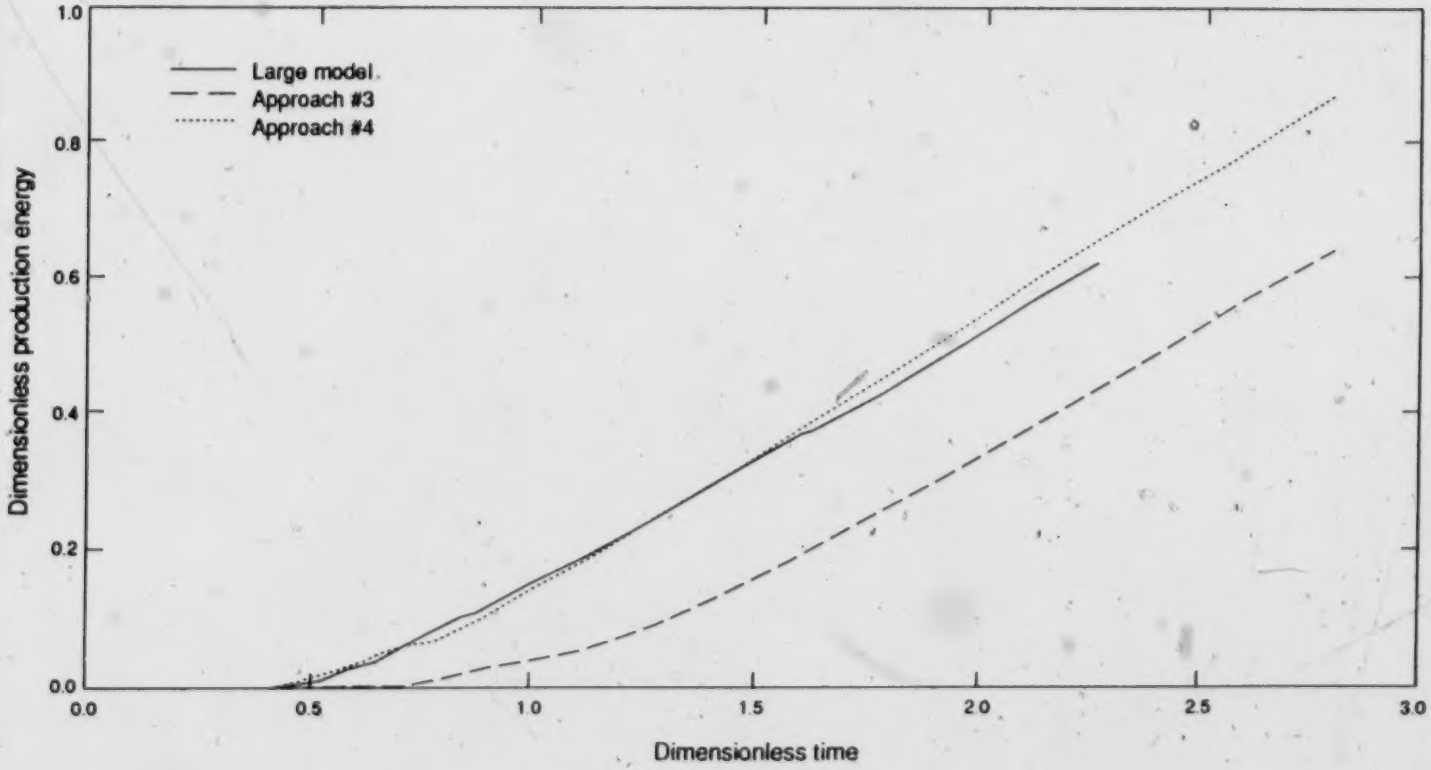

Figure 11. Comparison of the energy contained in the produced fluids of the large model to those predicted using Approaches §3 and §4 (Runs 44, 34, 24).

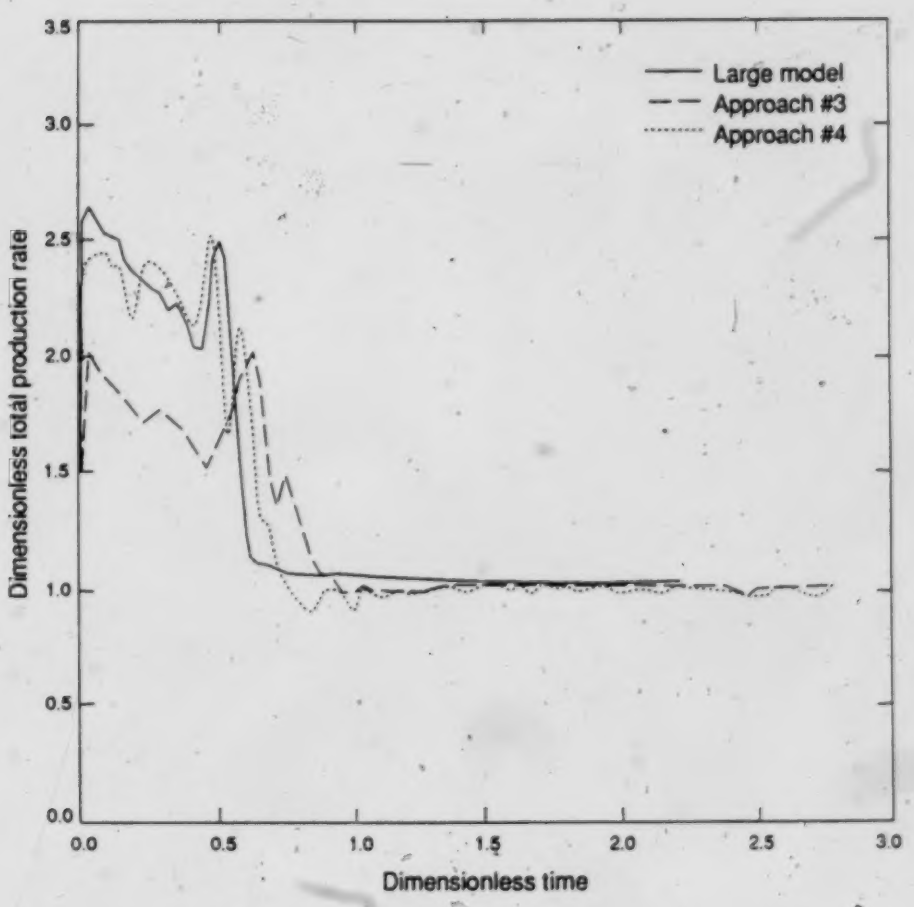

Figure 12. Comparison of the production rate of water and condensed steam in the large model to those predicted using Approaches #3 and #4 (Runs 44, 34, 24).

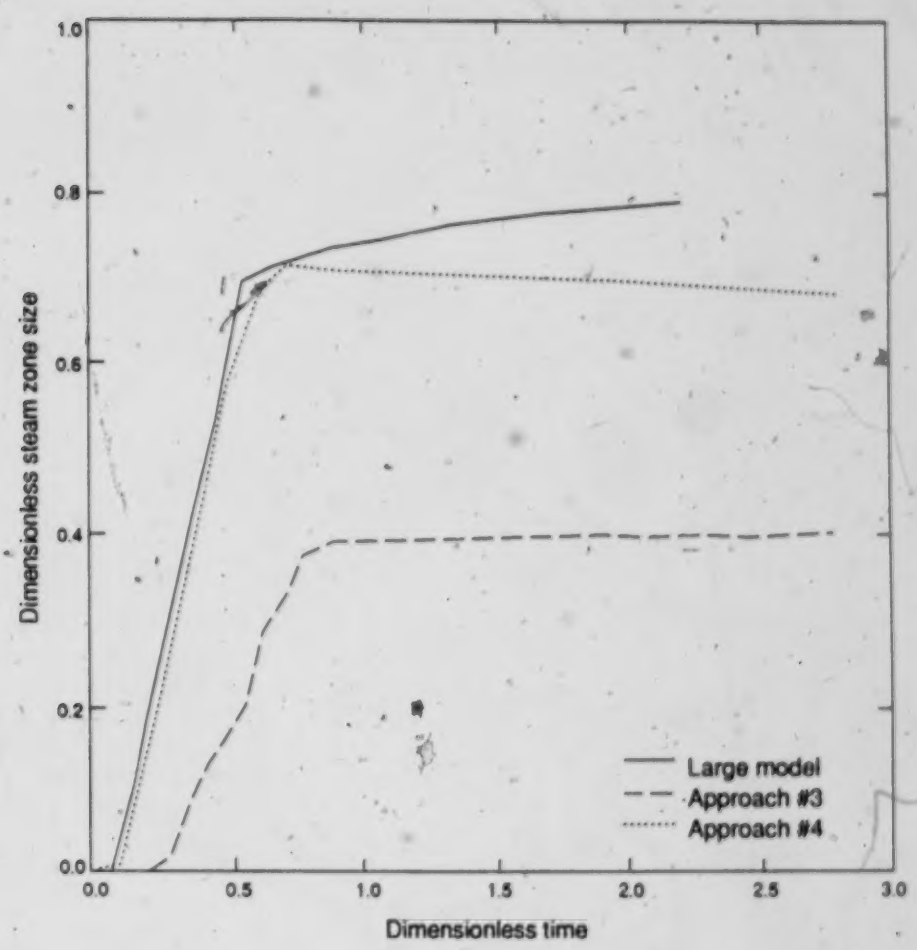

Figure 13. Comparison of the fraction of the reservoir occupied by steam in the large model to those predicted using Approaches #3 and #4 (Runs 44, 34, 24).

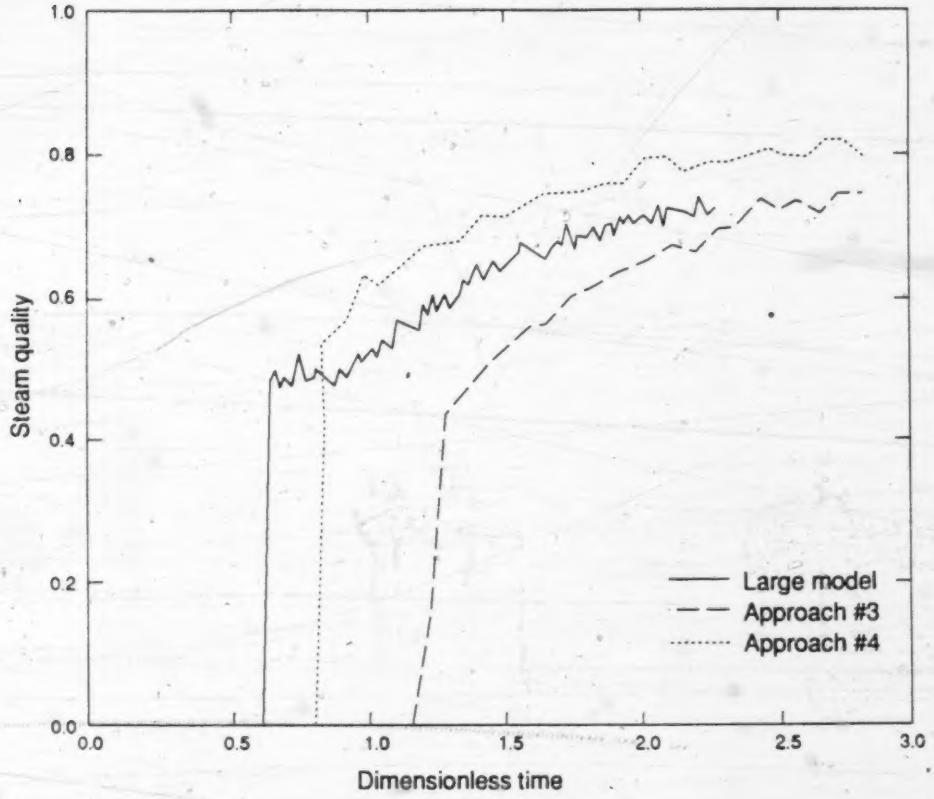

Figure 14. Comparison of the estimated quality of the produced steam from the large model to those predicted using Approaches #3 and #4 (Runs 44, 34, 24).

This design improvement was tested experimentally using Approach #3, the approach for which the change would be most dramatic. The results are shown in Figures 15-20. Redesigning the surrounding formations greatly improved Approach #3. This improved approach as well as Approaches #1 and #2 are discussed in detail in the following sections.

As previously noted, the predictions made using Approach #4 were considerably better than those made using Approach #3, even though both approaches alter geometric similarity (see Figures 9-14). In order to explain this, the requirements of the old design criteria for the surrounding formations were compared with those of the new criteria. Based on this comparison, the energy losses to the surrounding formations should have been overestimated by about 100% when using the old version of Approach #3, and underestimated by about 30% when using the old version of Approach #4. This explains why, even though the old versions of both approaches were in error, Approach #3 gave much less accurate predictions.

7.2 APPROACHES #1, #2 AND #3

In this section, a comparison of the capabilities of Approaches #1, #2, and #3 is presented. Results from the Phase I steam-water experiments as well as those from the Phase II steam-oil-water experiments are presented. Approach #1, which was first developed by Pujol and Boberg, allows the gravitational effects to be scaled but does not allow pressure conditions or any fluid properties that may depend on pressure to be scaled. In order to scale the pressure conditions using Approach

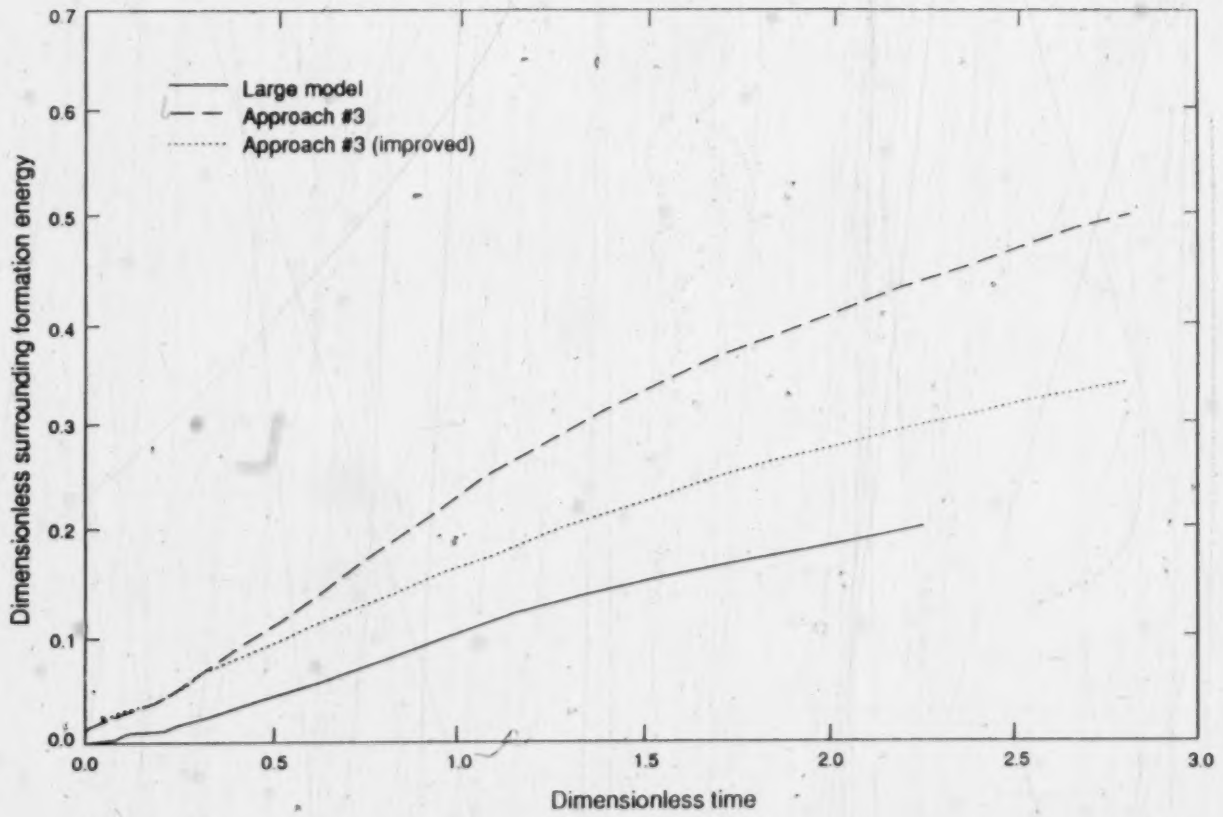

Figure 15. Improvement in predicting energy losses to the surrounding formations using Approach #3 (Run 46).

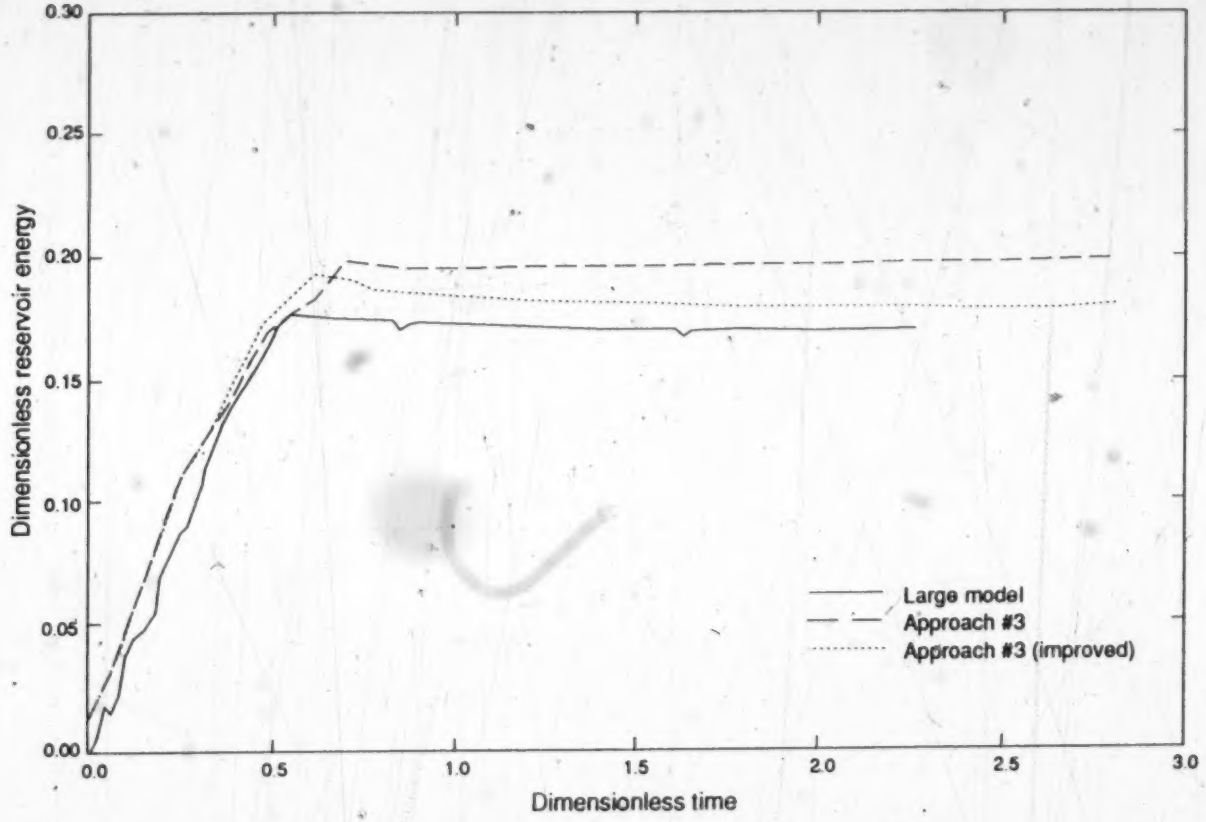

Figure 16. Improvement in prediction of energy contained within the reservoir using Approach #3 (Run 46).

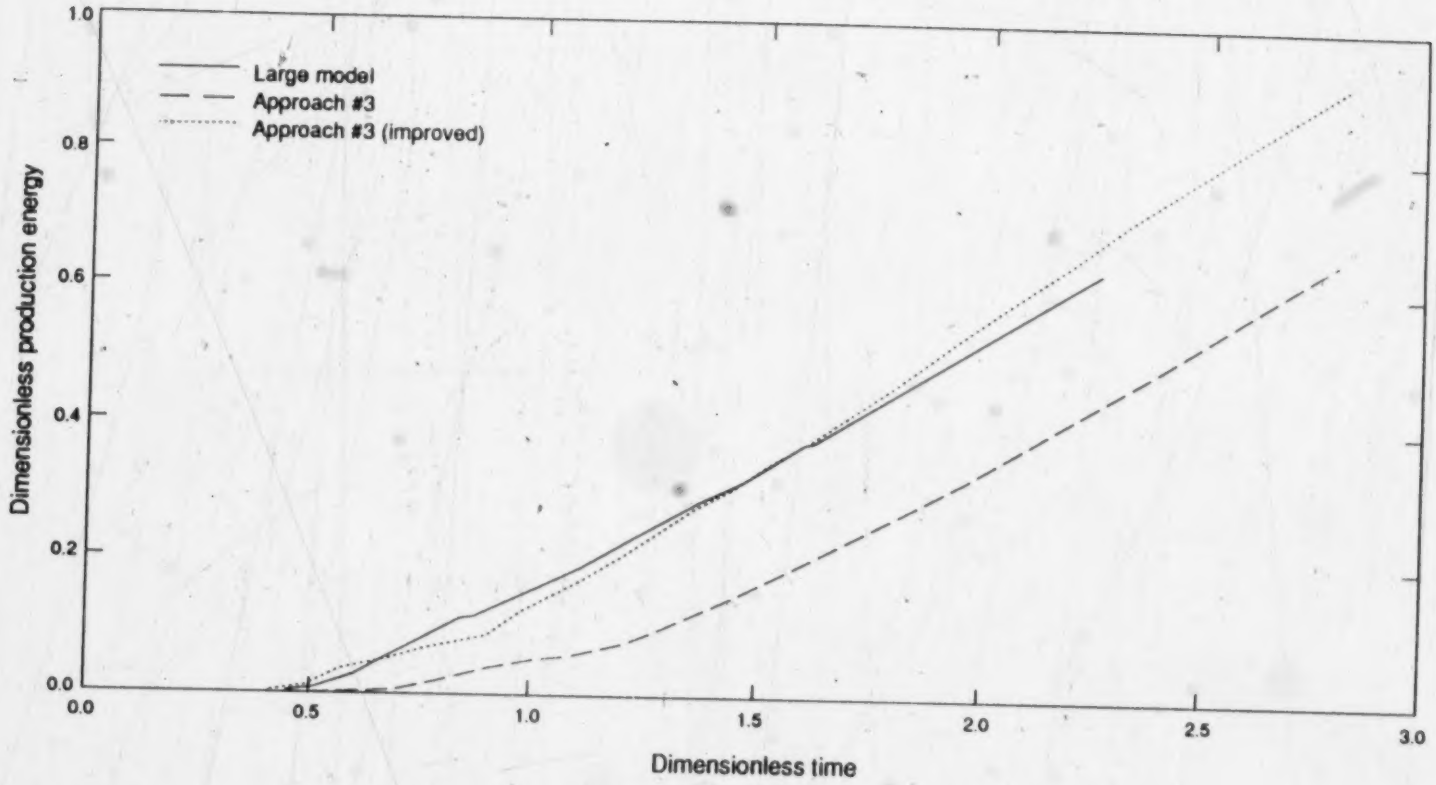

Figure 17. Improvement in predicting energy contained in the produced fluids using Approach #3 (Run 46).

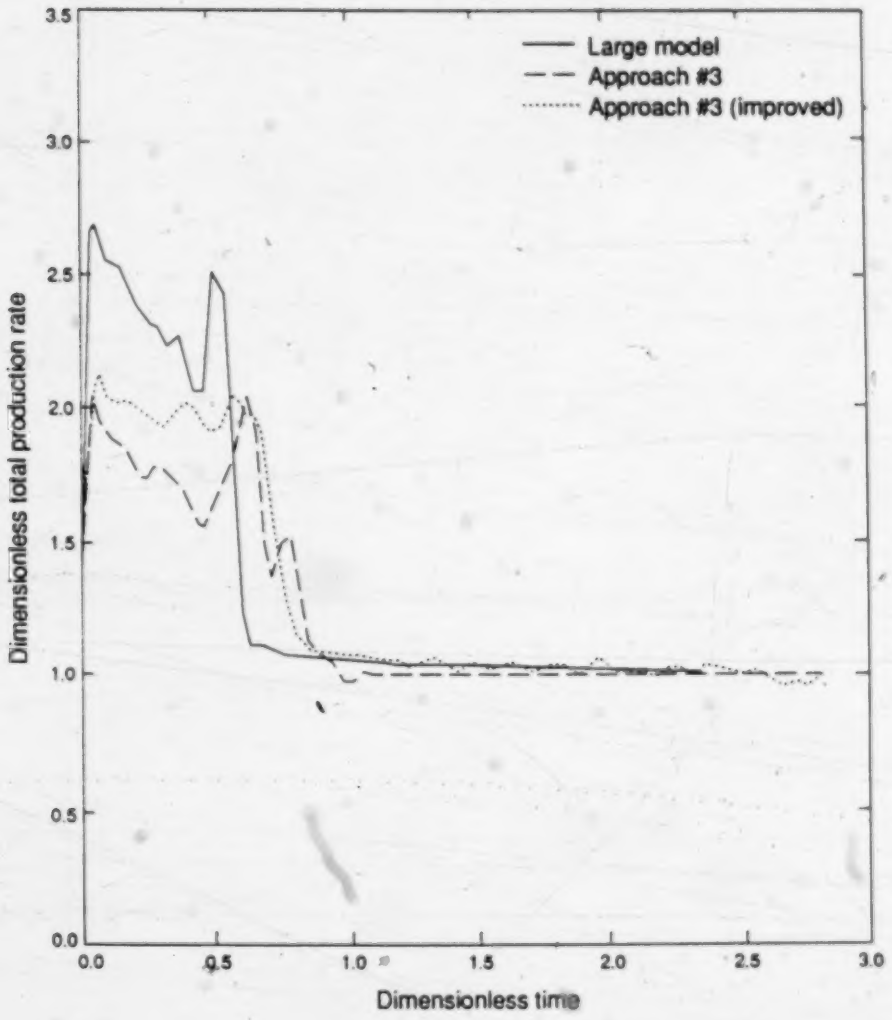

Figure 18. Improvement in predicted production rate using Approach #3 (Run 46).

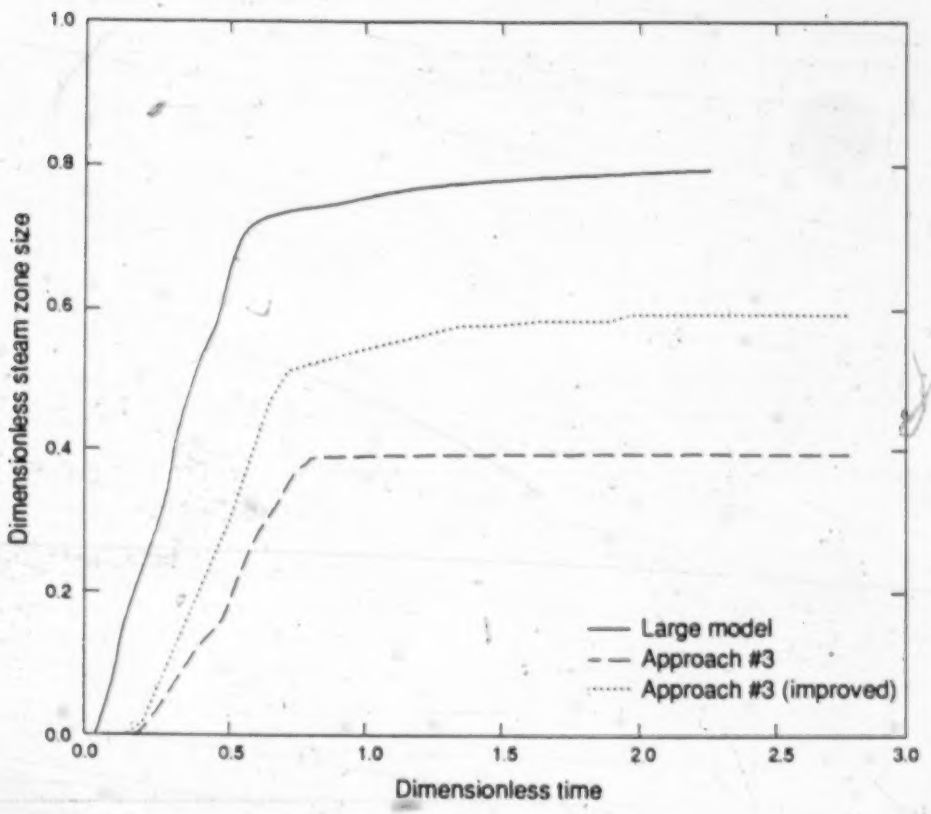

Figure 19. Improvement in prediction of steam zone volume using Approach #3 (Run 46).

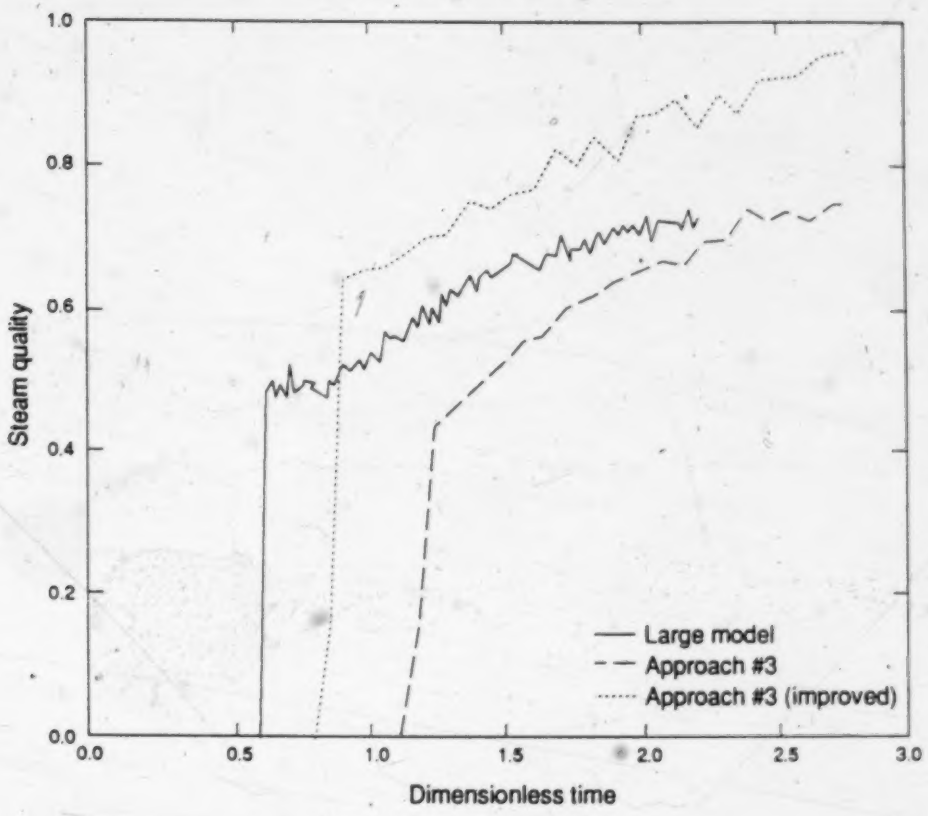

Figure 20. Improved estimate of the quality of the produced steam using Approach #3 (Run 46).

#2, the scaling requirements for the gravitational effects must be relaxed. Using Approach #3, the pressure conditions and the gravitational effects are scaled, but some of the requirements of geometric similarity must be relaxed. More specifically, the reservoir thickness is altered so that both pressure conditions and gravitational effects may be scaled. This approach is subject to a number of restrictive conditions, which together with Approaches #1 and #2, are discussed in detail in Chapter 4. Approaches #2 and #3 permit the use of reservoir porous media in the scaled model; Approach #1 requires an artificial medium.

The ability to predict temperature and energy distributions, steam zone development, production rates, steam breakthrough, produced steam quality, oil-water ratios, and pressure conditions, when using each of the different approaches, is compared in the following sections. The comparisons take the form of plots in which the predictions over the entire duration of the experiments are shown as well as estimates of the average error in predicting each parameter. The comparisons are of dynamic parameters, and as such, should match both in magnitude and in time.

7.2.1 Temperature Distribution

Heat transfer will take place largely due to convection and conduction. Proper scaling is critical in any effort to scale a thermal recovery process. For this reason it is important to scale the thermal properties of the fluids and rock as well as the distribution of fluids.

The temperature distribution is a very good indication of the degree of success achieved in scaling these mechanisms.

The temperature distribution in the large model can be compared to that of the small models at any instant in scaled time. Two-dimensional distributions are compared by taking cross sections through the model. These can be either horizontal or vertical sections. The vertical profiles give an indication of the effects of gravity override, heat losses to the surrounding formations, and the ability of each scaling approach to scale these mechanisms. Horizontal profiles can be used to show the ability of each approach to match horizontal conformance as well as to indicate the stability of the process. One vertical and one horizontal profile was selected. The location of each is shown in Figure 21.

Vertical Profiles. Temperature profiles discussed in this section are for a vertical cross section through the center of the overburden, reservoir and underburden (View A-A, Figure 21). Profiles obtained during the oil experiments are discussed as the degree of gravity override is more severe during these experiments than during the water-only experiments.

In Figure 22, the step-by-step advancement of the steam front in the large model is depicted. Initially, the steam appears to override ($t_D < 0.165$), but at later times this gravitational effect appears to die out ($0.179 < t_D < 0.265$). This observation is a result (at least in part) of the location of the thermocouples. After the steam front passes a

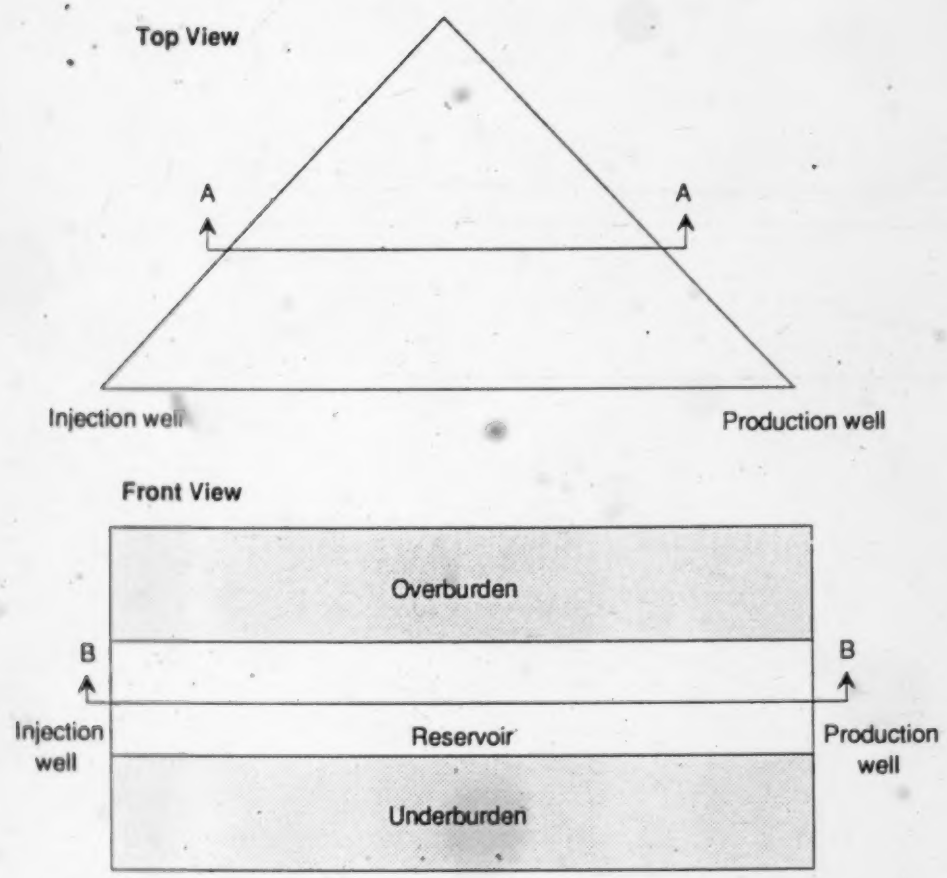

Figure 21. Sectioned views for vertical (View A-A) and horizontal (View B-B) temperature profiles.

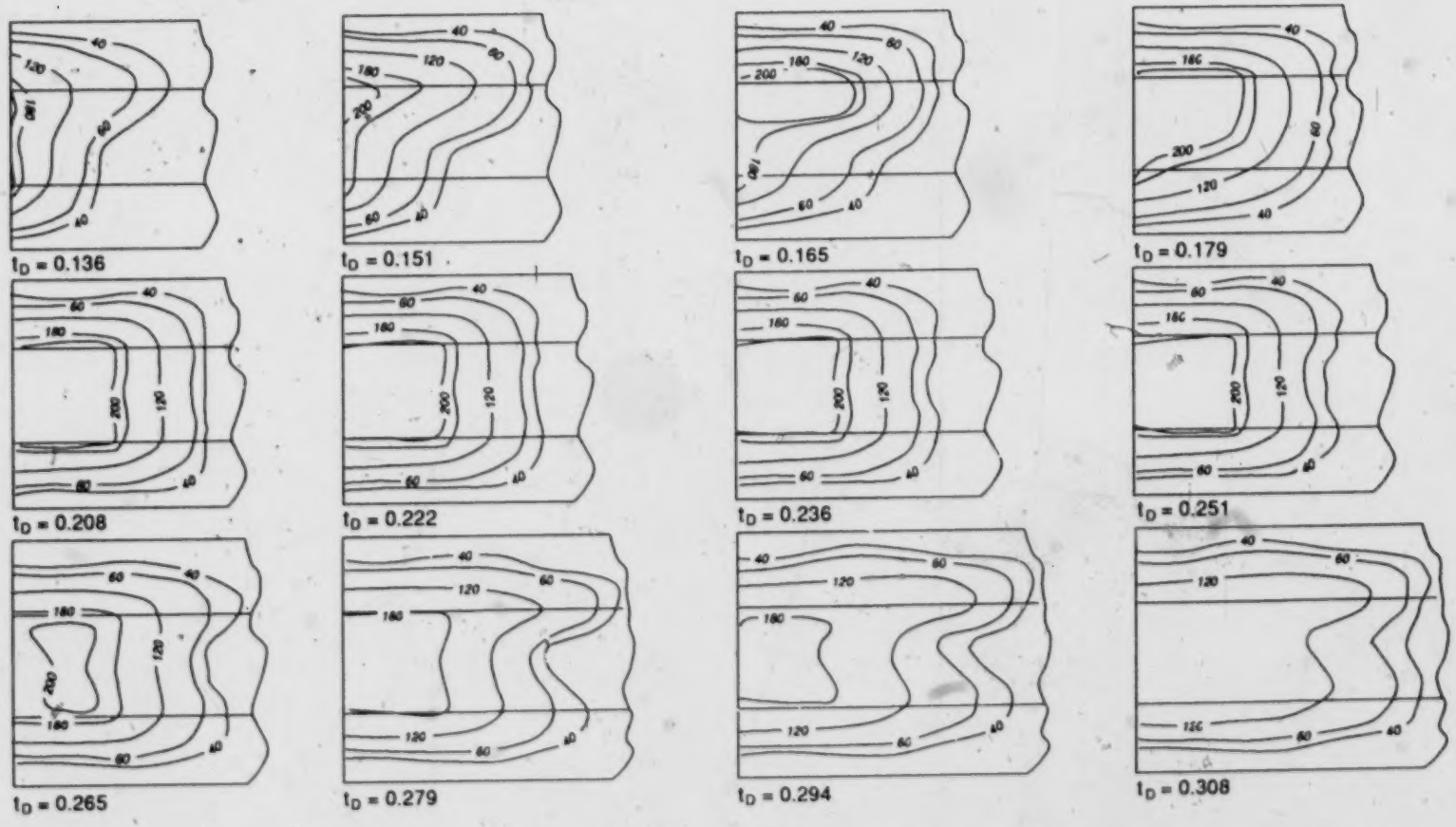

Figure 22. Step-by-step advancement of temperature within the large model (Run 45) during a steam-oil-water experiment.

column of thermocouples, all of them will indicate high temperatures, but before the steam front reaches the next column, the next column will read low temperatures. As a consequence the profiles will not indicate any gravity override even though it may exist. As the steam front advances past the next column of thermocouples, evidence of gravity override again appears ($t_D > 0.279$). Therefore, the shape of the steam front is best represented as the front passes through a column of thermocouples. It can also be seen from the profiles shown in Figure 22, that as warm fluids reach the production well and the pressure drop lowers, the temperatures near the injection well also drop (compare t_D=0.179 to t_D=0.308). This is one illustration of the importance of scaling the pressure conditions; the saturation temperature of steam depends on the pressure distribution.

The ability to predict the shape of these large model temperature profiles at any time using each approach is compared in Figure 23-25. A time step when the steam front is passing a column of thermocouples is selected for each approach. This results in the most realistic picture of the shape of the front. The large model profile that best matches this small model profile is then selected and a comparison of the two dimensionless times is made. If the process is scaled accurately, the times should be identical, but because of experimental variations (practical), inaccurate scaling (theoretical), and a finite number of sampling times (i.e. profile was not recorded at required time), they may not be.

Shown in Figures 23(a) and 23(b) is a comparison of the temperature profile for Approach #2 during an oil experiment, at a dimensionless

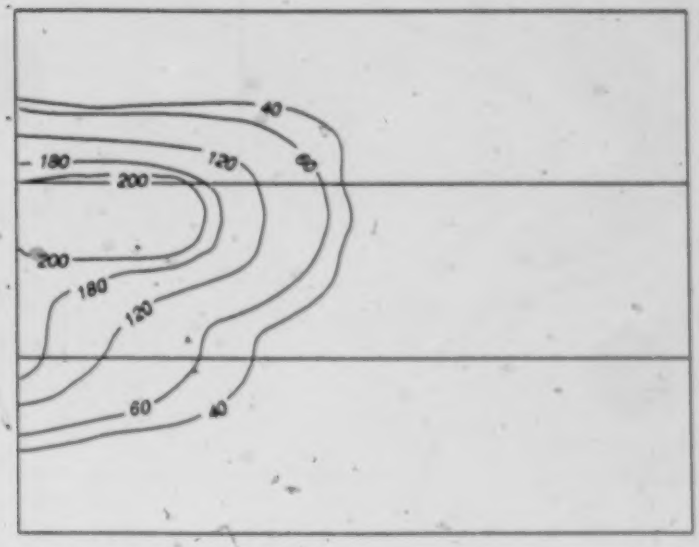

a) Large model, $t_D = 0.165$

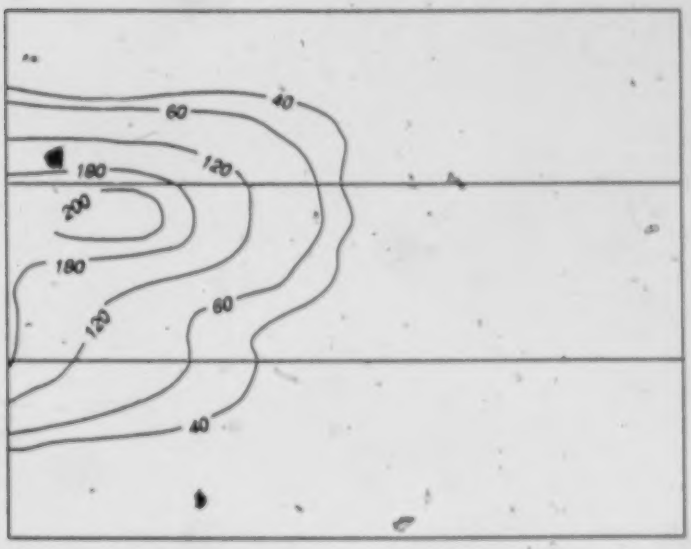

b) Approach #2, $t_D = 0.157$

Figure 23. Comparison of the vertical temperature profile for the large model (Run 45) at t_D=0.165 to that predicted using Approach #2 (Run 39).

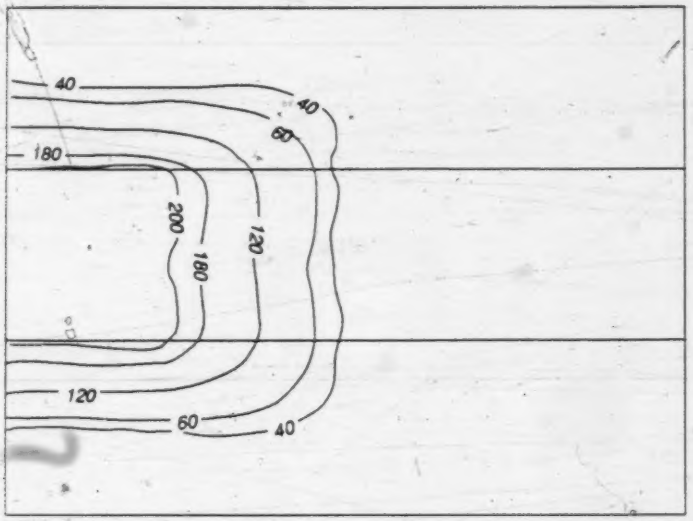

a) Large model, $t_D = 0.208$

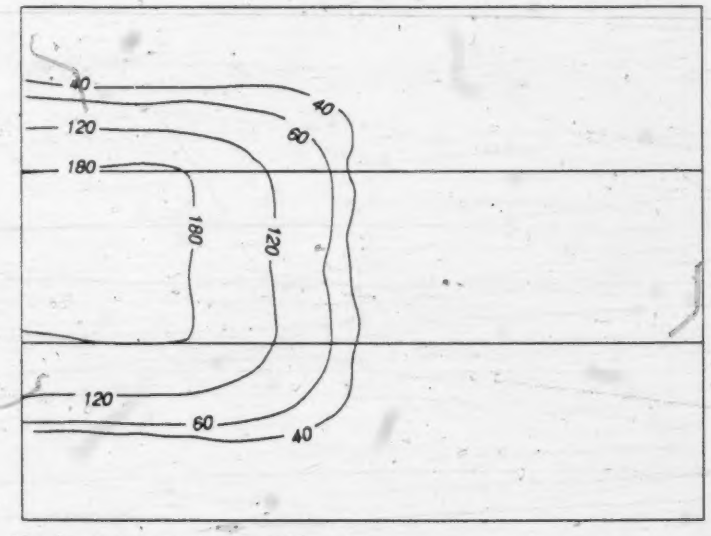

b) Approach #1, $t_D = 0.142$

Figure 24. Comparison of the vertical temperature profile for the large model (Run 45) at t_D=0.208 to that predicted using Approach #1 (Run 43).

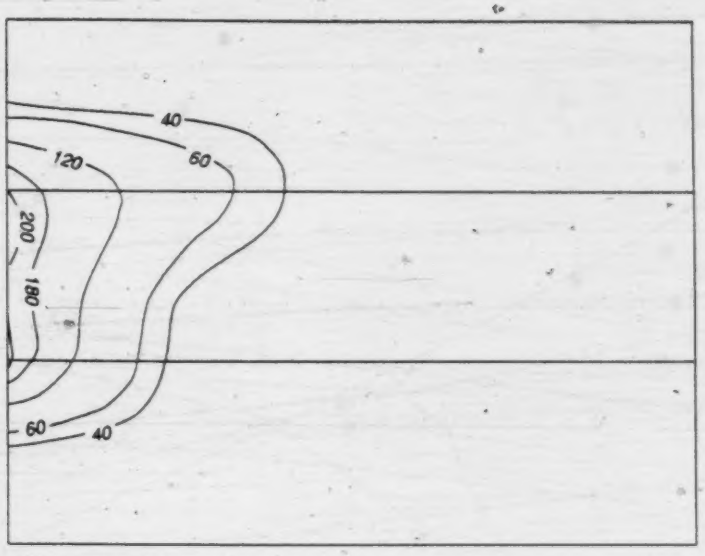

a) Large model, $t_D = 0.136$

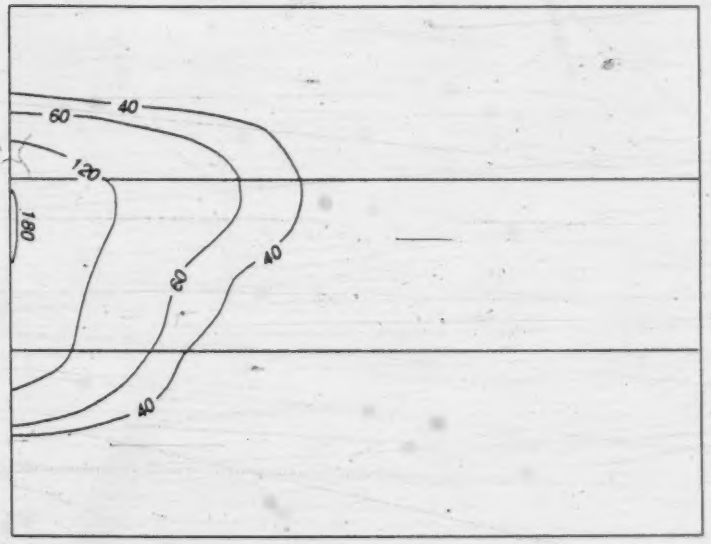

b) Approach #3, $t_D = 0.133$

Figure 25. Comparison of the vertical temperature profile for the large model (Run 45) at t_D=0.136 to that predicted using Approach #3 (Run 47).

time of 0.157, and the best fit for the large model which is at t_D=0.165. The dimensionless time interval for recording data for the large model is 0.014 and a match better than 0.007 should not be expected. Even though scaling of the gravitational effects are relaxed when using Approach #2, the override evident in the large model is well matched using this approach. A similar comparison for Approach #1 is shown in Figures 24(a) and 24(b). A dimensionless time of 0.142 for the small model corresponds with t_D=0.208, the dimensionless time at which the large model profile matches the small model one. Also note that, using this approach, the temperatures near the injection well are lower. Since the pressure conditions are not scaled using this approach, steam temperatures will be in error. This illustrates one of the effects of relaxing the scaling of pressure conditions using Approach #1. Vertical profiles are compared in Figures 25(a) and 25(b) for Approach #3 as well. Using this approach, the temperature profiles for the small model at a dimensionless time of 0.133 match most closely with the large model profiles at a dimensionless time of 0.136.

The dimensionless time differences, $|t_{D_{large}} - t_{D_{small}}|$, between the profiles matched in Figures 23 and 25 for Approaches #2 and #3 are 0.008 and 0.003, respectively. The profile match obtained using Approach #1 led to a much larger difference of 0.066. Similar comparisons were made for temperature profiles obtained at other times during the experiments. Table 13 lists the time of the profile for the small model, the time of the best match of that profile for the large model, and the dimensionless time difference for each case. Using Approach #1 an average difference of 0.093 was obtained; Approach #2, 0.007; and Approach #3, 0.008.

Table 13. Dimensionless time matches for each approach and the associated errors.

Approach	t_D(small)	t_D(large)	$\lvert\Delta t_D\rvert$
1	0.142	0.208	0.066
1	0.196	0.294	0.098
1	0.250	0.365	0.115
2	0.157	0.165	0.008
2	0.213	0.208	0.005
2	0.269	0.279	0.010
2	0.326	0.336	0.010
2	0.382	0.379	0.003
3	0.133	0.136	0.003
3	0.190	0.179	0.011
3	0.248	0.251	0.003
3	0.305	0.294	0.011
3	0.362	0.351	0.011

Horizontal Profiles. Horizontal temperature profiles are also compared. In Figures 26-29, the temperature profiles for a horizontal cross section through the center of the reservoir at four different injection rates are shown. The location of this cross section is shown in Figure 21. Steam is injected at the top left corner and fluids are produced at the lower right corner. An indication of the shape of the steam zone as well as the stability of the displacement can be obtained by examining these profiles. The results for the large model are shown in Figures 26(a)-29(a), with the corresponding predictions for Approaches #1 and #2 shown in Figures 26(b)-29(b) and 26(c)-29(c), respectively. A comparison using Approach #3 is shown in Figure 28(d); this was the only injection rate that was repeated using the improved version of Approach #3. Each profile is selected at the time step which most closely corresponds to a dimensionless time of 0.4.

The profiles shown in Figures 26-29 are for the water-only runs. The location and shape of the temperature profiles are predicted remarkably well using all three approaches. This indicates adequate scaling of heat transfer and fluid distribution within the reservoir. The ability to predict this parameter does not change with increasing injection rate (i.e. the quality of the predictions remains the same in Figures 26 through 29). However, because the time step increases with increasing injection rate, the ability to match times for the purpose of comparison becomes more difficult at higher rates.

For the same quantity of injected steam, the size of the steam zone becomes larger as the injection rate is increased. This is expected

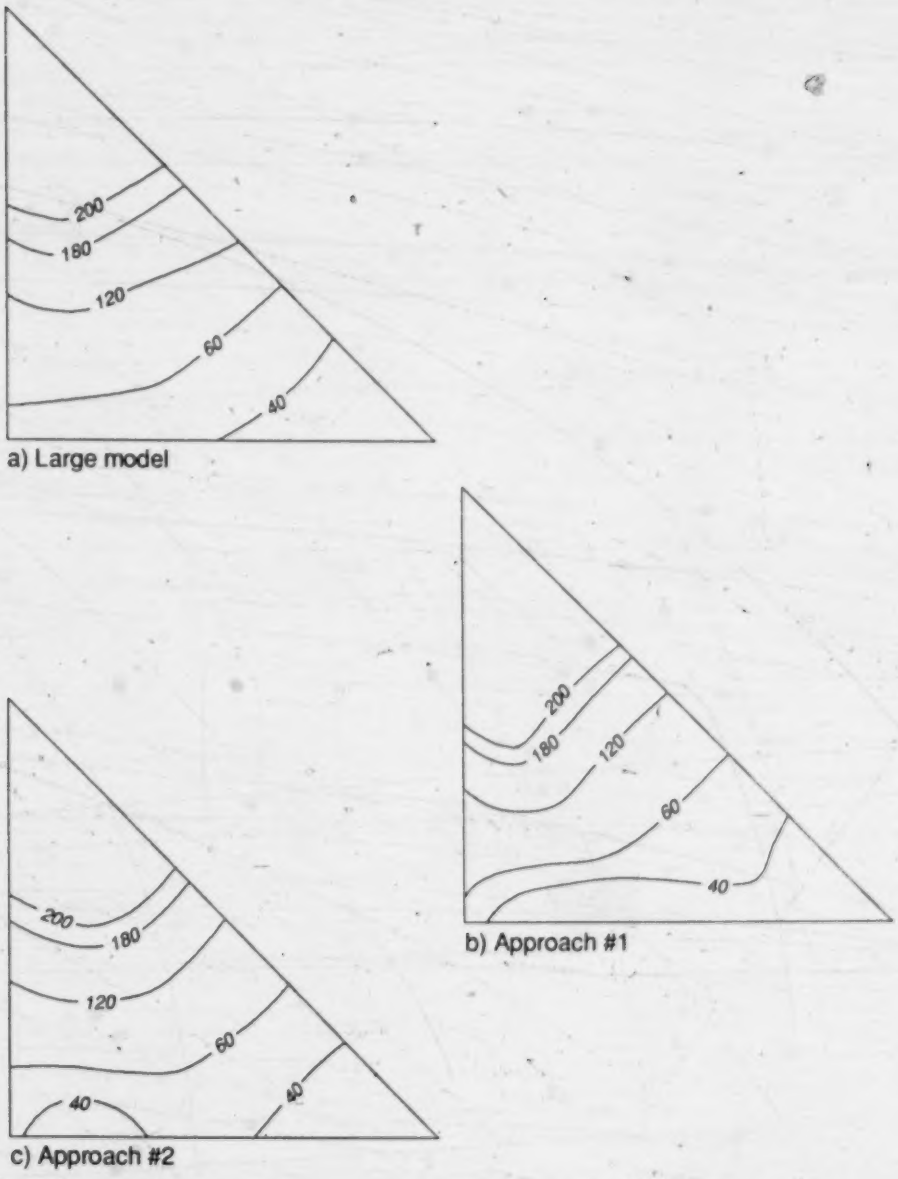

Figure 26. Comparison of the horizontal temperature profile for the large model (Run 8) to those predicted using Approach #1 (Run 28) and #2 (Run 13) at t_D=0.400. The scaled injection rate was 6.9 m^3/day for each.

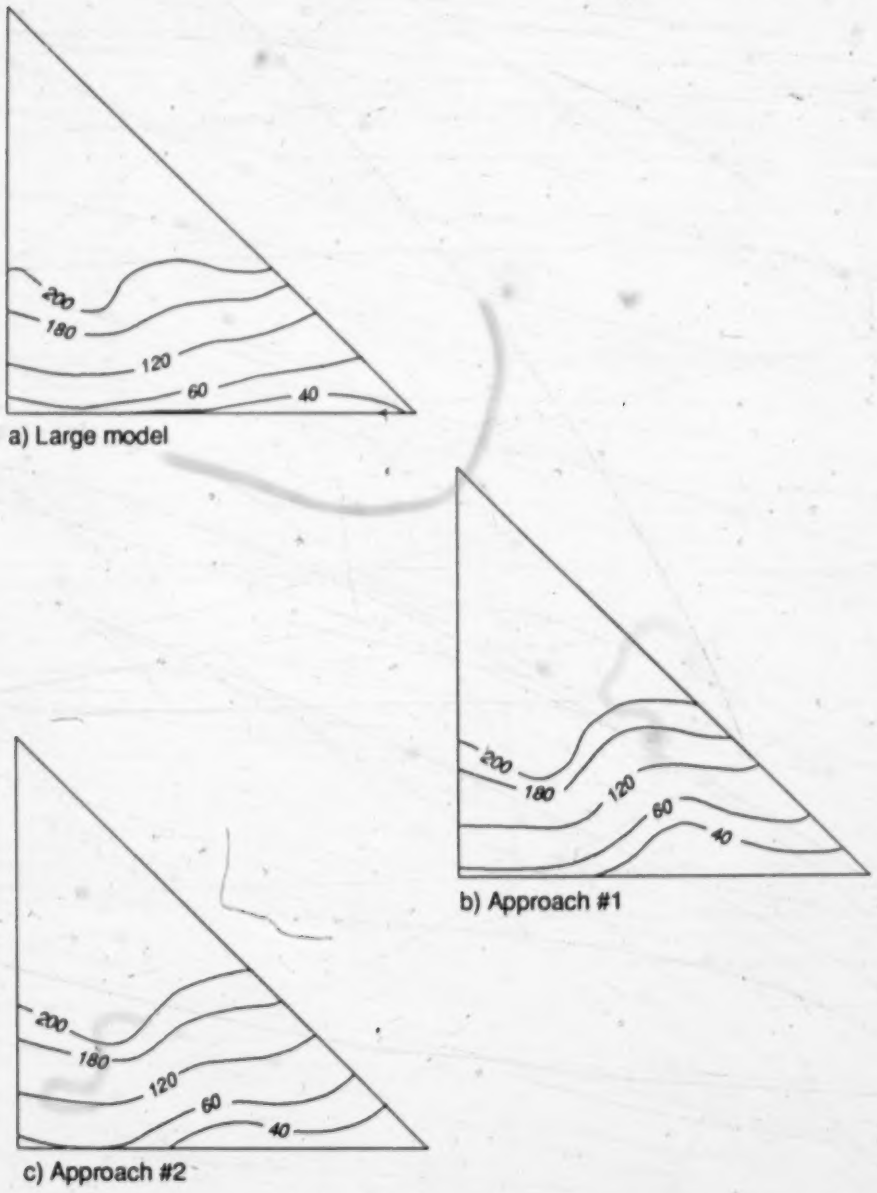

Figure 27. Comparison of the horizontal temperature profile for the large model (Run 11) to those predicted using Approach #1 (Run 27) and #2 (Run 16) at t_D=0.400. The scaled injection rate was 27.6 m^3/day for each.

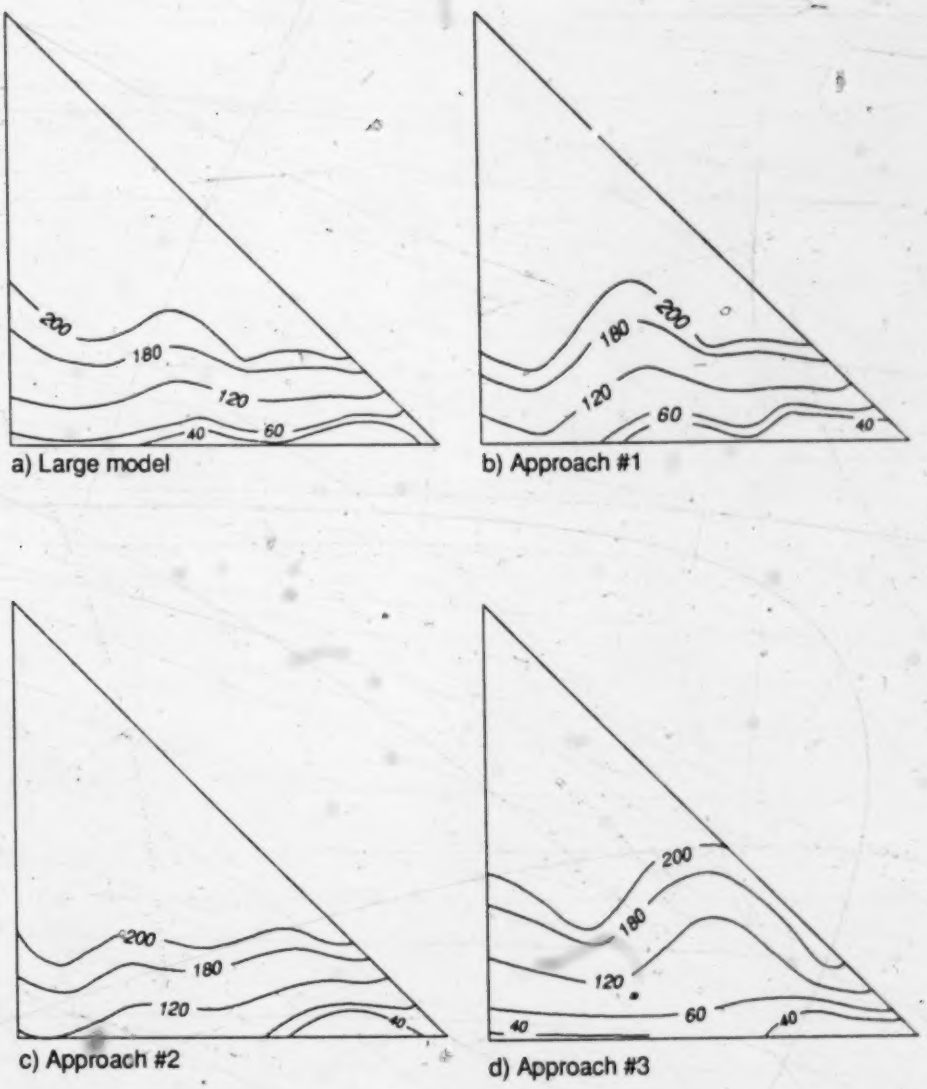

Figure 28. Comparison of the horizontal temperature profile for the large model (Run 44) to those predicted using Approach #1 (Run 42), #2 (Run 38) and #3 (Run 46) at t_D=0.400. The scaled injection rate was 55.3 m^3/day for each.

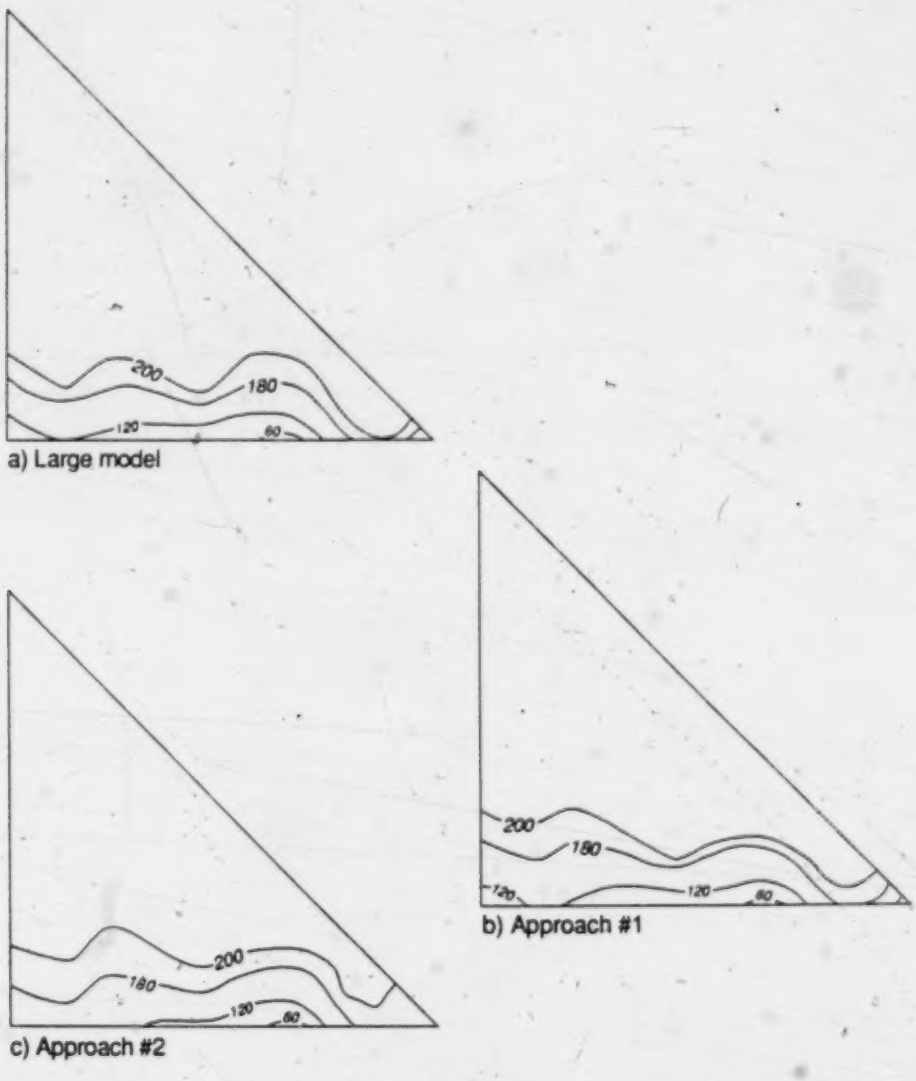

Figure 29. Comparison of the horizontal temperature profile for the large model (Run 10) to those predicted using Approach #1 (Run 30) and #2 (Run 15) at t_D=0.400. The scaled injection rate was 110.6 m^3/day for each.

because the fraction of the injected energy lost to the overburden and the underburden becomes smaller. As the steam zone advances, it is initially very radial in shape (see 200°C profiles in Figure 26) but as it moves toward the production well the five-spot geometry modifies this shape.

A similar comparison is shown in Figure 30 for the oil experiments. Using the scaling approaches, a good match for the temperature distributions is obtained again. Good predictions of both the shape of the profiles as well as the dimensionless time at which they match are obtained using Approaches #2 and #3. Approach #1 does not match as accurately, particularly near the production well. In this region the contours rely on the measurements of one or two thermocouples which if in error (i.e. malfunction or incorrectly positioned) can produce inaccurate profiles. A comparison of Figure 30 with Figures 26-29 reveals that with the presence of oil, the steam zone is less radial in shape and advances toward the production well more quickly.

7.2.2 Energy Distribution

Closely related to temperature distribution is the energy distribution. The unscaled energy distribution, for the lowest injection rate into the large model for the water-only case, is shown in Figure 31. The energy injected, the energy existing in the reservoir, underburden and overburden, and the energy produced are shown. The sum of these energies is shown as the total curve and represents the energy balance. The difference between the injected energy curve and the total curve represents

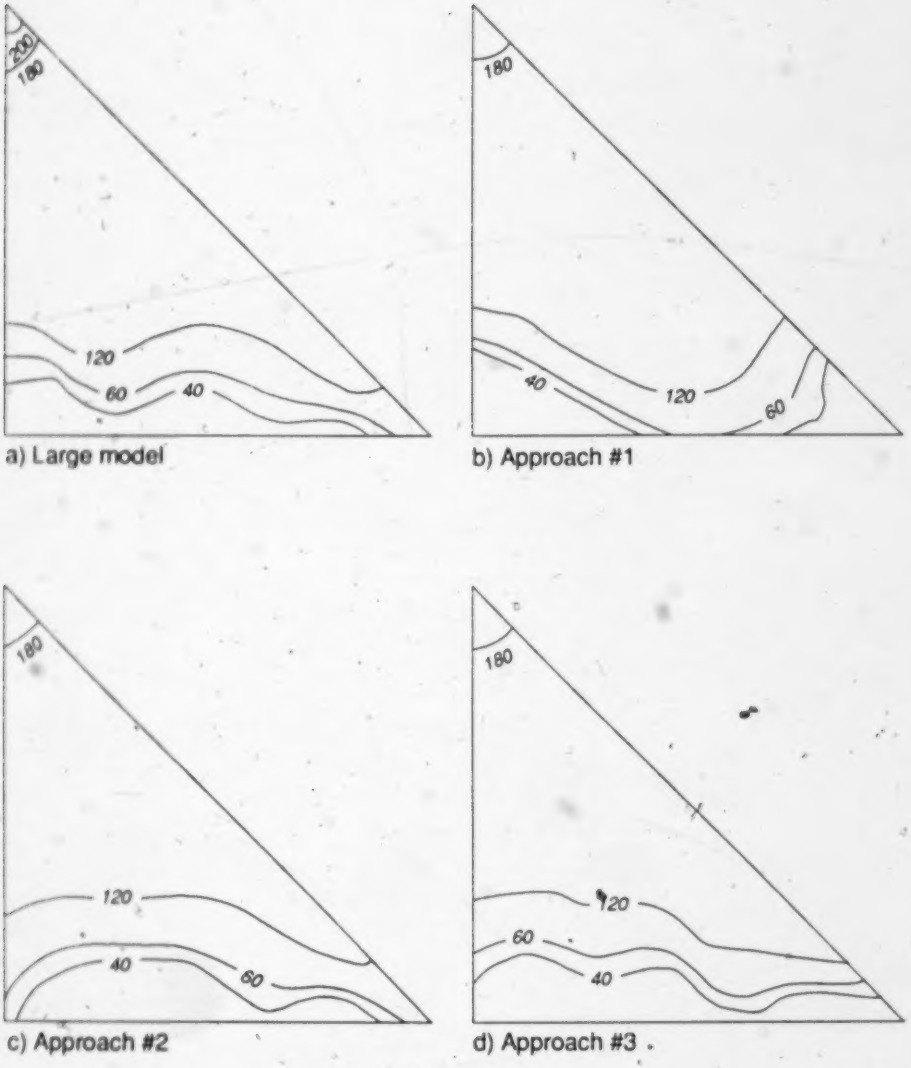

Figure 30. Comparison of the horizontal temperature profiles for the steam-oil-water experiments. The large model (Run 45) and Approaches #1 (Run 43), #2 (Run 39) and #3 (Run 47) are shown at t_D=0.300 for scaled injection rates of 41.5 m^3/day.

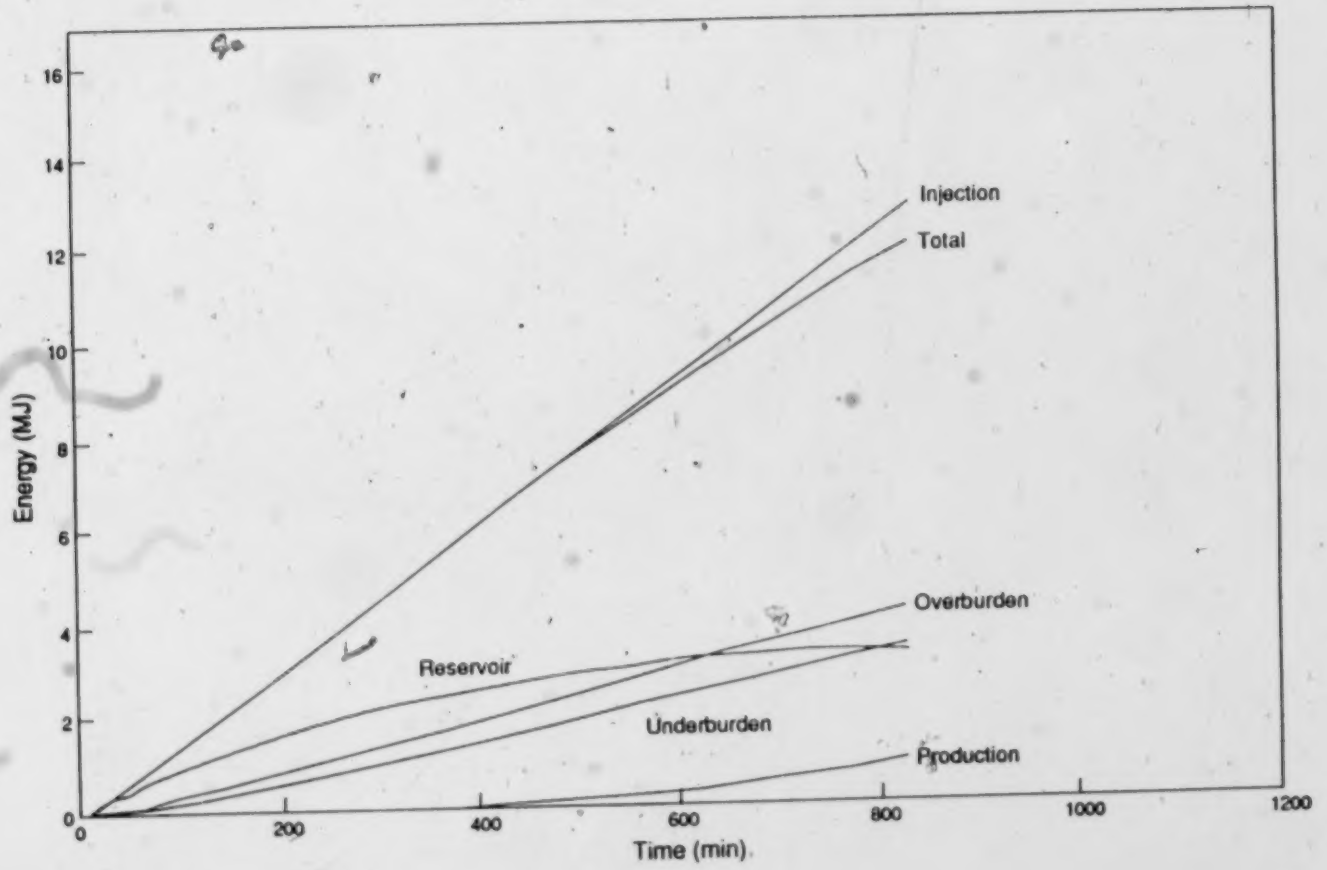

Figure 31. Energy distribution during a large model experiment (Run 8) at an injection rate of 6.9 m^3/day.

unaccounted energy losses such as that to the insulation surrounding the model.

In order to scale a thermal recovery process, in addition to supplying the correct amount of energy to the reservoir, the energy must be distributed to the proper areas at the correct scaled times. The energy contained in the overburden, the underburden, the reservoir, and the produced fluids are compared for each approach in Figures 32-37.

The energy lost to the surrounding formations (overburden and underburden), as predicted using each approach, is compared in Figures 32 and 33 to the actual losses for the large model. A series of water-only experiments with scaled injection rates of 55.3 m^3/d is shown in Figure 32. In Figure 33, the series of oil experiments with rates of 41.5 m^3/d are compared. It can be seen in both figures that these losses are slightly overestimated using the scaling approaches. In both cases, these losses are predicted most accurately using Approach #2, followed closely by Approach #1. The least accurate predictions of energy lost to the surrounding formations are obtained when using Approach #3. This illustrates one of the serious practical drawbacks associated with Approach #3. The scaling requirements for design of the surrounding formations using this approach are much more difficult to satisfy, and therefore, a greater error in predicting the energy losses is to be expected.

The amount of energy contained within the reservoir of the large model and the predictions made using each approach are compared in Figures 34

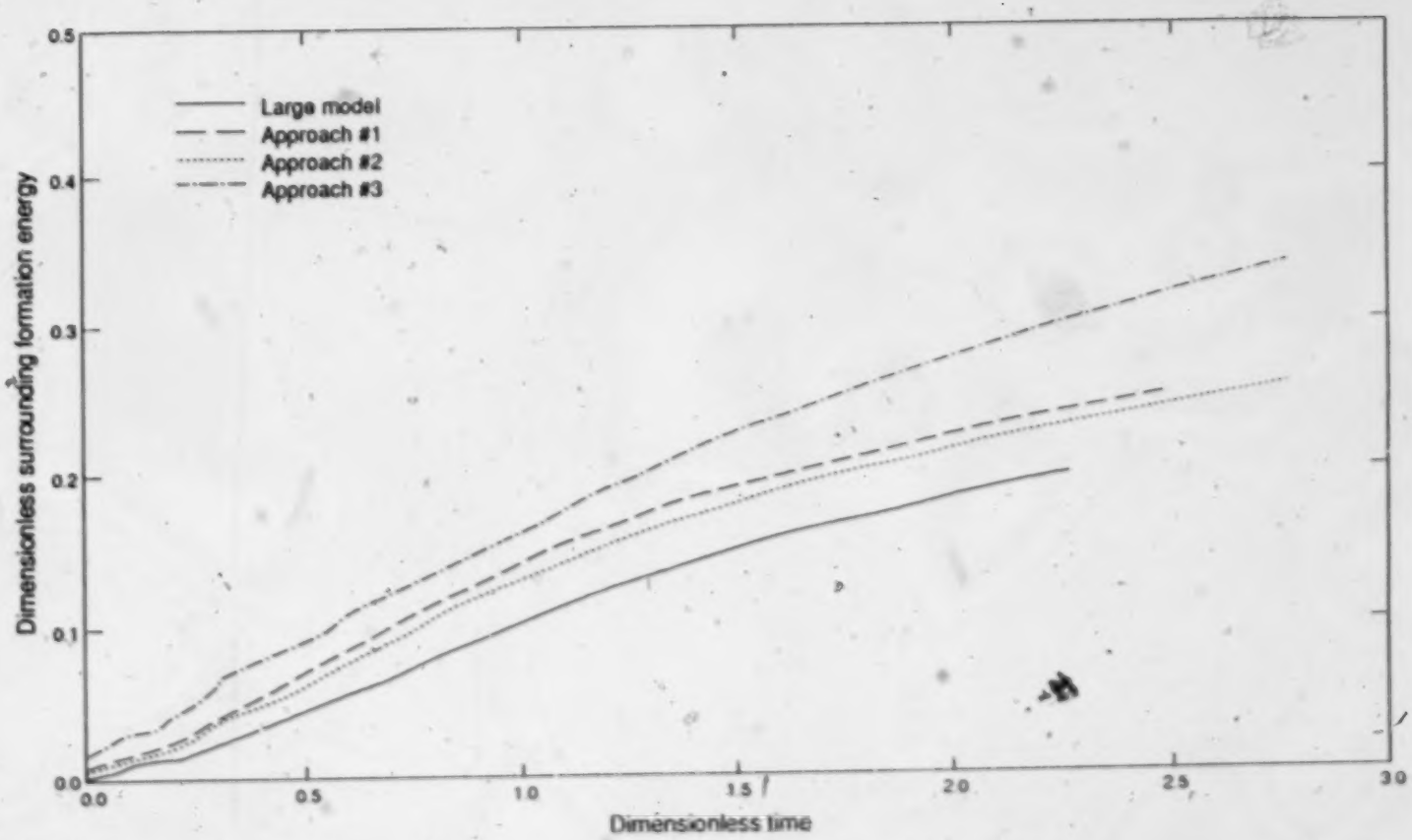

Figure 32. Comparison of energy lost to the surrounding formations of the large model (Run 44) to that predicted by each scaling approach (Runs 42, 38, 46). The scaled injection rate in these steam-water experiments was 55.3 m^3/day.

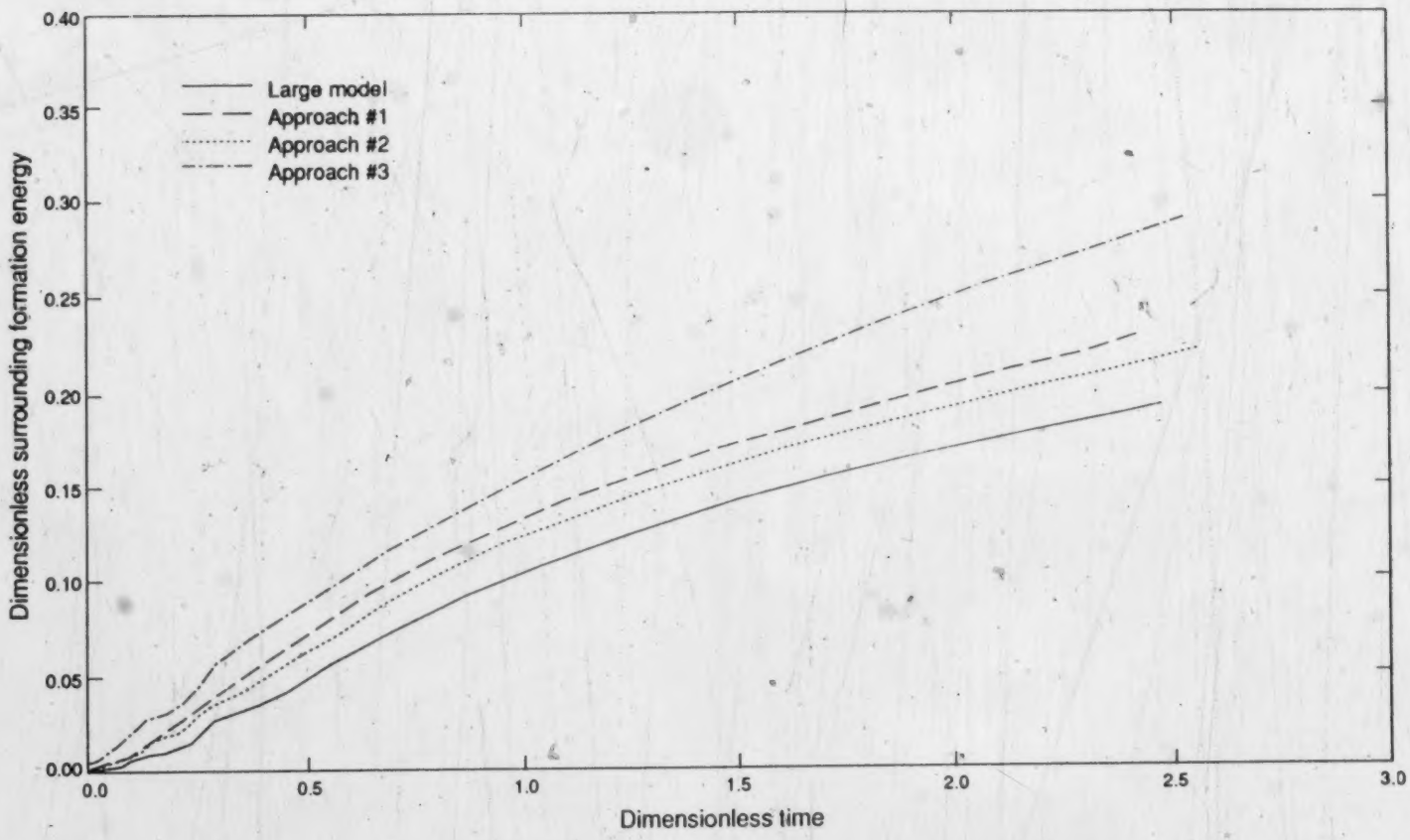

Figure 33. Comparison of energy lost to the surrounding formations of the large model (Run 45) to that predicted by each scaling approach (Runs 43, 39, 47). The scaled injection rate in these steam-oil-water experiments was 41.5 m^3/day.

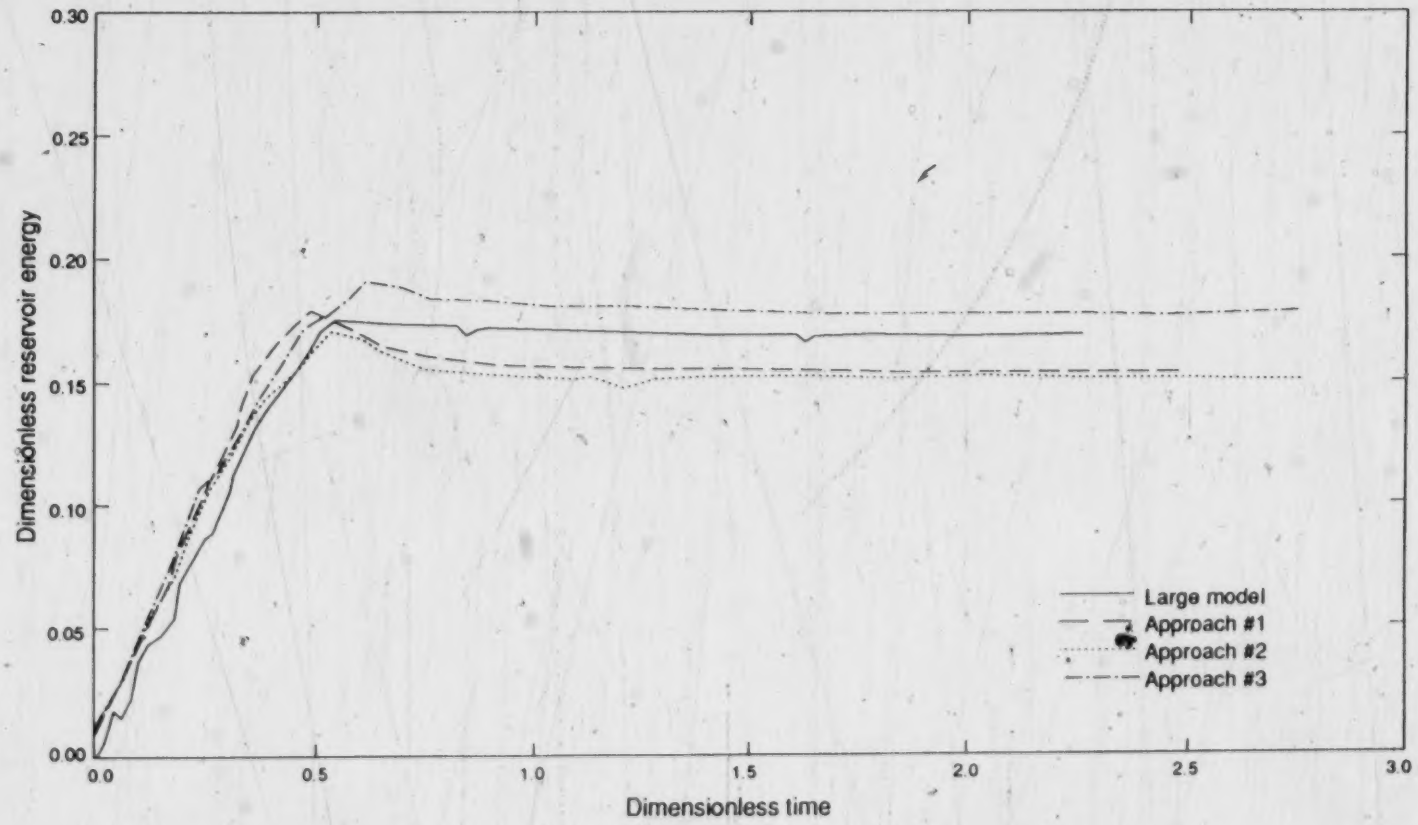

Figure 34. Comparison of the energy contained within the reservoir of the large model (Run 44) to that predicted by each scaling approach (Runs 42, 38, 46). The scaled injection rate in these steam-water experiments was 55.3 m^3/day.

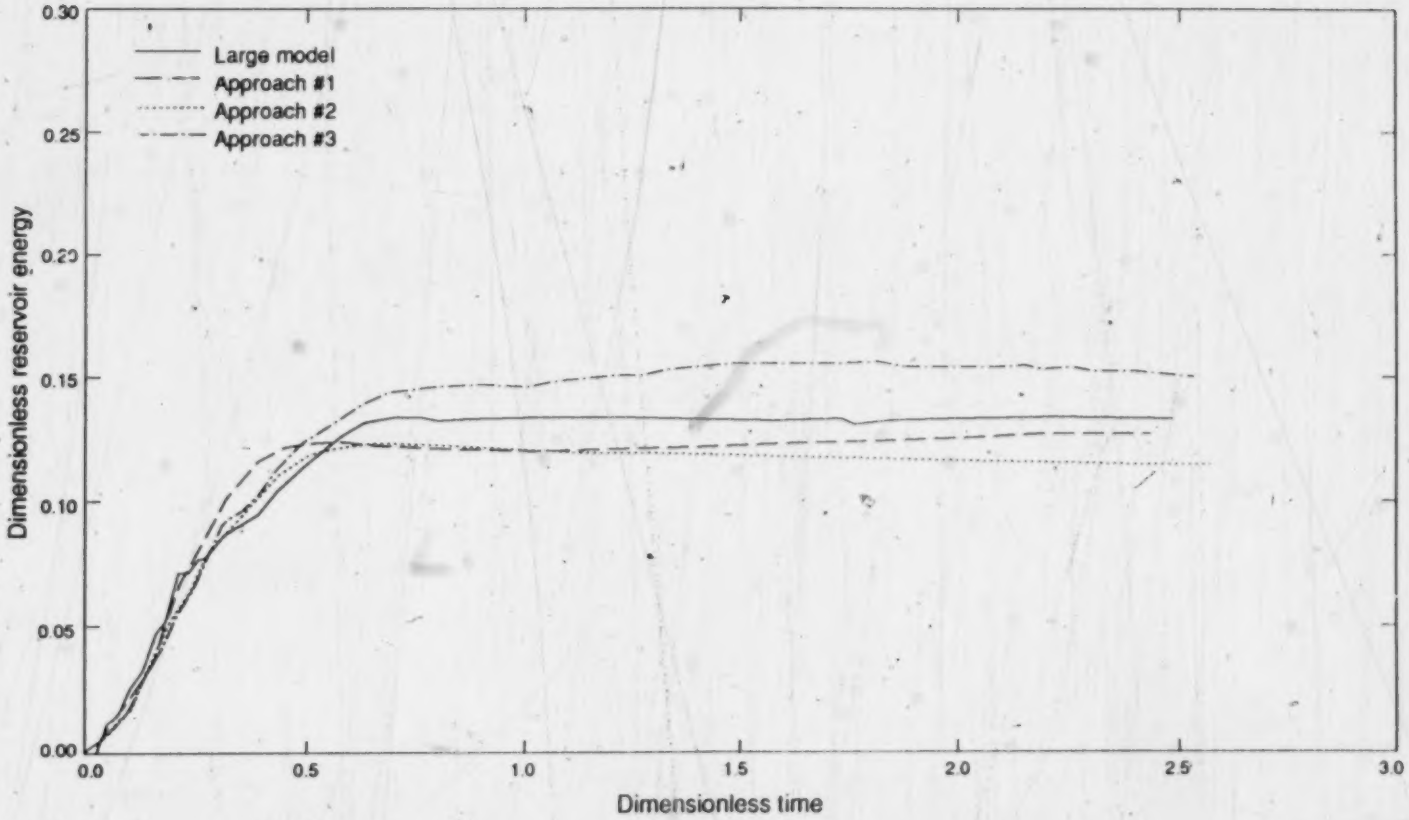

Figure 35. Comparison of the energy contained within the reservoir of the larger model (Run 45) to that predicted by each scaling approach (Runs 43, 39, 47). The scaled injection rate in these steam-oil-water experiments was 41.5 m^3/day.

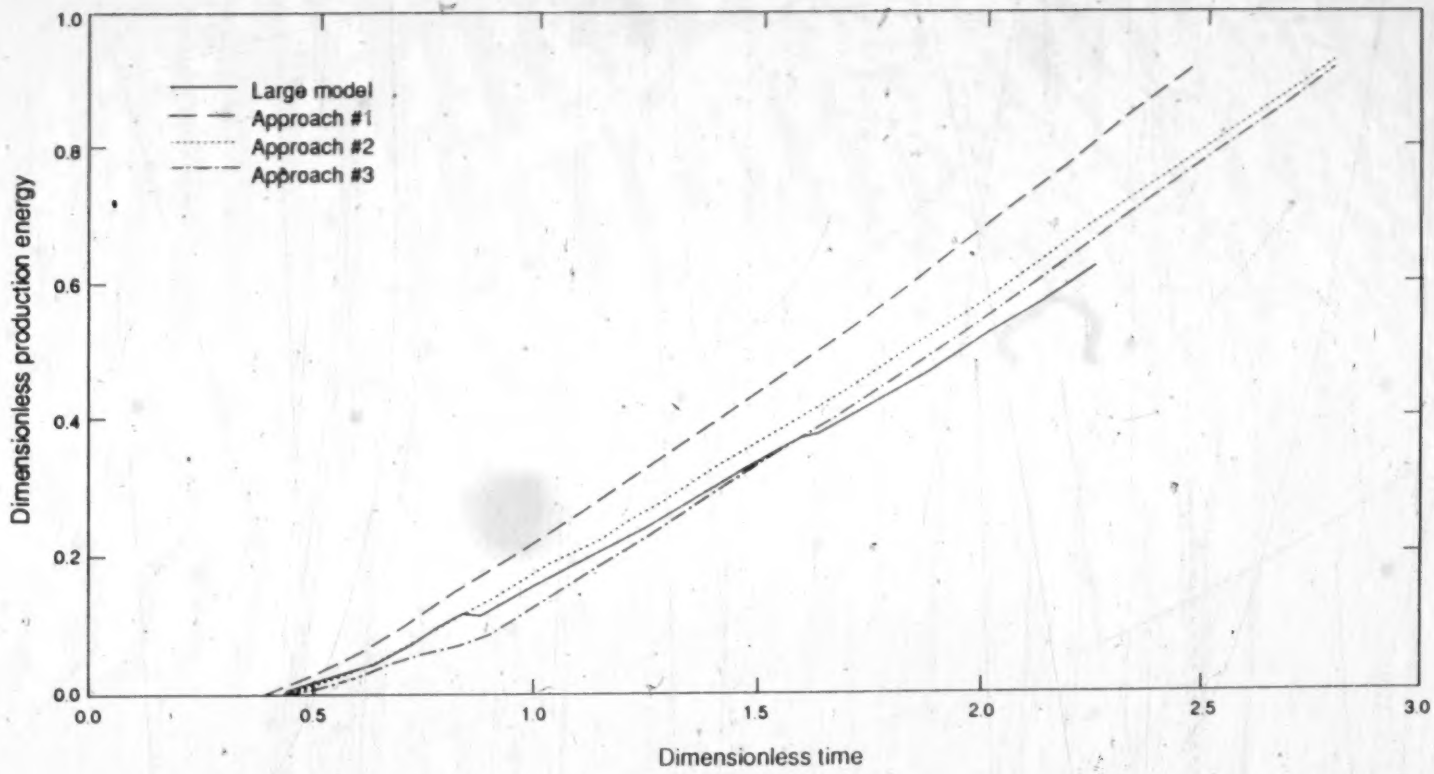

Figure 36. Comparison of the energy contained in the produced fluids of the large model (Run 44) to that predicted by each scaling approach (Runs 42, 38, 46). The scaled injection rate in these steam-water experiments was 55.3 m^3/day.

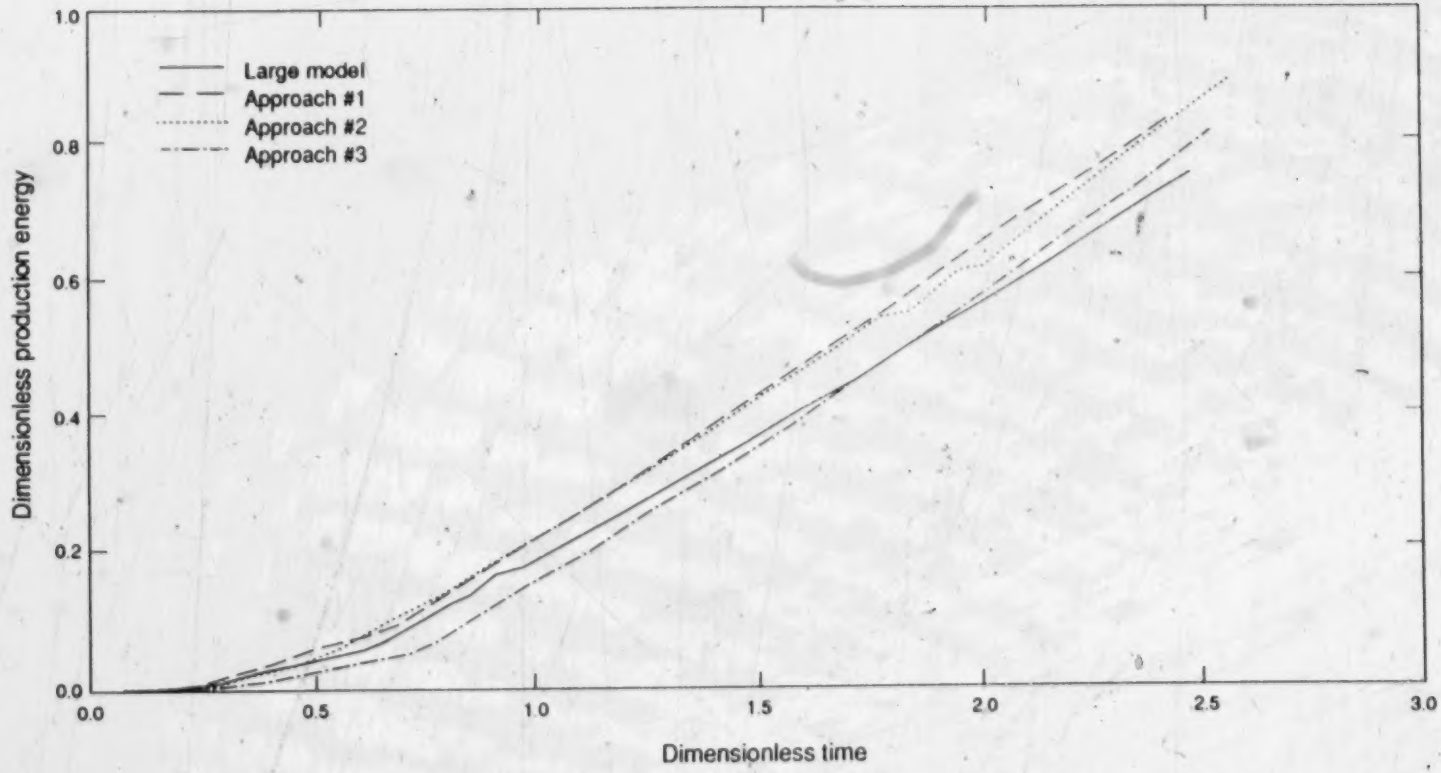

Figure 37. Comparison of the energy contained in the produced fluids of the large model (Run 45) to that predicted by each scaling approach (Runs 43, 39, 47). The scaled injection rate in these steam-oil-water experiments was 41.5 m^3/day.

and 35. A good estimate of this parameter is obtained using all three approaches. The reservoir energy increases as the steam zone develops and the reservoir is heated. The decline in reservoir energy later in the experiments is a result of lower density, higher energy steam replacing higher density, lower energy water. This results in less energy per unit volume.

The amount of energy in the produced fluids (steam, water, or oil is compared in Figures 36 and 37). The best prediction was obtained using Approach #3, while using Approaches #2 and #1 resulted in less accurate predictions. This comparison is the least reliable because the produced energy is not measured once the production well temperature reaches the saturation temperature but must be estimated from the energy balance.

To illustrate the effect of injection rate, the predictions made using Approach #2 for four injection rates are shown in Figures 38-41. As the rate of injection increased, the portion of injected energy contained in the produced fluids increased, and that lost to the surrounding formations decreased. No noticeable difference can be seen in the quality of the predictions made for the increasing injection rate cases shown in Figures 38-41. Therefore, the ability to predict these parameters using the scaling approaches does not appear to depend on injection rate.

7.2.3 Production

The rate of fluid production can also be compared. Production rate, rather than cumulative production, is compared as this parameter is more

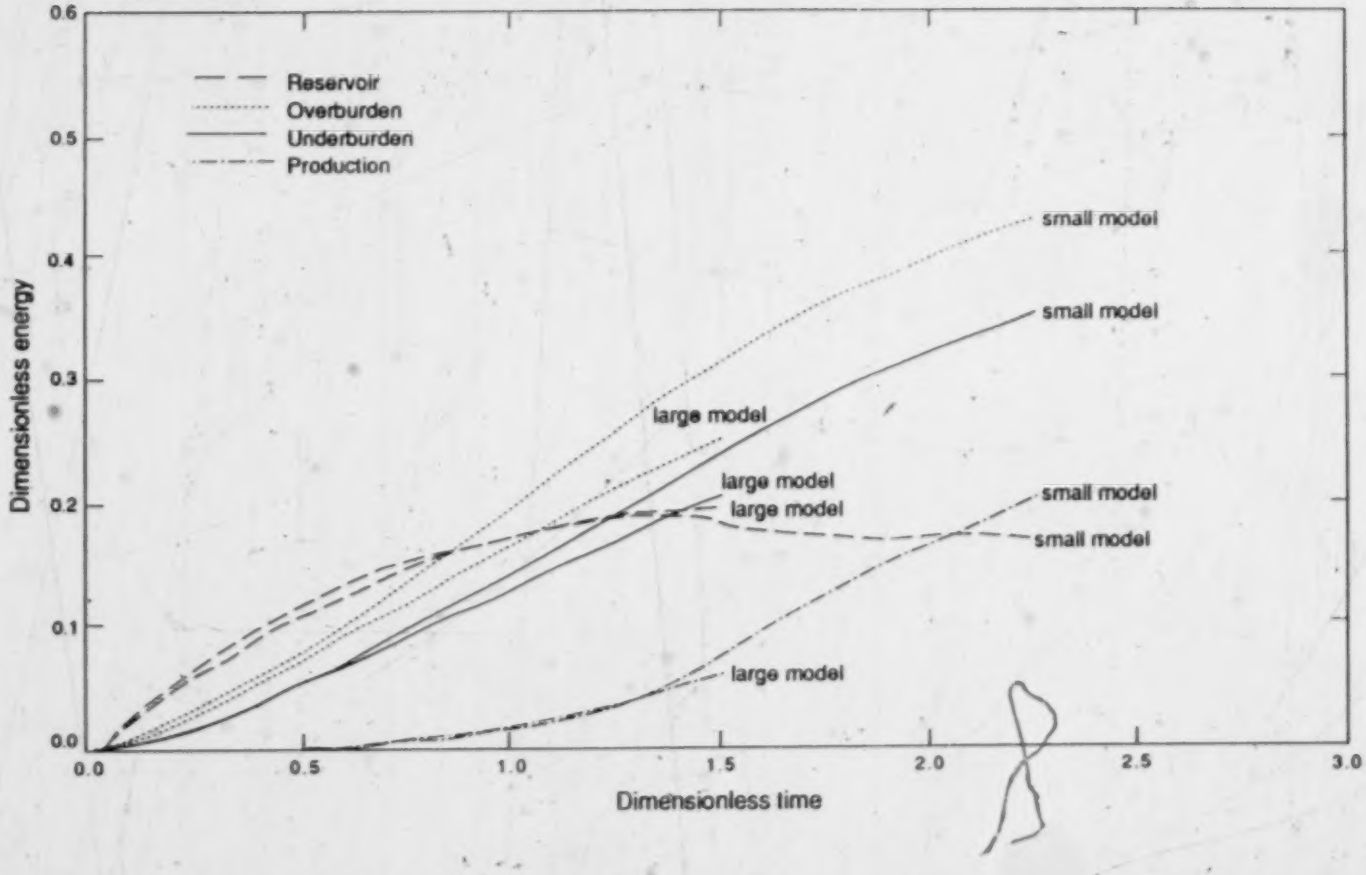

Figure 38. The energy distribution in the large model (Run 8) and that predicted using Approach #2 (small model, Run 13). The scaled injection rate in these steam-water experiments was 6.9 m^3/day.

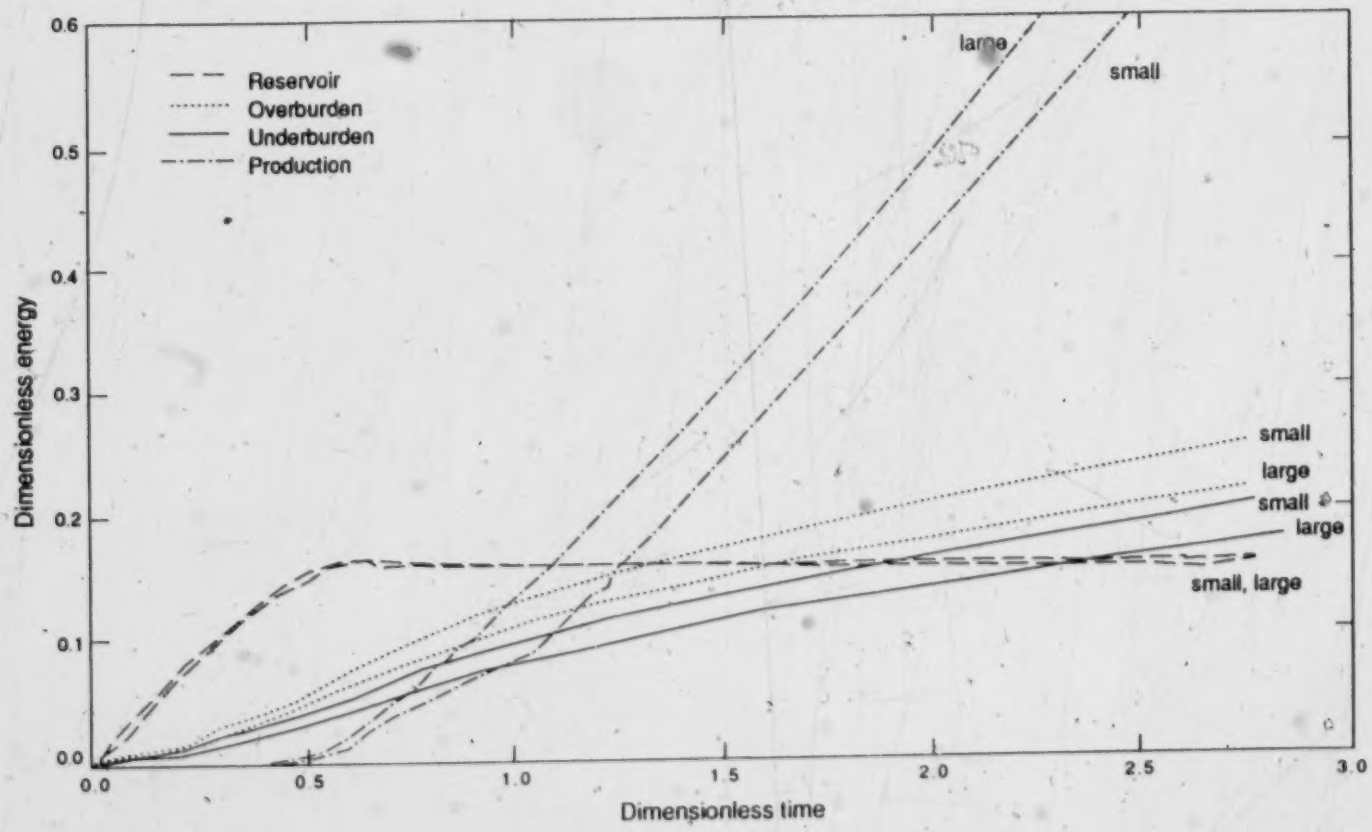

Figure 39. The energy distribution in the large model (Run 11) and that predicted using Approach #2 (small model, Run 16). The scaled injection rate in these steam-water experiments was 27.6 m^3/day.

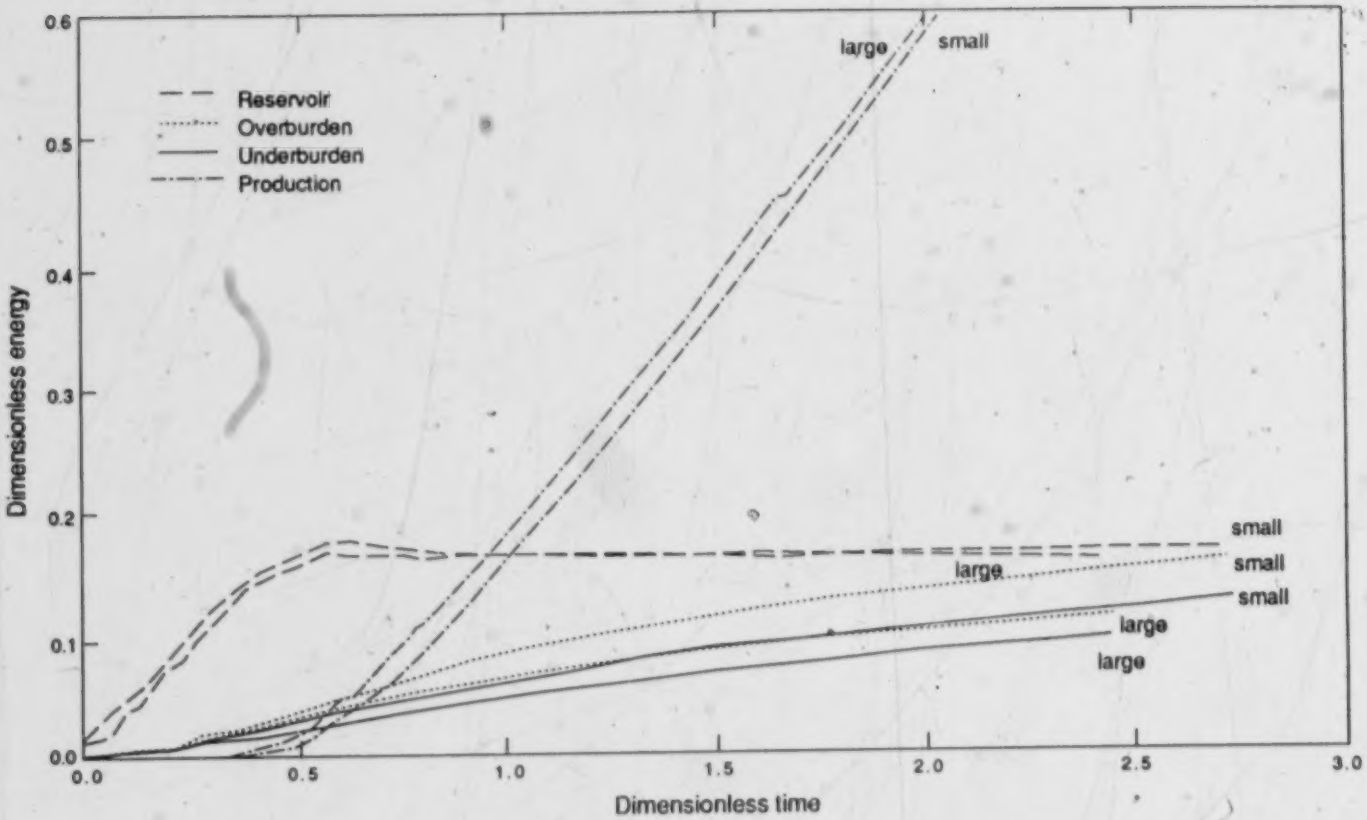

Figure 40. The energy distribution in the large model (Run 9) and that predicted using Approach #2 (small model, Run 14). The scaled injection rate in these steam-water experiments was 55.3 m^3/day.

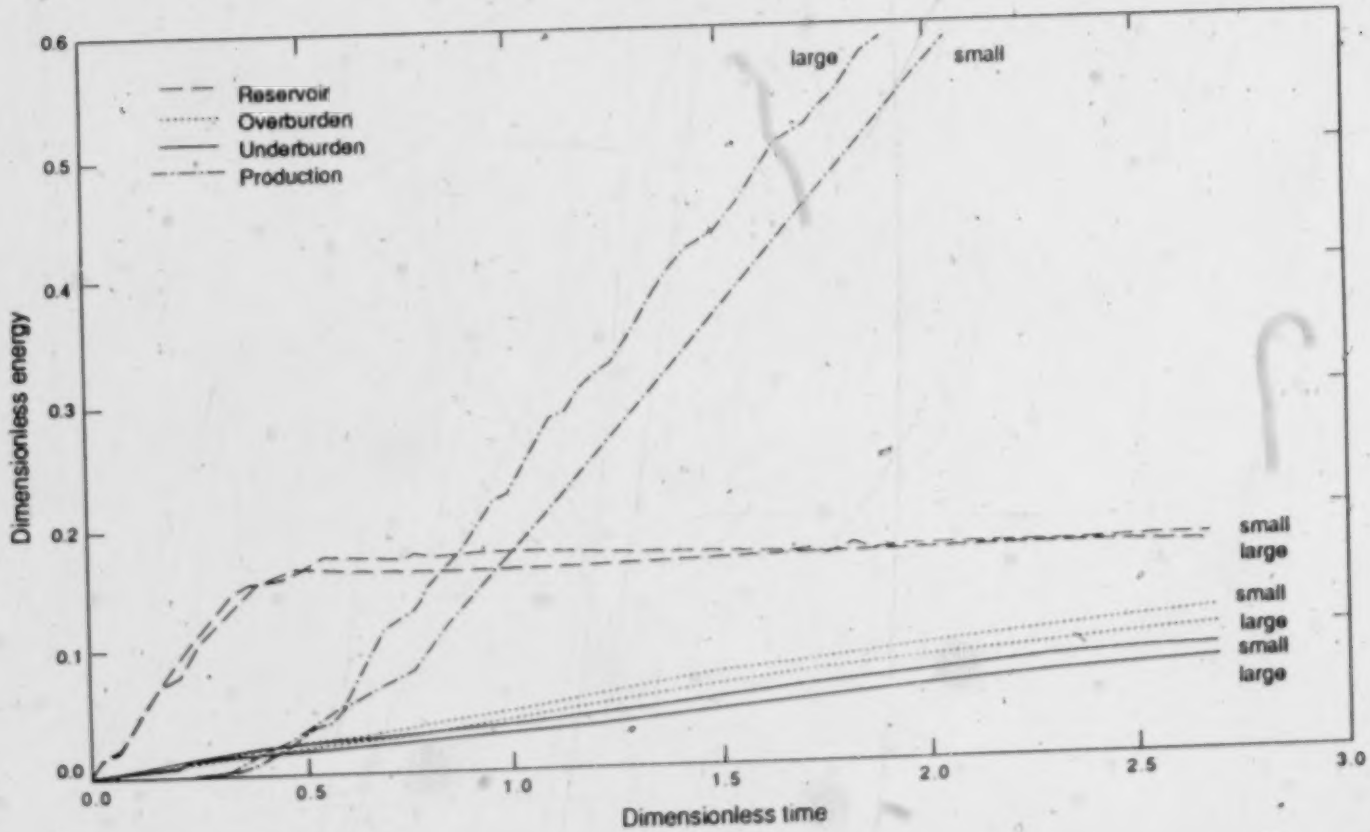

Figure 41. The energy distribution in the large model (Run 10) and that predicted using Approach #2 (small model, Run 15). The scaled injection rate in these steam-water experiments was 110.6 m^3/day.

sensitive to events such as steam breakthrough and maximum steam zone development and is therefore more meaningful to match. The production rate of water and/or steam is compared for the water-only experiments, and the oil production rate and the oil-water ratio are compared for the oil experiments.

The production rates predicted using Approaches #1, #2, and #3, are compared to the production rates for the large model for an injection rate of 55.3 m^3/d in Figures 42-44. The production rate is represented by the sum of water and condensed steam entering the production well. These curves are characterized by a high initial production rate as the steam zone develops, which levels off as the steam zone approaches its maximum size. A surge in production rate occurs near the point in time when steam breaks through at the production well (at $t_D \simeq 0.5$ in Figure 42-44). Breakthrough occurs earlier at increased injection rates (see Table 12). A considerable amount of water at saturation conditions may exist in the model when steam breaks through at the production well. A small reduction in pressure as steam breaks through at the well may result in flashing of this water and, therefore, the observed surge in production rate. The observed oscillations in production rate following the surge are difficult to account for; one explanation may be the stability of the flashing/production surge hypothesis. The overall comparison of production rate is still a valuable indication of the capabilities of a scaling approach. Results using Approaches #1 and #2 match well with the large model, including the surge in production near steam breakthrough. The predictions made using Approach #3 are slightly less accurate. As discussed in the previous section, the energy losses

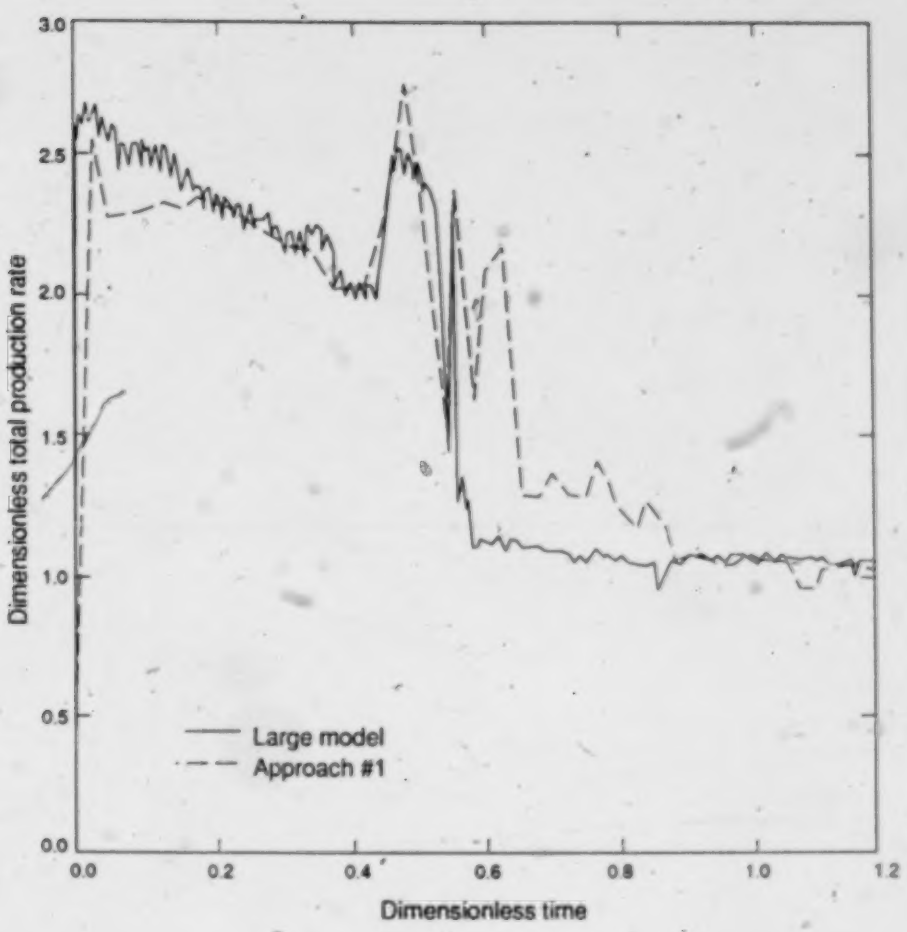

Figure 42. Comparison of the production rate of the large model (Run 44) to that predicted using Approach #1 (Run 42). The scaled injection rate in these steam-water experiments was 55.3 m^3/day.

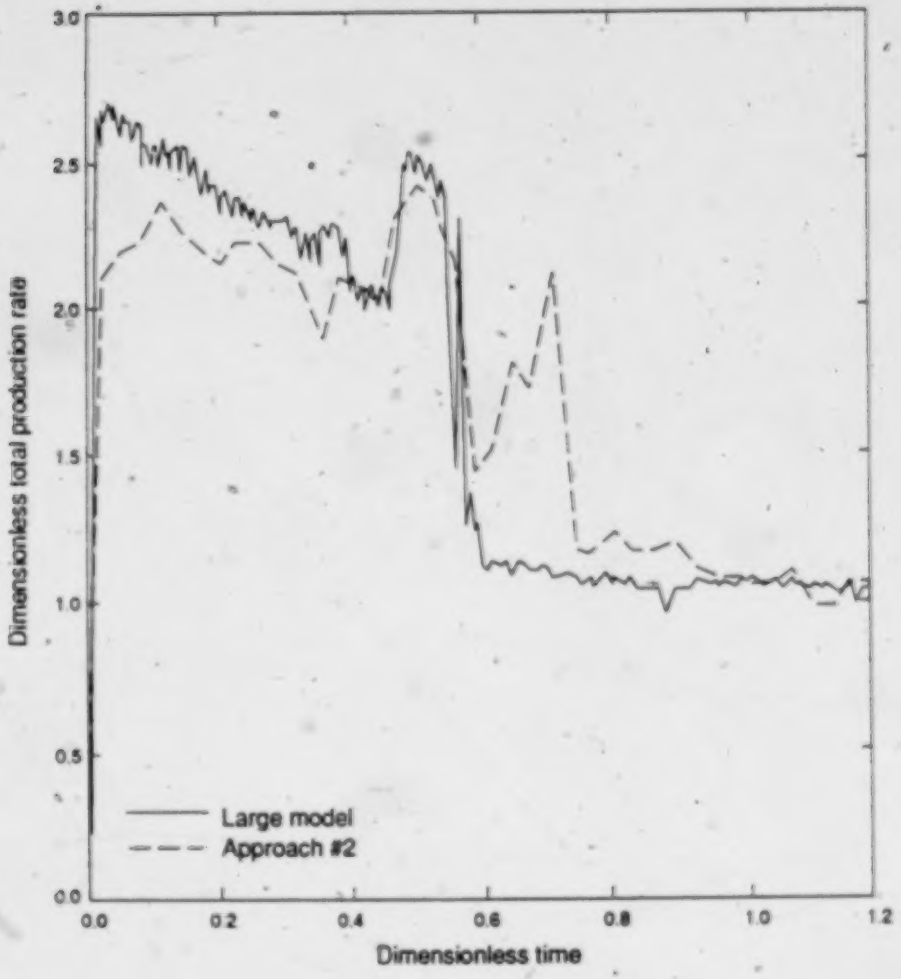

Figure 43. Comparison of the production rate of the large model (Run 44) to that predicted using Approach #2 (Run 38). The scaled injection rate in these steam-water experiments was 55.3 m^3/day.

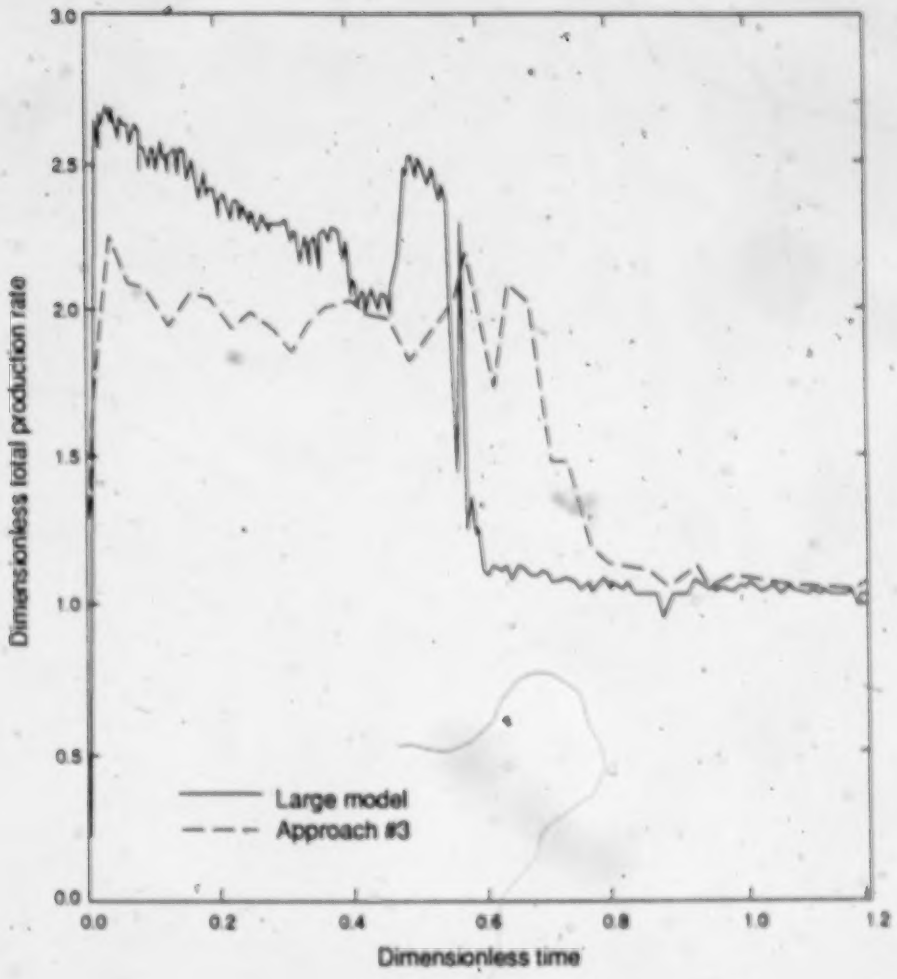

Figure 44. Comparison of the production rate of the large model (Run 44) to that predicted using Approach #3 (Run 46). The scaled injection rate in these steam-water experiments was 55.3 m^3/day.

to the surrounding formations are higher when using this approach. As a result, the steam zone develops more slowly leading to lower initial production rates and a delay in steam breakthrough (see Figure 44). A comparison of cumulative productions is shown in Figure 45, but many events, such as steam breakthrough, are more difficult to identify and therefore comparisons of this parameter are not as useful.

Compared in Figures 46-48 are the predicted oil production rates, made using Approaches #1, #2, and #3, for an injection rate of 41.5 m^3/d. As can be seen in Figures 46 and 47, very good predictions can be made using Approaches #1 and #2. These oil production curves are characterized by a high initial production rate as the steam zone develops (see $t_D < 0.3$ in Figure 46-48), which rapidly drops off as the oil-water ratio drops. The prediction made using Approach #3 is less accurate (see Figure 48) as initially ($t_D<0.1$) the predicted rate is lower and at later time it is higher. Two small surges in oil production occur late in the Approach #3 experiment ($t_D>0.8$) which did not occur in any other experiment. A slug of oil must have reached the production well after steam breakthrough; this is believed to be an artifact of this particular experiment.

A comparison of the predicted oil-water ratios using each approach is shown in Figure 49. Using Approaches #1 and #2, accurate predictions of this parameter are made. Slightly less accurate predictions are made using Approach #3, with the predicted arrival of the oil-water interface at the production well being late (i.e. the curve is shifted about 0.1 dimensionless time units to the right). The time at which a rapid fall

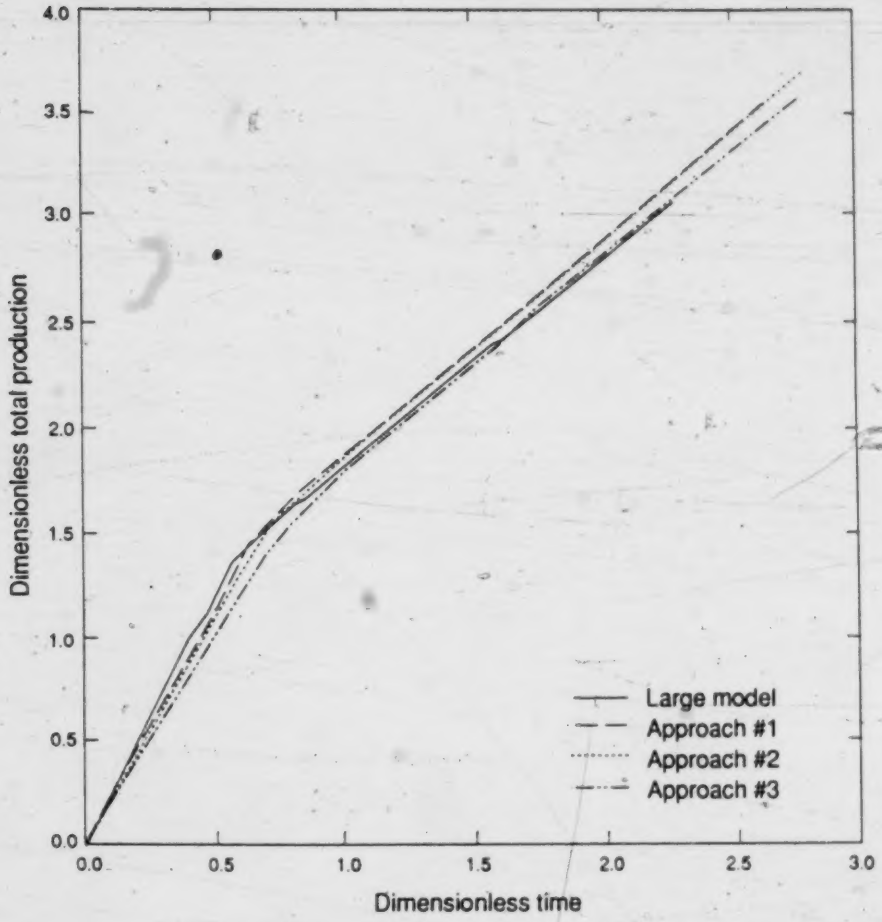

Figure 45. Comparison of the cumulative production from the large model (Run 44) to those predicted using Approaches #1 (Run 42), #2 (Run 38) and #3 (Run 46).

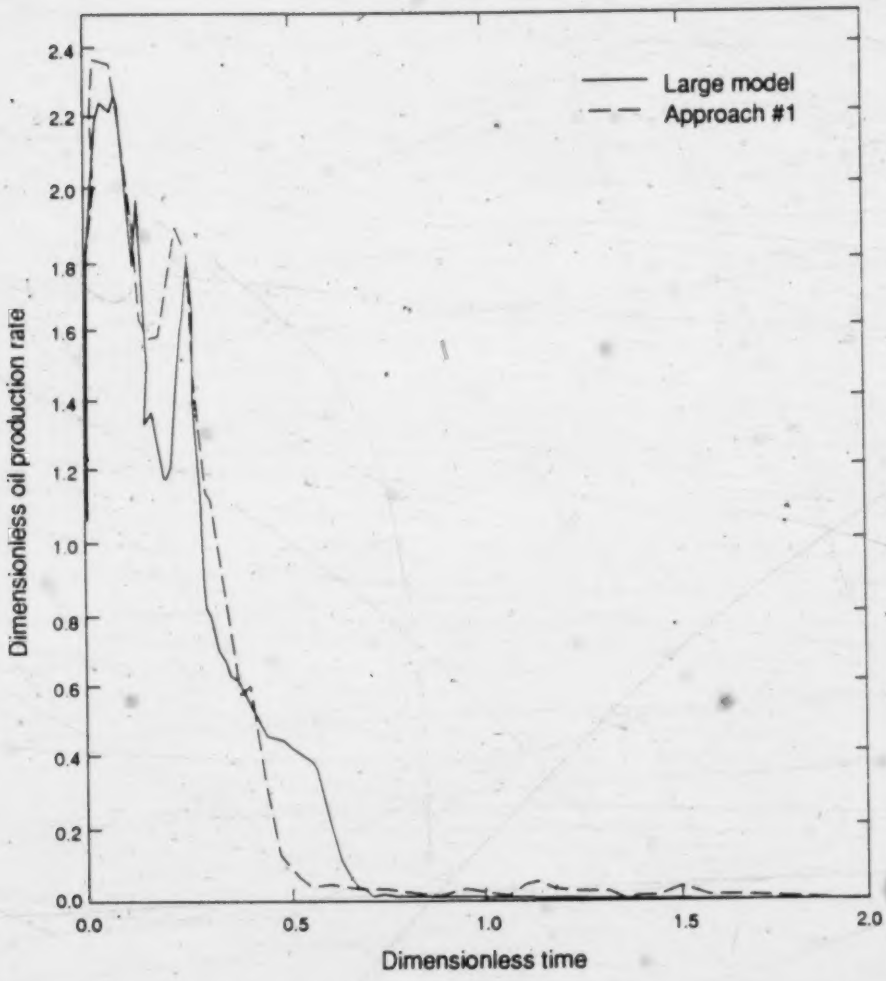

Figure 46. Comparison of the oil production rate of the large model (Run 45) to that predicted using Approach #1 (Run 43). The scaled injection rate in these steam-oil-water experiments was 41.5 m^3/day.

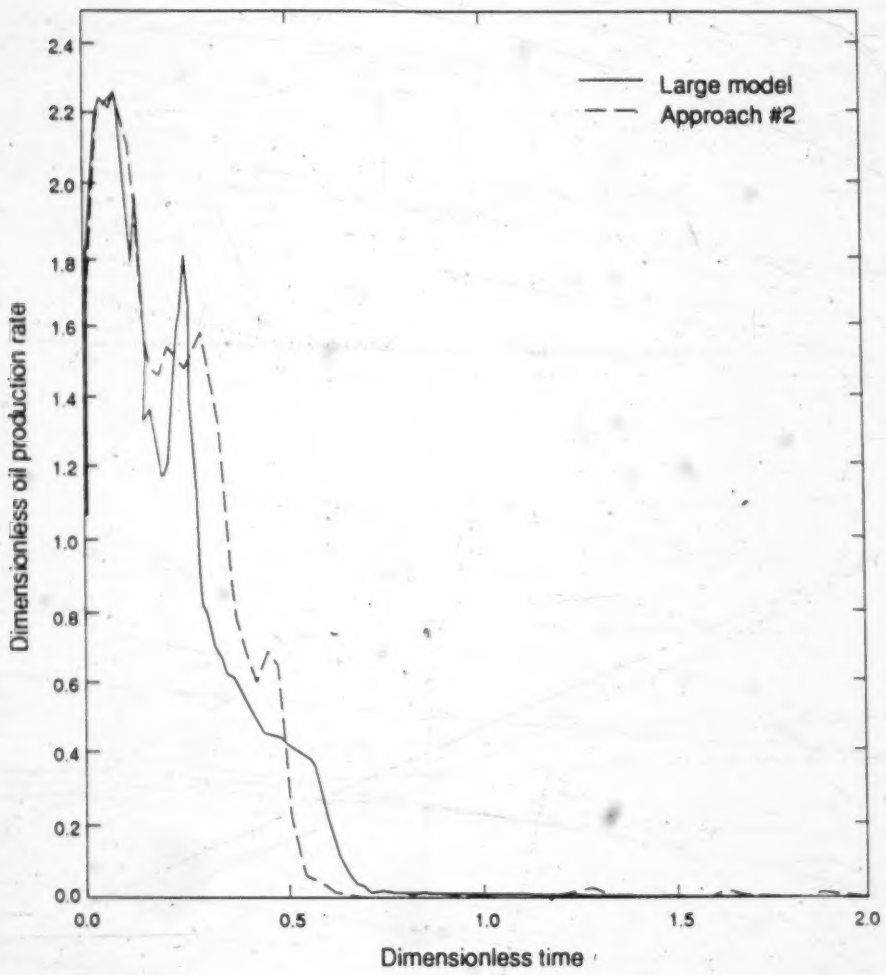

Figure 47. Comparison of the oil production rate of the large model (Run 45) to that predicted using Approach #2 (Run 39). The scaled injection rate in these steam-oil-water experiments was 41.5 m^3/day.

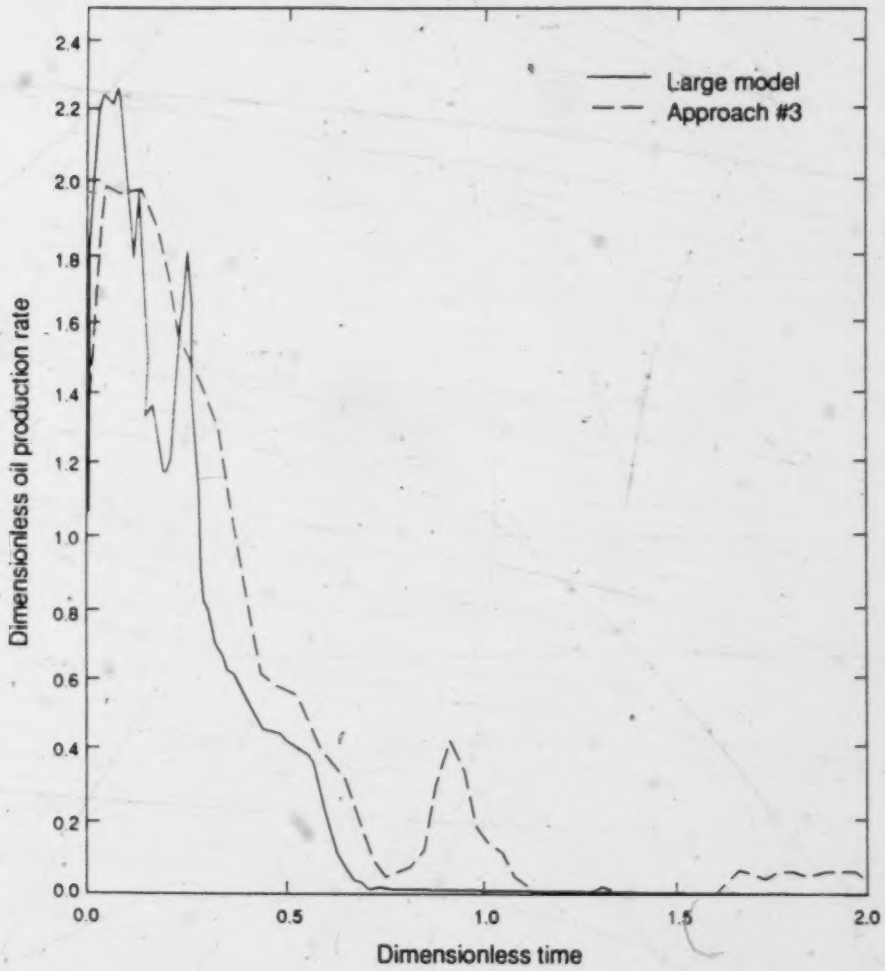

Figure 48. Comparison of the oil production rate of the large model (Run 45) to that predicted using Approach #3 (Run 47). The scaled injection rate in these steam-oil-water experiments was 41.5 m^3/day.

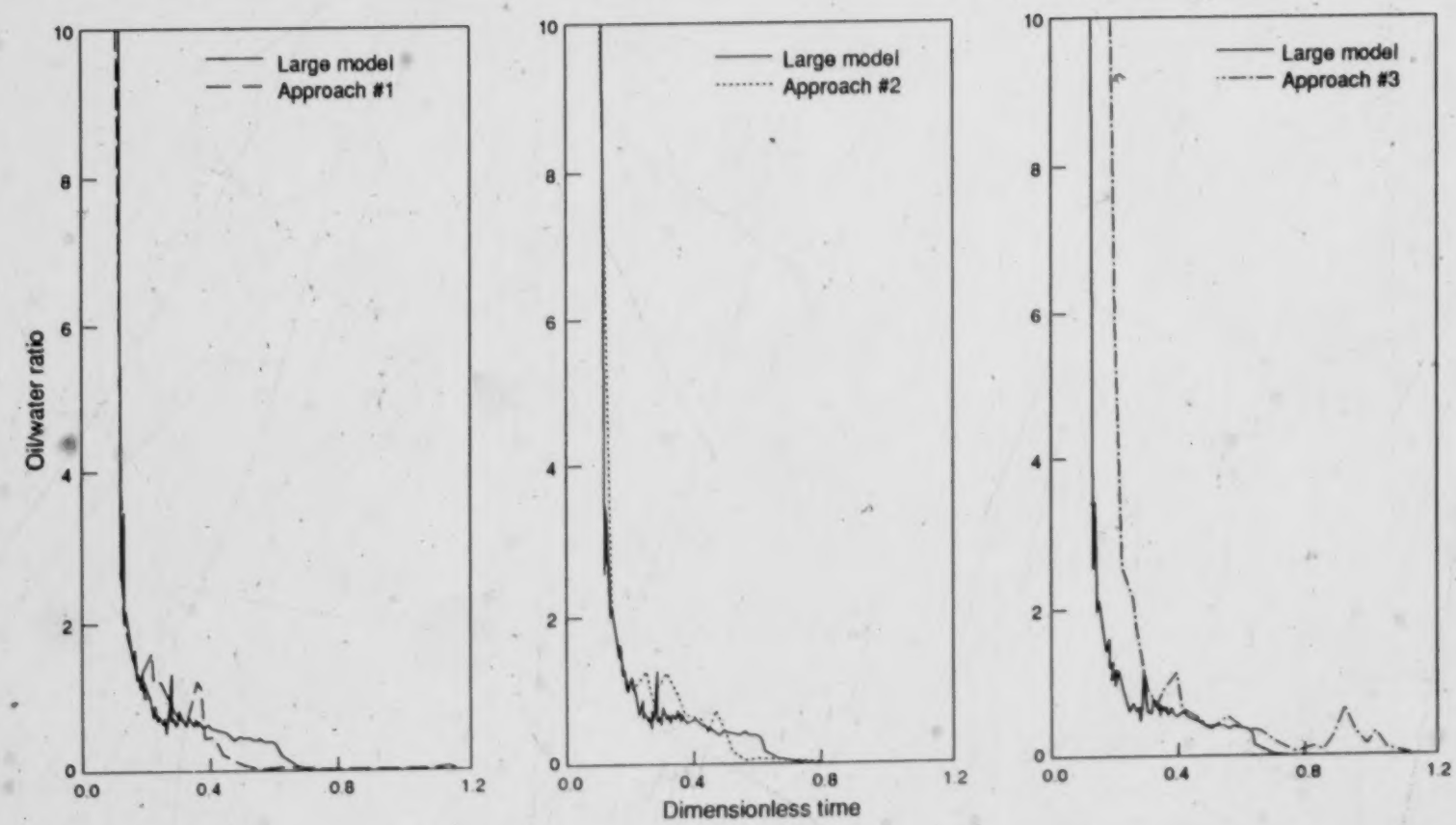

Figure 49. Comparison of the oil/water ratio for the large model (Run 45) to those predicted using Approaches #1 (Run 43), #2 (Run 39) and #3 (Run 47).

in oil-water ratio occurs is considered to correspond to arrival of the oil-water interface (see Figure 49).

7.2.4 Steam Zone Volume

Scaling the development of the steam zone is important in scaled steam injection experiments. Steam zone volume indicates the fraction of the reservoir occupied by steam. A limit exists for a given energy injection rate, at which the rate of heat loss equals the injection rate of latent energy. In Figures 50 and 51, the fraction of the pore volume occupied by steam in the large model is compared to that estimated by each of the small models using Approaches #1, #2, and #3 for the water-only and oil cases. The fraction of steam in the reservoir increases with time (see Figure 51, $t_D < 0.5$), leveling off as the rate of energy losses from the reservoir approach the rate of energy injected. In both figures, the steam zone volume is underestimated using Approach #3, while very reasonable predictions are made using Approaches #1 and #2. The higher energy losses to the surrounding formations which resulted when using Approach #3, caused the steam zone to develop more slowly and its ultimate size to be smaller.

7.2.5 Production Quality and Steam Breakthrough

Steam breakthrough and produced steam quality are also good indicators of the scaling of the mechanisms and properties responsible for the development of the steam zone. A good match of these, in combination with the steam zone volume, indicates good scaling of both the volume

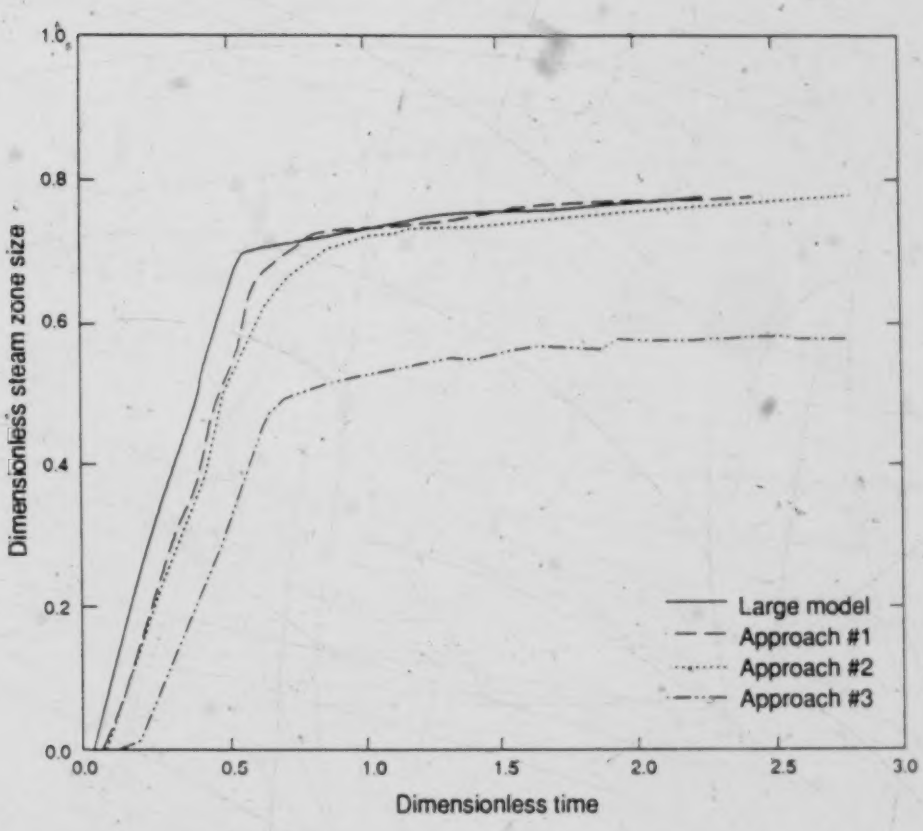

Figure 50. Comparison of the fraction of the pore volume occupied by steam in the large model (Run 44) to those estimated using Approaches #1 (Run 42), #2 (Run 38) and #3 (Run 46). The scaled injection rate for these steam-water experiments was 55.3 m^3/day.

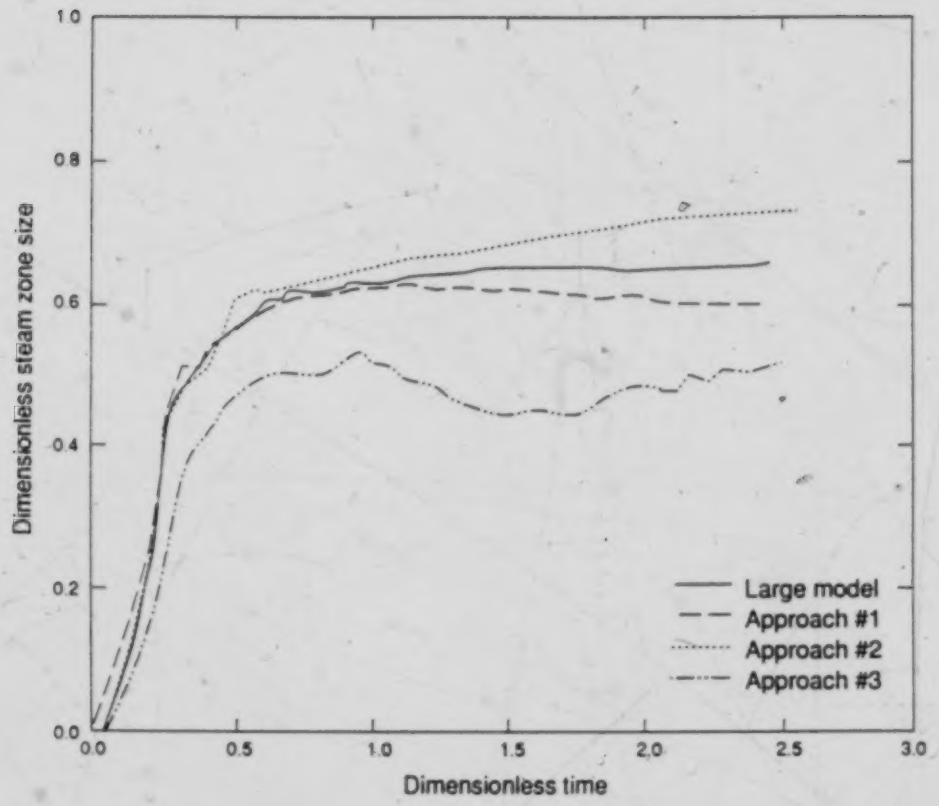

Figure 51. Comparison of the fraction of the pore volume occupied by steam in the large model (Run 45) to those estimated using Approaches #1 (Run 43), #2 (Run 39) and #3 (Run 47). The scaled injection rate for these steam-oil-water experiments was 41.5 m^3/day.

and shape of the steam zone. The steam quality at increasing injection rates for the large model experiments is shown in Figure 52. The point in time at which steam first appears indicates steam breakthrough. As would be expected, with increasing injection rates, the steam breaks through earlier and the quality of the produced steam levels off at a higher value. The experiment which used the lowest injection rate (6.9 m^3/day) did not achieve steam breakthrough (see Figure 52).

The ability to predict the quality of the produced steam for a series of water experiments and a series of oil experiments using each scaling approach is compared in Figures 53-56. The predictions made using Approaches #1, #2, and #3 and the actual results from the large model for the water experiments are shown in Figure 53. Satisfactory predictions of steam breakthrough at the production well are made using Approaches #1 and #2 (compare points at which steam quality first appears in Figure 53). The breakthrough is delayed when using Approach #3 due to a more slowly developing steam zone caused by higher heat losses to the surrounding formations. Higher steam quality at the production well was predicted using all three approaches ($t_D > 1$ in Figure 53). A similar comparison was made using the three approaches for a series of steam-oil-water experiments (Figures 54-56). Steam breakthrough occurs slightly earlier and steam quality at the production well is slightly higher for these experiments than for the steam-water experiments (Figure 53) even though the steam injection rate is lower for the former. This is to be expected because of the lower mobility of oil which leads to lower horizontal and vertical sweep efficiencies. Note this effect in the temperature profiles compared in Figure 57 where

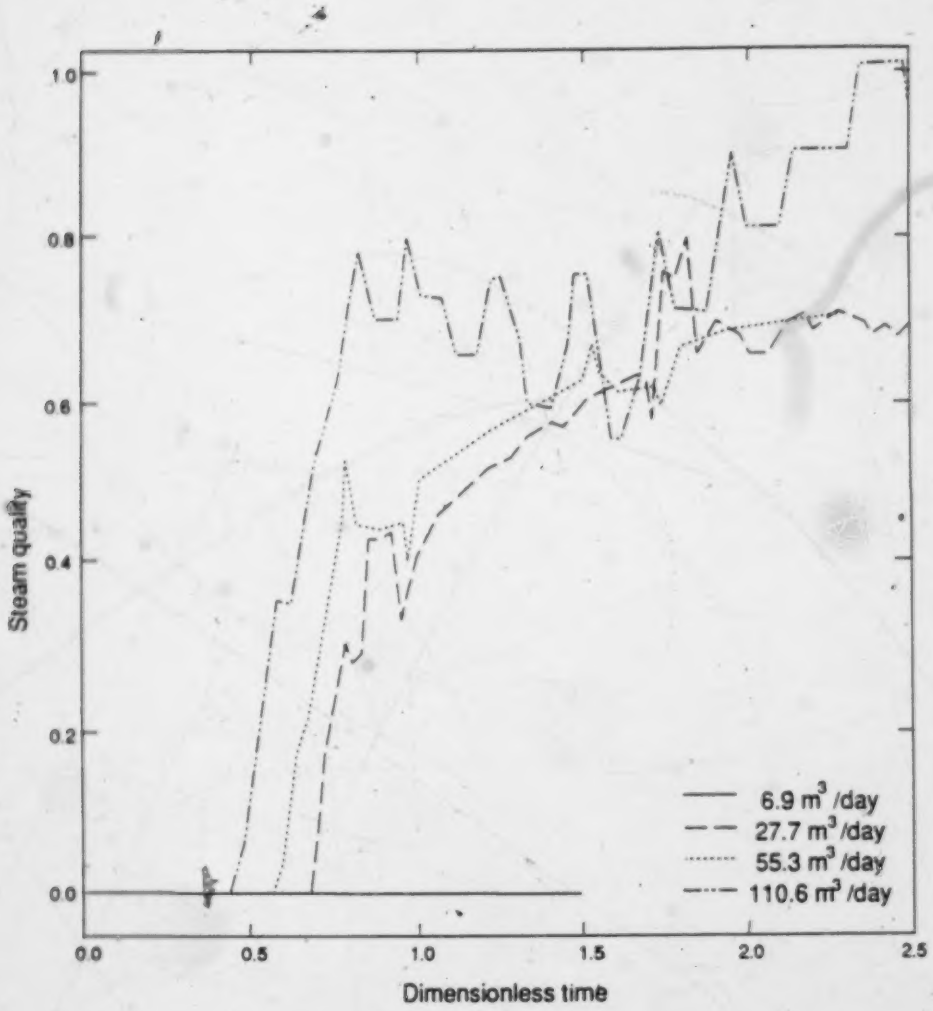

Figure 52. Estimated quality of the produced steam for large model experiments at various injection rates (Runs 8, 11, 44, 15).

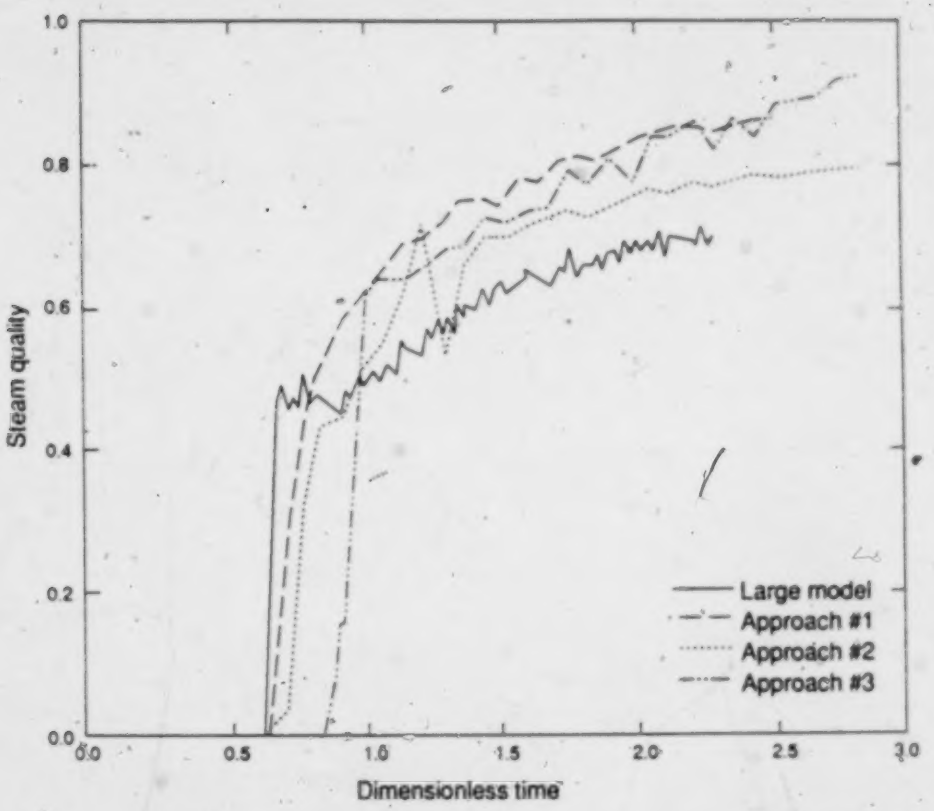

Figure 53. Comparison of the quality of the produced steam for the large model to the predictions of each scaling approach for a series of steam-water experiments with scaled injection rates of 55.3 m^3/day.

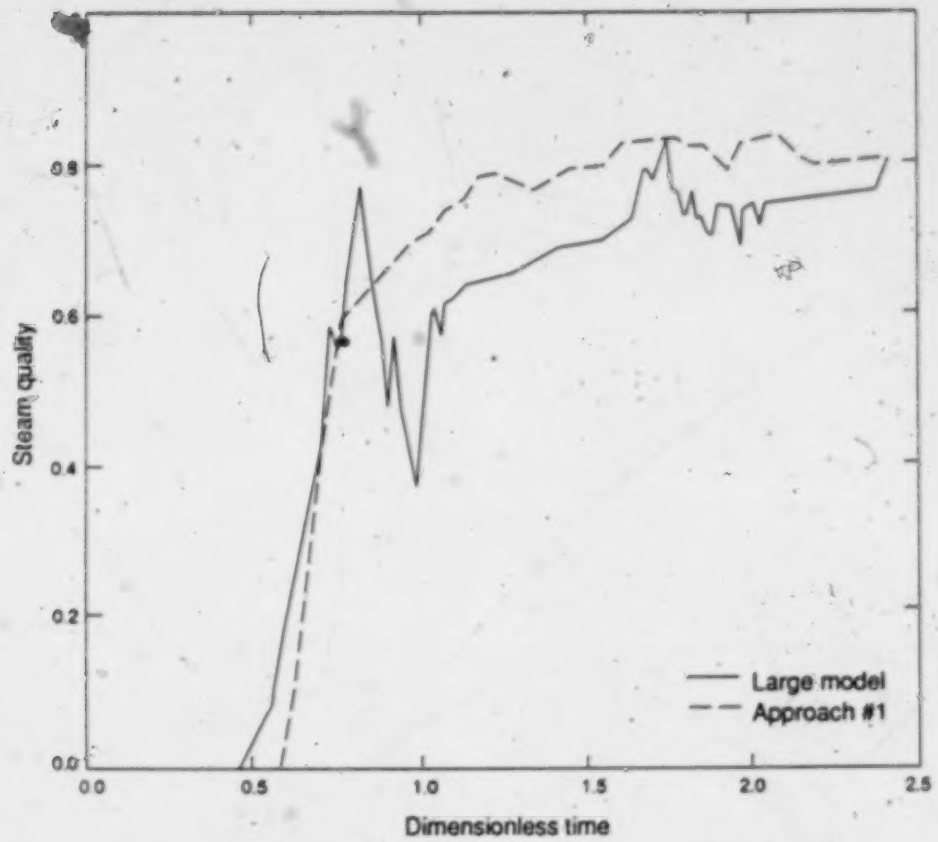

Figure 54. Comparison of the quality of the produced steam for the large model (Run 45) to the prediction made using Approach #1 (Run 43). The scaled injection rate for this series of steam-oil-water experiments was 41.5 m^3/day.

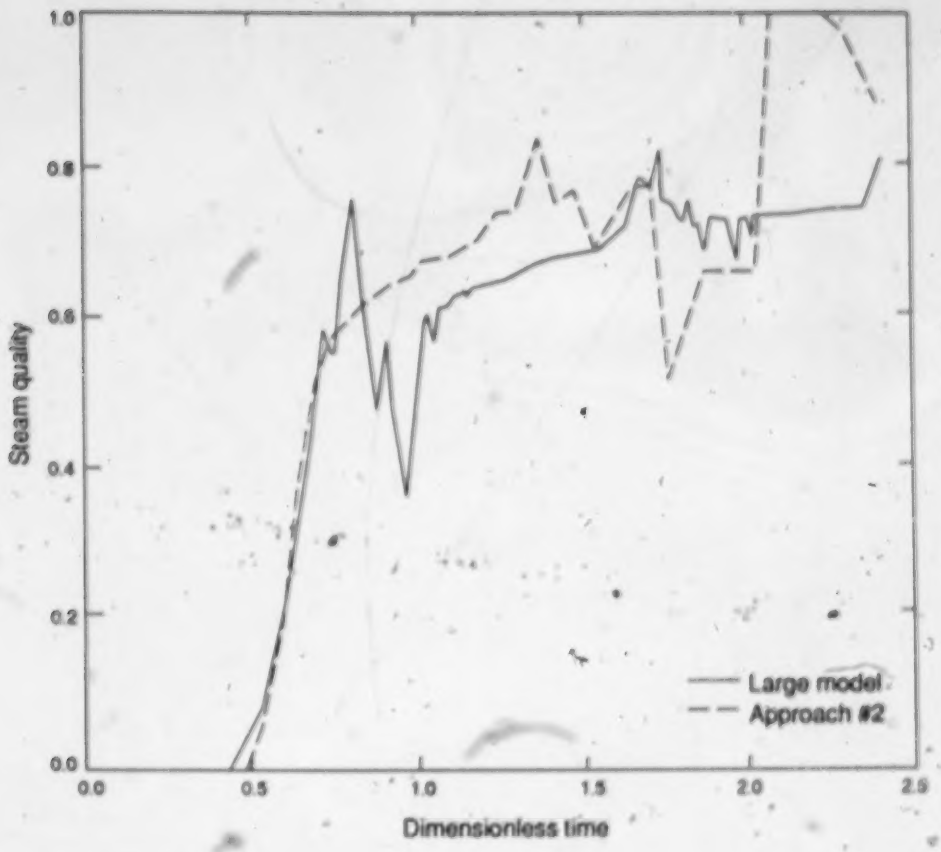

Figure 55. Comparison of the quality of the produced steam for the large model (Run 45) to the prediction made using Approach #2 (Run 39). The scaled injection rate for this series of steam-oil-water experiments was 41.5 m^3/day.

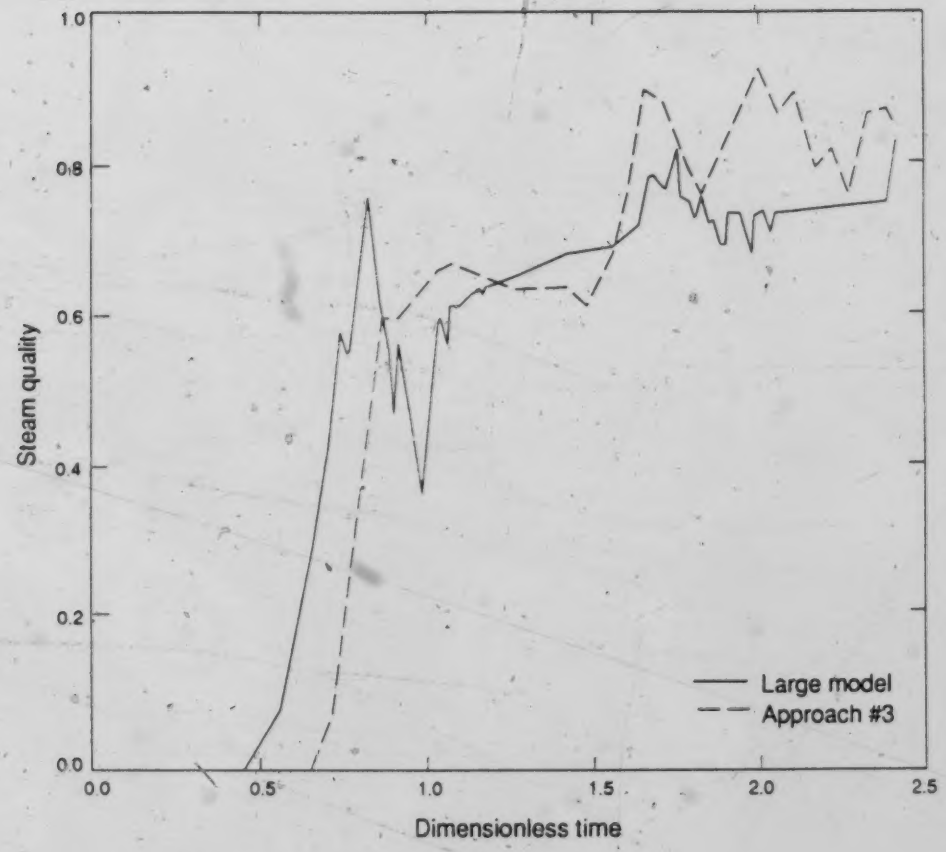

Figure 56. Comparison of the quality of the produced steam for the large model (Run 45) to the prediction made using Approach #3 (Run 47). The scaled injection rate for this series of steam-oil-water experiments was 41.5 m^3/day.

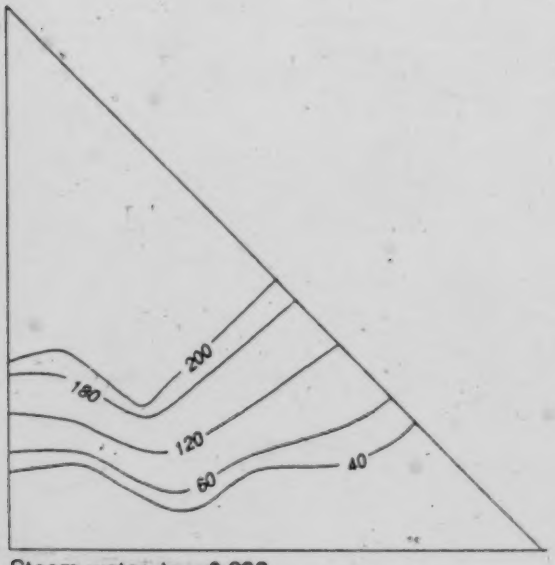

Steam-water, $t_D = 0.292$

Steam-oil-water, $t_D = 0.294$

Figure 57. Comparison of the horizontal temperature profiles for a steam-water experiment (Run 44) and a steam-oil-water experiment (Run 45). The injection rate for Runs 44 and 45 were 55.3 m^3/day and 41.5 m^3/day, respectively.

for the same quantity of steam, warm temperatures have reached the production well earlier in the steam-oil-water experiment. As was the case for the water experiments compared in Figure 53, the best predictions of steam breakthrough in the oil experiments were made using Approaches #1 and #2.

7.2.6 Pressure Data

One of the motivations for this study was to develop scaling criteria which better satisfy scaling of the pressure conditions and properties of fluids that depend on pressure. In Figures 58 and 59, a comparison of the injection pressures and pressure drops for the large model and those predicted by each of the three scaling approaches is shown. The pressures are expressed in dimensionless form, where the representative pressure selected for non-dimensionalizing is the saturation pressure of steam at 230°C (this selection is discussed in Section 6.9.6). Very good predictions are made using Approach #2, fair predictions using Approach #3, and rather poor predictions using Approach #1 (see Figures 58 and 59). This is not unexpected, as the major weakness of Approach #1 is the inability to scale the pressure conditions and any properties that may depend on them. An example of the scaled properties for steam was noted in Section 6.2.1

Some of the discrepancy between the predicted pressures and those of the large model (shown in Figures 58 and 59) is a result of experimental difficulties in achieving in the small models, exactly the desired permeability required to scale the large model. The actual permeability

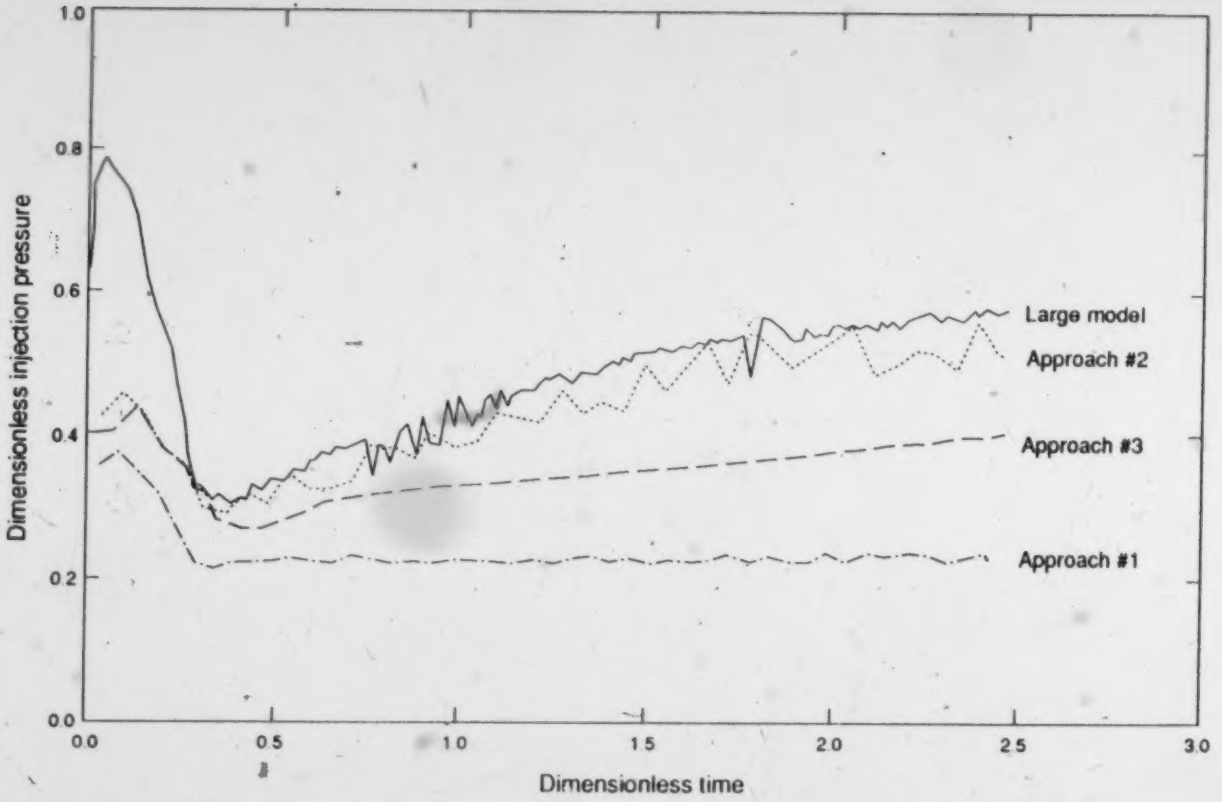

Figure 58. Comparison of the injection pressure for the large model (Run 45) to those predicted using Approaches #1 (Run 43), #2 (Run 39) and #3 (Run 47). The dimensionless injection pressure is defined as $p_D=p_i/p_R$.

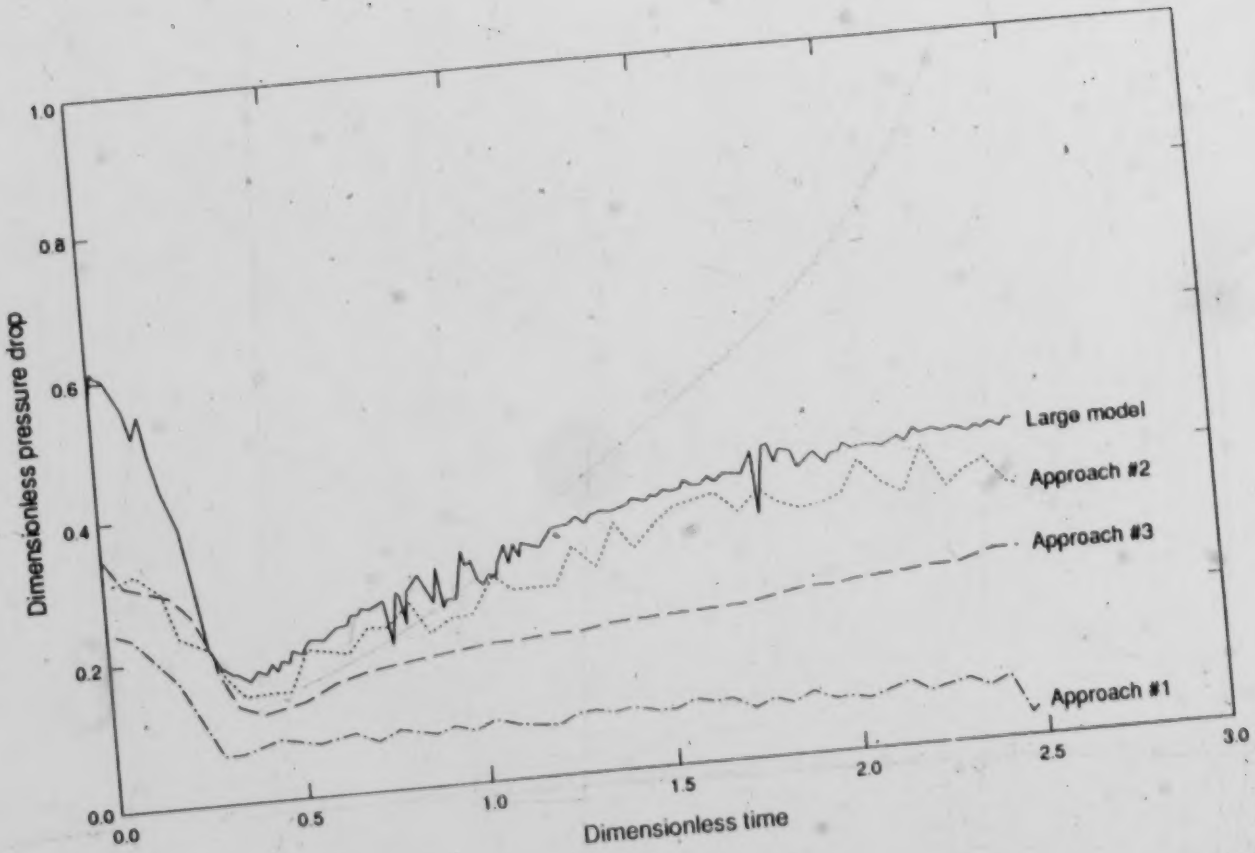

Figure 59. Comparison of the pressure drop across the large model (Run 45) to those predicted using Approaches #1 (Run 43), #2 (Run 39) and #3 (Run 47). The dimensionless pressure drop is defined as $\Delta p_D = \Delta p / p_R$.

for each experiment is listed in Table 12. Note that the models representing Approach #3 have higher permeability than the design requirement. These differences were minimized for all three approaches in these comparisons by multiplying each pressure by the ratio of its actual permeability to the ideal or desired permeability. The results are shown in Figures 60 and 61. In these figures, the predictions made using Approaches #2 and #3 match very closely with the large model results, except for very early times (t_D<0:25).

7.2.7 Quantitative Comparisons

To compare the capabilities of each approach in a more quantitative manner, the average error in predicting each parameter was calculated. The average error was estimated using the area between the curve of the parameter for the large model and that of the prediction made using each scaling approach. This error is defined for the general parameter "m" by:

$$e = \sum \left\{ \left| (m_L - m_S)_i \right| + \left| (m_L - m_S)_{i-1} \right| \right\} \cdot \frac{\Delta t_{Di}}{2}$$

For the energy predictions, the relative importance of the error was included by expressing it as a percentage of the average injected energy. Average errors for the other parameters were expressed as relative errors.

The average errors in predicting the reservoir energy, the overburden losses, and the underburden losses for each approach, for the series of water-only experiments is shown in Figure 62. A similar comparison is

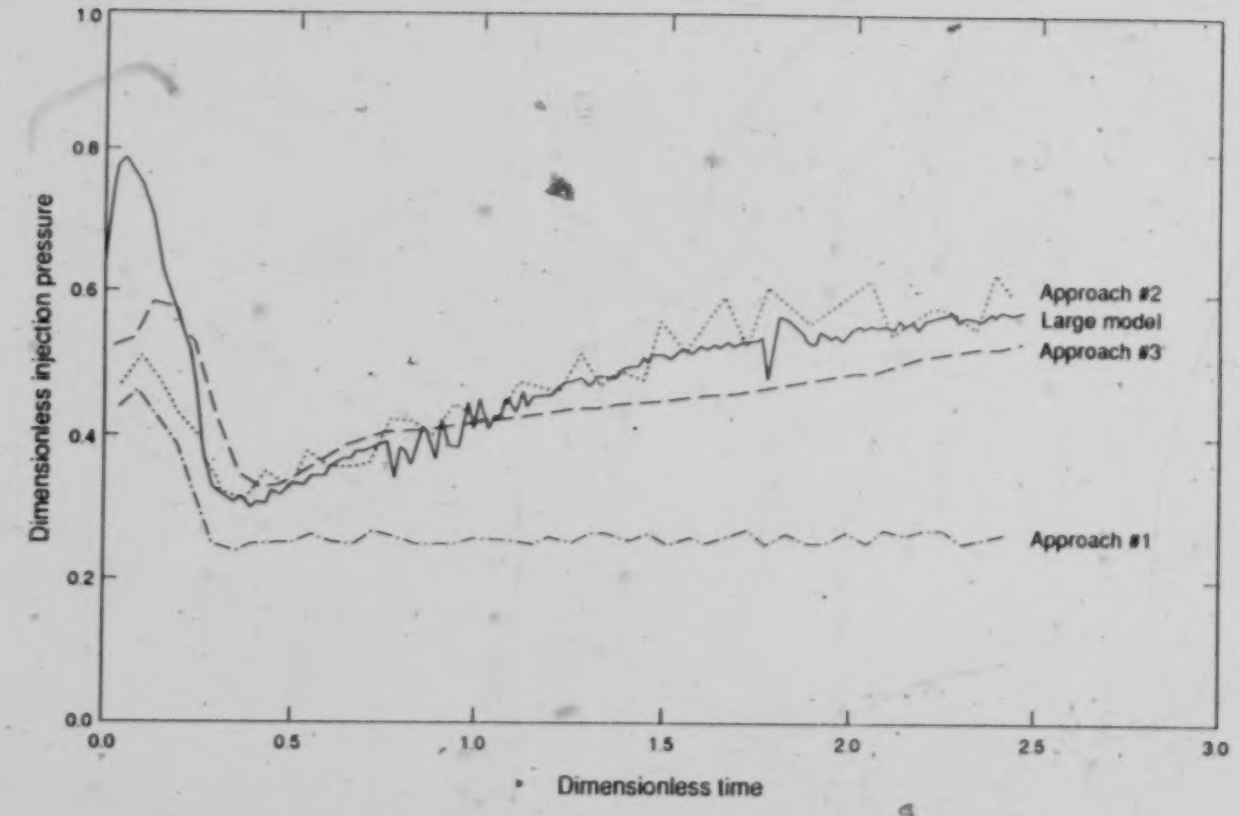

Figure 60. Injection pressure comparisons which minimize the effect of model permeability. The dimensionless injection pressure is defined as $[\Delta p(k/k_{ideal}) + p_{prod}]/p_R$.

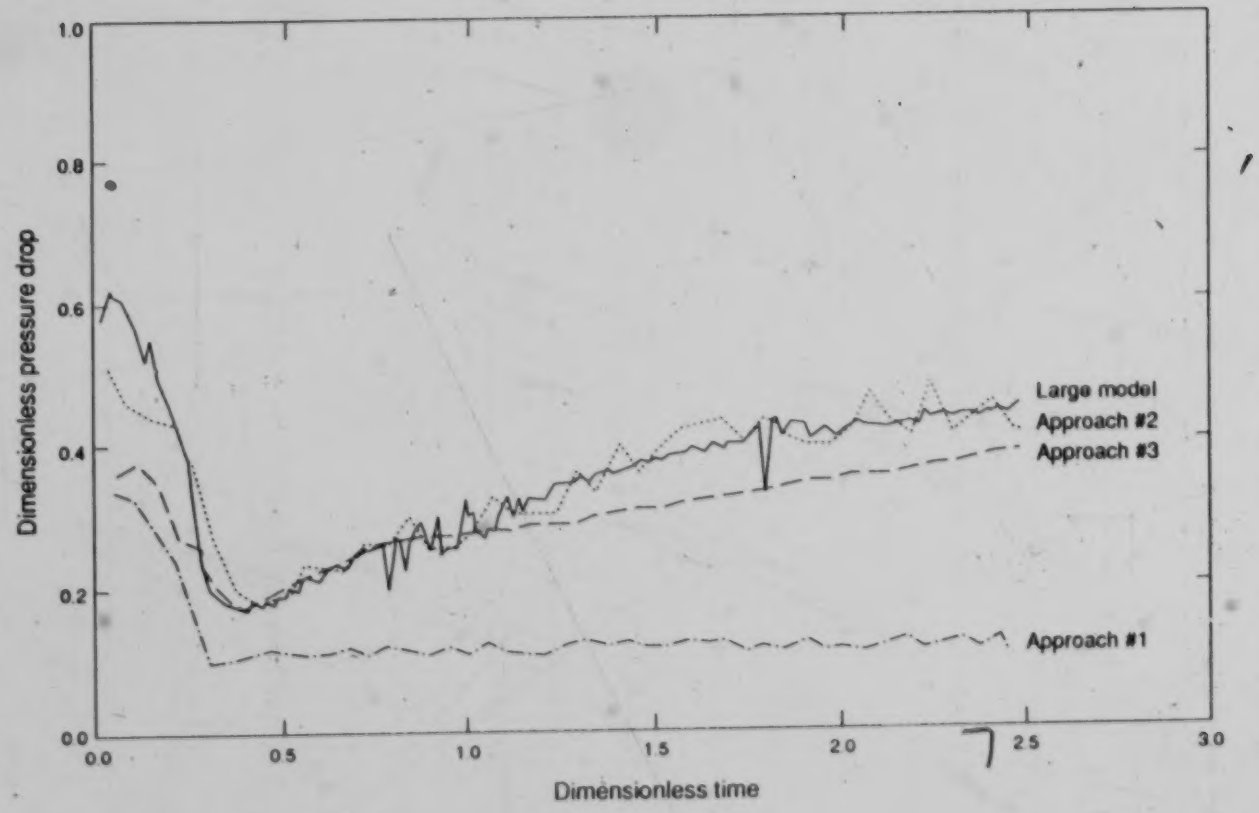

Figure 61. Pressure drop comparisons which minimize the effect of model permeability. The dimensionless pressure drop is defined as $\Delta p(k/k_{ideal})/p_R$.

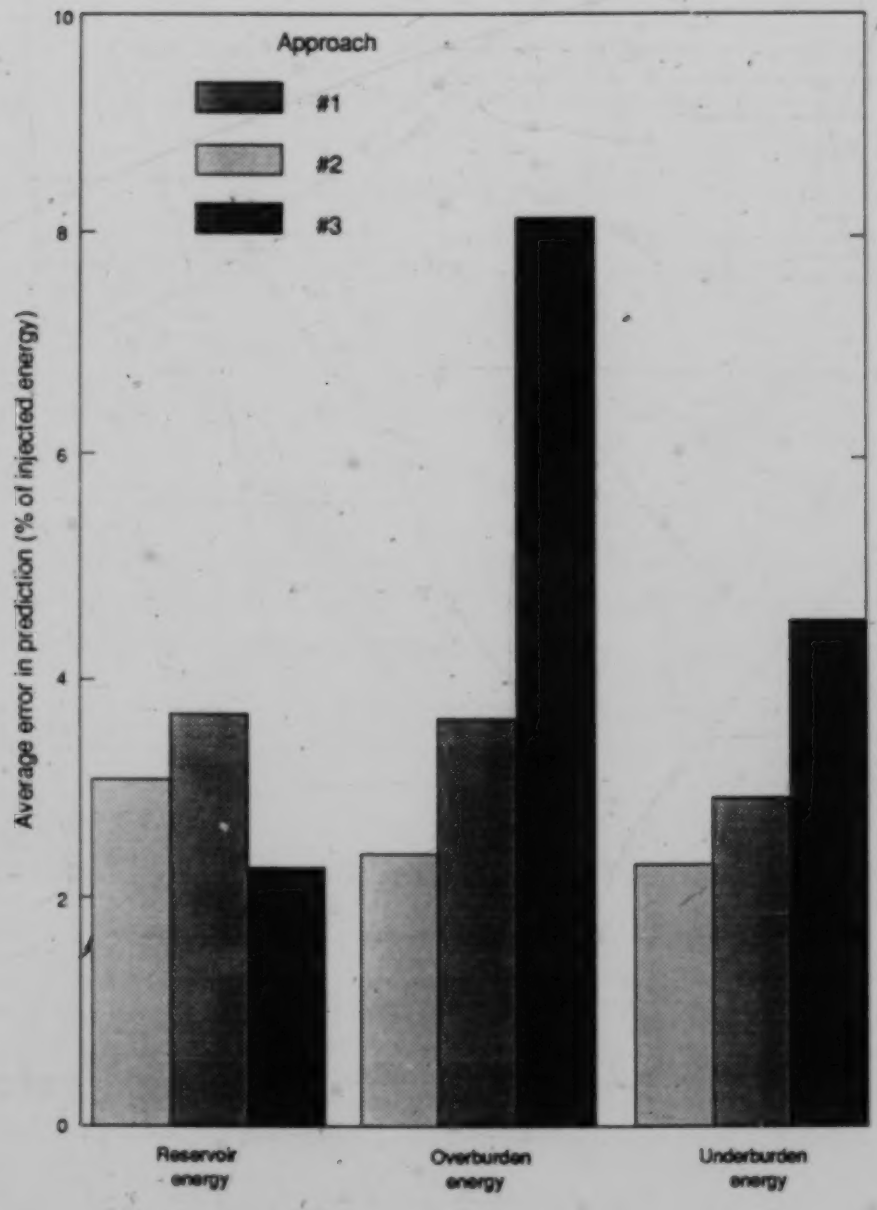

Figure 62. Average errors in predicting energy distribution for each scaling approach for a series of steam-water experiments (Runs 44, 42, 38, 46).

shown in Figure 63 for the series of oil experiments. The predictions made using Approach #2 are slightly better than those made using Approach #1, with the predictions made using Approach #3 being less accurate, particularly those of the energy losses to the surrounding formations. Superior scaling of the pressure conditions are obtainable using Approach #2; this leads to better scaling of the pressure-temperature relationship for steam and may explain the slightly better predictions. The somewhat less accurate predictions made using Approach #3 are attributed to the difficulty in finding material with the necessary thermal properties required to scale the surrounding formations, as the requirements are much more difficult to satisfy.

The average errors in the predictions of steam zone volume, produced steam quality, and production rate for each approach are shown in Figures 64 and 65. They are expressed as relative errors, where the average error for a parameter is divided by its average value. Again, slightly better predictions are made using Approach #2 than those made using Approach #1. The only exceptions are production rate for the steam-water experiment (Figure 64) and the steam zone volume for the steam-oil-water experiment (Figure 65). The better predictions made using Approach #2 may be attributed to better scaling of steam properties. The predictions, when using Approach #3, are less accurate because of greater heat losses to the surrounding formations creating a smaller steam zone and lower production rates.

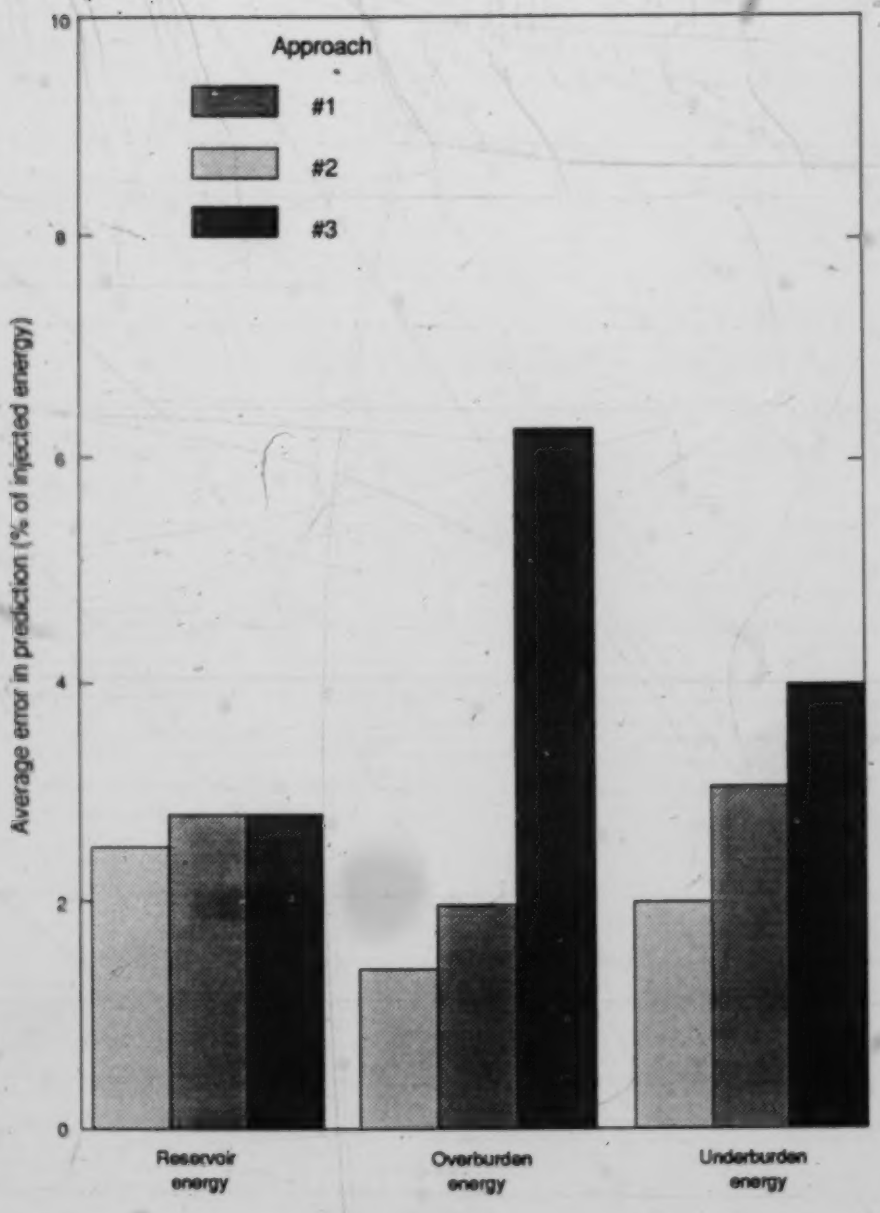

Figure 63. Average errors in predicting energy distribution for each scaling approach for a series of steam-oil-water experiments (Runs 45, 43, 39, 47).

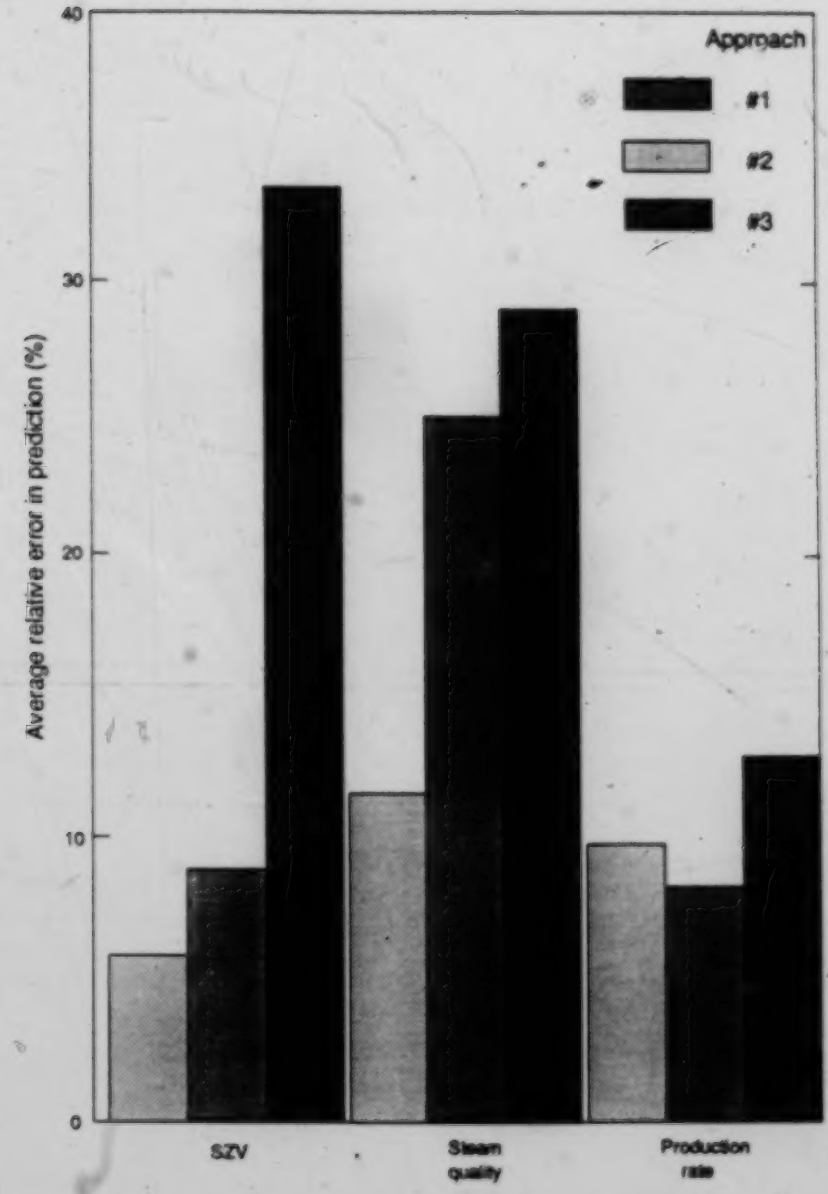

Figure 64. Average relative errors in predicting steam zone volume, produced steam quality, and production rate for a series of steam-water experiments (Runs 44, 42, 38, 46).

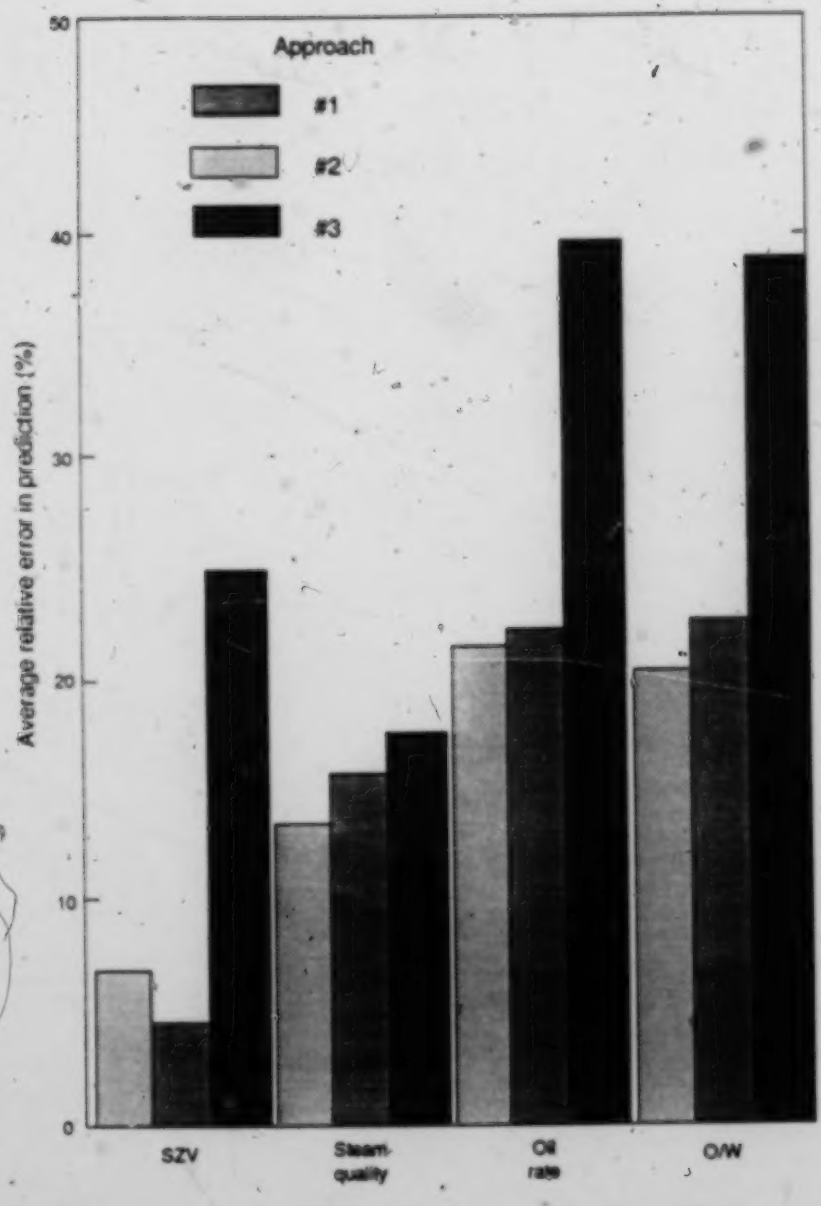

Figure 65. Average relative errors in predicting steam zone volume, produced steam quality, production rate and oil/water ratio for a series of steam-oil-water experiments (Runs 45, 43, 39, 47).

7.3 Heat Losses to the Insulation

Heat losses to the insulation are estimated from the total energy balance. After steam breakthrough, the fraction of the injected energy lost to the insulation is assumed to be constant as both the insulation losses and the produced energy must be inferred from the energy balance. The estimated losses to the insulation vary from about 1% of the injected energy for the higher injection rate experiments to about 7% for the lower injection rate experiments. These are calculated based on an assumed thermal conductivity for the rock wool insulation of 0.0415 W/m°C. Heat flux meters also were used to estimate the energy losses to the insulation. The measured fluxes were very low, the largest being approximately 25 W/m^2. For this experiment, assuming that all boundaries have this flux over the entire perimeter of the model, the losses would amount only to about 4% of the injected energy. Thermocouples were also placed in the insulation, 10 cm from the wall of the model. During the experiment temperatures increased very slightly, about 7°C over 400 minutes.

7.4 Repeatability

Experiments were repeated to determine their reproducibility. Some replicate experiments were performed in previously used models that were restored to their initial temperature and saturation. Other replicate experiments were performed in newly constructed and packed models. Four pairs of replicate runs were performed in the same models (7 & 11, 12 & 16, 27 & 31, and 37 & 38). Five sets of replicate experiments were

performed in different models (9 & 40 & 44, 41 & 45, 38 & 14, 19 & 34, and 29 & 42). The replicates performed in the same models gave relative errors of about 5% for the parameters examined; the replicates performed in the reconstructed models gave average errors of about 8%. This observation is not surprising as rebuilding and repacking the models often results in wider variations. This is evident from the measurements of porosity, permeability, and pore volume for the models (see Table 12). In Figures 66-69, comparisons of energy distributions, production rates, and steam zone volumes for similar experiments performed in the large model and Approaches #1, #2, and #3 are shown. Satisfactory repeatability was found in most cases. The only replicate experiments in different models, scaled using Approach #3, were Runs 19 and 34. This run was repeated because of equipment problems which may explain the larger differences in the comparisons.

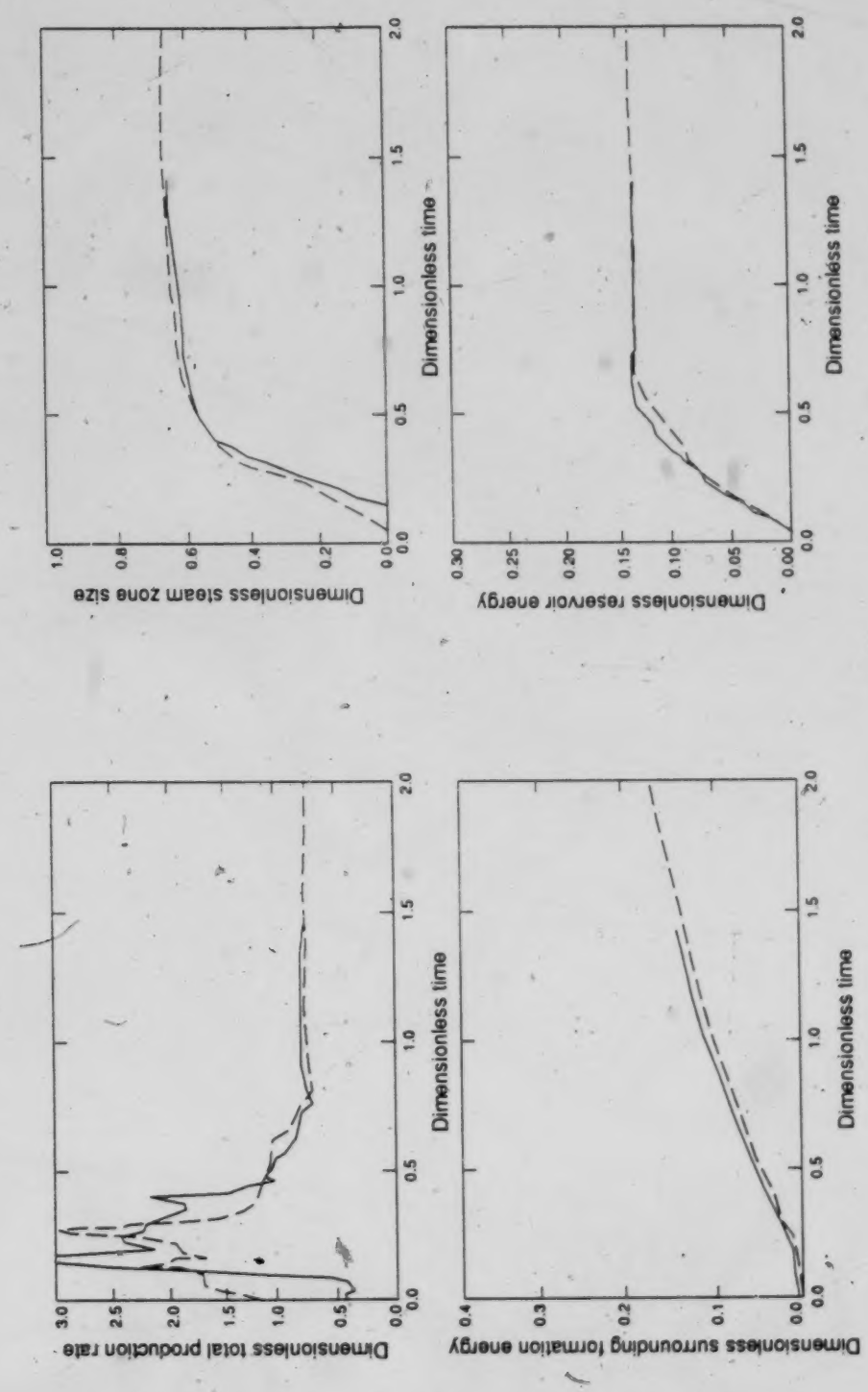

Figure 66. Repeatability of large model experiments (Runs 41 and 45).

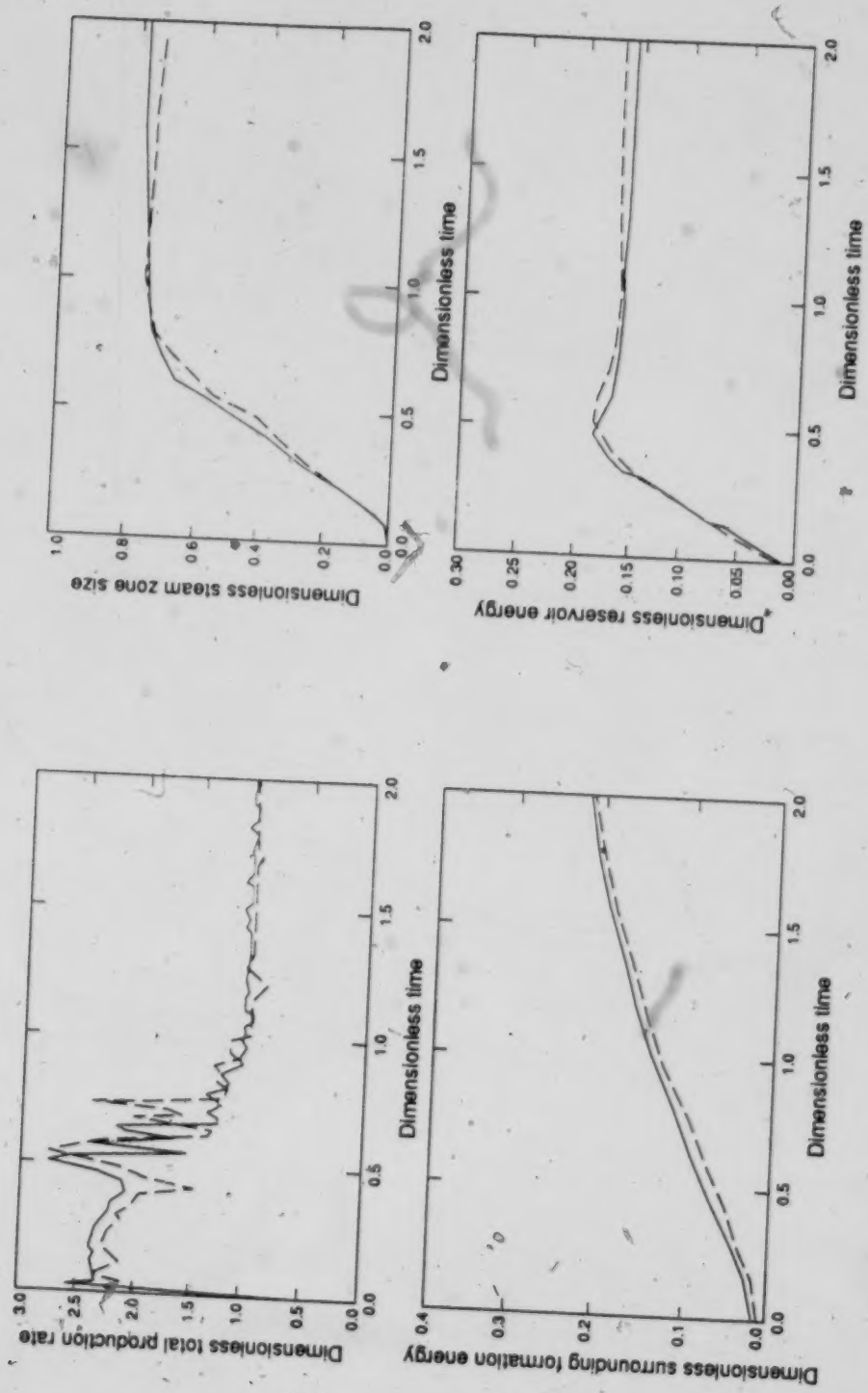

Figure 67. Repeatability of Approach #1 experiments (Runs 14 and 38).

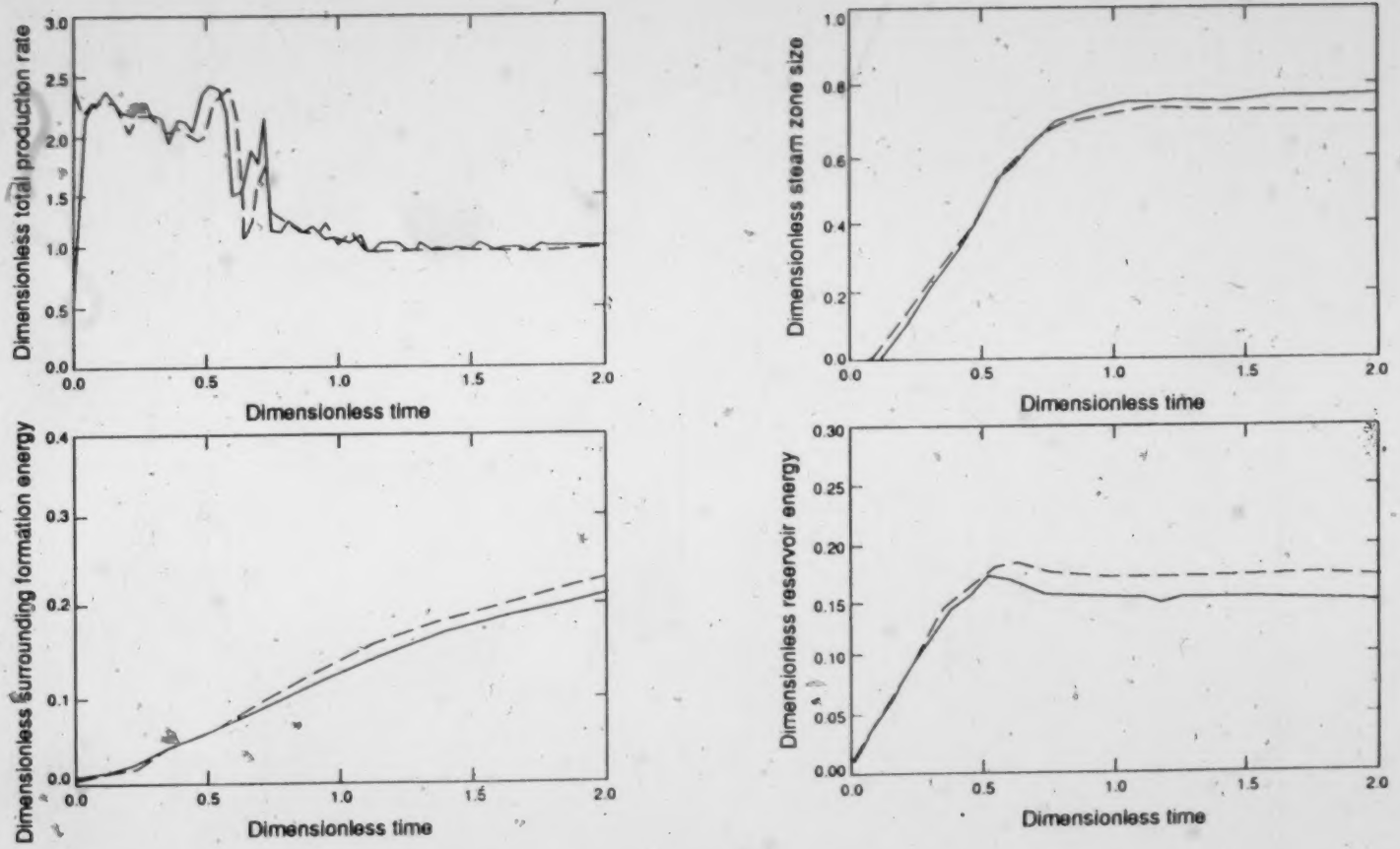

Figure 68. Repeatability of Approach #2 experiments (Runs 29 and 42).

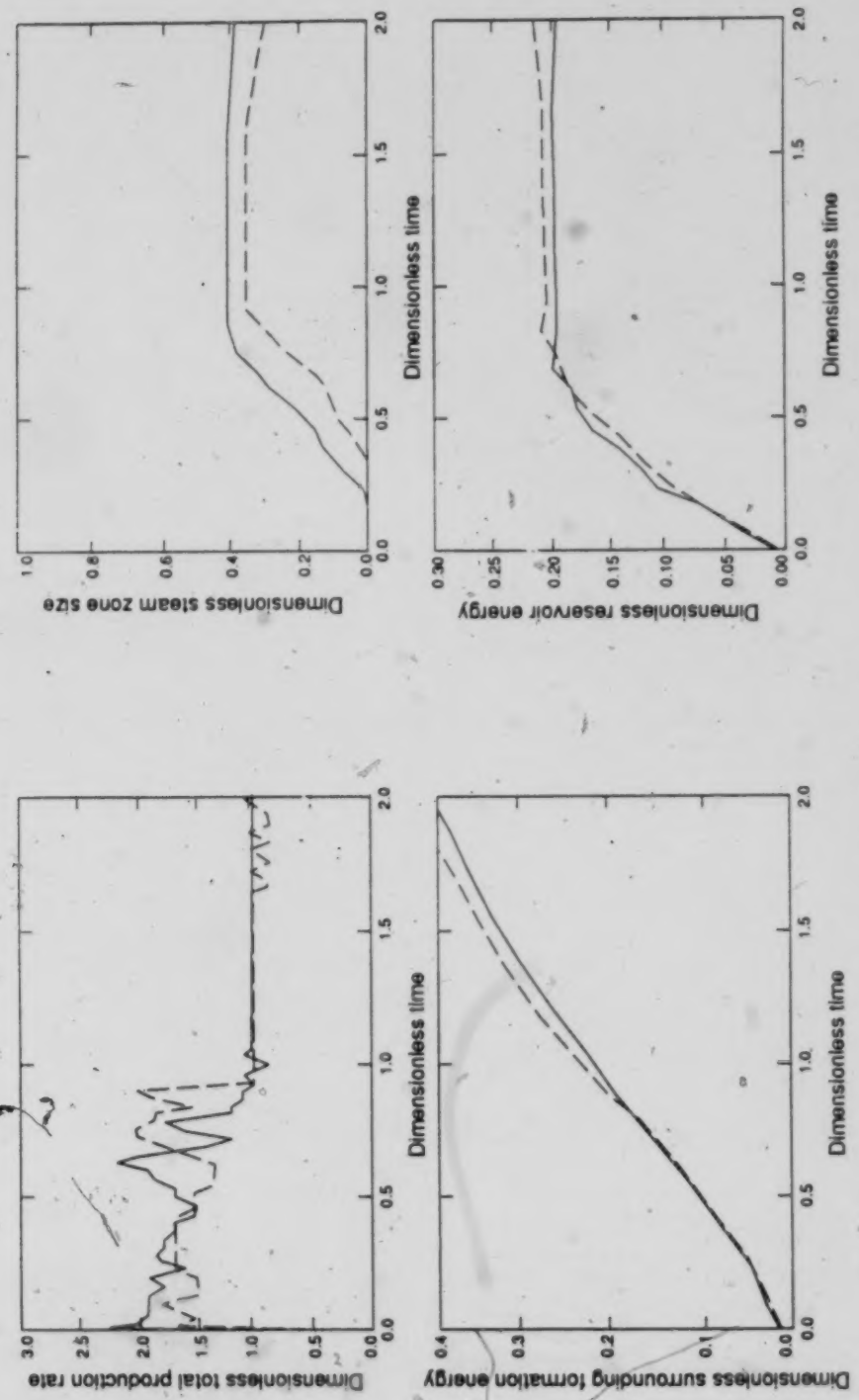

Figure 69. Repeatability of Approach #3 experiments (Runs 19 and 34).

8. SUMMARY AND CONCLUSIONS

A complete set of similarity groups required to scale the steam or steam-plus-additive process as defined by the stated governing differential equations, constraints, constitutive relationships, and initial and boundary conditions was derived. Five sets of scaling criteria, each representing a subset of this more complete set of scaling requirements were developed by rel ·ing the scaling of various phenomena. These criteria offer new options for high-pressure scaling techniques. Three of the approaches allow field porous media and field pressure conditions to be used in the physical models. Two of the approaches address the difficult task of scaling the effects of transverse dispersion in a thermal recovery process. None of these options were previously available.

A high-pressure scaled model facility was designed, constructed, and used to examine the capabilities of these scaling approaches. Some of the requirements of geometric similarity were relaxed in three of the approaches in order to scale other aspects of the process. This novel technique was first tested using a simpler steam-water system and then with a more complex steam-oil-water system. The simpler studies identified a problem in the scaling criteria for design of the surrounding formations for approaches which allow geometric similarity to be relaxed. Rather than scaling thermal diffusivity, it was found that thermal conductivity and heat capacity must be scaled independently using two scaling groups. Further testing using the improved approach in the steam-oil-water system showed that this technique could now be

used to make predictions comparable to those made by the other scaling approaches.

Qualitative and quantitative comparisons of the predictions of each approach were used to determine how well the energy and temperature distributions, the steam zone development, and oil production were scaled. The results indicate that reasonable predictions of all parameters could be made using Approaches #1, #2, or #3 under the conditions studied. Using Approach #2, slightly better predictions of energy distributions, steam zone volume, produced steam quality, and steam breakthrough are made. This is attributed to more accurate scaling of the steam properties. Using Approach #3, slightly less accurate predictions, which is largely attributable to the practical difficulties in satisfying the scaling requirements for design of the surrounding formations, are made. At this point, all three approaches appear to be suitable for scaling steam injection processes.

Approaches #2 and #3 were designed to scale the pressure conditions more accurately. This was tested and shown to be so. Better scaling of the pressure conditions resulted in better scaling of temperature distribution particularly near the injection well. Even though more accurate scaling of the gravitational effects was achieved using Approach #1, no noticeable improvement was observed in the predictions made for the processes that were studied. Perhaps for systems where gravitational override is more severe, significant improvement will result.

Since a number of approaches are available for scaling steam injection processes, the most appropriate one must be selected for the particular

process and conditions being studied. This usually involves making a compromise between the scaling of various mechanisms. The approach chosen should (1) correctly scale the major mechanisms of the process, and (2) not cause minor mechanisms in the process to have significant effects on the response of the experimental model. The selection of an approach can be simplified by using a comparison of approaches such as that presented in Table 8, which indicates the mechanisms that are scaled and estimates the degree by which the others are not. Some processes may not be scaled suitably by any of the approaches discussed here. Other subsets or approaches can be developed and a better approach might be derived in a manner similar to the one presented in this study.

The major conclusions corresponding to the list of objectives outlined in Chapter 2, are as follows:

1. Scaling techniques can be developed which offer new options for scaling steam injection processes. The four new techniques developed in this study could extend the usefulness of scaled models from the study of basic steam drive processes to the study of additives to steam processes, cyclic steam processes, and processes with distillable oils.

2. A high-pressure scaled model facility can be designed, constructed, and used to assess the capabilities of scaling techniques. Comparing the results of large and small model experiments is an extremely useful method by which to assess these capabilities.

3. Reasonable predictions of all parameters were achieved using Approaches #1, #2, and #3 in the two systems studied. Approach #2, in which pressure conditions were accurately scaled but gravitational effects were relaxed, resulted in slightly better predictions, and Approach #3, in which some of the requirements of geometric similarity were relaxed in order to simultaneously scale the pressure conditions and the gravitational effects, resulted in slightly less accurate predictions.

4. The thermal conductivity and heat capacity of the surrounding formations must be scaled independently when using scaling techniques that relax some of the requirements of geometric similarity.

5. Approaches #2 and #3 resulted in more accurate scaling of the pressure conditions, and therefore the fluid properties that depend on pressure. Better scaling of pressures resulted in better scaling of temperature, particularly near the injection well.

6. In order to scale a particular process, an appropriate approach must be selected. A comparison of approaches, such as the one given in this study, can be used to simplify this task.

9. RECOMMENDATIONS FOR FURTHER STUDIES

The new scaling approaches result in comparable predictions for the steam-water and the steam-oil-water systems studied. These new techniques offer various advantages over past approaches, but have some drawbacks as well. Continuing studies must extend the process of verification to include more viscous oils. Processes for which the advantages of the new techniques will be most powerful should be studied. These may include additives to steam processes, cyclic steam processes, and processes with significant distillation effects. Any future studies should include the use of numerical simulation as these are not competing techniques, but complementary ones. This study and future ones will assist in the calibration of numerical simulators. Ultimately, the verification of scaling techniques lies in their utility for field purposes. Final verification will come by comparing the usefulness of each approach when optimizing field recovery processes and designing field pilots.

REFERENCES

1. LEVERETT, M.C., LEWIS, W.B. and TRUE, M.E.: "Dimensional Model Studies of Oil Field Behavior," Trans. AIME, Vol. 146, 175, 1942.

2. RAPOPORT, L.A. and LEAS, W.J.: "Properties of Linear Waterfloods," Trans. AIME, Vol. 198, 139, 1953.

3. CROES, G.A. and SCHWARZ, N.: "Dimensionally Scaled Experiments and the Theories in the Water Drive Process," Trans. AIME, Vol. 204, 35, 1955.

4. GEERTSMA, J., CROES, G.A. and SCHWARZ, N.: "Theory of Dimensionally Scaled Models of Petroleum Reservoirs," Trans. AIME, Vol. 207, 118-127, 1956.

5. BAKER, P.E.: "An Experimental Study of Heat Flow in Steamflooding," SPEJ, 89-99, March 1969.

6. BAKER, P.E.: "Effect of Pressure and Rate on Steam Zone Development in Steamflooding," SPEJ, 274-284, October 1973.

7. FAROUQ ALI, S.M. and REDFORD, D.A.: "Physical Modeling of In Situ Recovery Methods for Oil Sands," Canada-Venezuela Oil Sands Symposium, Edmonton, Canada, CIM Special Volume No. 17, 319-326, 1977.

8. STEGEMEIER, G.L., VOLEK, C.W. and LAUMBACH, D.D.: "Representing Steam Processes with Vacuum Models," 52nd Annual Fall Technical Conference and Exhibition, Denver, SPE Paper No. 6787, 1977.

9. PUJOL, L. and BOBERG, T.C.: "Scaling Accuracy of Laboratory Steamflooding Models," 43rd Annual California Regional Meeting, Bakersfield, SPE Paper No. 4191, 1972.

10. BURSELL, C.G. and PITTMAN, G.M.: "Performance of Steam Displacement Kern River Field," 49th Annual Fall Meeting of SPE, Houston, SPE Paper No. 5017, 1974.

11. HUYGEN, H.H.A.: "Laboratory Steamfloods in Half of a Five-Spot," 51st Annual Meeting of the SPE of AIME, New Orleans, Louisiana, SPE Paper No. 6171, October 1976.

12. HUYGEN, H.H.A. and LOWRY, W.E.: "Steamflooding Wabasca Tar Sand Through The Bottom Water Zone -- Scaled Model Tests," SPEJ, 92-98, February 1983.

13. PURSLEY, S.A.: "Experimental Studies of Thermal Recovery Processes," Paper presented at the Heavy Oil Symposium, Maracaibo, Venezuela, 1974.

14. EHRLICH, R.: "Laboratory Investigation of Steam Displacement in the Wabasca Grand Rapids A Sand," Canada-Venezuela Oil Sands Symposium, Edmonton, Alberta, CIM Special Volume No. 17, 364-379, 1977.

15. NIKO, H. and TROOST, P.J.P.M.: "Experimental Investigation of Steam Soak Process in a Depletion Type Reservoir," JPT, 23, 1006-1014, August 1971.

16. PRATS, M.: "Peace River Steam Drive Scaled Model Experiments," Canada-Venezuela Oil Sands Symposium, Edmonton, Alberta, CIM Special Volume No. 17, 346-363, 1977.

17. PROCTOR, M.: "Steam Injection Experiments in a Scaled Physical Model," M.Sc. Thesis, University of Alberta, 1985.

18. SUFI, A.H.: "Injectivity Enhancement in Tar Sands - A Physical Model Study," 39th Annual Technical Meeting of the Petroleum Society of CIM, Calgary, 1988.

19. SINGHAL, A.K.: "Physical Model Study of Inverted Seven-Spot Steam Floods in a Pool Containing a Lloydminster Type Heavy Oil," Petroleum Recovery Institute, Research Report RR-38, November 1978.

20. DOSCHER, T.M.: "Scaled Physical Model Studies of the Steam Drive Process," First Annual Report, DOE/ET/12075-1, September 1977-September 1978.

21. YORTSOS, Y.C.: "Analytical Modeling of Oil Recovery by Steam Injection," Ph.D. Dissertation, California Institute of Technology, 1979.

22. BUTLER, R.M. and CHUNG, K.H.: "A Theoretical and Experimental Study of Steam-Assisted Gravity Drainage Process," 4th UNITAR/UNDP Conference, Paper No. 89, 1988.

23. NASR, T.: confidential report, 1988.

24. KENNEDY, W.A. and CRAWFORD, G.W.: "Derivation of the Dimensionless Scaling Groups Governing Miscible and Steam Drive Processes," Report No. UT 59-8, Texas Petroleum Research Committee, Austin, Texas, August 13 1959.

25. POZZI, A.L., Jr. and BLACKWELL, R.J.: "Design of Laboratory Models for the Study of Miscible Displacement," SPEJ, 28-40, March 1963.

26. ROJAS, G.A.: "Scaled Model Studies of Immiscible Carbon Dioxide Displacements of Heavy Oil," Ph.D. Thesis, University of Alberta, 1985.

27. BEAR, J. and BACHMAT, Y.: "Transport Phenomena in Porous Media Basic Equations," Presented at the NATO Advanced Study Institute on Mechanics of Fluids in Porous Media, Newark, Delaware, July 1982.

28. CHUOKE, R.L., VAN MEURS, P. and VAN DER POEL, C.: "The Instability of Slow, Immiscible, Viscous Liquid-Liquid Displacements in Permeable Media," Trans. AIME, Vol. 216, 188, 1959.

29. SAFFMAN, P.G. and TAYLOR, G.I.: "The Penetration of a Fluid into a Porous Medium or Hele-Shaw Cell Containing a More Viscous Liquid," Proc. Roy. Soc., 245A, 312, 1958.

30. MILLER, C.A.: "Stability of Moving Surfaces in Fluid Systems with Heat and Mass Transport III. Stability of Displacement Fronts in Porous Media," AIChE J., Vol. 21, 474, 1975.

31. BENTSEN, R.G.: "A New Approach to Instability Theory in Porous Media," SPEJ, 765, October 1985.

32. DE LA CRUZ, V., SPANOS, T.J.T. and SHARMA, R.C.: "The Stability of a Steam-Water Front in a Porous Medium," CJChE, 735-745, October 1985.

33. PRATS, M.: "Thermal Recovery," Monograph Volume 7, SPE-AIME, 1982.

34. COMBARNOUS, M. and SOURIEAU, P.: "Les Methodes Thermiques de Production des Hydrocarbares," Revue, Inst. Francais du Petrole, Chap. 3, 543, July-August 1976.

35. HIRASAKI, G.J.: "Scaling of Non-Equilibrium Phenomena in Surfactant Flooding," 1st Joint SPE/DOE Symposium on Enhanced Oil Recovery, April 1980.

36. LOOMIS, A.G. and CROWELL, D.C.: "Theory and Application of Dimensional and Inspectional Analysis to Model Study of Fluid Displacements in Petroleum Reservoirs," Bureau of Mines Report RI6546, 1964.

37. PETERS, E.J.: "Scaling Unstable Immiscible Displacements," unsolicited paper SPE 12331, 1983.

38. MUSKAT, M.: "Flow of Homogeneous Fluids," IHRDC, Boston, 1982.

39. CARSLAW, H.S. and JAEGER, J.C.: "Conduction of Heat in Solids," Oxford University Press, London, 1959.

40. STALKUP, F.I., Jr.: "Miscible Displacement," Monograph Volume 8, SPE-AIME, 1983.

41. PERKINS, T.K. and JOHNSTON, O.C.: "A Review of Diffusion and Dispersion in Porous Media," SPEJ, 70-84, March 1963.

APPENDIX A - INITIAL AND BOUNDARY CONDITIONS

Analysis of the partial differential equations representing the process shows that the system may be represented by four primitive variables,

i) two of S_g, S_o, S_w

ii) two of $T, p_o, C_{oo}, C_{ow}, C_{go}, C_{gw}$

By selecting S_g, S_w, T and p_o, the initial and boundary conditions may be defined as follows:

a) boundary conditions

i) lower boundary or upper boundary

$$\rho_o v_{on} = -\frac{\rho_o \bar{k}_o}{\mu_o} \cdot (\nabla_n p_o + \rho_o g \nabla_n z) = 0 \qquad \text{(A-1)}$$

$$k_{hr} \nabla_n T_r = k_{hc} \nabla_n T_c$$

where $T_c(t, x_1, x_2, x_3 \to \pm\infty) = T_i$

and $$(\rho C_p)_c \frac{\partial T_c}{\partial t} = \nabla \cdot (k_{hc} \nabla T_c) \qquad \text{(A-2)}$$

$$\rho_g v_{gn} = -\frac{\rho_g \bar{k}_g}{\mu_g} \cdot (\nabla_n p_g + \rho_g g \nabla_n z) = 0 \qquad \text{(A-3)}$$

$$\rho_w v_{wn} = -\frac{\rho_w \bar{k}_w}{\mu_w} \cdot (\nabla_n p_w + \rho_w g \nabla_n z) = 0 \qquad \text{(A-4)}$$

ii) walls or boundaries of symmetry of the pattern

$$\nabla_n p_o = -\rho_o g \nabla_n z \tag{A-5}$$

$$k_{hr} \nabla_n T = 0 \tag{A-6}$$

$$\nabla_n p_g = -\rho_g g \nabla_n z \tag{A-7}$$

$$\nabla_n p_w = -\rho_w g \nabla_n z \tag{A-8}$$

iii) injection well

$$\int_{A_{inj}} \frac{\rho_o}{\mu_o} \bar{\bar{k}}_o \cdot (\nabla p_o + \rho_o g \nabla z) \, dA = W_{os} \tag{A-9}$$

$$\int_{A_{inj}} \frac{\rho_w}{\mu_w} \bar{\bar{k}}_w \cdot (\nabla p_w + \rho_w g \nabla z) \, dA = W_{ww} \tag{A-10}$$

$$\int_{A_{inj}} \frac{\rho_g}{\mu_g} \bar{\bar{k}}_g \cdot (\nabla p_g + \rho_g g \nabla z) \, dA = W_{gs} + W_{gw} \tag{A-11}$$

$$\int_{A_{inj}} \left[k_{hr} \nabla_n T + \frac{\rho_g}{\mu_g} h_g \bar{\bar{k}}_g \cdot (\nabla_n p_g + \rho_g g \nabla_n z) + \frac{\rho_w}{\mu_w} h_w \bar{\bar{k}}_w \cdot (\nabla_n p_w + \rho_w g \nabla_n z) + \frac{\rho_o}{\mu_o} h_o \bar{\bar{k}}_o \cdot (\nabla_n p_o + \rho_o g \nabla_n z) \right] dA = W_{gs} h_{gs_{inj}} + W_{os} h_{os_{inj}} + W_{gw} h_{gw_{inj}} + W_{ww} h_{ww_{inj}} \tag{A-12}$$

iv) production well

$$p_o = p_{prod} \tag{A-13}$$

$$p_g = p_{prod} + P_{cgo} \tag{A-14}$$

$$p_w = p_{prod} + P_{cow} \tag{A-15}$$

$$\nabla_n T = 0 \tag{A-16}$$

b) initial conditions

$$S_g\ (0,x_1,x_2,x_3) = S_{gi}\ (0,x_1,x_2,x_3) \tag{A-17}$$

$$S_w\ (0,x_1,x_2,x_3) = S_{wi}\ (0,x_1,x_2,x_3) \tag{A-18}$$

$$p_o\ (0,x_1,x_2,x_3) = p_{oi}\ (0,x_1,x_2,x_3) \tag{A-19}$$

$$T\ (0,x_1,x_2,x_3) = T_i \tag{A-20}$$

APPENDIX B - DEVELOPMENT OF THE RELAXED SCALING CRITERIA

The method of deriving a relaxed set of scaling criteria is similar for all of the approaches. It is illustrated in this appendix for Approach #2. Based on the assumptions of an approach, the terms corresponding to these assumptions are eliminated from the governing balance equations which are in the form shown in Table 3. Each equation is then divided by one of the remaining coefficients to yield the dimensionless form of the equation. The coefficients represent the relaxed set of similarity groups which can then be reduced to their simplest form. The constitutive relationships, constraints, and initial and boundary conditions are treated in a similar manner.

For Approach #2, the effects of gravity and transverse and longitudinal dispersion are assumed to be negligible. For simplicity, the following model for diffusion was adopted.[40]

$$D^*_{eff} = D^*/F\phi \tag{B-1}$$

The following simple relationships given by Perkins and Johnston[41] for the dispersion coefficient were used when the effects of dispersion were considered.

$$D_L = D^*/F\phi + 0.5v\chi d_p \tag{B-2}$$

$$D_T = D^*/F\phi + 0.0157v\chi d_p \tag{B-3}$$

The equation from Table 3 then becomes:

$$\left[\frac{\phi_R S_{oR} C_{ooR} \rho_{oR}}{t_R}\right] \frac{\partial}{\partial t_D}(\phi_D S_{oD} C_{oD} \rho_{oD}) = \left[\frac{C_{ooR} \rho_{oR} k_{oR} P_{oR}}{x_{1R}^2 \mu_{oR}}\right] \frac{\partial}{\partial x_{1D}}$$

$$\left(C_{ooD} \rho_{oD} \frac{k_{oD}}{\mu_{oD}} \frac{\partial p_{oD}}{\partial x_{1D}}\right) + \left[\frac{C_{ooR} \rho_{oR} k_{oR} P_{oR}}{x_{2R}^2 \mu_{oR}}\right] \frac{\partial}{\partial x_{2D}} \left(C_{ooD} \frac{\rho_{oD} k_{oD}}{\mu_{oD}} \frac{\partial p_o}{\partial x_{2D}}\right) +$$

$$\left[\frac{C_{ooR} \rho_{oR} k_{oR} P_{oR}}{x_{3R}^2 \mu_{oR}}\right] \frac{\partial}{\partial x_{3D}} \left(C_{ooD} \rho_{oD} \frac{k_{oD}}{\mu_{oD}} \frac{\partial p_{oD}}{\partial x_{3D}}\right) +$$

$$\left[\frac{S_{oR} D^*_{ooR} C_{ooR} \rho_{oR}}{F_R x_{1R}^2}\right] \frac{\partial}{\partial x_{1D}} \left(S_{oD} \frac{D^*_{ooD}}{F_D} \frac{\partial}{\partial x_{1D}} (C_{ooD} \rho_{oD})\right) +$$

$$\left[\frac{S_{oR} D^*_{ooR} C_{ooR} \rho_{oR}}{F_R x_{2R}^2}\right] \frac{\partial}{\partial x_{2D}} \left(S_{oD} \frac{D^*_{ooD}}{F_D} \frac{\partial}{\partial x_{2D}} (C_{ooD} \rho_{oD})\right) +$$

$$\left[\frac{S_{oR} D^*_{ooR} C_{ooR} \rho_{oR}}{F_R x_{3R}^2}\right] \frac{\partial}{\partial x_{3D}} \left(S_{oD} \frac{D^*_{ooD}}{F_D} \frac{\partial}{\partial x_{3D}} (C_{ooD} \rho_{oD})\right) \qquad \text{(B-4)}$$

Dividing through by the coefficient, $\left[\frac{C_{ooR} \rho_{oR} k_{oR} P_{oR}}{x_{1R}^2 \mu_{oR}}\right]$,

yields the equation in dimensionless form:

$$\left[\frac{\phi_R S_{oR} x_{1R}^2 \mu_{oR}}{t_R k_{oR} P_{oR}}\right] \frac{\partial}{\partial t_D} (\phi_D S_{oD} C_{oD} \rho_{oD}) = \frac{\partial}{\partial x_{1D}} \left(C_{ooD} \rho_{oD} \frac{k_{oD}}{\mu_{oD}} \frac{\partial p_{oD}}{\partial x_{1D}}\right) +$$

$$\left[\frac{x_{1R}^2}{x_{2R}^2}\right] \frac{\partial}{\partial x_{2D}} \left(C_{ooD} \rho_{oD} \frac{k_{oD}}{\mu_{oD}} \frac{\partial p_{oD}}{\partial x_{2D}}\right) + \left[\frac{x_{1R}^2}{x_{3R}^2}\right] \frac{\partial}{\partial x_{3D}} \left(C_{ooD} \rho_{oD} \frac{k_{oD}}{\mu_{oD}} \frac{\partial p_{oD}}{\partial x_{3D}}\right) + \left[\frac{S_{oR} D^*_{ooR} \mu_{oR}}{F_R k_{oR} P_{oR}}\right] \frac{\partial}{\partial x_{1D}}$$

$$\left(S_{oD} \frac{D^*_{ooD}}{F_D} \frac{\partial}{\partial x_{1D}} (C_{ooD} \rho_{oD})\right) + \left[\frac{S_{oR} D^*_{ooR} \mu_{oR} x_{1R}^2}{F_R k_{oR} x_{2R}^2 P_{oR}}\right] \frac{\partial}{\partial x_{2D}} \left(S_{oD} \frac{D^*_{ooD}}{F_D} \frac{\partial}{\partial x_{2D}} (C_{ooD} \rho_{oD})\right) +$$

$$\left[\frac{S_{oR}D^{*}_{ooR}\mu_{oR}x^{2}_{1R}}{F_{R}x^{2}_{3R}k_{oR}P_{oR}}\right]\frac{\partial}{\partial x_{3D}}\left(S_{oD}\frac{D^{*}_{ooD}}{F_{D}}\frac{\partial}{\partial x_{3D}}\left(C_{ooD}\rho_{oD}\right)\right) \qquad \text{(B-5)}$$

The other mass balance equations, the energy balance equation, the constitutive relationships and constraints, and the initial and boundary conditions can be treated in a similar manner. This will lead to the following set of similarity groups.

$$\frac{L}{x_{1R}},\ \frac{H}{x_{2R}},\ \frac{W}{x_{3R}},\ \frac{x_{2R}}{x_{1R}},\ \frac{x_{3R}}{x_{1R}},\ \frac{\phi_{R}S_{oR}x^{2}_{1R}\mu_{oR}}{t_{R}k_{oR}P_{oR}},\ \frac{k_{oR}\rho_{oR}h_{oR}P_{oR}}{\mu_{oR}k_{hrR}T_{R}},\ \frac{\rho_{rR}U_{rR}}{\rho_{wR}h_{wR}},\ \frac{h_{oR}}{h_{wR}},\ \frac{h_{qR}}{h_{wR}},$$

$$\frac{\mu_{oR}k_{qR}}{\mu_{gR}k_{oR}},\ \frac{\mu_{oR}k_{wR}}{\mu_{wR}k_{oR}},\ \frac{\rho_{oR}}{\rho_{wR}},\ \frac{\rho_{qR}}{\rho_{wR}},\ \frac{W_{osR}}{W_{wwR}},\ \frac{W_{qwR}}{W_{wwR}},\ \frac{W_{qsR}}{W_{wwR}},\ \phi_{R},\ \frac{k_{hcR}}{k_{hrR}},\ \frac{S_{wiR}}{S_{wR}},\ \frac{S_{qiR}}{S_{wR}},\ \frac{T_{iR}}{T_{R}},$$

$$\frac{P_{iR}}{P_{oR}},\ \frac{P_{pwR}}{P_{oR}},\ \frac{W_{wwR}\mu_{wR}}{\rho_{wR}k_{wR}P_{wR}x_{2R}},\ \frac{A_{iwR}}{x_{1R}x_{2R}},\ \frac{S_{oR}\mu_{oR}D^{*}_{ooR}}{k_{oR}P_{oR}F_{R}},\ \frac{D^{*}_{ooR}}{D^{*}_{osR}},\ \frac{D^{*}_{qsR}}{D^{*}_{osR}},\ \frac{D^{*}_{qwR}}{D^{*}_{osR}}$$

The reference quantities for the independent variables, x_1, x_2, x_3 and t can be written in terms of the reference quantities of the dependent variables by setting a group containing each reference quantity to one.

By setting $\frac{L}{x_{1R}} = 1$, $\quad x_{1R} = L$

By setting $\frac{x_{2R}}{x_{1R}} = 1$, $\quad x_{2R} = L$

By setting $\frac{x_{3R}}{x_{1R}} = 1$, $\quad x_{3R} = L$

By setting $\frac{\phi_{R}S_{oR}x^{2}_{1R}\mu_{oR}}{t_{R}k_{oR}P_{oR}} = 1$

$$t_R = \frac{\phi_R S_{oR} L^2 \mu_{oR}}{k_{oR} P_{oR}}$$

Substituting these into the set of similarity groups shown before, the set of relaxed scaling criteria for Approach #2 becomes:

$$\frac{H}{L}, \frac{W}{L}, \frac{k_{oR}\rho_{oR}h_{oR}P_{oR}}{\mu_{oR}k_{hrR}T_R}, \frac{\rho_{rR}U_{rR}}{\rho_{wR}h_{wR}}, \frac{h_{oR}}{h_{wR}}, \frac{h_{gR}}{h_{wR}}, \frac{\mu_{oR}k_{gR}}{\mu_{gR}k_{oR}}, \frac{\mu_{oR}k_{wR}}{\mu_{wR}k_{oR}}, \frac{\rho_{oR}}{\rho_{wR}}, \frac{\rho_{gR}}{\rho_{wR}},$$

$$\frac{W_{osR}}{W_{wwR}}, \frac{W_{gwR}}{W_{wwR}}, \frac{W_{gsR}}{W_{wwR}}, \phi_R, \frac{k_{hcR}}{k_{hrR}}, \frac{S_{wiR}}{S_{wR}}, \frac{S_{giR}}{S_{wR}}, \frac{T_{iR}}{T_R}, \frac{P_{iR}}{P_{oR}}, \frac{P_{pwR}}{P_{oR}}, \frac{W_{wwR}\mu_{wR}}{\rho_{wR}k_{wR}P_{wR}L},$$

$$\frac{A_{iwR}}{L^2}, \frac{S_{oR}\mu_{oR}D^*_{ooR}}{k_{oR}P_{oR}F_R}, \frac{D^*_{ooR}}{D^*_{osR}}, \frac{D^*_{gsR}}{D^*_{osR}}, \frac{D^*_{gwR}}{D^*_{osR}}$$

APPENDIX C - DIFFERENTIAL EQUATIONS IN DIMENSIONLESS FORM

1) Mass Balance For Solvent

$$\left[\frac{\phi_R S_{oR} C_{osR} \rho_{oR}}{t_R}\right] \frac{\partial}{\partial t_D} (\phi_D S_{oD} C_{osD} \rho_{oD} + \left[\frac{S_{gR} C_{gsR} \rho_{gR}}{S_{oR} C_{osR} \rho_{oR}}\right] (\phi_D S_{gD} C_{gsD} \rho_{gD})$$

$$= \left[\frac{C_{osR} \rho_{oR} k_{oR} p_{oR}}{x_{1R}^2 \mu_{oR}}\right] \frac{\partial}{\partial x_{1D}} (C_{osD} \rho_{oD} \frac{k_{oD}}{\mu_{oD}} \frac{\partial p_{oD}}{\partial x_{1D}}) + \left[\frac{C_{osR} \rho_{oR}^2 k_{oR} g_R z_R}{x_{1R}^2 \mu_{oR}}\right] \frac{\partial}{\partial x_{1D}}$$

$$(C_{osD} \rho_{oD}^2 \frac{k_{oD}}{\mu_{oD}} g_D \frac{\partial z_D}{\partial x_{1D}}) + \left[\frac{C_{osR} \rho_{oR} k_{oR} p_{oR}}{x_{2R}^2 \mu_{oR}}\right] \frac{\partial}{\partial x_{2D}} (C_{osD} \rho_{oD} \frac{k_{oD}}{\mu_{oD}} \frac{\partial p_{oD}}{\partial x_{2D}})$$

$$+ \left[\frac{C_{osR} \rho_{oR}^2 k_{oR} g_R z_R}{\mu_{oR} x_{2R}^2}\right] \frac{\partial}{\partial x_{2D}} (C_{osD} \rho_{oD}^2 \frac{k_{oD}}{\mu_{oD}} g_D \frac{\partial z_D}{\partial x_{2D}}) + \left[\frac{C_{osR} \rho_{oR} k_{oR} p_{oR}}{x_{3R}^2 \mu_{oR}}\right] \frac{\partial}{\partial x_{3D}}$$

$$(C_{osD} \rho_{oD} \frac{k_{oD}}{\mu_{oD}} \frac{\partial p_{oD}}{\partial x_{3D}}) + \left[\frac{C_{osR} \rho_{oR}^2 k_{oR} g_R z_R}{\mu_{oR} x_{3R}^2}\right] \frac{\partial}{\partial x_{3D}} (C_{osD} \rho_{oD}^2 \frac{k_{oD}}{\mu_{oD}} g_D \frac{\partial z_D}{\partial x_{3D}})$$

$$+ \left[\frac{C_{gsR} \rho_{gR} k_{gR} p_{gR}}{x_{1R}^2 \mu_{gR}}\right] \frac{\partial}{\partial x_{1D}} (C_{gsD} \rho_{gD} \frac{k_{gD}}{\mu_{gD}} \frac{\partial p_{gD}}{\partial x_{1D}}) + \left[\frac{C_{gsR} \rho_{gR}^2 k_{gR} g_R z_R}{\mu_{gR} x_{1R}^2}\right] \frac{\partial}{\partial x_{1D}}$$

$$(C_{gsD} \rho_{gD} \frac{k_{gD}}{\mu_{gD}} g_D \frac{\partial z_D}{\partial x_{1D}}) + \left[\frac{C_{gsR} \rho_{gR} k_{gR} p_{gR}}{x_{2R}^2 \mu_{gR}}\right] \frac{\partial}{\partial x_{2D}} (C_{gsD} \rho_{gD} \frac{k_{gD}}{\mu_{gD}} \frac{\partial p_{gD}}{\partial x_{2D}})$$

$$+ \left[\frac{C_{gsR} \rho_{gR}^2 k_{gR} g_R z_R}{\mu_{gR} x_{2R}^2}\right] \frac{\partial}{\partial x_{2D}} (C_{gsD} \rho_{gD}^2 \frac{k_{gD}}{\mu_{gD}} \frac{\partial z_D}{\partial x_{2D}}) + \left[\frac{C_{gsR} \rho_{gR} k_{gR} p_{gR}}{x_{3R}^2 \mu_{gR}}\right] \frac{\partial}{\partial x_{3D}}$$

$$(C_{gsD} \rho_{gD} \frac{k_{gD}}{\mu_{gD}} \frac{\partial p_{gD}}{\partial x_{3D}}) + \left[\frac{C_{gsR} \rho_{gR}^2 k_{gR} g_R z_R}{\mu_{gR} x_{3R}^2}\right] \frac{\partial}{\partial x_{3D}} (C_{gsD} \rho_{gD}^2 \frac{k_{gD}}{\mu_{gD}} g_D \frac{\partial z_D}{\partial x_{3D}})$$

MASS BALANCE FOR SOLVENT (continued)

$$+\left[\frac{\phi_R S_{oR} D_{LosR} C_{osR} \rho_{oR}}{x_{1R}^2}\right]\frac{\partial}{\partial x_{1D}}\left(\phi_D S_{oD} D_{LosD}\frac{\partial}{\partial x_{1D}}(C_{osD}\rho_{oD})\right)$$

$$+\left[\frac{\phi_R S_{oR} D_{TosR} C_{osR} \rho_{oR}}{x_{2R}^2}\right]\frac{\partial}{\partial x_{2D}}\left(\phi_D S_{oD} D_{TosD}\frac{\partial}{\partial x_{2D}}(C_{osD}\rho_{oD})\right)$$

$$+\left[\frac{\phi_R S_{oR} D_{TosR} C_{osR} \rho_{oR}}{x_{3R}^2}\right]\frac{\partial}{\partial x_{3D}}\left(\phi_D S_{oD} D_{TosD}\frac{\partial}{\partial x_{3D}}(C_{osD}\rho_{oD})\right)$$

$$+\left[\frac{\phi_R S_{gR} D_{LgsR} C_{gsR} \rho_{gR}}{x_{1R}^2}\right]\frac{\partial}{\partial x_{1D}}\left(\phi_D S_{gD} D_{LgsD}\frac{\partial}{\partial x_{1D}}(C_{gsD}\rho_{gD})\right)$$

$$+\left[\frac{\phi_R S_{gR} D_{TgsR} C_{gsR} \rho_{gR}}{x_{2R}^2}\right]\frac{\partial}{\partial x_{2D}}\left(\phi_D S_{gD} D_{TgsD}\frac{\partial}{\partial x_{2D}}(C_{gsD}\rho_{gD})\right)$$

$$+\left[\frac{\phi_R S_{gR} D_{TgsR} C_{gsR} \rho_{gR}}{x_{3R}^2}\right]\frac{\partial}{\partial x_{3D}}\left(\phi_D S_{gD} D_{TgsD}\frac{\partial}{\partial x_{3D}}(C_{gsD}\rho_{gD})\right)$$

2) Mass Balance For Water

$$\left[\frac{\phi_R S_{gR} C_{gwR} \rho_{gR}}{t_R}\right] \frac{\partial}{\partial t_D} \left(\phi_D S_{gD} C_{gwD} \rho_{gD} + \left[\frac{S_{wR} \rho_{wR}}{S_{gR} C_{gwR} \rho_{gR}}\right] \phi_D S_{wD} \rho_{wD}\right)$$

$$= \left[\frac{C_{gwR} \rho_{gR} k_{gR} p_{gR}}{\mu_{gR} x_{1R}^2}\right] \frac{\partial}{\partial x_{1D}} \left(C_{gwD} \rho_{gD} \frac{k_{gD}}{\mu_{gD}} \frac{\partial p_{gD}}{\partial x_{1D}} + \left[\frac{C_{gwR} \rho_{gR}^2 k_{gR} g_R z_R}{\mu_{gR} x_{1R}^2}\right] \frac{\partial}{\partial x_{1D}}\right.$$

$$\left(C_{gwD} \rho_{gD}^2 \frac{k_{gD}}{\mu_{gD}} g_D \frac{\partial z_D}{\partial x_{1D}}\right) + \left[\frac{C_{gwR} \rho_{gR} k_{gR} p_{gR}}{\mu_{gR} x_{2R}^2}\right] \frac{\partial}{\partial x_{2D}} \left(C_{gwD} \rho_{gD} \frac{k_{gD}}{\mu_{gD}} \frac{\partial p_{gD}}{\partial x_{2D}}\right)$$

$$+ \left[\frac{C_{gwR} \rho_{gR}^2 k_{gR} g_R z_R}{\mu_{gR} x_{2R}^2}\right] \frac{\partial}{\partial x_{2D}} \left(C_{gwD} \rho_{gD}^2 \frac{k_{gD}}{\mu_{gD}} g_D \frac{\partial z_D}{\partial x_{2D}}\right) + \left[\frac{C_{gwR} \rho_{gR} k_{gR} p_{gR}}{\mu_{gR} x_{3R}^2}\right] \frac{\partial}{\partial x_{3D}}$$

$$\left(C_{gwD} \rho_{gD} \frac{k_{gD}}{\mu_{gD}} \frac{\partial p_{gD}}{\partial x_{3D}}\right) + \left[\frac{C_{gwR} \rho_{gR}^2 k_{gR} g_R z_R}{\mu_{gR} x_{3R}^2}\right] \frac{\partial}{\partial x_{3D}} \left(C_{gwD} \rho_{gD}^2 \frac{k_{gD}}{\mu_{gD}} g_D \frac{\partial z_D}{\partial x_{3D}}\right)$$

$$+ \left[\frac{\rho_{wR} k_{wR} p_{wR}}{x_{1R}^2 \mu_{wR}}\right] \frac{\partial}{\partial x_{1D}} \left(\rho_{wD} \frac{k_{wD}}{\mu_{wD}} \frac{\partial p_{wD}}{\partial x_{1D}}\right) + \left[\frac{\rho_{wR}^2 k_{wR} g_R z_R}{\mu_{wR} x_{1R}^2}\right] \frac{\partial}{\partial x_{1D}} \left(\rho_{wD}^2 \frac{k_{wD}}{\mu_{wD}} g_D \frac{\partial z_D}{\partial x_{1D}}\right)$$

$$+ \left[\frac{\rho_{wR} k_{wR} p_{wR}}{x_{2R}^2 \mu_{wR}}\right] \frac{\partial}{\partial x_{2D}} \left(\rho_{wD} \frac{k_{wD}}{\mu_{wD}} \frac{\partial p_{wD}}{\partial x_{2D}}\right) + \left[\frac{\rho_{wR}^2 k_{wR} g_R z_R}{\mu_{wR} x_{2R}^2}\right] \frac{\partial}{\partial x_{2D}} \left(\rho_{wD}^2 \frac{k_{wD}}{\mu_{wD}} g_D \frac{\partial z_D}{\partial x_{2D}}\right)$$

$$+ \left[\frac{\rho_{wR} k_{wR} p_{wR}}{x_{3R}^2 \mu_{wR}}\right] \frac{\partial}{\partial x_{3D}} \left(\rho_{wD} \frac{k_{wD}}{\mu_{wD}} \frac{\partial p_{wD}}{\partial x_{3D}}\right) + \left[\frac{\rho_{wR}^2 k_{wR} g_R z_R}{\mu_{wR} x_{3R}^2}\right] \frac{\partial}{\partial x_{3D}} \left(\rho_{wD}^2 \frac{k_{wD}}{\mu_{wR}} g_D \frac{\partial z_D}{\partial x_{3D}}\right)$$

$$+ \left[\frac{\phi_R S_{gR} D_{LgwR} C_{gwR} \rho_{gR}}{x_{1R}^2}\right] \frac{\partial}{\partial x_{1D}} \left(\phi_D S_{gD} D_{LgwD} \frac{\partial}{\partial x_{1D}} \left(C_{gwD} \rho_{gD}\right)\right)$$

$$+ \left[\frac{\phi_R S_{gR} D_{TgwR} C_{gwR} \rho_{gR}}{x_{2R}^2}\right] \frac{\partial}{\partial x_{2D}} \left(\phi_D S_{gD} D_{TgwD} \frac{\partial}{\partial x_{2D}} \left(C_{gwD} \rho_{gD}\right)\right)$$

$$+ \left[\frac{\phi_R S_{gR} D_{TgwR} C_{gwR} \rho_{gR}}{x_{3R}^2}\right] \frac{\partial}{\partial x_{3D}} \left(\phi_D S_{gD} D_{LgwD} \frac{\partial}{\partial x_{3D}} \left(C_{gwD} \rho_{gD}\right)\right)$$

3) Energy Balance

$$\left[\frac{\phi_R \rho_{gR} S_{gR} U_{gR}}{t_R}\right] \phi_D \frac{\partial}{\partial t_D} (\rho_{gD} S_{gD} U_{gD} + \left[\frac{\rho_{wR} S_{wR} U_{wR}}{\rho_{gR} S_{gR} U_{gR}}\right] \rho_{wD} S_{wD} U_{wD} + \left[\frac{\rho_{oR} S_{oR} U_{oR}}{\rho_{gR} S_{gR} U_{gR}}\right]$$

$$\rho_{oD} S_{oD} U_{oD}) + \left[\frac{\rho_{rR} U_{rR}}{t_R}\right] (1 - [\phi_R]\phi_D) \rho_{rD} \frac{\partial U_{rD}}{\partial t_D} = \left[\frac{k_{hrR} T_R}{x_{1R}^2}\right] \frac{\partial}{\partial x_{1D}} (k_{hrD} \frac{\partial T_D}{\partial x_{1D}})$$

$$+ \left[\frac{k_{hrR} T_R}{x_{2R}^2}\right] \frac{\partial}{\partial x_{2D}} (k_{hrD} \frac{\partial T_D}{\partial x_{2D}}) + \left[\frac{k_{hrR} T_R}{x_{3R}^2}\right] \frac{\partial}{\partial x_{3D}} (k_{hrD} \frac{\partial T_D}{\partial x_{3D}}) + \left[\frac{\rho_{gR} h_{gR} k_{gR} p_{gR}}{\mu_{gR} x_{1R}^2}\right] \frac{\partial}{\partial x_{1D}}$$

$$(\rho_{gD} h_{gD} \frac{k_{gD}}{\mu_{gD}} \frac{\partial p_{gD}}{\partial x_{1D}}) + \left[\frac{\rho_{gR}^2 h_{gR} k_{gR} g_R z_R}{\mu_{gR} x_{1R}^2}\right] \frac{\partial}{\partial x_{1D}} (\rho_{gD}^2 h_{gD} \frac{k_{gD}}{\mu_{gD}} g_D \frac{\partial z_D}{\partial x_{1D}})$$

$$+ \left[\frac{\rho_{gR} h_{gR} k_{gR} p_{gR}}{\mu_{gR} x_{2R}^2}\right] \frac{\partial}{\partial x_{2D}} + (\rho_{gD} h_{gD} \frac{k_{gD}}{\mu_{gD}} \frac{\partial p_{gD}}{\partial x_{2D}}) + \left[\frac{\rho_{gR}^2 h_{gR} k_{gR} g_R z_R}{\mu_{gR} x_{2R}^2}\right] \frac{\partial}{\partial x_{2D}}$$

$$(\rho_{gD}^2 h_{gD} \frac{k_{gD}}{\mu_{gD}} g_D \frac{\partial z_D}{\partial x_{2D}}) + \left[\frac{\rho_{gR} h_{gR} k_{gR} p_{gR}}{\mu_{gR} x_{3R}^2}\right] \frac{\partial}{\partial x_{3D}} (\rho_{gD} h_{gD} \frac{k_{gD}}{\mu_{gD}} \frac{\partial p_{gD}}{\partial x_{3D}})$$

$$+ \left[\frac{\rho_{gR}^2 h_{gR} k_{gR} g_R z_R}{\mu_{gR} x_{3R}^2}\right] \frac{\partial}{\partial x_{3D}} (\rho_{gD}^2 h_{gD} \frac{k_{gD}}{\mu_{gD}} g_D \frac{\partial z_D}{\partial x_{3D}}) + \left[\frac{\rho_{wR} h_{wR} k_{wR} p_{wR}}{\mu_{gR} x_{1R}^2}\right] \frac{\partial}{\partial x_{1D}}$$

$$(\rho_{wD} h_{wD} \frac{k_{wD}}{\mu_{wD}} \frac{\partial p_{wD}}{\partial x_{1D}}) + \left[\frac{\rho_{wR}^2 h_{wR} k_{wR} g_R z_R}{\mu_{wR} x_{1R}^2}\right] \frac{\partial}{\partial x_{1D}} (\rho_{wD}^2 h_{wD} \frac{k_{wD}}{\mu_{gD}} g_D \frac{\partial z_D}{\partial x_{1D}})$$

$$+ \left[\frac{\rho_{wR} h_{wR} k_{wR} p_{wR}}{\mu_{gR} x_{2R}^2}\right] \frac{\partial}{\partial x_{2D}} (\rho_{wD} h_{wD} \frac{k_{wD}}{\mu_{wD}} \frac{\partial p_{wD}}{\partial x_{2D}}) + \left[\frac{\rho_{wR}^2 h_{wR} k_{wR} g_R z_R}{\mu_{wR} x_{2R}^2}\right] \frac{\partial}{\partial x_{2D}}$$

ENERGY BALANCE (continued)

$$\left(\rho_{wD}^2 h_{wD} \frac{k_{wD} g_D}{\mu_{wD}} \frac{\partial z_D}{\partial x_{2D}}\right) + \left[\frac{\rho_{wR} h_{wR} k_{wR} p_{wR}}{\mu_{gR} x_{3R}^2}\right] \frac{\partial}{\partial x_{3D}} \left(\rho_{wD} h_{wD} \frac{k_{wD}}{\mu_{wD}} \frac{\partial p_{wD}}{\partial x_{3D}}\right)$$

$$+ \left[\frac{\rho_{wR}^2 h_{wR} k_{wR} g_R z_R}{\mu_{wR} x_{3R}^2}\right] \frac{\partial}{\partial x_{3D}} \left(\rho_{wD}^2 h_{wD} \frac{k_{wD}}{\mu_{wD}} g_D \frac{\partial z_D}{\partial x_{3D}}\right) + \left[\frac{\rho_{oR} h_{oR} k_{oR} p_{oR}}{\mu_{oR} x_{1R}^2}\right] \frac{\partial}{\partial x_{1D}}$$

$$\left(\rho_{oD} h_{oD} \frac{k_{oD}}{\mu_{oD}} \frac{\partial p_{oD}}{\partial x_{1D}}\right) + \left[\frac{\rho_{oR}^2 h_{oR} k_{oR} g_R z_R}{\mu_{oR} x_{1R}^2}\right] \frac{\partial}{\partial x_{1D}} \left(\rho_{oD}^2 h_{oD} \frac{k_{oD}}{\mu_{oD}} g_D \frac{\partial z_D}{\partial x_{1D}}\right)$$

$$+ \left[\frac{\rho_{oR} h_{oR} k_{oR} p_{oR}}{\mu_{oR} x_{2R}^2}\right] \frac{\partial}{\partial x_{2D}} \left(\rho_{oD} h_{oD} \frac{k_{oD}}{\mu_{oD}} \frac{\partial p_{oD}}{\partial x_{2D}}\right) + \left[\frac{\rho_{oR}^2 h_{oR} k_{oR} g_R z_R}{\mu_{oR} x_{2R}^2}\right] \frac{\partial}{\partial x_{2D}}$$

$$\left(\rho_{oD}^2 h_{oD} \frac{k_{oD} g_D}{\mu_{oD}} \frac{\partial z_D}{\partial x_{2D}}\right) + \left[\frac{\rho_{oR} h_{oR} k_{oR} p_{oR}}{\mu_{oR} x_{3R}^2}\right] \frac{\partial}{\partial x_{3D}} \left(\rho_{oD} h_{oD} \frac{k_{oD}}{\mu_{oD}} \frac{\partial p_{oD}}{\partial x_{3D}}\right)$$

$$+ \left[\frac{\rho_{oR}^2 h_{oR} k_{oR} g_R z_R}{\mu_{oR} x_{3R}^2}\right] \frac{\partial}{\partial x_{3D}} \left(\rho_{oD}^2 h_{oD} \frac{k_{oD}}{\mu_{oD}} g_D \frac{\partial z_D}{\partial x_{3D}}\right)$$

APPENDIX D - SCALING ANISOTROPIC POROUS MEDIA

Let the permeability tensor for anisotropic porous media having a vertical permeability different from the horizontal permeability be,

$$\bar{\bar{k}} = \begin{pmatrix} k_x & 0 & 0 \\ 0 & k_y & 0 \\ 0 & 0 & k_x \end{pmatrix} .$$

Then, assuming a horizontal reservoir in which the vertical pressure gradient is relatively small, the mass balance for oil becomes,

$$\frac{\partial}{\partial t}(\phi S_o C_{oo} \rho_o) = \frac{\partial}{\partial x_1}\left[\frac{C_{oo}\rho_o k_{ox}}{\mu_o}\frac{\partial p_o}{\partial x_1}\right] + \frac{\partial}{\partial x_2}\left[\frac{C_{oo}\rho_o^2 g k_{oy}}{\mu_o}\frac{\partial z}{\partial x_2}\right] + \frac{\partial}{\partial x_3}\left[\frac{C_{oo}\rho_o k_{ox}}{\mu_o}\frac{\partial p_o}{\partial x_3}\right]$$

$$+ \frac{\partial}{\partial x_1}\left[\phi S_{oo} D_{Loo}\frac{\partial (C_{oo}\rho_o)}{\partial x_1}\right] + \frac{\partial}{\partial x_2}\left[\phi S_{oo} D_{Too}\frac{\partial (C_{oo}\rho_o)}{\partial x_2}\right] + \frac{\partial}{\partial x_3}\left[\phi S_{oo} D_{Too}\frac{\partial (C_{oo}\rho_o)}{\partial x_3}\right]$$

Non-dimensionalizing, and collecting the coefficients yields the following similarity groups:

$$\frac{W}{L}, \frac{\rho_{oR} g_R k_{oyR} L^2}{H k_{oxR} p_{oR}}, \frac{\phi_R S_{oR} \mu_{oR} L^2}{t_R k_{oxR} p_{oR}}, \frac{\phi_R S_{oR} \mu_{oR} D_{LooR}}{k_{oxR} p_{oR}}, \frac{\phi_R S_{oR} \mu_{oR} D_{TooR} L^2}{k_{oxR} p_{oR} H^2}, \frac{D_{TooR}}{D_{LooR}}$$

The other governing equations are treated in a similar manner. The same conclusions are reached. Using Approaches #1 and #3, the gravitational group can be satisfied using a uniform sand in the model (i.e. $k_{xm}=k_{ym}$) when,

$$\Delta p_m = \left(\frac{L^2}{H}\right)_m \left(\frac{H\, k_x \Delta p}{L^2 k_y}\right)_p .$$

APPENDIX E - OIL PROPERTIES

i) Oil viscosity as a function of temperature

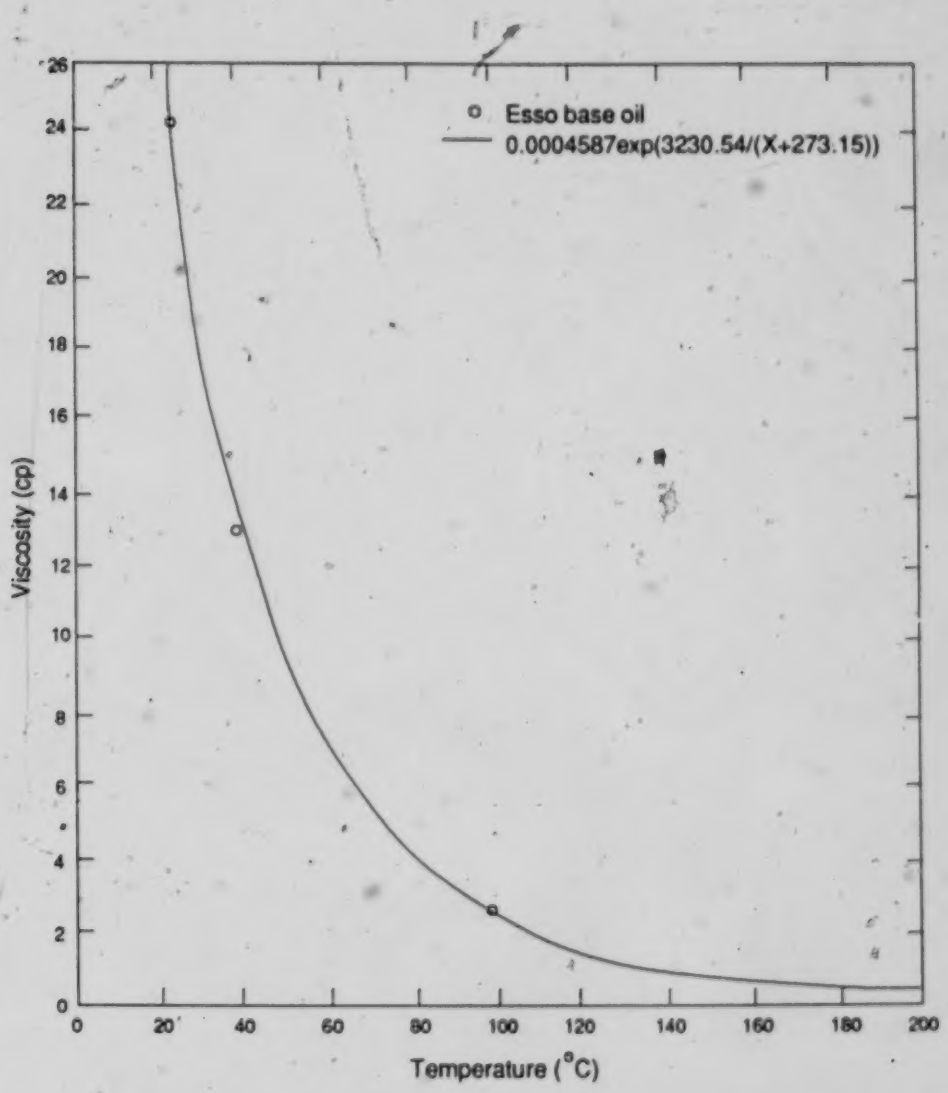

ii) Oil density as a function of temperature

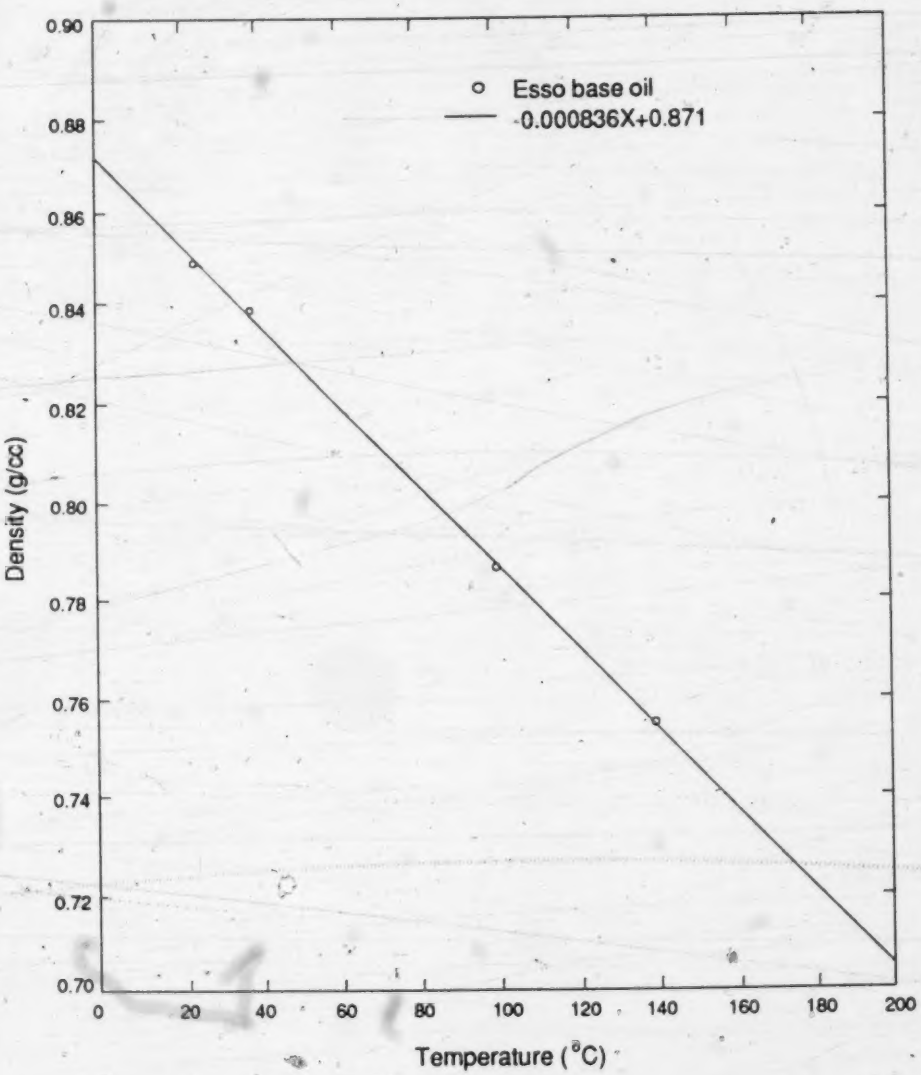

iii) Simulated distillation of the oil

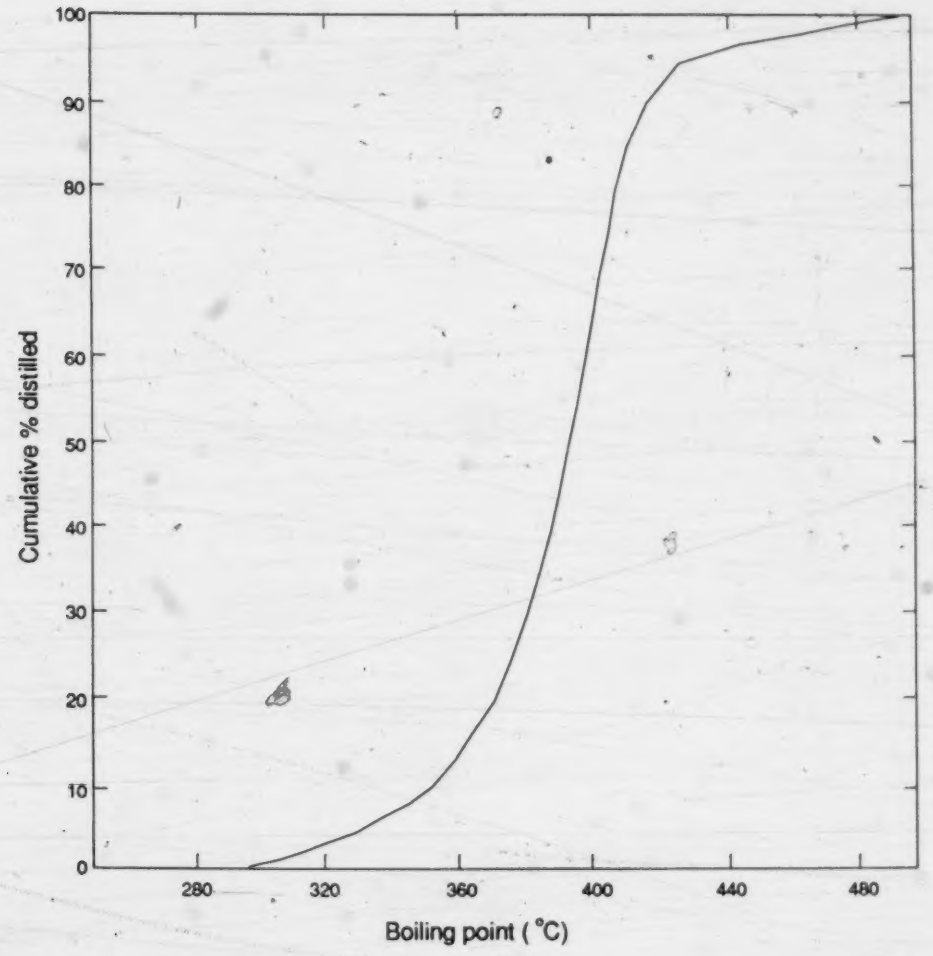

APPENDIX F - AVERAGE BLOCK TEMPERATURE

The average temperature of the triangular block (see figure) is:

$$\bar{T} = \frac{1}{A} \int\int T(x,y)\, dx\, dy$$

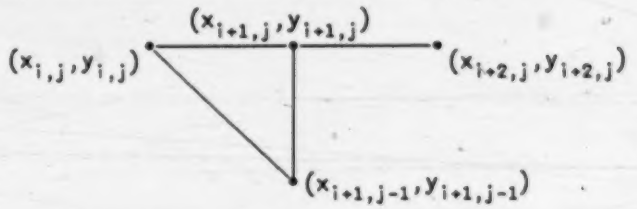

Temperature was assumed to vary linearly in the y-direction between y_j and y_{j+1}.

$$T(x,y) = T(x) + C_1 y + C_3$$

$$\bar{T} = \frac{1}{A} \int_{x_i}^{x_{i+1}} \left[Ty + \frac{C_1 y^2}{2} + C_3 y \right]_{m_2 x + b_2}^{y_j} dx$$

$$\bar{T} = \frac{1}{A} \left[D_1 \int_{x_i}^{x_{i+1}} Tx\, dx + D_2 \int_{x_i}^{x_{i+1}} T\, dx + D_3 (x_{i+1}^3 - x_i^3) + D_4 (x_{i+1}^2 - x_i^2) + D_5 (x_{i+1} - x_i) \right.$$

$$C_1 = (T_{i+1,j} - T_{i+1,j-1}) / (y_{i+1,j} - y_{i+1,j-1})$$

$$C_3 = -y_{i,j} (T_{i+1,j} - T_{i+1,j-1}) / (y_{i+1,j} - y_{i+1,j-1})$$

$$b_1 = y_{i,j}$$

$$m_2 = (y_{i,j} - y_{i,j-1}) / (x_{i,j} - x_{i+1,j-1})$$

$$b_2 = y_{i,j} - m_2 x_{i,j}$$

$$D_1 = -m_2$$

$$D_2 = b_1 - b_2$$

$$D_3 = -(C_1 m_2^2/2 + C_2 m_2)/3$$

$$D_4 = -(C_1 m_2 b_2 - C_2 (b_1 - b_2) + C_3 m_2)/2$$

$$D_5 = C_1 (b_1^2 - b_2^2) + C_3 (b_1 - b_2)$$

Assuming $T(x) = a_1/(1+a_2x+a_3x^2)$,

where a_1, a_2, and a_3 are calculated using $T_{i,j}$, $T_{i+1,j}$, and $T_{i+2,j}$,

then $$D_1 \int_{x_i}^{x_{i+1}} Tx\, dx = D_1 \int_{x_i}^{x_{i+1}} \frac{a_1 x}{1+a_2x+a_3x^2}\, dx$$

$$= \frac{D_1 a_1}{2\, a_3} \left[\ln\left(\frac{R(x_{i+1})}{R(x_i)}\right) - a_2 \int_{x_i}^{x_{i+1}} \frac{dx}{R} \right]$$

and $$D_2 \int_{x_i}^{x_{i+1}} T\, dx = D_2 \int_{x_i}^{x_{i+1}} \frac{a_1 x}{1+a_2x+a_3x^2}\, dx$$

$$= D_2 a_1 \int_{x_i}^{x_{i+1}} \frac{dx}{R}$$

where

$$R = 1+a_2x+a_3x^2$$

$$q = 4a_3 - a_2^2$$

$$\int_{x_i}^{x_{i+1}} \frac{dx}{R} = \begin{cases} \dfrac{2}{\sqrt{q}} \tan^{-1} \dfrac{2cx+b}{\sqrt{q}} & q > 0 \\ \dfrac{-2}{\sqrt{-q}} \tanh^{-1} \dfrac{2cx+b}{\sqrt{-q}} & \left|\dfrac{2cx+b}{\sqrt{-q}}\right| < 1 \text{ and } q < 0 \\ \dfrac{1}{\sqrt{-q}} \ln \dfrac{2cx+b-\sqrt{-q}}{2cx+b+\sqrt{-q}} & q < 0 \end{cases}$$

APPENDIX G - NEW CRITERIA FOR APPROACHES #3 AND #4

Conductive heat transfer within the reservoir is not scaled in the vertical direction when using Approaches #3 and #4 (i.e. vertical geometric similarity is relaxed), therefore, the boundary condition,

$$k_{hc} \frac{\partial T}{\partial x_{3c}} = k_{hr} \frac{\partial T}{\partial x_{3r}}$$

can not be used. Instead,

$$k_{hc} \frac{\partial T}{\partial x_{3c}} = \left(\frac{Q}{A} \right)_n$$

should be used, where Q is the energy lost to the surrounding formations from the reservoir. The rate of energy conducted away from the reservoir should be scaled in a similar manner as the rate of energy injected. This leads to the scaling group,

$$\frac{k_{hc} \Delta T L}{W_{st} h_w}$$

As with all approaches, the similarity groups associated with the energy balance equation within the surrounding formations must be satisfied as well. The groups are,

$$\frac{k_{hc} t}{(\rho C_p)_c L^2} \quad , \quad \frac{H_c}{L} \quad , \quad \frac{W_c}{L}$$